Development of Homogeneous Manganese and Iron Catalysts for Organic

Transformations and Renewable Fuel Production

by

Tufan K. Mukhopadhyay

A Dissertation Presented in Partial Fulfillment
of the Requirements for the Degree of
Doctor of Philosophy

ARIZONA STATE UNIVERSITY

August 2016

ABSTRACT

The late first row transition metals, being inexpensive and environmentally benign, have become very attractive for sustainable catalyst development. However, to overcome the detrimental one electron redox processes exhibited by these metals, the employment of redox non-innocent chelates turned out to be very useful. The Trovitch group has designed a series of pentadentate bis(imino)pyridine ligands (pyridine diimine, PDI) that are capable of binding the metal center beyond their κ^3-*N,N,N* core and also possess coordination flexibility. My research is focused on developing PDI-supported manganese catalysts for organic transformations and renewable fuel production.

The thesis presents synthesis and characterization of a family of low valent (PDI)Mn complexes. Detailed electronic structure evaluation from spectroscopic and crystallographic data revealed electron transfer from the reduced metal center to the accessible ligand orbitals. One particular (PDI)Mn variant, (κ^5-^{Ph2PPr}PDI)Mn has been found to be the most efficient carbonyl hydrosilylation catalyst reported till date, achieving a maximum turnover frequency of up to 4950 min^{-1}. This observation demanded a thorough investigation of the operative mechanism. A series of controlled stoichiometric reactions, detailed kinetic analysis, and relevant intermediate isolation suggest a mechanism that involves oxidative addition, carbonyl insertion, and reductive elimination. Noticing such remarkable efficiency of the (PDI)Mn system, it has been tested for application in renewable fuel generation. A modest efficiency for H_2 production at an apparent pH of 8.4 have been achieved using a cationic Mn complex, [(^{Ph2PPr}PDI)Mn(CO)]Br. Although, a detailed mechanistic investigation remained

i

challenging due to complex instability, a set of relevant Mn(-I) intermediates have been isolated and characterized thoroughly.

The dissertation also includes synthesis, characterization, and electronic structure evaluation of a series of Triphos supported iron complexes. Using this pincer chelate and either 2,2'-bipyridine (bpy) or 1,3,5,7-cyclooctatetraene (COT), a set of electronically interesting complexes have been isolated. Detailed electronic structure investigation using spectroscopy, magnetometry, crystallography, and DFT calculations revealed redox non-innocent behavior in the Bpy and COT ligands. Additionally, CO binding to the (Triphos)Fe system followed by reaction with borohydride reagents allowed for the isolation of some catalytically relevant and reactive iron hydride complexes.

Dedicated to

My parents
Tapan Kumar Mukhopadhyay
&
Dipa Mukhopadhyay

discussion regarding my research and teaching some of the important concepts related to electrochemistry and synthetic organic chemistry.

While working in Prof. Trovitch's laboratory I had the nicest and talented crew around me who were all very helpful and friendly. With a small number of equipment in the beginning of our laboratory set up, all of my colleagues were very cooperative.

Importantly, I would take this opportunity to thank those who provided constant encouragement to me. My father Late Tapan Kumar Mukhopadhyay was the first person who ignited the passion of pursuing higher studies in science within me. My physical chemistry teacher Dr. Nimai C. Dey has constantly inspired me during the time of disappointments and helped me to chose a career in chemistry. During the M.Sc. dissertation at IIT Madras in Prof. Santosh J. Gharpure's laboratory, I learnt the fundamentals of professional academic research, where I also acquired strong experimental skills in synthetic organic chemistry. Last but not the least, I would thank

my mother Dipa Mukhopadhyay from the bottom of my heart for her constant encouragement to thrive and for her sacrifices to see me in a successful platform.

TABLE OF CONTENTS

LIST OF TABLES

LIST OF FIGURES

LIST OF SCHEMES

xviii

CHAPTER 1

SYNTHESES AND ELECTRONIC STRUCTURE OF PENTADENTATE

BIS(IMINO)PYRIDINE SUPPORTED MANGANESE COMPLEXES

1.1. Abstract:

A series of low valent manganese complexes have been prepared using bis(imino)pyridine (pyridine diimine, PDI) ligands containing phosphine, pyridine, or amine co-ligand arms. Heating a mixture of ^{Ph2PPr}PDI ligand and $(THF)_2MnCl_2$ resulted in formation of the dichloride $(^{Ph2PPr}PDI)MnCl_2$, which possesses a κ^3-*N,N,N*-chelate. Reduction of this dichloride using excess Na/Hg in presence of catalytic 1,3,5,7-cyclooctatetraene (COT) allowed for the isolation of the paramagnetic complex, $(\kappa^5$-*N,N,N,P,P*-PDI)Mn, with a formally zerovalent Mn center. Detailed electron structure investigation of this reduced complex using a combination of multinuclear NMR spectroscopy, magnetometry, X-ray crystallography, EPR spectroscopy, and DFT calculations revealed a Mn(II) center that is antiferromagnetically coupled to a triplet dianionic PDI-chelate (PDI^{2-}). Additionally, treating $(^{Ph2PPr}PDI)MnCl_2$ with 2.1 equiv. of $NaEt_3BH$ afforded a diamagnetic hydride complex, $(\kappa^5$-*N,N,N,P,P*-PDI)MnH, which features a ^1H NMR hydride resonance at -2.98 ppm (t). Reduction of a slightly modified dichloride, $(^{Ph2PEt}PDI)MnCl_2$ using excess Na/Hg and catalytic COT produced a dimeric paramagnetic complex $[(\kappa^4$-$^{Ph2PEt}PDI)Mn]_2$. The metrical parameters of $(\kappa^5$-*N,N,N,P,P*-PDI)MnH and $[(\kappa^4$-$^{Ph2PEt}PDI)Mn]_2$ obtained from X-ray diffraction analysis suggests significant reduction of the PDI chelate. Interestingly, two electron reduction of $(^{PyEt}PDI)MnCl_2$ containing pyridine as co-donor arms instead of phosphine, resulted in

the deprotonation of backbone methyl groups to give (κ^5-^{PyEt}PDEA)Mn. This fact clearly explains the role of π-accepting phosphine σ-P co-donors in the stabilization of low oxidation state Mn.

1.2. Introduction:

Synthetically important catalytic transformations like hydrogenation, hydrosilylation, metathesis, and C-C bond formation have mostly relied upon the use of soluble precious metal catalysts.[1] While the efficiency is remarkable, high price and toxicity associated with these metals are a potential problem for large-scale industrial use. The search for cheap and sustainable surrogates for these noble metals have been an area of immense study in organometallic chemistry over the past decade.[2] The late first row transition metals, being inexpensive and environmentally benign, are excellent choices for this application.[2c] However, the detrimental one electron redox processes initiated by first row transition metals in their low oxidation states, is a crucial point to address while developing catalysts for organometallic transformations. In the past few years, the use of redox non-innocent ligands to stabilize the reduced state of these metals, has escalated.[3] Redox non-innocent ligands, owing to their extended π network, can stabilize low-valent metals in their preferred oxidation state by accepting electrons from reduced metal centers (Figure 1.1).[3] As a consequence, the reactivity of such complexes are also controlled by the ligand cooperativity. Using these type of chelates, a handful of Co, Ni, and Fe complexes are reported,[3a] which are known to catalyze useful transformations such as water reduction,[4a] proton reduction,[4b] and alcohol oxidation.[4c] Notably, the bis(imino)pyridine (pyridine diimine, PDI) family is one such redox non-innocent

chelate, which has been one of the most investigated systems among organometallic chemists in the last few years.[5] It was first introduced by Brookhart and Gibson, where Fe and Co complexes supported by this tridentate chelate were shown to catalyze olefin polymerization.[6] Later, Chirik and coworkers have developed PDI-supported bis(dinitrogen) complexes of iron and cobalt, which can catalyze a variety of reactions such as hydrogenation, hydrosilylation, 2+2 cyclization and polymerization.[7] It is also known that the electronic structure and the metal oxidation state of these complexes can be accurately determined from spectroscopic, crystallographic, and computational methods,[8, 3b] which is beyond the definition of redox "non-innocence" introduced by Jørgensen in 1966.[9, 3a] Herein, we have designed an extended version of PDI ligands, where the traditional κ^3-chelate is tethered to two or three carbon bridged phosphine or amine co-donor arms (Figure 1.1).[10]
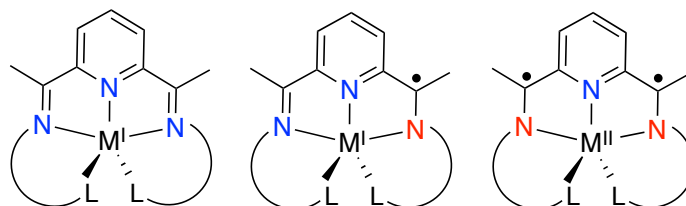
Figure 1.1. Design of redox non-innocent bis(imino)pyridine ligands and their reduction.

The advantages associated with this approach are now two fold: (i) these chelates are capable of accepting one, two, or three electrons as usual[11] and (ii) due to the additional modular co-ligand arms, they can coordinate to a metal center beyond their κ^3-core. Additionally, modular imine arms can dissociate to allow substrate(s) to approach the metal center during a catalytic transformation and coordinate back to the metal once the cycle is finished, hence preventing catalyst decomposition pathways. Also, knowing

the simplicity of preparing these ligands, the co-donor atom can be varied to tune the catalytic activity. Using these set of ligands,[10] we sought to develop manganese-based homogeneous catalysts, concerning the scarcity of Mn complexes in catalytic applications.[12] Except a very few important catalytic transformations such as olefin epoxidation,[13a] ketone and ester hydrosilylation,[13b] and electrocatalytic CO_2 reduction,[13c] the organometallic chemistry of manganese has yet to be developed.
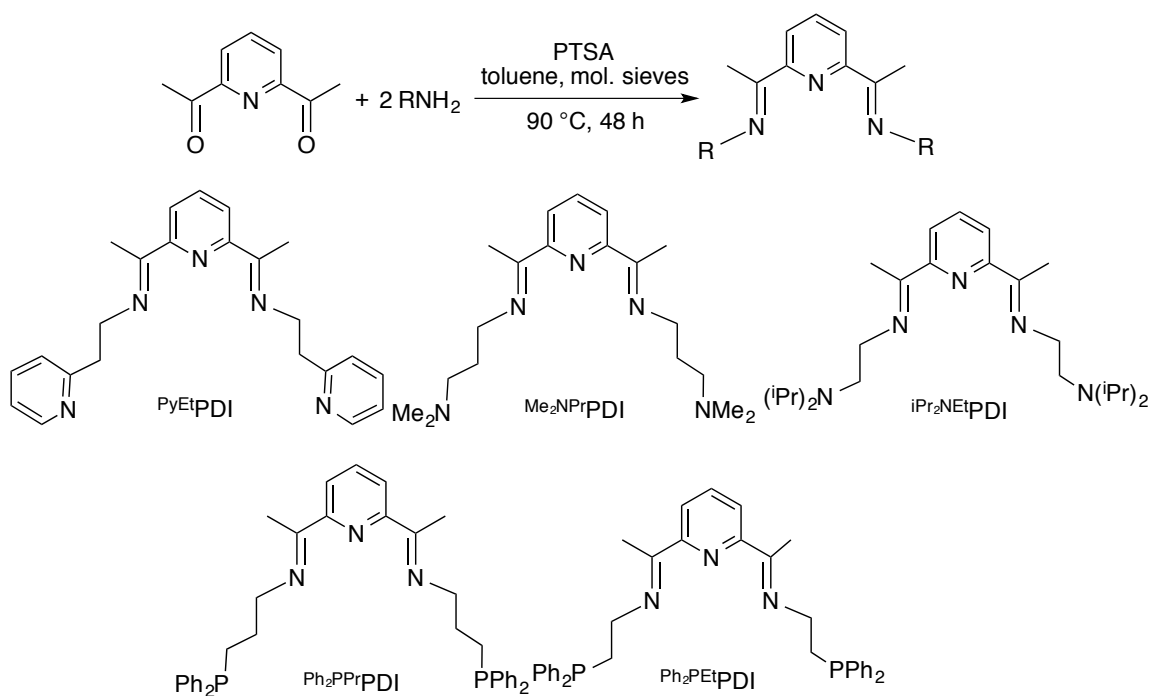
Scheme 1.1. Synthesis of different PDI variants following Schiff's base condensation.

1.3. Synthesis of PDIMnCl$_2$ complexes:

This venture began with heating a mixture of ^{PyEt}PDI and $MnCl_2$ in tetrahydrofuran at 90 °C for 3 d, which produced the paramagnetic dichloride ^{PyEt}PDIMnCl$_2$ **(1-Cl$_2$)** albeit in poor yields. Performing this reaction with ligand and $(THF)_2MnCl_2$[14] in toluene at 90 °C for 48 h improved the yield. ^{1}H NMR spectra of **1-Cl$_2$** showed three broadened resonances at 62.76, 13.51, and -31.63 ppm. Magnetic

susceptibility measurements using a Gouy's balance suggested it to possess a high spin Mn(II) center with a magnetic moment of 6.3 μ_B at 25 °C. The electronic spectrum of **1-Cl$_2$** showed two absorbance maxima at 306 nm (ε = 3844 M^{-1}cm^{-1}) and 318 nm (ε = 2601 M^{-1}cm^{-1}). Similarly, using other variants of the PDI family, four additional dichloride complexes have been isolated (Scheme 1.2). Although none of these dichloride complexes displayed conclusive ^{1}H NMR resonances, a few broad resonances for **2-Cl$_2$** were noticed at 70.31, 7.34, and 37.59 ppm. The solid-state magnetic moment collected for all these complexes showed values consistent with five unpaired electrons (**2-Cl$_2$** (5.9 μ_B), **3-Cl$_2$** (6.0 μ_B), **4-Cl$_2$** (6.0 μ_B), **5-Cl$_2$** (6.2 μ_B),).
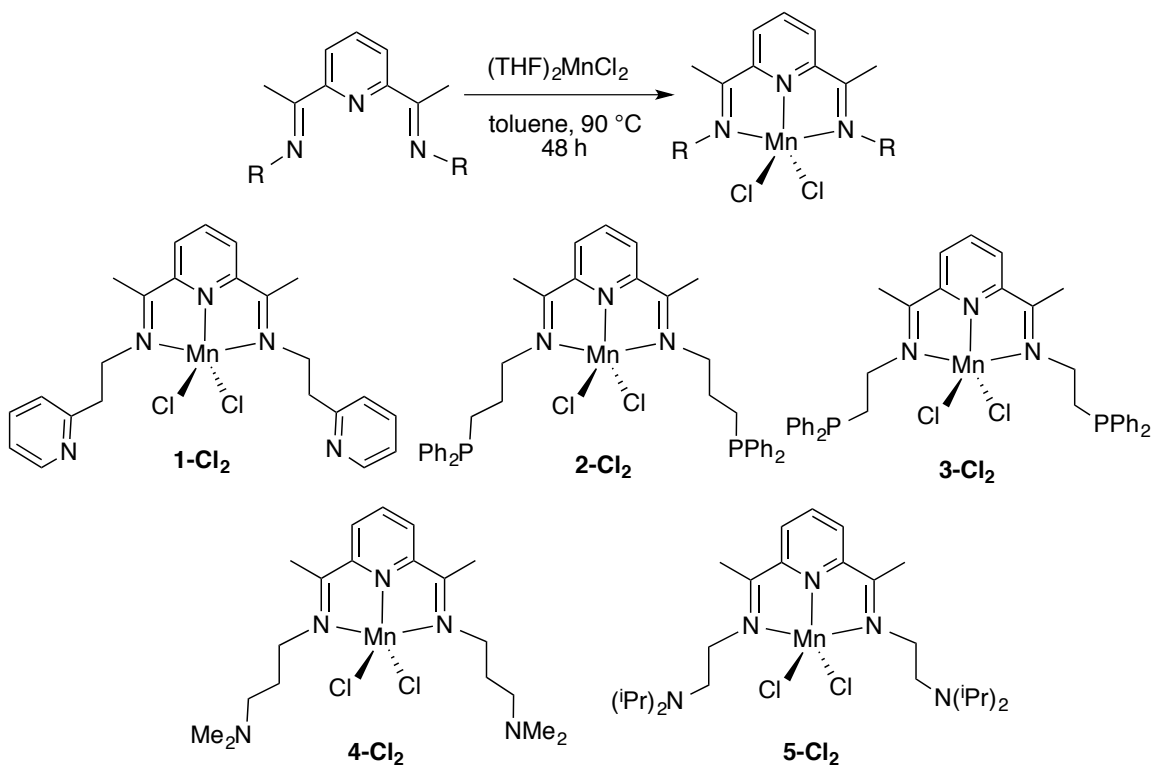
Scheme 1.2. Preparation of PDI-supported manganese dichloride complexes.

To confirm tridentate ligation of the PDI chelate, crystallization of some of these dichloride complexes was attempted. Cooling concentrated chloroform solutions of **1-Cl$_2$**

5

at -35 ºC, produced light orange crystals suitable for X-ray diffraction. Crystals of **2-Cl₂**

were obtained from a concentrated THF solution at ambient temperature. The solid-state

structures of **1-Cl₂** and **2-Cl₂** (Figure 1.2) clearly indicated κ^3-chelation of the PDI core,

while the imine arms are uncoordinated. The average N(1)-Mn(1)-N(1A/3) angle of

142.05(3)° and N(1)-Mn(1)-Cl(1) angle of 100.23(11)° for **1-Cl₂** and 98.64(6)° for **2-Cl₂**

confirmed a distorted trigonal bipyramid geometry around Mn in both complexes.

Comparing the C_{imine}-N_{imine} (average distance of 1.285 Å) and C_{imine}-$C_{pyridine}$ (average

distance of 1.501 Å) bond distances (Table 1.1) to reported values for unreduced PDI

chelate,[11] suggested a neutral PDI in both **1-Cl₂** and **2-Cl₂**, except minimal backbonding.

Highly broadened ^{1}H NMR resonances, an average magnetic moment of 6.0 μ_B, and the

Mn(1)-N_{imine} distances of 2.264(4) Å for **1-Cl₂** and 2.300(2) and 2.338(2) Å for **2-Cl₂**,

suggest a high spin Mn(II) center.
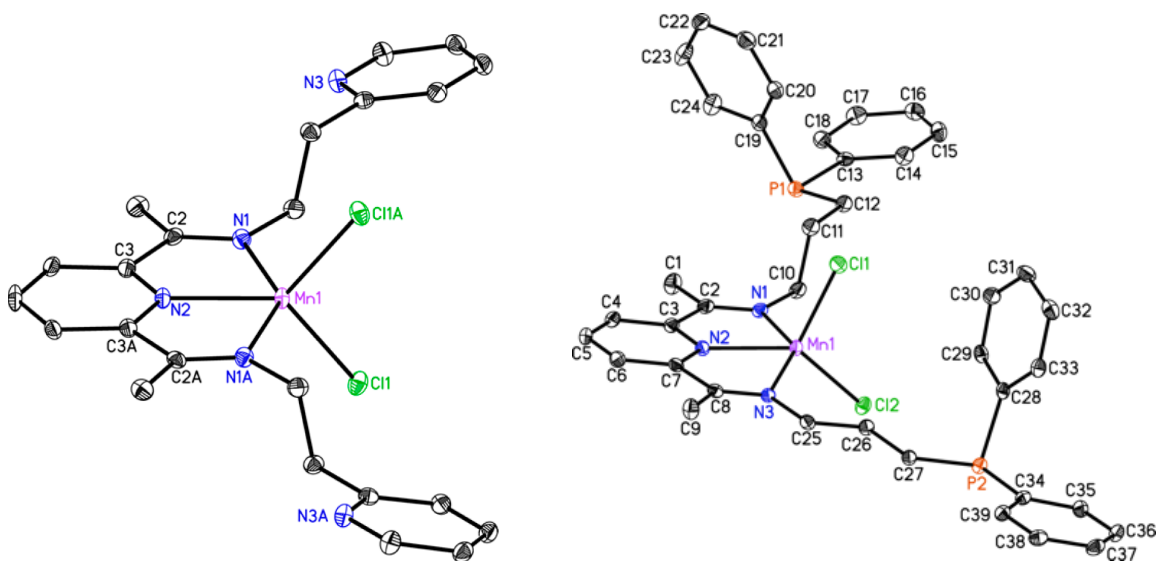
Figure 1.2. Solid-state structure of **1-Cl₂** (left) and **2-Cl₂** (right) shown at 30% probability ellipsoids. Hydrogen atoms and co-crystallized solvent molecules are omitted for clarity.

Table 1.1. Relevant bond lengths (Å) and bond angles (°) of **1-Cl₂** and **2-Cl₂**.

	1-Cl₂	**2-Cl₂**
Mn(1)-N(1)	2.264(4)	2.300(2)
Mn(1)-N(2)	2.224(6)	2.196(2)
Mn(1)-N(3)	-	2.338(2)
Mn(1)-Cl(1)	2.3740(15)	2.3514(8)
Mn(1)-Cl(2)	-	2.3748(8)
C(2)-N(1)	1.291(7)	1.274(4)
C(8)-N(3)	-	1.282(3)
C(2)-C(3)	1.505(7)	1.493(4)
C(7)-C(8)	-	1.502(4)
N(1)-Mn(1)-N(1A)	142.3(2)	-
N(1)-Mn(1)-N(3)	-	141.81(3)
N(2)-Mn(1)-Cl(1)	126.97(4)	113.63(6)
N(1)-Mn(1)-C1(1)	100.23(11)	98.64(6)
N(1)-Mn(1)-N(2)	-	71.47(8)

1.4. Synthesis of low-valent manganese complexes

1.4.1. Reduction of 1-Cl₂:

With the dichloride complexes in hand, we determined to reduce these PDI-bound Mn(II) precursors in order to isolate reactive Mn complexes. Reacting **1-Cl₂** with excess Na/Hg in THF resulted in the formation of a greenish-brown solid after 72 h. Using 0.5 equiv. of 1,3,5,7-cyclooctatetraene (COT) during the reduction reduced the reaction time to 12 h (Scheme 1.3). ^{1}H NMR spectra of this complex showed paramagnetically broadened resonances over a 100 ppm range. A solution magnetic moment was found to be 3.9 μ_B, which is an indicative of three unpaired electrons. Cooling a concentrated toluene/diethylether (1:1) solution at -35 °C afforded dark green crystals suitable for X-ray diffraction. Analysis of the single crystal X-ray diffraction data confirmed the formation of C_2 symmetric (κ^5-*N,N,N,N,N*-^{PyEt}PDEA)Mn complex (**1**, Figure 1.3)

featuring a doubly deprotonated bis(enamide) tris(pyridine) (PDEA) chelate (Scheme 1.3) with C(1)-C(2) and C(1A)-C(2A) bond distance of 1.363(3) Å (Table 1.2).[11] The imine C-N bond length of 1.369(3) Å is indicative of a C-N single bond. Also, the shorter Mn(1)-N(1) and Mn(1)-N(2) lengths compared to **1-Cl₂** is consistent with a PDEA^{2-} coordination. The N(1)-Mn(1)-N(1A) and N(2)-Mn(1)-N(3) angles of 148.67° and 126.59° indicate a distorted trigonal bipyramid geometry around manganese.
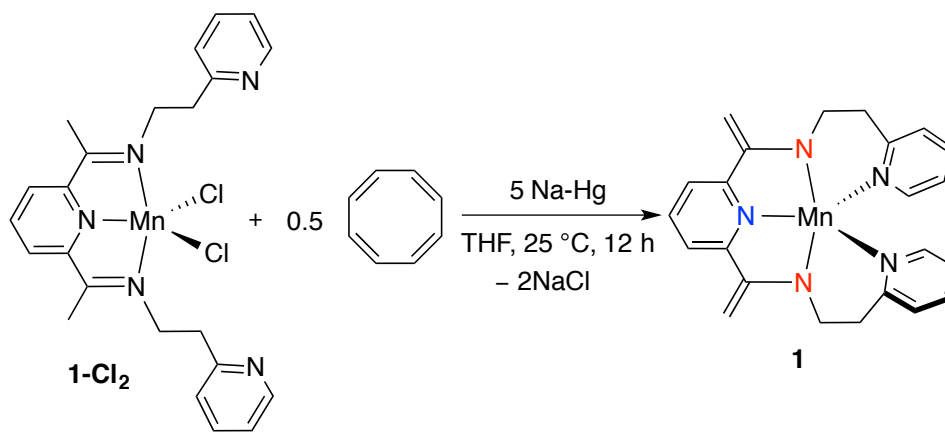
Scheme 1.3. Synthesis of (^{PyEt}PDEA)Mn **(1)**.
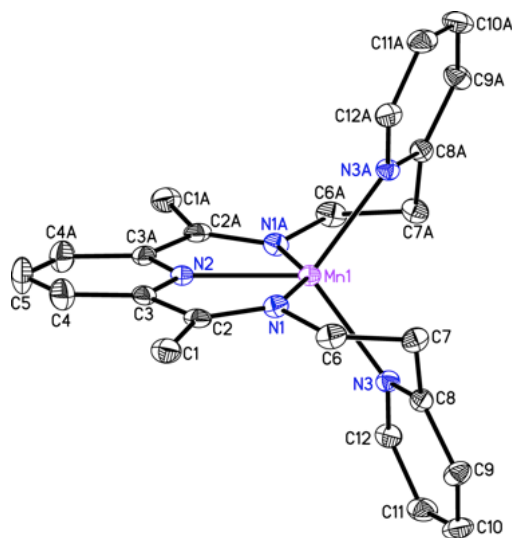
Figure 1.3. Solid-state structure of **1** shown at 30% probability ellipsoids. Hydrogen atoms and co-crystallized solvent molecules are omitted for clarity.

Table 1.2. Relevant bond lengths (Å) and angles (°) for **1**.

Mn(1)-N(1)	2.1123(18)	C(3)-N(2)	1.347(3)
Mn(1)-N(2)	2.158(3)	C(6)-N(1)	1.444(3)
Mn(1)-N(3)	2.2178(17)	N(1)-Mn(1)-N(1A)	148.67(10)
C(2)-N(1)	1.369(3)	N(2)-Mn(1)-N(3)	126.59(5)
C(2)-C(1)	1.363(3)	N(1)-Mn(1)-N(3)	86.38(7)
C(2)-C(3)	1.491(3)	N(1)-Mn(1)-N(2)	74.33(5)
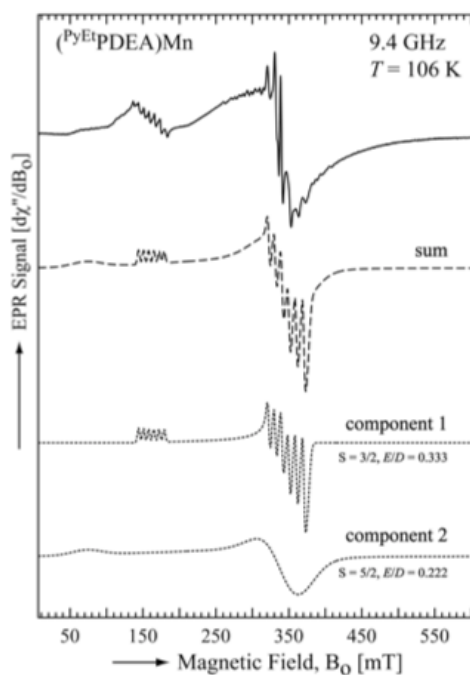
Figure 1.4. EPR spectrum of **1** at 106 K.

To further explore the electronic structure of **1**, the X-band (9.44 GHz) electron paramagnetic resonance (EPR) spectrum of **1** was collected in a toluene glass at 106 K, which displayed (Figure 1.4) a multiline pattern at 330 mT (g_{eff} = 2.0) consistent with a S = 3/2 Mn(II) species. Notably, another resonance was observed at 150 mT (g_{eff} = 4.3) due to a S = 5/2 impurity. These features are in good agreement to an intermediate spin [55]Mn center (S = 3/2; I = 5/2). Furthermore, the UV-vis spectrum of **1** showed two weak absorbance maxima at 512 nm (ε = 524 $M^{-1}cm^{-1}$) and 624 nm (ε = 504 $M^{-1}cm^{-1}$) that

9

correspond to d-d transitions, is additional supportive evidence for intermediate spin Mn(II) center. It is evident that the deprotonation of methyl backbone of the κ^5-*N,N,N,N,N*-PDI chelate under reducing conditions is switching off the redox communication between metal center and ligand which is opposed to our original ligand design approach. Although an exact mechanism of deprotonation is difficult to determine in this reduction, it is believed that the five σ-donating nitrogen donors around Mn are likely to be responsible for facilitating a putative imine-enamine tautomerism.

1.4.2. Reduction of 2-Cl$_2$:

Having observed backbone methyl group deprotonation of **1** under reducing conditions, the phosphine containing PDI variant, ^{Ph2PPr}PDI ligand was employed. It was hypothesized that π-accepting phosphine donors may allow for the isolation of κ^5-PDI supported Mn complex with persistent redox non-innocence in the chelate. Reducing **2-Cl$_2$** with excess Na/Hg in presence of a catalytic quantity of COT afforded a paramagnetic dark brown solid identified as (κ^5-*N,N,N,P,P*-^{Ph2PPr}PDI)Mn (**2**) (Scheme 1.4). The ^{1}H NMR of **2** features 10 paramagnetically broadened resonances ranging over 200 ppm (Figure 1.5). Solution state magnetic moment of this complex was found to be 2.2 μ_B at 25 °C, which is indicative of one unpaired electron. Determination of the solid-state structure of **2** was sought to further confirm the ligation and the extent of chelate reduction. A concentrated toluene solution of **2** was layered with diethylether and cooled to isolate dark brown crystals suitable for X-ray diffraction. Analysis of the diffraction data bolstered the formation of a pentadentate PDI bound Mn complex (Figure 1.6).
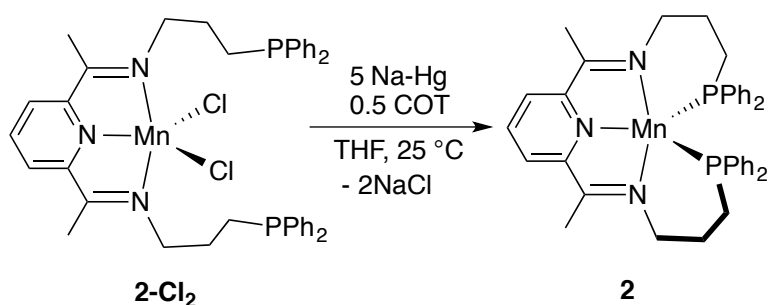
Scheme 1.4. Synthesis of **2** from reduction of **2-Cl₂**.
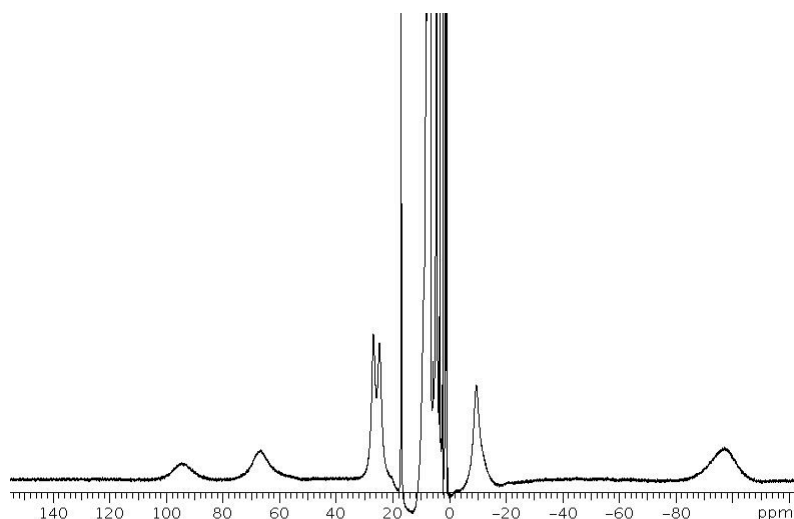
Figure 1.5. ^{1}H NMR spectrum of **2** in benzene-d_6.

The geometry about the Mn center is trigonal bipyramidal with N(1)-Mn(1)-N(3), N(2)-Mn(1)-P(1) and N(2)-Mn(1)-P(2) angles of 157.54(9)°, 130.90(6)°, and 123.14(6)° respectively. The average Mn(1)-N$_{imine}$ and Mn(1)-P bond lengths (Table 1.3) are within the covalent radii of a low spin Mn center.[15] While the imine bonds of the PDI chelate, C(2)-N(1) and C(8)-N(3) are fairly elongated to 1.354(3) and 1.355(3) Å respectively, the C(2)-C(3) and C(7)-C(8) bonds are contracted to 1.416(4) and 1.414(3) Å respectively. The elongation of imine bonds and concomitant shortening of the C$_{imine}$-C$_{pyridine}$ bonds[11] are highly consistent to those reported for ($^{2,6-iPr2Ph}$PDI)Mn(THF)$_2$[16] and suggest that **2**

11

possesses a low spin Mn(II) center supported by a doubly reduced PDI^{2-} dianion (Figure 1.9, left).
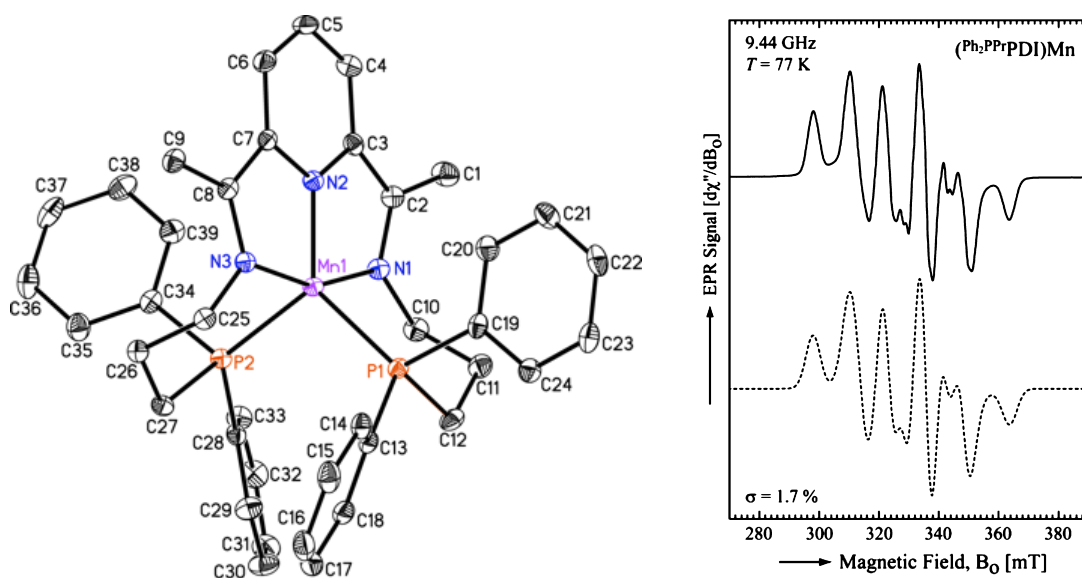
Figure 1.6. Solid-state structure of **2** shown at 30% probability ellipsoids (left). Hydrogen atoms and co-crystallized solvent molecules are omitted for clarity. The X-band (9.44 GHz) spectrum of **2** at 77 K (right).

Table 1.3. Relevant bond lengths (Å) and angles (°) for **2**.

Mn(1)-N(1)	2.1123(18)	C(3)-N(2)	1.347(3)
Mn(1)-N(2)	2.158(3)	C(6)-N(1)	1.444(3)
Mn(1)-N(3)	2.2178(17)	N(1)-Mn(1)-N(1A)	148.67(10)
C(2)-N(1)	1.369(3)	N(2)-Mn(1)-N(3)	126.59(5)
C(2)-C(1)	1.363(3)	N(1)-Mn(1)-N(3)	86.38(7)
C(2)-C(3)	1.491(3)	N(1)-Mn(1)-N(2)	74.33(5)

To obtain further supporting evidence for the electronic structure description of **2**, the X-band (9.44 GHz) EPR spectrum of **2** was collected in a toluene glass at 77 K. Although a signal consistent with the presence of Mn(II) was observed (Figure 1.6, right), the spin state of the metal center and its hyperfine coupling interaction could not be determined by simple inspection of the spectrum. To obtain the EPR parameters, the

respective spin Hamiltonian was fit to the data (Figure 1.6, right, dashed line). The spectral features observed for **2** were well-fit (σ = 1.7%) considering a low-spin ^{55}Mn center (S = 1/2, I = 5/2) with anisotropic g values (g_X = 2.079, g_y = 2.037, g_z = 2.017) and large anisotropic hyperfine couplings ($|A_X|$ = 161.2, $|A_y|$ = 375.4, $|A_z|$ = 164.8 MHz). Both properties are consistent with the crystallographically determined coordination environment about the Mn in **2** and are characteristic of a low spin Mn(II) complex.[17]

1.4.3. Synthesis of 2-H:

After isolating and characterizing the formal Mn(0) complex, preparation of a dihydride complex was attempted starting from the dichloride complexes. Treating **2-Cl$_2$** with two equivalents of NaEt$_3$BH in toluene afforded a green diamagnetic solid after workup and drying, which was identified as (^{Ph2PPr}PDI)MnH **(2-H)** (Scheme 1.5). ^{1}H NMR spectra of this complex showed a triplet at -2.98 ppm (J_{P-H} = 111.74 Hz) (Figure 1.7) split by two phosphines, which turned into a singlet peak after ^{31}P decoupling and hence bolsters the presence of the hydride. ^{31}P NMR of **2-H** displayed a single resonance at 69.60 ppm suggesting top-bottom equivalence of the PDI chelate (Scheme 1.5). Layering a toluene solution of **2-H** with diethyl ether and cooling at -35 °C yielded dark greenish-brown crystals.
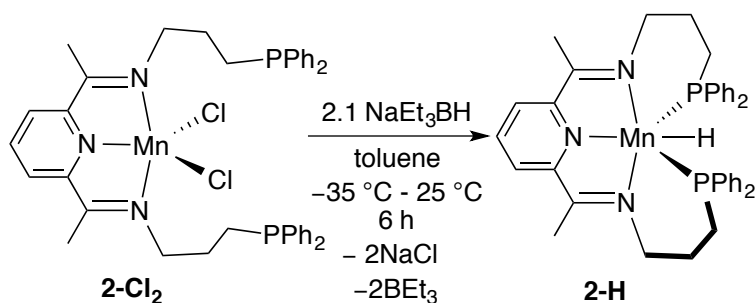
Scheme 1.5. Synthesis of **2-H** from **2-Cl$_2$**.
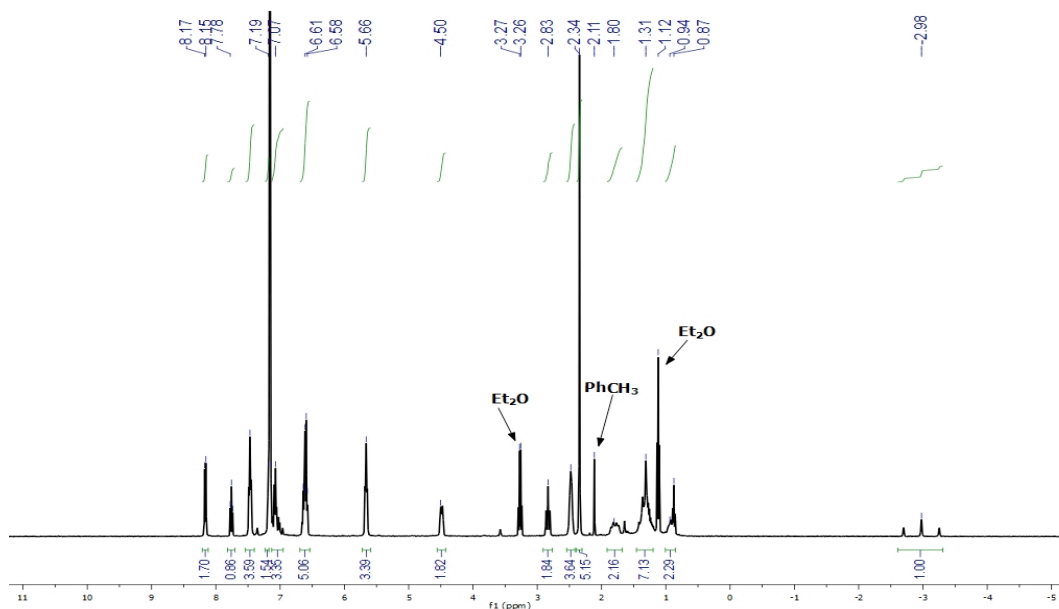
Figure 1.7. ^{1}H NMR spectrum of **2-H** in benzene-d_6.

The crystal structure of **2-H** (Figure 1.8) confirmed the presence of hydride with a Mn(1)-H(1) bond distance of 1.57(3) Å, which is within the range of the sum of covalent radii of a low spin Mn and H.[15] The average Mn(1)-N distances and Mn(1)-P distances are very similar to those of **2**, which further supports the assumption of low spin Mn(II) center.[15] While the C(2)-N(1) and C(8)-N(3) bonds are elongated to 1.351(3) and 1.342(3) Å, the C(2)-C(3) and C(7)-C(8) bonds are contracted to 1.424(4) and 1.418(3) Å, which is very similar to the values obtained for **2**. It was also found that **2-H** possesses a distorted trigonal bipyramidal geometry about Mn center with N(1)-Mn(1)-N(3), N(2)-Mn(1)-P(1), and P(1)-Mn(1)-P(2) angles of 158.81(9)°, 114.01(6)°, and 123.85(3)° respectively, despite the fact that **2-H** is a six coordinated complex. Presumably, this is a consequence of significantly large energy gap between hydride based atomic orbitals and the metal based orbitals, which results in a reasonably weak overlap to fully destabilize the e_g set (x^2-y^2 and z^2) to attain an octahedral geometry. However, the x^2-y^2 orbital

14

(Figure 1.9 right) is slightly destabilized by the Mn-H bond while the xy orbital remains singly occupied. Comparing the metrical parameters to **2** it can be inferred that **2-H** features a low spin Mn(III) center that is antiferromagnetically coupled to a doubly reduced PDI^{2-} chelate (Figure 1.9, right).
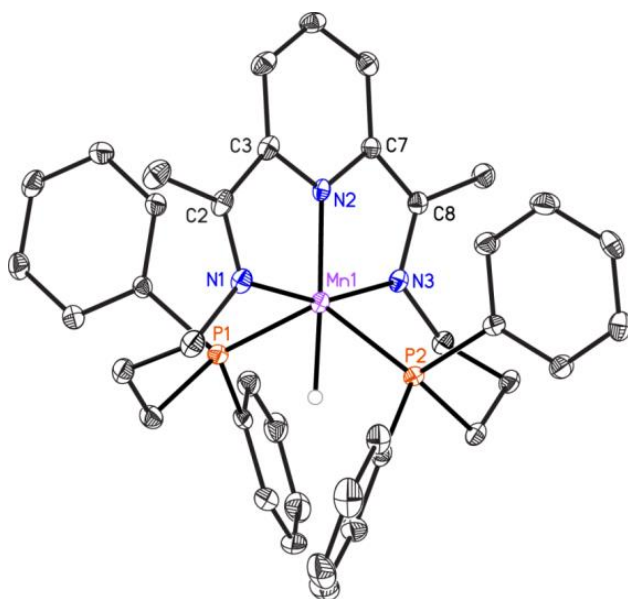
Figure 1.8. Solid-state structure of **2-H** shown at 30% probability ellipsoid. Hydrogen atoms and co-crystallized solvent molecules are omitted for clarity.

Table 1.4. Relevant bond lengths (Å) and angles (°) for **2-H**.

Mn(1)-N(1)	2.1123(18)	C(3)-N(2)	1.347(3)
Mn(1)-N(2)	2.158(3)	C(6)-N(1)	1.444(3)
Mn(1)-N(3)	2.2178(17)	N(1)-Mn(1)-N(1A)	148.67(10)
C(2)-N(1)	1.369(3)	N(2)-Mn(1)-N(3)	126.59(5)
C(2)-C(1)	1.363(3)	N(1)-Mn(1)-N(3)	86.38(7)
C(2)-C(3)	1.491(3)	N(1)-Mn(1)-N(2)	74.33(5)

Similar attempts to prepare a hydride complex from **1-Cl₂** have remained unsuccessful as under the reaction conditions ^{PyEt}PDI has been found to disintegrate to produce an intractable mixture, which supports the advantage of using phosphine containing PDI ligands.
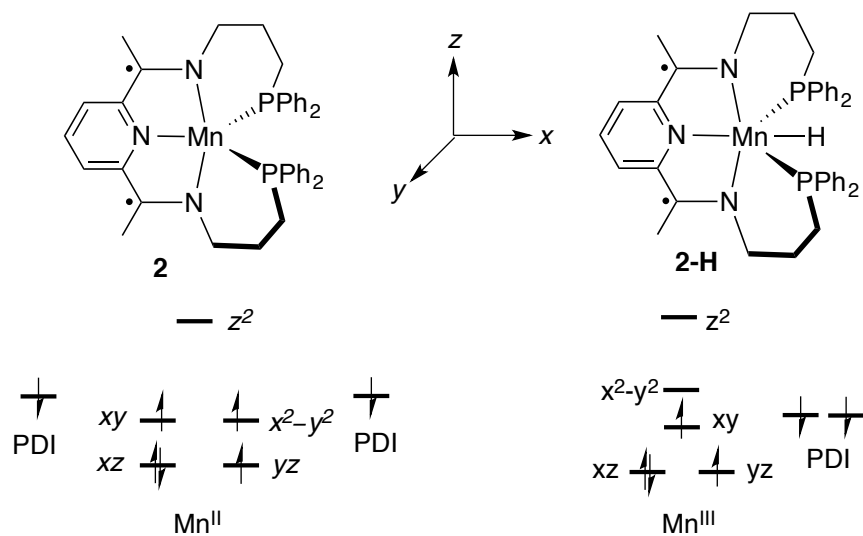
Figure 1.9. Qualitative *d*-orbital splitting of **2** (left) and **2-H** (right) shown with antiferromagnetically coupled PDI^{2-} chelate.

1.4.4. Reduction of 3-Cl$_2$:

Similarly, reduction of **3-Cl$_2$** using excess Na-Hg and catalytic COT afforded a red paramagnetic complex, which was identified as **3** (Scheme 1.6) identified as [(^{Ph2PEt}PDI)Mn]$_2$. The ^{1}H NMR spectrum obtained for this complex showed highly shifted broad resonances over a range of 300 ppm. A single broad resonance was observed in the ^{31}P NMR spectrum at -58.42 ppm (Figure 1.10) for the uncoordinated phosphine arm. Solution state magnetic moment was found to be 3.3 μ_B at 298 K indicative of two unpaired electrons in the ground state.

Crystals for **3** were grown from a concentrated toluene solution layered with diethylether. Single crystal X-ray diffraction of complex **3** confirmed the dimeric structure containing a κ^4-PDI chelate (Figure 1.11). Each metal center has distorted trigonal bipyramidal geometry with N(1)-Mn(1)-N(3), N(2)-Mn(1)-P(1), and N(2)-Mn(1)-C(8A) angles of 150.9, 129.2, and 137.5° respectively. Interestingly, it was found

16

that the Mn center from one (PDI)Mn moiety is coordinated to the imine bond of the neighboring (PDI)Mn moiety in an η^2-fashion with Mn(1)-C(8A) and Mn(1)-N(3A) distances of 2.233(3) and 1.977(3) Å respectively. As a consequence, the C(8)-N(3) and C(8A)-N(3A) bonds are unusually elongated to 1.395(3) Å compared to the uncoordinated side of PDI. The uncoordinated imine bond C(2)-N(1) is stretched to 1.338(4) Å from the standard C=N distances of 1.28 Å.[11]
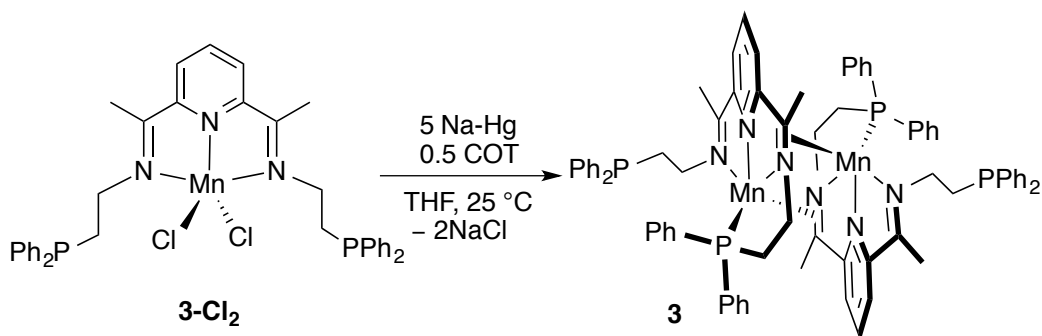
Scheme 1.6. Synthesis of **3** from the reduction of **3-Cl₂**.
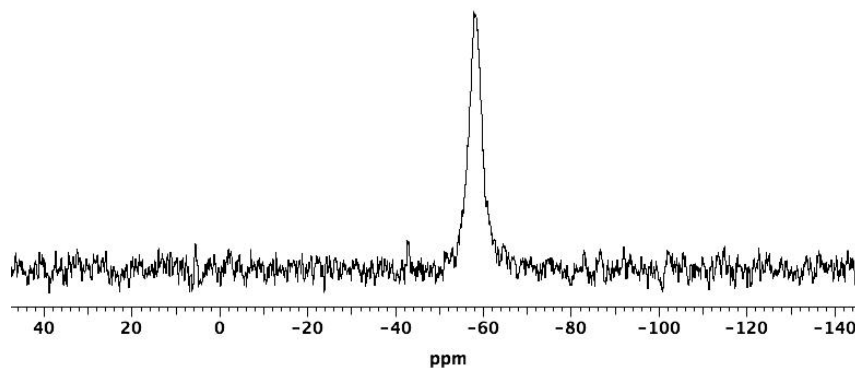
Figure 1.10. ^{31}P NMR spectrum of **3** in benzene-d_6.

The Mn(1)-N(1), Mn(1)-N(2), and Mn(1)-N(3) distances are 2.022(3), 1.947(3), and 2.091(3) Å, which indicates a low spin manganese center.[15] Also, the two Mn centers

are 2.789(4) Å apart, which is exactly the sum of the covalent radii of two Mn atoms when they are low spin. Considering these crucial metrical parameters, NMR and the effective magnetic moment, it can be proposed that **3** features two low spin Mn(I) centers with each metal antiferromagnetically coupled to a singly reduced pseudo diimine fragment (N1-C2-C3-N2, Figure 1.12, right), along with significant metal to ligand backbonding to the coordinated imine bonds C(8)-N(3) and C(8A)-N(3A) in a Dewar-Chatt extreme (Figure 1.12, right). Two antiferromagnetic coupling results in one unpaired electrons on each Mn giving rise to a observed magnetic moment of 3.3 μ_B. Having this reduced dimer isolated, $NaEt_3BH$ was added to **3-Cl$_2$** in order to isolate a hydride complex, but rather ligand disintegration was observed, which is very likely due to instability imparted by a κ^4 coordination mode of this ethyl bridged PDI ligand.
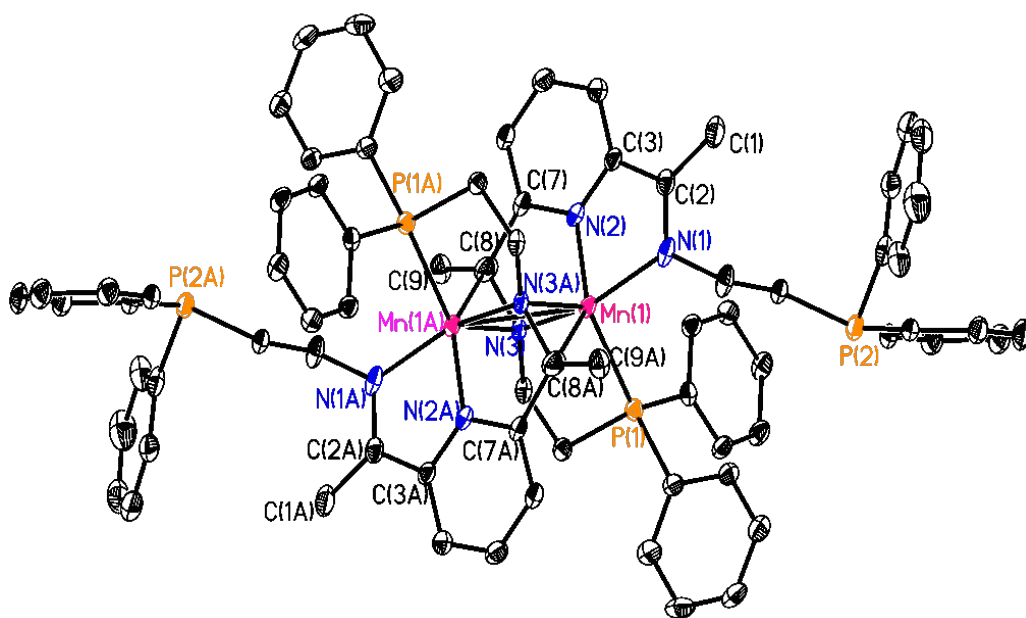
Figure 1.11. **S**olid-state structure of **3** shown at 30% probability ellipsoid. Hydrogen atoms and co-crystallized solvent molecules are not shown for clarity.

18

Table 1.5. Relevant bond lengths (Å) and angles (°) for **3**.

Mn(1)-N(1)	2.022(4)	C(8)-N(3)	1.395(6)
Mn(1)-N(2)	1.947(4)	C(7)-C(8)	1.462(7)
Mn(1)-N(3)	2.092(4)	N(2)-Mn(1)-P(1)	129.25(12)
Mn(1)-N(3A)	1.977(4)	N(2)-Mn(1)-N(3)	100.30(15)
Mn(1)-C(8A)	2.233(6)	N(1)-Mn(1)-N(3)	150.85(16)
Mn(1)-P(1)	2.3525(15)	N(2)-Mn(1)-C(8A)	102.86(18)
Mn(1)-Mn(1A)	2.7889(14)	N(2)-Mn(1)-N(1)	77.00(16)
C(2)-N(1)	1.338(6)	N(1)-Mn(1)-P(1)	103.71(12)
C(2)-C(3)	1.425(7)		

Electron paramagnetic resonance spectrum of **3** was collected (Figure 1.12) in a toluene glass at 107 K to gain more insight into the electronic structure of **3**. A complicated multiline pattern was obtained that is consistent with a $S = 1/2$ Mn center and the observed hyperfine splitting are due to the coupling of Mn nuclear spin ($I = 5/2$). Although, theoretically a 10-line spectrum is expected with this hypothesis, the anisotropy present in the structure of **3** results a more complicated pattern.
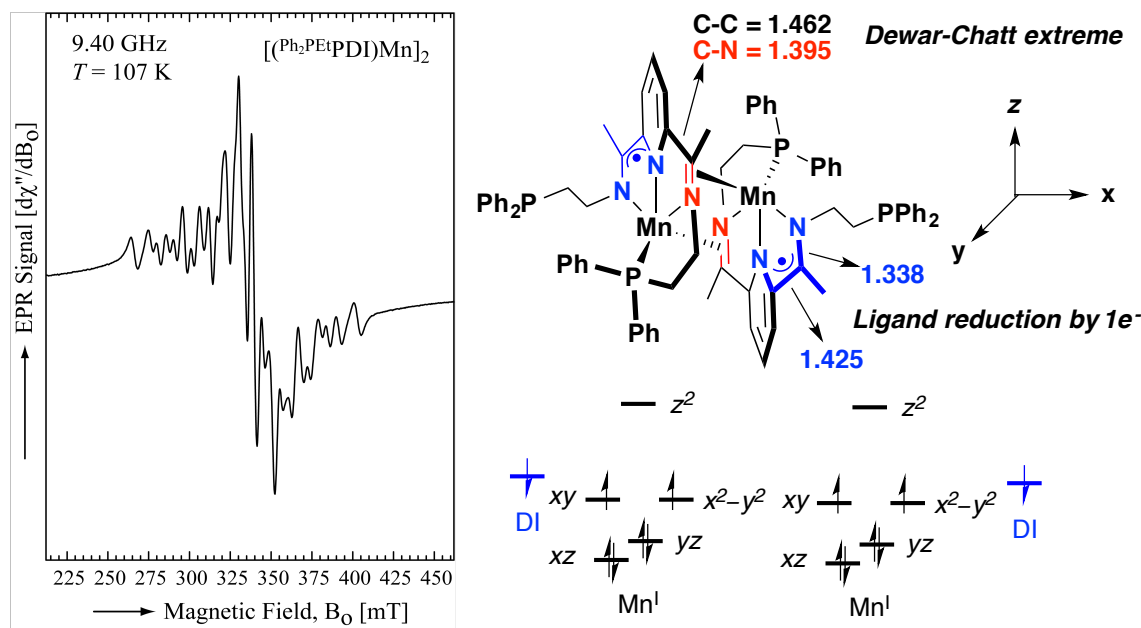
Figure 1.12. The X-band EPR spectrum of **3** (left). Qualitative *d*-orbital splitting of **3** with a model of the primary coordination sphere (right).

19

1.4.5. Reduction of (^{R2N}PDI)MnCl$_2$:

When the amine containing PDI supported dichloride precursors **4-Cl$_2$** and **5-Cl$_2$** were reduced under identical conditions, chelate decomposition has been observed. Also, attempts to prepare corresponding hydride complexes by adding NaEt$_3$BH separately led to chelate dissociation. These results prove the ^{R2N}PDI ligands to be highly labile under reducing conditions and these ligands may not be used to stabilize low oxidation states of manganese.

1.5. Concluding remarks:

In summary, a series of low valent Mn complexes have been successfully isolated and characterized using a combination of spectroscopy, magnetometry, EPR, X-ray crystallography, and DFT calculations. Unlike the tethered phosphine co-donors, amine containing PDI ligands have been found to be difficult to handle under reducing conditions. Presumably, it can be inferred that the π-accepting ability of the phosphine co-donors aid to the stabilization of the reduced Mn complexes. Moreover, it has also been noted that manipulation of the co-ligand imine arms and the terminal donor atom has a direct influence on the electronic behavior and stability of these complexes, which shows promising correlation to our initial proposition on ligand design. This observation is crucial for investigating the reactivity of these complexes.

1.6. Experimental Procedures:

General Considerations. All synthetic reactions were performed in an MBraun glovebox under an atmosphere of purified nitrogen. Aldrich or Acros anhydrous solvents were purified using a Pure Process Technology solvent system and stored in the glovebox over activated 4Å molecular sieves and sodium before use. Benzene-d_6 and chloroform-d were purchased from Cambridge Isotope Laboratories and dried over 4Å molecular sieves before use. $(THF)_2MnCl_2$ was purchased from Acros. 3-(diphenylphosphino)-1-propylamine and 2-(diphenylphosphino)-1-ethylamine was used as received from Strem. 1,3,5,7-Cyclooctatetraene and mercury were used as received from Sigma-Aldrich. ^{Ph_2PPr}PDI, ^{PyEt}PDI, ^{iPr2NEt}PDI, ^{Me2NPr}PDI, and ^{Ph2PEt}PDI were prepared according to the reported procedure.[10]

Solution ^{1}H nuclear magnetic resonance (NMR) spectra were recorded at room temperature on a Varian 400-MR 400 MHz NMR spectrometer. All ^{1}H and ^{13}C NMR chemical shifts (ppm) are reported relative to $Si(CH_3)_4$ using ^{1}H (residual) and ^{13}C chemical shifts of the solvent as secondary standards. ^{31}P NMR data is reported relative to H_3PO_4. Elemental analyses were performed at Robertson Microlit Laboratories Inc. (Ledgewood, NJ) and the Arizona State University CLAS Goldwater Environmental Laboratory (Tempe, AZ). Solid state magnetic susceptibilities were determined at 23 °C using a Johnson Matthey magnetic susceptibility balance calibrated with $HgCo(SCN)_4$ and $K_3Fe(CN)_6$. Solution state magnetic susceptibility was determined from Evans method using Varian 400 MHz NMR spectrometer.

X-ray Crystallography. Diffraction data were collected and analyzed by Dr. Thomas L. Groy at Arizona State University. Single crystals suitable for X-ray diffraction were

coated with polyisobutylene oil in the glovebox and transferred to glass fiber with Apiezon N grease, which was then mounted on the goniometer head of a Bruker APEX Diffractometer equipped with Mo K$_\alpha$ radiation. A hemisphere routine was used for data collection and determination of the lattice constants. The space group was identified and the data was processed using the Bruker SAINT+ program and corrected for absorption using SADABS. The structures were solved using direct methods (SHELXS) completed by subsequent Fourier synthesis and refined by full-matrix, least-squares procedures on [F^2] (SHELXL). The solid-state structure of (^{Ph_2,PPr}PDI)MnCl$_2$ was found to possess a disordered THF molecule near an inversion center that was successfully modeled in three orientations.

Electron Paramagnetic Resonance Spectroscopy.

Studies were performed at the EPR Facility of Arizona State University. Continuous wave EPR spectra were recorded at 77 K using a Bruker ELEXSYS E580 continuous wave X-band spectrometer (Bruker, Rheinstetten, Germany) equipped with an Oxford Model ESR900 liquid helium cryostat (Oxford Instruments, Oxfordshire, UK). The magnetic field modulation frequency was 100 kHz with a field modulation of 1 mT peak-to-peak. The microwave power was 0.25 mW, the microwave frequency was 9.44 GHz and the sweep time was 84 seconds.

Preparation of ^{PyEt}PDIMnCl$_2$ (1-Cl$_2$): A 100 mL thick-walled glass bomb was charged with 0.275 g (1.018 mmol) of (THF)$_2$MnCl$_2$, 0.728 g (1.962 mmol) of ^{PyEt}PDI, and approximately 20 mL of toluene under an inert atmosphere. The bomb was then sealed under N$_2$, taken out of the glovebox, and heated to 125 °C in an oil bath for 48 h while its contents were being stirred. Upon cooling, the reaction vessel was brought back into the

glovebox; the resulting light orange solid was collected by vacuum filtering the solution, ollowed by washinf with toluene (4 × 5 mL) and diethyl ether (3 × 5 mL) to remove the excess ligand. The solid material was then dried under vacuum to afford 0.473 g of 1 (93% yield) as a light orange solid. Single crystals suitable for X- ray diffraction were obtained following recrystallization from dichloromethane. Analysis for $C_{23}H_{25}N_5MnCl_2$: Calcd. C, 55.55%; H, 5.07%; N, 14.08%. Found: C, 55.27%; H, 4.90%; N, 13.79%. Magnetic susceptibility (Guoy balance, 23 °C): μ_{eff} = 6.3 μ_B. ^{1}H NMR spectroscopy (benzene-d_6, 23 °C): δ 62.76 (peak width at half-height of 9830 Hz), 13.51 (2020 Hz), −31.63 (3000 Hz). UV−vis (from five independent concentrations in chloroform): λ_{max} = 306 (ε = 3844 M^{-1} cm^{-1}), 318 nm (ε = 2601 $M^{-1}cm^{-1}$).

Preparation of ^{Ph_2PPr}PDIMnCl$_2$ (2-Cl$_2$): Under an inert atmosphere, a thick-walled glass bomb was charged with 0.199 g (0.737 mmol) of (THF)$_2$MnCl$_2$, 0.452 g (0.737 mmol) of ^{Ph_2PPr}PDI, and approximately 30 mL of toluene. The bomb was then sealed and brought out of the glove box. The mixture was heated at 90 °C in an oil bath for 48 h. The resulting light orange precipitate was collected by vacuum filtering the solution, followed by washing with toluene and diethyl ether. Finally, it was dried under vacuum to isolate 0.509 g (0.689 mmol, 93% yield) of **1** as a light orange solid. Analysis for $C_{39}H_{41}N_3Cl_2MnP_2$: Calcd. C, 63.34%; H, 5.59%; N, 5.68%. Found: C, 62.97%; H, 5.66%; N, 5.41%. Magnetic susceptibility (Guoy balance, 23 °C) μ_{eff} = 6.0 μ_B. ^{1}H NMR (chloroform-d, 23 °C): 70.31 (9210 Hz), 7.34 (265 Hz), −37.59 (2872 Hz).

Preparation of ^{Ph2PEt}PDIMnCl$_2$ (3-Cl$_2$): A thick walled glass tube was charged with 0.390 g of ^{Ph2PEt}PDI (0.665 mmol), and 0.180 g of (THF)$_2$MnCl$_2$ (0.665 mmol) in approximately 20 mL toluene. The tube was sealed under N$_2$ and heated at 90 °C for 72

hours. The resulting pale orange solid was collected by vacuum filtering the solution and the solid was washed with toluene (4x5 mL) and diethylether (3x5 mL) to remove any excess of ligand. Finally, it was dried to isolate 0.433 g of pale orange solid. Magnetic moment (Guoy's balance) $\mu_{eff} = 6.0 \mu_B$.

Preparation of ^{Me2NPr}PDIMnCl$_2$ (4-Cl$_2$): Under an inert atmosphere, a thick-walled glass bomb was charged with 0.296 (2.354 mmol) of MnCl$_2$, 0.779 g (0.2.354 mmol) of ^{Me2NPr}PDI, and approximately 25 mL of toluene. The bomb was sealed under N$_2$ and heated at 90 °C for 72 h. The resulting precipitate was collected by vacuum filtering the solution and the faint yellow solid was washed several times with Et$_2$O. Finally dried to isolate 0.850 g (1.860 mmol, 78% yield) faint yellow solid identified as (^{Me2NPr}PDI)MnCl$_2$. Magnetic susceptibility (Evans method, 23 °C): $\mu_{eff} = 6.0 \mu_B$. Analysis for C$_{19}$H$_{33}$N$_5$MnCl$_2$: Calcd. C, 49.89%; H, 7.27%; N, 15.31%. Found: C, 49.55%; H, 7.02%; N, 14.83%.

Preparation of ^{iPr2NEt}PDIMnCl$_2$ (5-Cl$_2$): Under an inert atmosphere, a thick-walled glass bomb was charged with 0.1004 (0.798 mmol) of MnCl$_2$, 0.331 g (0.798 mmol) of ^{iPr2NEt}PDI, and approximately 25 mL of THF. The bomb was sealed under N$_2$ and heated at 90 °C for 24 h. The resulting precipitate was collected by vacuum filtering the solution and the faint yellow solid was washed several times with Et$_2$O. Finally dried to isolate 0.323 g (0.597 mmol, 75% yield) faint yellow solid identified as (^{Me2NEt}PDI)MnCl$_2$. Magnetic susceptibility (Evans method, 23 °C): $\mu_{eff} = 6.2 \mu_B$.

Preparation of (^{PyEt}PDEA)Mn (1): In the glovebox, a 20 mL scintillation vial was charged with 8.12 g (40.62 mmol) of Hg^0 in approximately 6 mL of dry THF. To this was added 0.047 g (2.030 mmol) of freshly cut Na^0, and the resulting amalgam was stirred for

25 min. After this, 0.017 g (0.162 mmol) of 1,3,5,7-cyclooctatetraene was added and the mixture stirred for 5 min while it turned yellow in color. Then a 10 mL THF slurry of **1-Cl$_2$** (0.202 g, 0.406 mmol) was added. An instant color change to a greenish-brown solution was observed. The reaction mixture was stirred at ambient temperature for 12 h, after which time it was filtered through Celite under vacuum and the THF was evacuated. The resulting residue was washed with pentane (2 × 5 mL) and dried. The residue was dissolved in toluene (15 mL) and filtered through a Celite column. This was repeated once again, and the filtrate was dried under vacuum to afford **1** (0.084 g, 49% yield). Single crystals suitable for X-ray diffraction were grown from a concentrated toluene solution layered with diethyl ether (1:1). Analysis for C$_{23}$H$_{23}$N$_5$Mn.C$_7$H$_8$: Calcd. C, 69.76%; H, 6.05%; N, 13.56%. Found: C, 68.39%; H, 5.78%; N, 13.10%. Complex **1** quickly decomposes in the presence of air or water. Magnetic susceptibility (Evans method, 23 °C): μ_{eff} = 3.8 μ_B. ^{1}H NMR spectroscopy (benzene-d_6, 23 °C): δ 52.85 (7320 Hz), 33.10 (31850 Hz), −8.08 (16000 Hz, shoulder), −48.20 (3600 Hz). UV−vis: 428 (ε = 2528 M^{-1} cm^{-1}), 512 (ε = 524 M^{-1} cm^{-1}), 624 nm (ε from five independent concentrations in toluene): λ_{max} = 348 (ε = 5066 M = 504 M^{-1} cm^{-1}).

Preparation of (^{Ph_2PPr}PDI)Mn (2): Under an inert atmosphere, a 20 mL scintillation vial was charged with 4.33 g (21.66 mmol) of mercury, 0.025 g (1.083 mmol) of sodium, and approximately 4 mL of tetrahydrofuran. The mixture was stirred at ambient temperature for 20 minutes, after which time 0.011 g (0.108 mmol) of cyclooctatetraene was added. A slurry of **2-Cl$_2$** (0.160 g, 0.216 mmol) and approximately 10 mL of tetrahydrofuran was then added to the vial. After stirring at ambient temperature for 15 h, the resulting deep brown solution was filtered through a Celite pad and the solvent was evacuated to obtain

a brown solid. This solid was scraped off the sides of the flask in the presence of pentane (2 x 10 mL) and dried again to remove any residual solvent. The solid was dissolved in 15 mL toluene and filtered through a Celite column to ensure NaCl removal. After evacuating the toluene, the resulting solid was crystallized from diethyl ether to yield 0.068 g (47%) of dark brown crystals identified as **2**. Analysis for $C_{39}H_{41}N_3MnP_2$: Calcd. C, 70.05%; H, 6.18%; N, 6.28%. Found: C, 69.75%; H, 5.96%; N, 5.99%. Magnetic susceptibility (Evans method, 23 °C) μ_{eff} = 2.2 μ_B. ^{1}H NMR (benzene-d_6, 23 °C): δ 96.28 (2265 Hz), 68.38 (2176 Hz), 28.59 (2176 Hz), 18.77 (55.3 Hz), 8.15 (30.7 Hz), 6.90 (16.6 Hz), 6.68 (16.6 Hz), 4.56 (45.4 Hz), −7.79 (1014 Hz), −95.61 (3502 Hz).

Preparation of (^{Ph_2PPr}PDI)MnH (2-H): Under N_2 atmosphere, a 250 mL round bottom flask was charged with 0.344 g (0.466 mmol) of **2-Cl₂** in approximately 80 mL of toluene. The slurry was cooled in a cold well (liquid N_2 temperature) for 30 min. A 20 mL scintillation vial was charged with 0.114 mg (0.932 mmol) of $NaEt_3BH$ (1 M in toluene) in approximately 10 mL of toluene and it was also cooled for 30 min. Then the $NaEt_3BH$ solution was added to the slurry of **2-Cl₂** slowly at cold condition while it was stirred. The flask was then allowed to stir at room temperature. A deep brownish-green color was noticed after 20 min, which darkened over time. After 6 h the brownish-green solution was filtered through Celite and the toluene was evacuated to obtain a dark solid. The solid was washed with pentane (4 x 5 mL) and dried again. It was washed quickly with 10 mL of ether (2 x 5 mL) to remove any free ligand generated in the reaction and dissolved in 15 mL of toluene. The toluene solution was filtered throught Celite and solvent was removed *in vacuo*. The residue was dissolved in minimum diethyl ether and placed at −35 °C for overnight. Dark green crystals (125 mg, 0.187 mmol) were collected

after drying and identified as [Ph2PPr]**PDIMnH**. ^{1}H NMR 500 MHz (benzene-d_6), δ (ppm) = 8.17 (d, J_{H-H} = 8.1 Hz, 2H, *pyridine*), 7.76 (t, J_{H-H} = 8.1 Hz, 1H, *pyridine*), 7.47 (t, J_{H-H} = 8.1 Hz, 4H, *phenyl*), 7.09 (m, 4H, *phenyl*), 6.61 (m, 6H, *phenyl*), 5.66 (t, J_{H-H} = 8.1 Hz, 4H, *phenyl*), 4.50 (d, J_{H-H} = 11.4 Hz, 2H, *phenyl*), 2.83 (t, J_{H-H} = 11.2 Hz, 2H, -CH_2), 2.48 (broad m, 4H, -CH_2), 2.34 (s, 6H, 2CH_3), 1.78 (broad m, 2H, -CH_2), 1.36 (broad m, 2H, -CH_2), 1.26 (broad m, 2H, -CH_2), −2.98 (t, J_{P-H} = 112.4 Hz, 1H, Mn-*H*). ^{13}C NMR 500 MHz (benzene-d_6) δ (ppm) = 231.5, 189.9, 170.8, 154.6, 151.5, 133.6, 133.5, 133.3, 129.9, 129.7, 128.0, 120.9, 115.5, 110.4, 75.2, 74.9, 57.5, 29.9, 14.6. ^{31}P{^{1}H} NMR (benzene-d_6) δ (ppm) = 69.60 (s).

Preparation of [([Ph2PEt]PDI)Mn]$_2$ (3): A 20 mL scintillation vial was charged with 5.53 g of Hg[0] in 5 mL THF and 0.032 g of freshly cut Na[0] was added to it. The amalgam was stirred for 25 minutes while it became clear. Then 0.012 g (0.110 mmol) of 1,3,5,7-cyclooctatetraene was added and stirred for 5 minutes while it turned pale yellow. Then a 10 mL THF slurry of **3-Cl$_2$** was added and an instantaneous color change to red was noticed. The mixture was stirred at room temperature for 8 hours. The red solution was then filtered through Celite and THF was removed *in vacuo*. The resulting red film was washed with pentane (2 x 5 mL) and dried again. Then it was dissolved in 10 mL toluene and filtered through a Celite column. The filtrate was concentrated and layered with diethyl ether and placed at −35 °C for crystallization. 0.087g red crystals were isolated after removing the mother liquor and drying. ^{1}H NMR (benzene-d_6), δ (ppm): 88.98 (50.19 Hz), 32.41 (1316 Hz), 26.22 (195.08 Hz), -134.78 (174.87 Hz), -172.83 (14.86 Hz). {^{1}H}^{31}P NMR δ (ppm): 58.42 (486.83 Hz). Magnetic moment (Evans method): μ_{eff}

= 3.3 μ_B. Elemental analysis for $C_{74}H_{74}N_6P_4Mn_2$: calcd. C, 69.37%; H, 5.82%; N, 6.56%;

Found C, 69.36%; H, 6.35%; N, 6.21%.

1.7. References:

1. Role of homogeneous precious metal catalysts: (a) Chirik, P. J.; Wieghardt, K. *Science.* **2010**, *327*, 794-795. (b) Osborn, J. A.; Jardine, F. H.; Young, J. F.; Wilkinson, G. *J. Chem. Soc. A* **1966**, 1711-1732. (c) Yi, C. S.; Lee, D. W. *Organometallics* **1999**, *18*, 5152-5156. (d) Speier, J. L.; Webster, J. A.; Barnes, G. H. *J. Am. Chem. Soc.* **1957**, *79*, 974−979. (e) Troegel, D.; Stohrer, J. *Coord. Chem. Rev.* **2011**, *255*, 1440−1459. (f) Vougioukalakis, G. C.; Grubbs, R. H. *Chem. Rev.* **2010**, *110*, 1746-1787. (g) Nicolaou, K. C.; Bulger, P. G.; Sarlah, D. *Angew. Chem. Int. Ed.* **2005**, *44*, 4442-4489. (h) Beletskaya, I. P.; Cheprakov, A. V.; *Chem. Rev.* **2000**, *100*, 3009-3066.

2. (a) Junge, K.; Schröder, K.; Beller, M. *Chem. Commun.* **2011**, *47*, 4849−4859. (b) Le Bailly, B. A. F.; Thomas, S. P. *RSC Adv.* **2011**, *1*, 1435. (c) Bullock, R. M. *Catalysis without Precious Metals*; Wiley-VCH: Weinheim, Germany, **2010**. (d) Gosmini, C.; Beǵouin, J.-M.; Moncomble, A. *Chem. Commun.* **2008**, 3221−3233. (e) Gaillard, S.; Renaud, J.-L. *ChemSusChem* **2008**, *1*, 505−509. (f) Enthaler, S.; Junge, K.; Beller, M. *Angew. Chem. Int. Ed.* **2008**, *47*, 3317.

3. (a) Luca O. R.; Crabtree, R. H. *Chem. Soc. Rev.* **2013**, *42*, 1440-1459. (b) Chirik P. J.; Wieghardt, K. *Science* **2010**, *327*, 794-795.

4. (a) Stubbert, B. D.; Peters, J. C.; Gray, H. B. *J. Am. Chem. Soc.*, **2011**, *133*, 18070. (b) Luca, O. R.; Konezny, S. J.; Blakemore, J. D.; Saha, S.; Colosi, D. M.; Brudvig, G. W.; Batista, V. S.; Crabtree, R. H. *New J. Chem.*, **2012**, *36*, 1149. (c) Chaudhuri, P.; Hess, M.; Müller, J.; Hildenbrand, K.; Bill, E.; Weyhermüller, T.; Wieghardt, K. *J. Am. Chem. Soc.* **1999**, *121*, 9599.

5. Gibson, V. C.; Redshaw, C.; Solan, G. A. *Chem. Rev.* **2007**, *107*, 1745-1776.

6. (a) Small, B. L.; Brookhart, M.; Bennett, A. M. A. *J. Am. Chem. Soc.* **1998**, *120*, 4049-4050. (b) Britovsek, G. J. P.; Gibson, V. C.; Kimberley, B. S.; Maddox, P. J.; McTavish, S. J.; Solan, G. A.; White, A. J. P.; Williams, D. J. *Chem. Commun.* **1998**, 849-850.

7. (a) Bart, S. C.; Lobkovsky, E.; Bill, E.; Chirik, P. J. *J. Am. Chem. Soc.* **2004**, *126*, 13794-13807. (b) Trovitch, R. J.; Lobkovsky, E.; Bill, E.; Chirik, P. J. *Organometallics* **2008**, *27*, 1470. (c) Sylvester, K. T.; Chirik, P. J. *J. Am. Chem. Soc.* **2009**, *131*, 8772-8774. (d) Hoyt, J. M.; Schmidt, V. A.; Tondreau, A. M.; Chirik, P. J. *Science,* **2015**, *349*, 960-963.

8. (a) de Bruin, B.; Bill, E.; Bothe, E.; Weyhermüller, T.; Wieghardt, K. *Inorg. Chem.*

2000, *39*, 2936-2947. (b) Knijnenburg, Q.; Gambarotta, S.; Budzelaar, P. H. M. *Dalton Trans.* **2006**, 5442-5448.

9. (a) Jørgensen, C. K. *Coord. Chem. Rev.*, **1966**, *1*, 164.   (b) Baker-Hawkes, M. J.; Billig, E.; Gray, H. B. *J. Am. Chem. Soc.*, **1966**, *88*, 4870-4875.
10. (a) Ben-Daat, H.; Hall, G. B.; Groy, T. L.; Trovitch, R. J. *Eur. J. Inorg. Chem.* **2013**, 4430−4442. (b) Pal, R.; Groy, T. L.; Bowman, A. C.; Trovitch, R. J. *Inorg. Chem.* **2014**, *53*, 9357-9365.

11. (a) Knijnenburg, Q.; Gambarotta, S.; Budzelaar, P. H. M. *Dalton Trans.* **2006**, 5442-5448. (b) Chirik, P. J.; Wieghardt, K. *Science* **2010**, *327*, 794-795.

12. (a) Valyaev, D. A.; Lavigne, G.; Lugan, N. *Coord. Chem. Rev.* **2016**, *308*, 191-235.
(b) Trovitch, R. J. *Synlett* **2014**, *25*, 1638−1642.

13. (a) Zhang, W.; Loebach, J. L.; Wilson, S. R.; Jacobsen, E. N. *J. Am. Chem. Soc.* **1990**, *112*, 2801-2803. (b) Cavanaugh, M. D.; Gregg, B. T.; Cutler, A. R. *Organometallics* **1996**, *15*, 2764-2769. (c) Sampson, M. D.; Nguyen, A. D.; Grice, K. A.; Moore, C. E.; Rheingold, A. L.; Kubiak, C. P. *J. Am. Chem. Soc.* **2014**, *136*, 5460-5471.

14. Reardon, D.; Aharonian, G.; Gambarotta, S.; Yap, G. P. A. *Organometallics* **2002**, *21*, 786-788.

15. B. Cordero, V. Gómez, A. E. Platero-Prats, M. Revés, J. Echeverría, E. Cremades, F. Barragán, S. Alvarez, *Dalton Trans.* **2008**, 2832-2838.

16. Russell, S. K.; Bowman, A. C.; Lobkovsky, E.; Wieghardt, K.; Chirik, P. J. Eur. J. *Inorg*. *Chem*. **2012**, *2012*, 535−545.

17. (a) Weil, J. A.; Bolton, J. R. Electron paramagnetic resonance: Elementary theory and practical applications; Wiley: Hoboken, NJ, **2007**. (b) Rieger, P. H. *Coord. Chem. Rev.* **1994**, *135/136*, 203−286.

CHAPTER 2

BIS(IMINO)PYRIDINE SUPPORTED MANGANESE COMPLEXES AS EFFICIENT

CATALYSTS FOR CARBONYL AND ESTER HYDROSILYLATION

2.1. Abstract:

Bis(imino)pyridine supported low-valent manganese complexes, (^{Ph2PPr}PDI)Mn, (^{Ph2PPr}PDI)MnH, (^{PyEt}PDEA)Mn, and [(^{Ph2PEt}PDI)Mn]$_2$ were found to be highly active precatalysts for the hydrosilylation of ketones, aldehydes, acetates, and formates. Ketones were efficiently hydrosilylated to silyl ethers using (^{Ph2PPr}PDI)Mn in presence of PhSiH$_3$ with a maximum turnover frequency (TOF) of up to 1280 min^{-1}. Acetates were also converted to a mixture of silyl ethers with modest rate. A TOF of up to 990 min^{-1} for ketone hydrosilylation and 2475 min^{-1} for aldehyde hydrosilylation was achieved using (^{PyEt}PDEA)Mn as a catalyst under neat conditions. When aldehydes were assayed using (^{Ph2PPr}PDI)Mn or [(^{Ph2PEt}PDI)Mn]$_2$, the highest TOFs of up to 4950 min^{-1} were obtained under solvent free conditions. Fourteen different aldehydes containing varying functional groups were hydrosilylated in an efficient manner and subsequent hydrolysis of the silyl ethers with aq. NaOH solution afforded the corresponding alcohol with high purity and decent yield. It has also been found that the catalysts can tolerate a wide range of functionalities including halides, nitriles, olefins, ethers, and heterocylces. Furthermore, (^{Ph2PPr}PDI)Mn was found to hydrosilylate fomates under solvent free conditions with TOFs of up to 330 min^{-1}. Hydrolysis of the resulting silyl ether mixture furnished the corresponding alcohols. A comparative analysis has also been presented on the leading first row metal hydrosilylation catalysts among which these PDI supported Mn

complexes are found to be the best carbonyl hydrosilylation catalysts. This fact further supports the promising application of Mn in silicone rubber manufacturing.

2.2. Introduction:

Reductions of carbonyl compounds are frequently encountered during the synthesis of various organic alcohols and commodity chemicals. Typically, inorganic hydride reagents or transfer hydrogenation is used to execute this process. But, due to the harsh conditions and poor selectivity of such protocols, hydrosilylation of unsaturated carbon-oxygen bonds has been employed as a complementary route to silyl ethers and alcohols.[1] Silyl ethers are useful synthetic equivalents for alcohols and are also used in the industrial preparation of silicone containing polymers.[2] Furthermore, the operational conditions required for hydrosilylations either on a bench top or in large scale, are simple and inexpensive.[2d]

Although a number of precious metal catalysts are known to catalyze this transformation,[2b-c, 3] poor selectivity, narrow applicability, toxicity, and high prices of these catalysts have prompted the search for more sustainable substitutes. For instance, Karstedt's Pt catalyst is extensively used for C-Si bond formation in the silicone rubber industry,[3c-d] however, the inexpensive and nontoxic late first row metals are excellent alternatives.[2a] Although, many base metal hydrosilylation catalysts are known, further improvement of turnover number (TON) and turnover frequency (TOF) are still a challenge. Despite the intractable one-electron chemistry of these metals, recently a handful of Fe-based aldehyde and ketone hydrosilylation catalysts have been documented.[4] There are also several leading examples of carbonyl hydrosilylation

31

catalysts using Co,[5] Ni,[6] Cu,[7] and Zn.[8] Surprisingly, catalysts based on Mn in such transformations are underdeveloped.[9] In 1991, the first evidence of Si-H bond addition across the acyl bond of $(CO)_5MnCOR$ (R = Me, Ph)[10] was observed by the Cutler group when a stoichiometric amount of dihydro- or monohydrosilane was added. After a few years, they improvised the first catalytic hydrosilylation of ketone[11a] and ester[11b] using $(Ph_3P)(CO)_4MnC(O)Me$ with TOFs of up to 27 min^{-1} and 4 min^{-1} respectively. After that $(\eta^5\text{-}C_{10}H_9)Mn(CO)_3$[12] and $[(\eta^5\text{-}C_{10}H_9)Mn(CO)_3][BF_4]$[13] were found to have modest efficiencies towards ketone hydrosilylation. Another effective aldehyde hydrosilylation has been reported using (salen-3,5-^{t}Bu)MnN catalyst but, it requires higher temperature.[14] This document encompasses a detailed hydrosilylation study on ketones, aldehydes, acetates, and formates using (PDI)Mn complexes (Figure 2.1) as catalysts. Unprecedented efficiencies have been observed for ketone and aldehyde hydrosilylation, rendering these Mn complexes promising for silicone polymer synthesis.
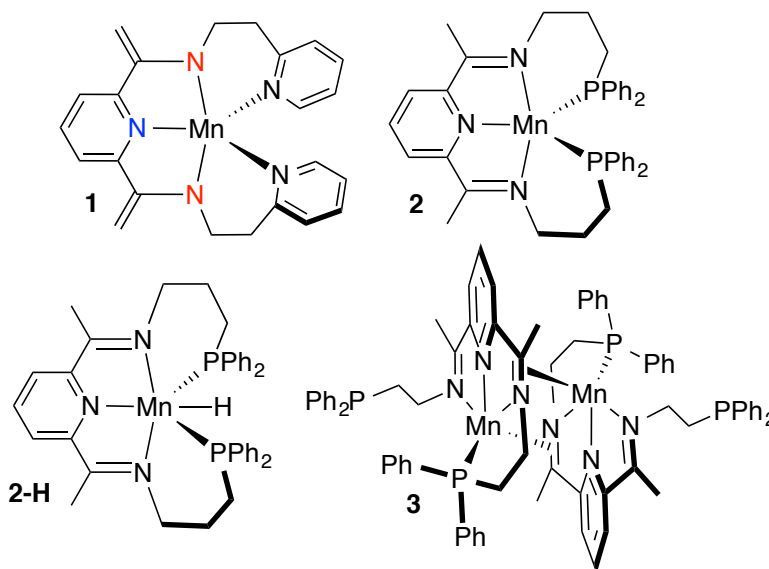
Figure 2.1. PDI supported low valent manganese complexes.

2.3. Ketone hydrosilylation:[15]

Having synthesized the low valent PDI supported manganese complexes (Figure 2.1) in Chapter 1, catalytic hydrosilylation was investigated. The study commenced with adding 1 mol% of (^{Ph2PPr}PDI)Mn **(2)** to an equimolar solution of cyclohexanone and PhSiH$_3$ in benzene-d_6, which afforded complete ketone reduction after 4 min (TOF = 1,485 h^{-1}, Table 2.2, Entry 1). In addition to PhSiH(OCy)$_2$, a significant quantity of residual PhSiH$_3$ was identified by ^{1}H NMR spectroscopy. Since efficient hydrosilylation was achieved in the presence of PhSiH$_3$, the reductant was systematically varied to probe whether steric or electronic effects influence the rate of ketone reduction (Table 2.1). Although 26% conversion was observed after 4 min with Ph$_2$SiH$_2$ (Table 2.1, Entry 2), no reaction was observed for tertiary silanes such as Ph$_3$SiH (Table 2.1, Entry 3) or Et$_3$SiH (Table 2.1, Entry 7). In contrast, 28% conversion was achieved over the same time period in the presence of (EtO)$_3$SiH (Table 2.1, Entry 4), confirming that quaternary silane products can be formed when using **2** as a catalyst. The activity noted for (EtO)$_3$SiH (TOF = 7 min^{-1}) and the inactivity of Et$_3$SiH, imply that silyl ether linkages formed during ketone reduction enhance the reactivity of remaining Si-H bonds. This also provides an explanation for why the hydrosilylation of cyclohexanone with PhSiH$_3$ results in the formation of PhSiH(OCy)$_2$ rather than PhSiH$_2$(OCy).

Table 2.1. 2-catalyzed hydrosilylation of cyclohexanone[a] in presence of various silanes.
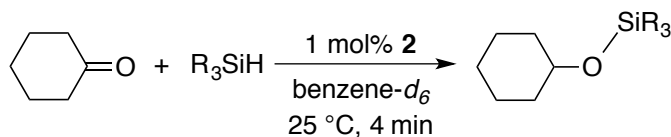
Entry	Silane	Product	Conv.(%)[b]
1	PhSiH₃	PhSiH(OCy)₂	>99
2	Ph₂SiH₂	Ph₂SiH(OCy)	26
3	Ph₃SiH	-	-
4	(EtO)₃SiH	(EtO)₃Si(OCy)	28
5	(EtO)₂MeSiH	(EtO)₂MeSi(OCy)	5
6	(EtO)Me₂SiH	(EtO)Me₂Si(OCy)	3
7	Et₃SiH	-	-

[a] Reactions conducted in 0.7 mL of benzene-d_6 with approximately 0.003 mmol of **2**, 0.3 mmol of silane, and 0.3 mmol of substrate. [b] Conversion determined by ^{1}H NMR spectroscopy.

Encouraged by these results, the scope of **2**-catalyzed ketone hydrosilylation was then investigated (Table 2.2). Using an equimolar quantity of PhSiH₃ and 1 mol% of **2**, acetophenone was fully reduced after 4 min at 25 °C to yield a 3:1 ratio of PhSiH(OCH(Me)(Ph))₂ to PhSi(OCH(Me)(Ph))₃ (Entry 1). Varying the phenyl group of acetophenone to include electron donating (Entries 2 and 3) or withdrawing substituents (Entries 4 and 5) greatly extended the time required to achieve reaction completion. A similar effect was observed for 2,2,2-trifluoroacteophenone (Entry 6); however, this reaction turned into an uncharacteristic bluish-green color upon **2** addition. Steric bulk about the ketone functionality was also found to significantly influence turnover rates (Entries 8-10). Importantly, the hydrosilylation of acetophenone, cyclohexanone, and 2-hexanone with PhSiH₃ was also conducted using 0.1 mol% of **2** in the absence of solvent (Entries 11-13). These reactions were exothermic in nature and had reached completion after 4 min (TOF = 247.5 min^{-1}). Since cyclohexanone and 2-hexanone produced only one product, these two substrates were hydrosilylated using 0.01 mol% of **2** in order to

achieve a higher TOF. Complete conversion was noticed after 4 min and the corresponding silyl ethers $PhSiH(OCy)_2$ (64%; TOF = 1280 min^{-1}) and $PhSiH(OCH(Me)(^nBu))_2$ (62%; TOF = 1240 min^{-1}) were isolated with high purity (Figure 2.1 and 2.2).
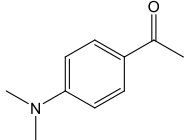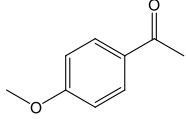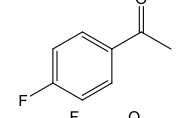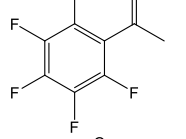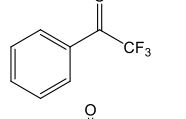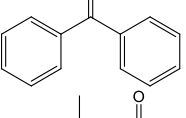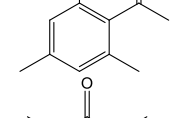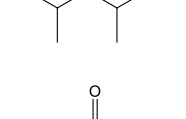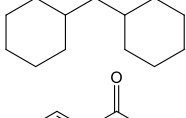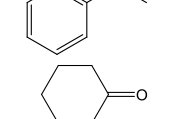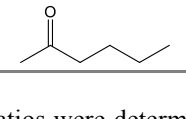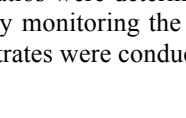
Since two hydrosilylation products were identified for many of the ketones in Table 2.2, efforts were made to improve the selectivity and atom-efficiency of this transformation by decreasing the relative amount of $PhSiH_3$ admitted to the reaction. Adding 0.33 mol% of **2** to a benzene-d_6 solution containing 3 eq. of either cyclohexanone or acetophenone per $PhSiH_3$ eq. resulted in complete Si-H bond utilization and the sole formation of $PhSi(OCy)_3$ or $PhSi(OCH(Me)(Ph))_3$, respectively (Table 2.3, Entries 1 and 2). Likewise, the hydrosilylation of diisopropyl ketone to selectively yield $PhSiH(OCH(^iPr)_2)_2$ was achieved within 30 min of **2** addition (TOF = 6.6 min^{-1}). When 3 eq. of 2-hexanone were admitted per $PhSiH_3$ eq., the reaction did not reach completion after 24 h at 25 °C (Entry 4), as $PhSiH(OCH(Me)(^nBu))_2$ was fairly unreactive under these conditions.

Table 2.2. Hydrosilylation of ketone using **2**.
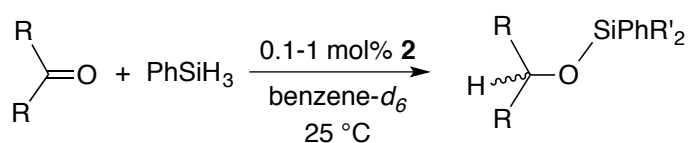
Entry	Substrate	Product(s)[a] (Ratio)	Time	Conv. (%)[b]
1		$PhSiH(OCH(Me)(Ph))_2$ $PhSi(OCH(Me)(Ph))_3$ (3:1)	4 min	>99

Entry	Substrate	Silane	Time	Conversion
2		PhSiH(OCH(Me)(Ar))$_2$	6 h	>99
3		PhSiH(OCH(Me)(Ar))$_2$ PhSi(OCH(Me)(Ar))$_3$ (5:1)	25 min	>99
4		PhSiH(OCH(Me)(Ar))$_2$ PhSi(OCH(Me)(Ar))$_3$ (7:1)	4 h	>99
5		PhSiH(OCH(Me)(Ar))$_2$ PhSi(OCH(Me)(Ar))$_3$ (3:1)	3.5 h	>99
6		PhSi(OCH(CF$_3$)(Ph))$_3$	12 h	>99
7		PhSiH(OCH(Ph)$_2$)$_2$ PhSi(OCH(Ph)$_2$)$_3$ (7:1)	20 min	>99
8		PhSiH(OCH(Me)(Ar))$_2$	5 d	80
9		PhSiH$_2$(OCH(^{i}Pr)$_2$) PhSiH(OCH(^{i}Pr)$_2$)$_2$ (4:1)	36 min	>99
10		PhSiH(OCH(Cy)$_2$)$_2$ PhSiH$_2$(OCH(Cy)$_2$) (3:1)	24 h	>99
11[c]		PhSiH(OCH(Me)(Ph))$_2$ PhSi(OCH(Me)(Ph))$_3$ (5:1)	4 min	>99
12[c]		PhSiH(OCy)$_2$	4 min	>99
13[c]		PhSiH(OCH(Me)(^{n}Bu))$_2$	4 min	>99

[a] Product ratios were determined by integrating the corresponding ^{1}H NMR spectra. [b] Conversions are determined by monitoring the disappearance of starting ketone in ^{1}H NMR over time. [c] Hydrosilylation of these substrates were conducted using 0.01 mol% catalysts under solvent free condition.

Table 2.3. Atom-efficient hydrosilylation reactions.

$$R_2C=O \xrightarrow[\text{25 °C}]{\substack{\text{0.33-0.5 mol\% 2} \\ \text{0.33-0.5 eq. PhSiH}_3 \\ \text{benzene-}d_6}} \text{H-CR}_2\text{-O-SiPhR'}_2$$
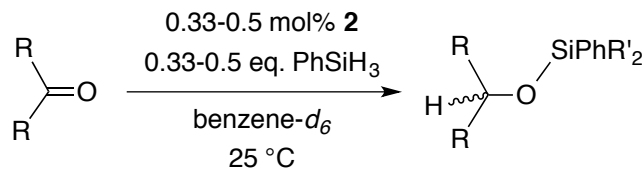
Entry	Substrate	Product(s) (Ratio)	Time	Conv. (%)[a]
1[b]		$PhSi(OCy)_3$	4 h	>99
2[b]		$PhSi(OCH(Me)(Ph))_3$	6.5 h	>99
3[c]		$PhSiH(OCH(^iPr)_2)_2$ $PhSiH_2(OCH(^iPr)_2)$ (9:1)	42 min	>99
4[b]		$PhSiH(OCH(Me)(^nBu))_2$ $PhSi(OCH(Me)(^nBu))_3$ (3:1)	24 h	74

[a] Conversion determined by ^{1}H NMR spectroscopy. [b] Reaction conducted in 0.7 mL of benzene-d_6 with ~0.0027 mmol of 2, 0.27 mmol of silane, and 0.81 mmol of substrate. [c] Reaction conducted in 0.7 mL of benzene-d_6 with 0.0036 mmol of 2, 0.36 mmol of silane, and 0.72 mmol of substrate.
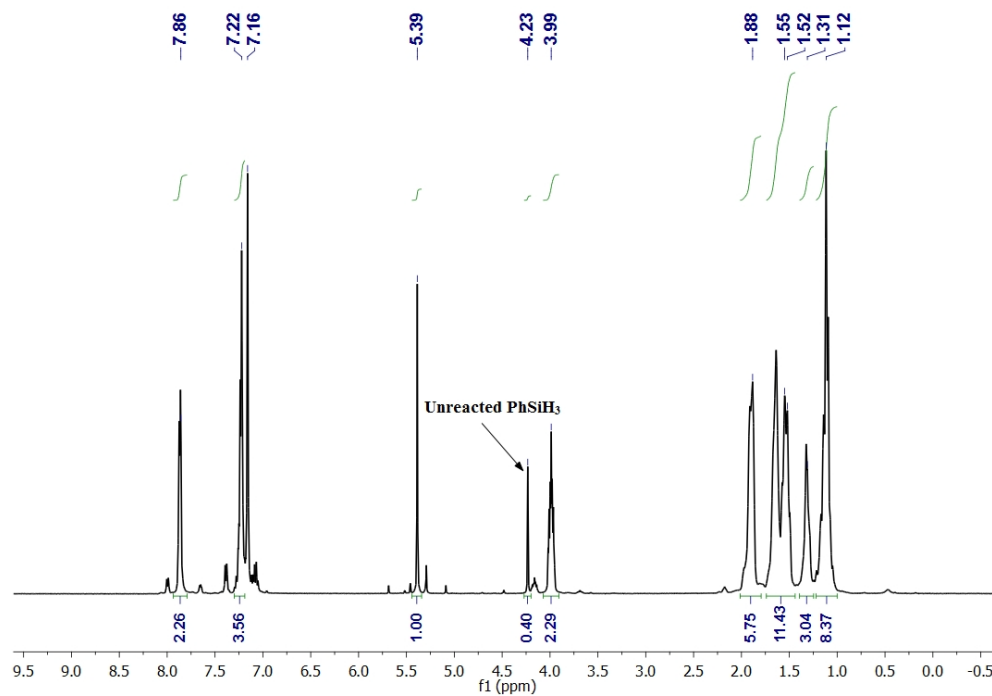
Figure 2.2. ^{1}H NMR spectra of $PhSiH(OCy)_2$.
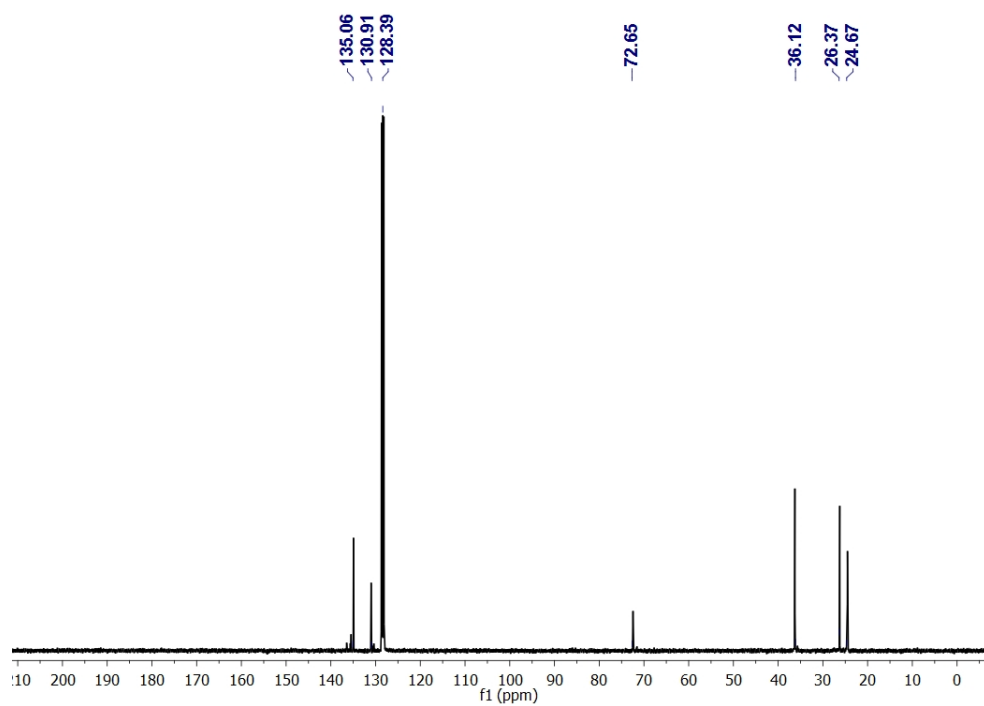
Figure 2.3. ^{13}C NMR spectra of PhSiH(OCy)$_2$.
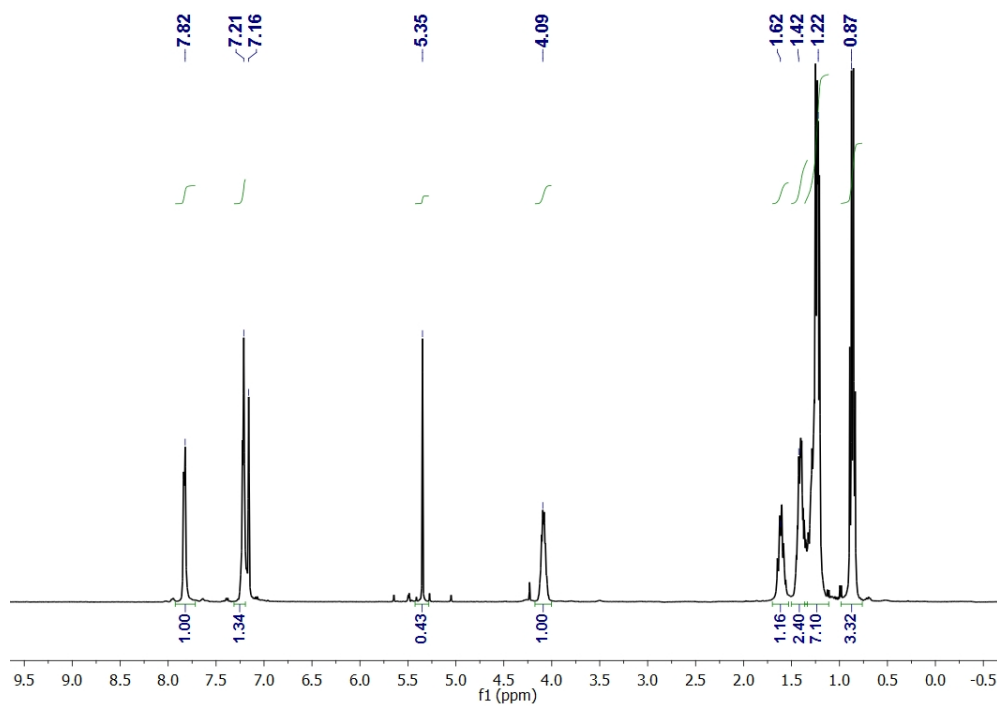
Figure 2.4. ^{1}H NMR spectra of PhSiH(OCH(Me)(^{n}Bu))$_2$.
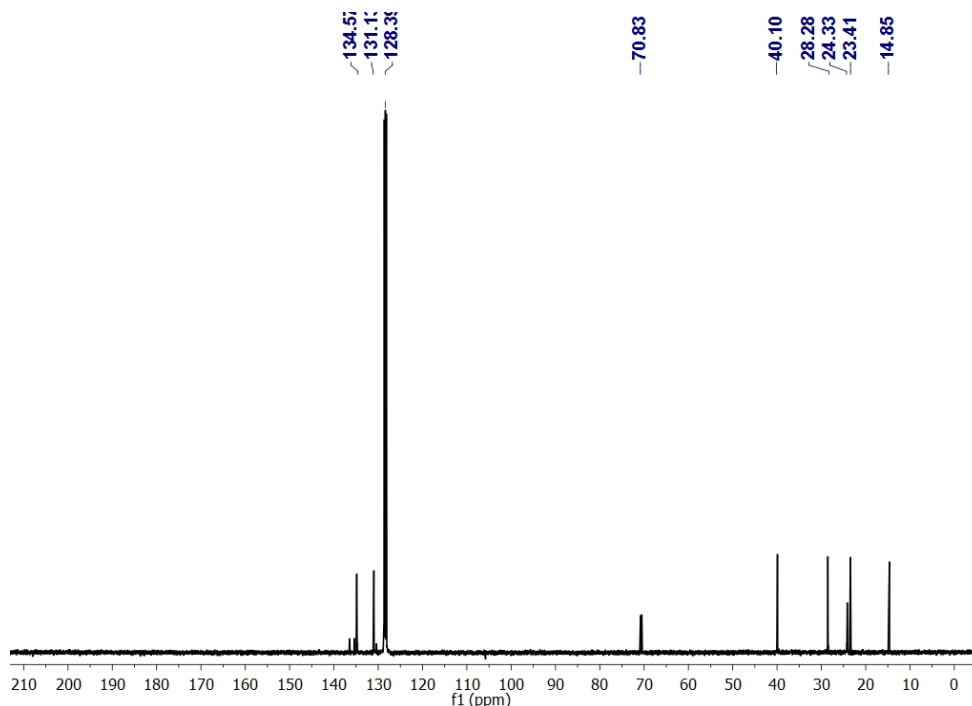
Figure 2.5. ^{13}C NMR spectra of PhSiH(OCH(Me)(^{n}Bu))$_2$.

Knowing the remarkable efficiency of **2** for ketone hydrosilylation, the deprotonated complex (^{PyEt}PDEA)Mn **(1)** was also screened for this reaction. Despite the fact that **1** has a redox innocent chelate, it is still capable of hydrosilylating ketones with comparable TOF of up to 990 min^{-1}.[16] Although a full substrate scope for [(^{Ph2PEt}PDI)Mn]$_2$ **(3)** catalyzed ketone hydrosilylation has not been established, it was found that **3** can also hydrosilylate ketones with similar TOFs as **2**.

2.4. Aldehyde hydrosilylation:[17]

Aldehydes, being more reactive than ketones, were also assayed for hydrosilylation using these low valent manganese complexes. A thorough investigation of substrate scope and functional group tolerance was sought using **2** and **3** side by side

39

as catalysts. When a neat mixture of benzaldehyde and PhSiH$_3$ was added to 0.1 mol% of catalyst at room temperature, complete conversion to the corresponding silyl ether was observed after 2 min and the reaction was exothermic. Hydrolysis with 10% aq. NaOH solution following extraction allowed the isolation of benzyl alochol with high purity. Thirteen different aldehydes were assayed for hydrosilylation and summarized in Scheme 2.2. Both catalysts can tolerate the electron withdrawing halide and cyanide substituents on benzaldehyde except in the case of 4-iodobenzaldehyde, where **2** shows 32% conversion and **3** is inactive. Electron donating substituents on the benzene ring also do not influence efficiency, as can be seen in the case of *p*-tolualdehyde and *p*-anisaldehyde. The nitro group of *p*-nitrobenzaldehyde remains unreduced during the course of hydrosilylation, as identified from ^{1}H NMR of the alcohol. Similarly, 2-naphthaldehyde was hydrosilylated using **2** and **3** with decent TOFs. Heteroaromatic aldehydes are also hydrosilylated without any difficulties using both catalysts. It is also to be noted that both the catalysts can selectively reduce aldehydes in presence of olefin/conjugated olefin bonds (as in the case of 3-cyclohexene-1-carboxaldehyde and citral). However, **3** can convert only 32% of the 3-cyclohexene-1-carboxaldehyde.
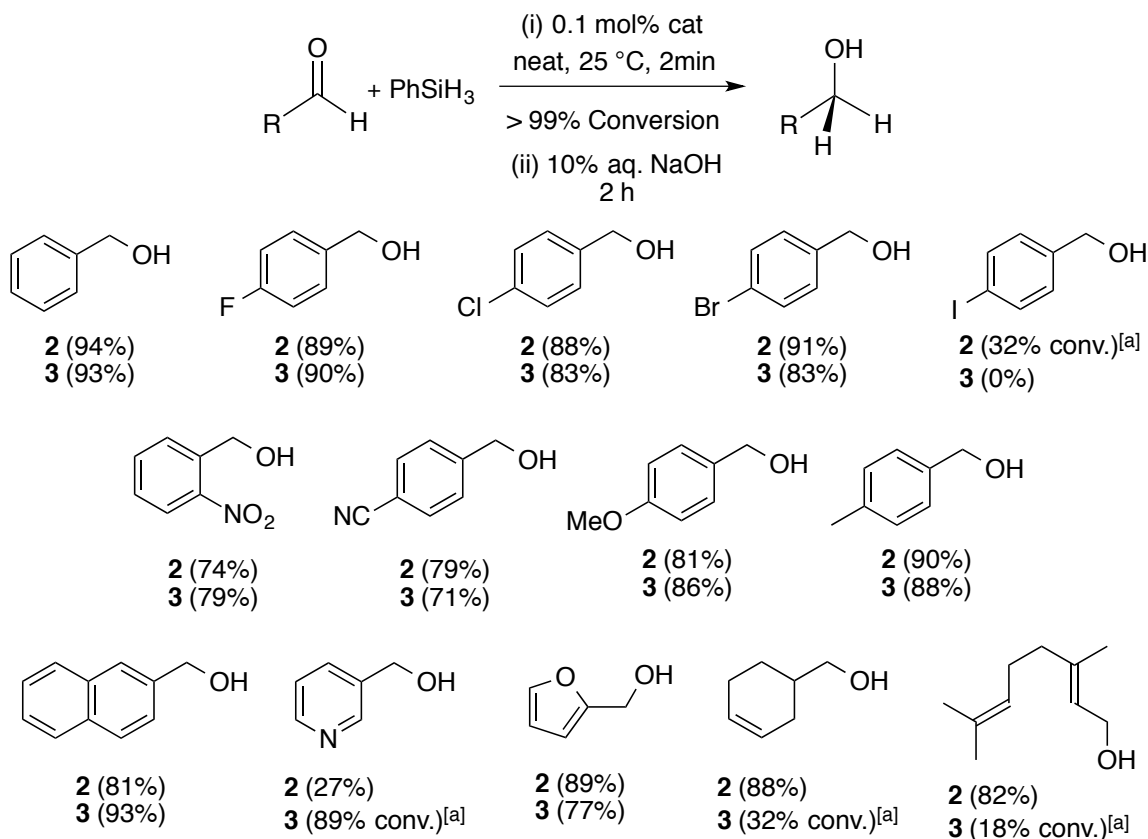
Scheme 2.1. Substrate scope and functional group tolerance for **2-** and **3**-catalyzed aldehyde hydrosilylation. (a) The silyl ethers were not hydrolysed to isolate alcohols.

A series of controlled reactions were carried out to prove the homogeniety and feasibility of **2-** and **3**-catalyzed hydrosilylation (Table 2.4). Attempts to hydrosilylate benzaldehyde using the precursors (^{Ph2PPr}PDI)MnCl$_2$ and (^{Ph2PEt}PDI)MnCl$_2$ separately as catalysts has been unsuccessful. Conducting this reaction in presence of excess Hg^0 did not affect the reactivity. Also, Mn^0 powder and (THF)$_2$MnCl$_2$ unable to hydrosilylate benzaldehyde under the identical catalytic conditions. All these facts suggest the presence of a homogeneous reduced complex in the reaction mixture during catalytic hydrosilylation. Furthermore, the TOF is not affected by performing this reaction in absence of light using **2** and **3** separately, which excludes the possibility of photocatalytic

reduction of aldehydes. Employing AIBN ($t_{1/2}$ = 1 h at 85 °C) as a catalyst for benzaldehyde hydrosilylation was also found to be unsuccessful, ruling out a radical chain process.

Table 2.4. Controlled hydrosilylation of benzaldehyde.
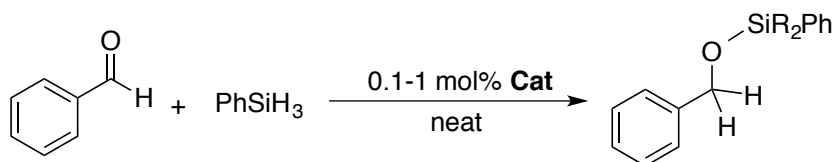
Entry	Catalyst	Time (min)	Temp (°C)	Conv. (%)[a]
1	^{Ph2PEt}PDIMnCl$_2$	5	25	0
2	^{Ph2PPr}PDIMnCl$_2$	5	25	0
3	(THF)$_2$MnCl$_2$	5	25	0
4	Mn^0	5	25	0
7	**2** + 50,000 Hg^0	2	25	>99
8	**2** in dark	2	25	>99
9	**3** + 50,000 Hg^0	2	25	>99
10	**3** in dark	2	25	>99
11	AIBN[b]	120	90	0

[a] Conversions were determined by ^{1}H NMR. [b] 1 mol% of AIBN was used as a catalyst and this reaction was conducted in benzene-d_6.

After exploring the reactivity and functional group tolerance, both catalysts were tested for stability under higher substrate loading (Scheme 2.3). When a manganese loading of 0.01 mol% was used, benzaldehdye was completely consumed in 2 min (TOF of 4950 min^{-1}) using either **2** or **3**. Notably, **2** has been found to hydrosilylate 4-

fluorobenzaldehdyde and 2-nitrobenzaldehyde with decent turnover frequencies (Scheme 2.3) while catalyst **3** showed poor efficiency towards these substrates. It is believed that the relatively poor reactivity of **3** compared to **2**, is due to slow dissociation of the dimer to monomeric (PDI)Mn unit during the course of hydrosilylation.

2, >99% (92%), 4950 min^{-1}   **2**, >99% (87%), 4950 min^{-1}   **2**, 72%,[a] 3600 min^{-1}
3, >99% (91%), 4950 min^{-1}   **3**, 18%,[a] 900 min^{-1}   **3**, 5%,[a] 250 min^{-1}
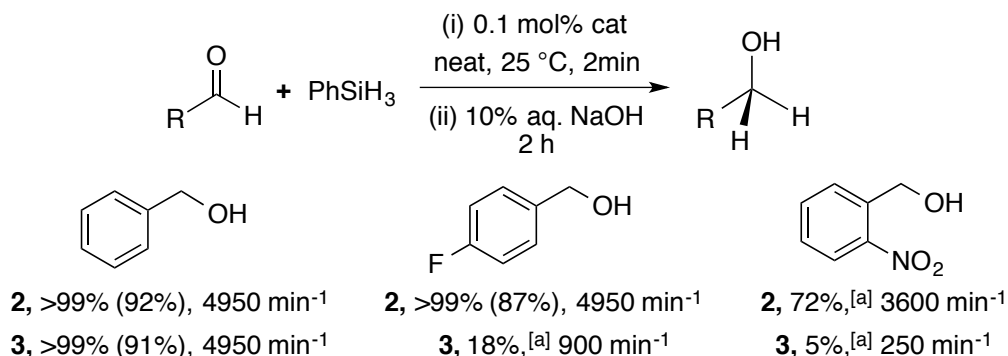
Scheme 2.2. Aldehyde hydrosilylation with low catalyst loading. [a] The corresponding silyl ethers were not hydrolyzed.

In summary, **2** and **3** can catalyze aldehyde hydrosilylation with unprecedented TOFs of up to 4950 min^{-1} rendering these complexes to be the most efficient first row transition metal carbonyl hydrosilylation catalysts reported to date. Similarly, Ghosh *et al.* has shown that **1** can also hydrosilylate aldehydes with TOFs of up to 2475 min^{-1} with a reasonably good functional group tolerance.[16] Considering the wide functional group tolerance and stability under low catalyst loading, it can be concluded that **2** is the best carbonyl hydrosilylation precatalyst among these low valent Mn complexes of discussion.

2.5. Acetate Hydrosilylation:[15]
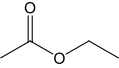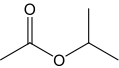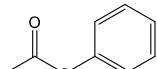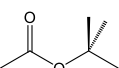
The ability of **2** to catalyze the hydrosilylation of esters was also investigated. Five different acetates with varying bulkiness were assayed and are shown in Table 2.5. To our surprise, adding 1 mol% of **2** to an equimolar benzene-d_6 solution of

43

MeOAc and PhSiH$_3$ afforded a mixture of quaternary silanes that included PhSi(OMe)$_3$,

PhSi(OEt)$_3$, PhSi(OMe)$_2$(OEt), and PhSi(OEt)$_2$(OMe) (Entry 1).

Table 2.5. Reductive cleavage and dihydrosilylations of ester using **2**.

$$R \overset{O}{\underset{}{\|}} O\text{-}R' \xrightarrow[\substack{\text{benzene-}d_6 \\ 25\text{ - }80\ °C}]{\substack{1\ \text{mol}\%\ \mathbf{2} \\ \text{PhSiH}_3}} \text{PhSi(H)}_x(\text{OCH}_2R)_y(\text{OR'})_z$$

x = 0 or 1; y = 0, 1, 2, or 3
z = 0, 1, 2, or 3
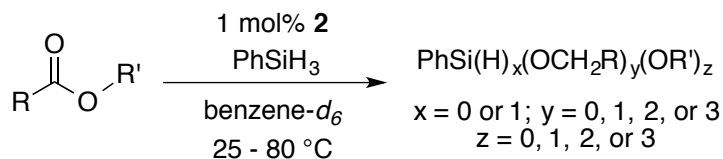
Entry	Substrate	Product(s) (Ratio)	Time	Conv. (%)[b]
1[c]		PhSi(OEt)$_2$(OMe) PhSi(OMe)$_3$ PhSi(OEt)$_3$ PhSi(OMe)$_2$(OEt) (2:1.5:1.2:1)	24 h	>99
2[c]		PhSi(OEt)$_3$ PhSiH(OEt)$_2$ (9:1)	5.5 h	>99
3[d]		PhSi(OEt)$_3$ PhSiH(O^{i}Pr)$_2$ PhSi(O^{i}Pr)$_3$ PhSiH(OEt)$_2$ (2:1.5:1:1)	3 d	>99
4[c]		PhSi(OPh)$_3$ PhSi(OEt)$_3$ PhSi(OEt)$_2$(OPh) (1.25:1.25:1)	10 d	95
5[a]		PhSiH(O^{t}Bu)$_2$ PhSiH(OEt)(O^{t}Bu) PhSi(OEt)$_3$ (1.25:1.25:1)	10 d	85

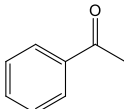[a] Reactions were conducted in 0.7 mL of benzene-d_6 with ~0.003 mmol of **2**, 0.3 mmol of silane, 0.3 mmol of substrate. [b] Conversion determined by ^{1}H NMR spectroscopy. [c] Reactions were conducted at 25 °C. [d] Reactions were conducted at 80 °C.

When this reaction was repeated using PhSiD$_3$, deuterium incorporation into the

methylene position of each ethoxysilane product was observed by ^{1}H and ^{2}H NMR

spectroscopy (Scheme 2), confirming the ethoxide substituents are formed following

ketone reduction and reductive cleavage of the MeOAc acyl C-O bond. Although the

reduction of MeOAc was not complete after 16 h at 25 °C, the dihydrosilylation of

EtOAc to form a 9:1 mixture of PhSi(OEt)$_3$ to PhSiH(OEt)$_2$ took only 5.5 h to reach

completion (Entry 2). In contrast, the reduction of ^{i}PrOAc, PhOAc, or ^{t}BuOAc to tertiary

and quaternary silane products required up to 10 d or heating to 80 °C to reach

appreciable conversion (Entries 3-5).
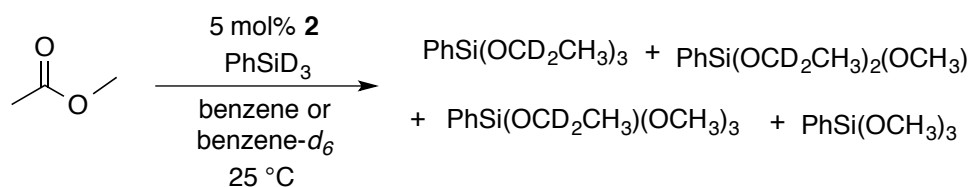
Scheme 2.3. The deuterosilylation of methyl acetate as observed by ^{1}H and ^{2}H NMR spectroscopy.
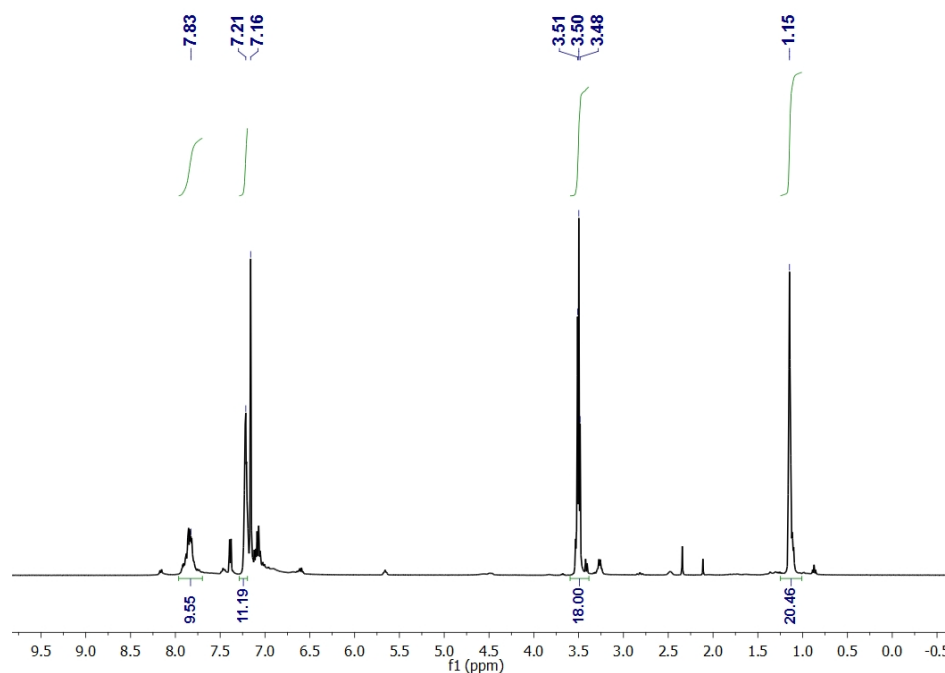
Figure 2.6. ^{1}H NMR of **2**-catalyzed MeOAc deuterosilylation using PhSiD$_3$.
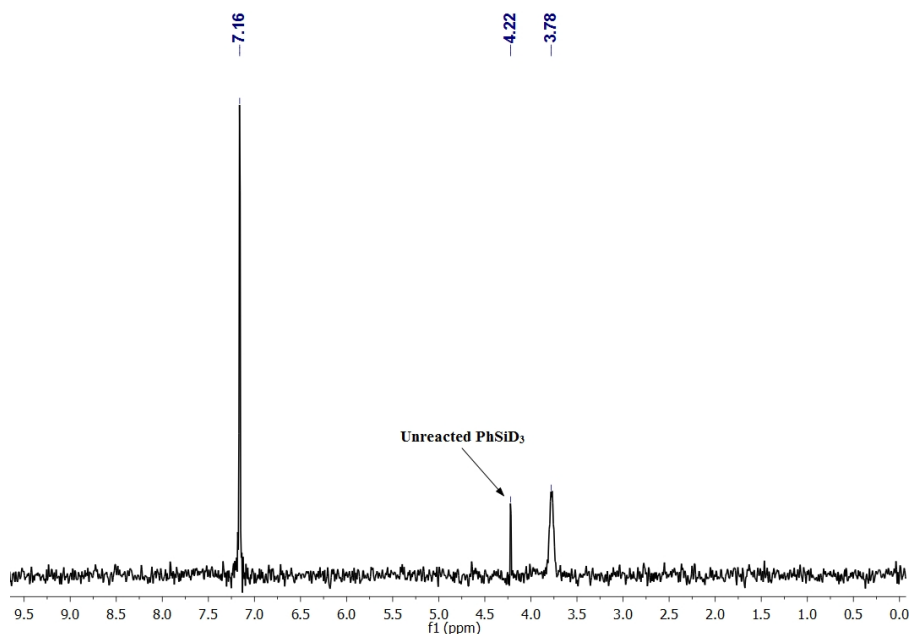
Figure 2.7. ^{2}H NMR spectra of **2**-catalyzed MeOAc deuterosilylation using PhSiD$_3$.

Based on Table 2.5 (and the fact that **2** does not mediate the reduction of ethyl benzoate under these conditions), it appears that the relative rates of ester dihydrosilylation closely correlate to the acyl C-O bond cleavage preferences reported for ($^{2,6\text{-iPr2Ph}}$PDI)Fe(N$_2$)$_2$.[22] Although efforts to elucidate the mechanism of **2**-catalyzed ester reduction remain underway, the tendency of esters to undergo acyl C-O bond cleavage appears to be important for achieving their dihydrosilylation.

2.6. Formate Hydrosilylation:[17]

With the knowledge that **2** can cleave the C-O bond of acetates,[15] hydrosilylation of formates using **2** have been sought. When a neat equimolar mixture of methylformate (or ethylformate) and PhSiH$_3$ was added to 0.02 mol% of **2**, an exothermic reaction occurs with >99% substrate conversion in 15 min. Analysis of the reaction mixture by [1]H

46

NMR spectroscopy, revealed a mixture of silyl ethers. Attempts to hydrolyze these silyl ethers in order to isolate the corresponding alcohols by fractional distillation did not allow for adequate separation. Choosing heavier formates such as shown in Table 2.6 allowed for the isolation of corresponding heavier alcohols.

Table 2.6. Hydrosilylation of formates catalyzed by **2**.
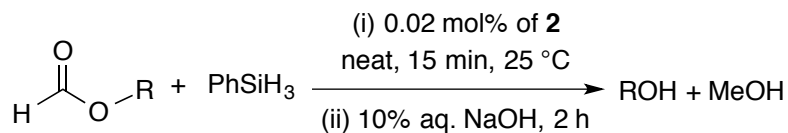
Entry	Substrate	Alcohols	Isolated yield (%)
1			88
2			86
3[a]		-	<2% conversion
4			64
5			60
6[a]		-	<2% conversion

[a] These substrates showed no conversion after 1 h.

47

Addition of an equimolar quantity of benzyl formate and PhSiH$_3$ to 0.02 mol% of either **2** resulted in vigorous bubbling and the reaction mixture became hot. ^{1}H NMR analysis after 15 minutes following catalyst deactivation revealed complete consumption of starting formate. Hydrolysis using 10% aq. NaOH followed by extraction and evaporation afforded pure benzyl alcohol with excellent yield (Entry 1, Table 2.6). Similarly, phenylethyl formate, isoamyl formate, hexyl formate, were hydrosilylated with >99% substrate consumption rate and corresponding alcohols were obtained in good yield. Geranyl formate and *p*-anisyl formate showed no conversion even after 1 h. Unlike the acetates, the TOFs of formate reduction are found to be unaffected upon varying the ester group. A TOF of 330 min^{-1} (based on substrate conversion) has been achieved for each substrate except geranyl formate (198 min^{-1}). Performing these reactions in presence of excess Hg^0 and in absence of light did not affect the conversion. Mixing PhSiH$_3$ and substrate in absence of catalyst did not result any conversion. Employing the corresponding dichlorides and Mn powder as catalysts separately, showed no reaction. Catalyst **3** showed comparable efficiencies towards hydrosilylation of ethyl formate, benzyl formate, phenylethyl formate, and hexyl formate, *p*-anisylformate, isoamyl formate, and geranyl formate and the corresponding alcohols were isolated in decent yields and high purity.

2.7. Leading first row metal carbonyl hydrosilylation catalysts:

To further contextualize the activity of **1**, **2**, and **3** a comparison to prominent first-row metal catalysts is warranted (Table 2.7). Relative to the late metals, early transition metal catalysts have been sparingly used for carbonyl hydrosilylation. Of the examples

reported, the most effective Sc,[18] Ti,[19] and Cr[20] catalysts exhibit maximal TOFs of <1 min^{-1}. Late first-row metal catalysts for this transformation have been more extensively investigated. A recent report by Sydora, Turculet, and Stradiotto described an N-phosphinoamidinate Fe complex that mediates acetophenone hydrosilylation with TOFs of up to 393 min^{-1} (23600 h^{-1}).[4a] While the most efficient Co,[5f] Ni,[6c] and Zn[8m] catalysts for this transformation operate with maximal TOFs lower than those determined for **2**, comparison to leading Cu catalysts is more difficult. The reaction proceeds with TOFs of up to 660 min^{-1}; however, this is calculated relative to ligand instead of Cu because the authors sought to minimize the most expensive reagent, (S)-Xyl-P-Phos.[7k] Using a similar methodology, Lipshutz and co-workers reported an asymmetric acetophenone hydrosilylation TOF of 77 min^{-1} at −50 °C,[7n] suggesting greater TOFs might have been achieved at or near ambient temperature. A number of well-defined Cu−H hydrosilylation catalysts have since been described; however, they have mostly been used for low-temperature asymmetric ketone hydrosilylation and have not been evaluated for their maximal TOF.[7]

Table 2.7. Leading first row metal carbonyl hydrosilylation catalysts

M	Catalyst	Silane	Substrate[a]	T (°C)	TOF (min^{-1})
Sc[17]	$(\kappa^4\text{-}N_3O)Sc$ $(O_2CCH_2SiMe_2Ph)\cdot(BC_6F5)_3$[b]	Et_3SiH	Carbon dioxide	65	0.2[c]
Ti[18]	$(Cp)_2TiCl_2 + 2\ ^nBuLi$	$(EtO)_3SiH$	Methyl benzoate	25	0.7[d]
V	-	-	-	-	-

49

Cr[19]	$(\eta^6\text{-}C_6H_6)_2Cr$	Ph_2SiH_2	*p*-Anisaldehyde	70	0.1
Mn	**1, 2**, **3**	$PhSiH_3$	Benzaldehyde	25	2475 (**1**)[16] 4950 (**2, 3**)
Fe[4a]	$(\kappa^2\text{-}PN)Fe(N(SiMe_3)_2)$ [e]	$PhSiH_3$	Acetophenone	25	393
Co[5f]	$(DPB)Co(N_2)$ [f]	Ph_2SiH_2	Propanal	25	49.5
Ni[6c]	$(Cp^*\text{-}NHC^{Me})Ni(O^tBu)$	$PhSiH_3$	*p*-CF$_3$-benzaldehyde	25	38.4
Cu[7k]	CuF_2 + (S)-Xyl-P-Phos	$PhSiH_3$	*p*-NO$_2$-acetophenone	25	660[g]
Zn[8m]	$((\kappa^3\text{-}Tptm)ZnH$ [h]	$PhSiH_3$	Acetaldehyde	25	20

[a] Least-substituted example. [b] N$_3$O = analido(bipyridyl)carboxylate. [c] TOF based on Si−H bond utilization. [d] TOF based on ester dihydrosilylation, assuming a reaction time of 0.5 h. [e] PN = N-phosphinoamidinate. [f] DPB = bis(o-diisopropylphosphinophenyl)phenylborane. [g] Calculated relative to ligand, not Cu loading. [h] Tptm = tris(2-pyridylthio)methyl.

2.8. Concluding Remarks:

In conclusion, a thorough investigation on the catalytic hydrosilylation of carbonyls and carboxylates using a set of low-valent redox-active ligand supported Mn complexes has been demonstrated. These catalysts have also been found to tolerate a wide range of functional groups and chemoselectively reduce carbonyls and formates over alkenes. While excellent activities were observed for the hydrosilylation of aldehydes (TOF of up to 4950 min^{-1}) and ketones (TOF of up to 1280 min^{-1}) a decent TOF of up to 330 min^{-1} has been obatined for formate reduction. It was also noticed that the dihydrosilylation of acetates proceeds thorough acyl C-O bond cleavage with modest TOFs. Notably, such high

efficiency for Si-O bond formation renders these complexes promising for siloxane polymer synthesis applications. Although Mn reduction catalysts remain underutilized, it is hoped that the transformations reported herein will open a new chapter in the book of sustainable transition metal catalysis and highlight the potential value of high-denticity redox-active chelates in catalyst design.

2.9. Experimental Procedure

General procedure for silane screening: In the glovebox, an ambient temperature benzene-d_6 (approximately 0.7 mL) solution of silane (0.3 mmol) and cyclohexanone (0.030 mL, 0.3 mmol) was added to a 20 mL scintillation vial containing 2 mg (0.003 mmol) of complex **2**. The resulting brown solution was stirred for 4 min and then exposed to air to deactivate the catalyst. The colorless solution was then filtered through Celite directly into an NMR tube. The progress of the reaction was determined following analysis by ^{1}H NMR spectroscopy.

General procedure for hydrosilylation of ketones: An ambient temperature benzene-d_6 (0.7 mL) solution of PhSiH$_3$ (0.33 mmol) and ketone (0.33 mmol) was added to a vial containing 0.0033 mmol of **2**. The resulting brown solution was then transferred into a J. Young tube and the progress of the reaction was monitored by NMR spectroscopy at ambient temperature. In the case of acetophenone and substituted acetophenones, enantiomeric product mixtures were observed. A control experiment was performed in a similar fashion by adding 0.3 mmol of PhSiH$_3$ and 0.3 mmol of acetophenone to 0.7 mL of benzene-d_6 in the absence of complex **2**. The solution was monitored by ^{1}H NMR spectroscopy over time and no reaction was observed after 24 h at room temperature.

Semimicro scale hydrosilylation of acetophenone: In the glovebox, a benzene-d_6 (0.7 mL) solution of PhSiH$_3$ (27.6 μL, 0.224 mmol) and acetophenone (26.2 μL, 0.224 mmol) was added to a 20 mL scintillation vial containing 1.5 mg (0.00224 mmol) of complex **2**. The resulting brown solution was stirred for 4 min and then exposed to air to deactivate the catalyst. The colorless solution was filtered through Celite and analyzed by NMR spectroscopy. Complete disappearance of the acetophenone resonances was observed along with the formation of PhSiH(OCH(Me)(Ph))$_2$[5] (75%) and PhSi(OCH(Me)(Ph))$_3$[6] (25%). Product ratio was determined from the corresponding CH peaks at 5.02 ppm (PhSiH(OCH(Me)(Ph))$_2$) and 5.19 ppm (PhSi(OCH(Me)(Ph))$_3$). Unreacted PhSiH$_3$ was observed at 7.38, 7.07 and 4.23 ppm.

PhSiH(OCH(Me)(Ph))$_2$: ^{1}H NMR (benzene-d_6): δ = 7.72 (m, 2H, *phenyl*), 7.25 (m, 4H *phenyl*), 7.15 (m, 9H, phenyl), 5.28 (s, 1H, Si*H*), 5.02 (m, 2H, C*H*), 1.40 (m, 6H, C*H$_3$*).

PhSi(OCH(Me)(Ph))$_3$: ^{1}H NMR (benzene-d_6): δ = 7.80 (m, *phenyl*), 7.23 (m, *phenyl*), 7.20-7.10 (m, *phenyl*), 5.19 (m, C*H*MePh), 1.36 (m, C*H$_3$*).

Neat hydrosilylation of acetophenone (0.1 mol% catalyst loading): In the glovebox, a mixture of PhSiH$_3$ (922 μL, 7.48 mmol), and acetophenone (874 μL, 7.48 mmol) was added to a 20 mL scintillation vial containing 5 mg (0.00748 mmol) of complex **2**. The mixture was then stirred vigorously and significant heat generation was noticed. After 4 min the mixture was exposed to air to deactivate the catalyst. The resulting colorless solution was filtered through Celite and analysis by ^{1}H NMR spectroscopy revealed the complete conversion of acetophenone into a mixture of PhSiH(OCH(Me)(Ph))$_2$ (83%) and PhSi(OCH(Me)(Ph))$_3$ (17%). Product ratio was determined from the integration of the peaks at 5.02 ppm (PhSiH(OCH(Me)(Ph))$_2$) and 5.19 ppm (PhSi(OCH(Me)(Ph))$_3$).

52

Atom-efficient hydrosilylation of acetophenone: In the glovebox, a benzene-d_6 (0.7 mL) solution of PhSiH$_3$ (33.2 μL, 0.269 mmol) and acetophenone (94.4 μL, 0.808 mmol) was added to a vial containing 1.8 mg (0.00269 mmol) of complex **2**. The resulting brown solution was transferred into a J. Young tube and the progress of the reaction was monitored by ^{1}H NMR spectroscopy. Complete conversion to PhSi(OCH(Me)(Ph))$_3$ was observed after 6.5 h at room temperature.

Semimicro scale hydrosilylation of 4'-dimethylaminoacetophenone: In the glovebox, a benzene-d_6 (0.7 mL) solution of PhSiH$_3$ (33.2 μL, 0.269 mmol) and 4'-dimethylaminoacetophenone (43.9 mg, 0.269 mmol) was added to a vial containing 1.8 mg (0.00269 mmol) of complex **2**. The brown solution was then transferred into a J. Young tube and the progress of reaction was monitored by NMR spectroscopy. The resonance at 5.15 ppm for the two methylene protons in ^{1}H NMR spectroscopy revealed complete conversion to PhSiH(OCH(Me)(p-NMe$_2$C$_6$H$_4$))$_2$ after 6 h at room temperature. Unreacted PhSiH$_3$ was also observed at 7.38, 7.07, and 4.23 ppm.

PhSiH(OCH(Me)(p-NMe$_2$C$_6$H$_4$))$_2$: ^{1}H NMR (benzene-d_6): δ = 7.85 (m, 2H, *phenyl*), 7.33 (m, 4H, *phenyl*), 7.19 (m, 3H, *phenyl*), 6.60 (m, 4H, *phenyl*), 5.41 (s, 1H Si*H*), 5.15 (m, 2H, C*H*), 2.53 (12H, *NMe$_2$*), 1.55 (d, J_{H-H} = 6.2 Hz, 6H, C*H$_3$*).

Semimicro scale hydrosilylation of *p*-methoxyacetophenone: In the glovebox, a benzene-d_6 (0.7 mL) solution of PhSiH$_3$ (46.1 μL, 0.374 mmol) and *p*-methoxyacetophenone (56.1 μL, 0.374 mmol) was added to a vial containing 2.5 mg (0.00374 mmol) of complex **2**. The brown solution was then transferred into a J. Young tube and the progress of reaction was monitored by NMR spectroscopy. Complete conversion to a mixture of PhSiH(OCH(Me)(p-OMeC$_6$H$_4$))$_2$ (80%) and

PhSi(OCH(Me)(p-OMeC$_6$H$_4$))$_3$ (20%) was observed after 25 min by ^{1}H NMR spectroscopy. Product ratio was determined from the integration of the peaks at 5.04 ppm (PhSiH(OCH(Me)(p-OMeC$_6$H$_4$))$_2$) and 5.20 ppm (PhSi(OCH(Me)(p-OMeC$_6$H$_4$))$_3$), which correspond to the methylene proton.

PhSiH(OCH(Me)(p-OMeC$_6$H$_4$))$_2$: ^{1}H NMR (benzene-d_6): δ = 7.78 (m, 2H, *phenyl*), 7.20-7.10 (m, 6H, *phenyl*), 6.77 (m, 5H, *phenyl*), 5.33 (s, 1H Si*H*), 5.04 (m, 2H, C*H*), 3.33 (s, 6H, OC*H$_3$*), 1.44 (m, 6H, C*H$_3$*).

PhSi(OCH(Me)(p-OMeC$_6$H$_4$))$_3$: ^{1}H NMR (benzene-d_6, selected resonances): δ = 5.20 (m, 3H, C*H*), 1.51 (m, 9H, C*H$_3$*).

Semimicro scale hydrosilylation of *p*-fluoroacetophenone: In the glovebox, a benzene-d_6 (0.7 mL) solution of PhSiH$_3$ (20.3 μL, 0.165 mmol) and *p*-fluoroacetophenone (19.9 μL, 0.165 mmol) was added to a vial containing 1.1 mg (0.00165 mmol) of complex **2**. The brown solution was then transferred to a J. Young tube and the progress of reaction was monitored via ^{1}H NMR spectroscopy. Complete conversion to a mixture of PhSiH(OCH(Me)(p-F-C$_6$H$_4$))$_2$ (87%) and PhSi(OCH(Me)(p-F-C$_6$H$_4$))$_3$ (13%) was identified after 4 h by ^{1}H NMR spectroscopy. Product ratio was determined from the integration of the methylene proton resonances at 4.85 ppm (*PhSiH(OCH(Me)(p-F-C$_6$H$_4$))$_2$*) and 5.01 ppm (*PhSi(OCH(Me)(p-F-C$_6$H$_4$))$_3$*). Unreacted PhSiH$_3$ was also observed at 7.38, 7.07 and 4.23 ppm.

PhSiH(OCH(Me)(p-F-C$_6$H$_4$))$_2$: ^{1}H NMR (benzene-d_6): δ = 7.69 (m, 2H, *phenyl*), 7.19 (m, 3H, *phenyl*), 6.98 (m, 4H, *phenyl*), 6.77 (m, 4H, *phenyl*), 5.22 (s, 1H, Si*H*), 4.85 (m, 2H C*H*), 1.28 (d, J_{H-H} = 6.5 Hz, 6H, C*H$_3$*).

PhSi(OCH(Me)(p-F-C₆H₄))₃: ¹H NMR (benzene-*d₆*, selected resonance): δ = 5.01 (m, 3H, C*H*).

Semimicro scale hydrosilylation of 2',3',4',5',6'-pentafluoroacetophenone: In the glovebox, a benzene-*d₆* (0.7 mL) solution of PhSiH₃ (22.1 μL, 0.179 mmol) and 2',3',4',5',6'- pentafluoroacetophenone (25.5 μL, 0.179 mmol) was added to a vial containing 1.2 mg (0.00179 mmol) of complex **2**. The brown solution was then transferred into a J. Young tube and the progress of the reaction was monitored by ¹H NMR spectroscopy. Complete conversion to a mixture of PhSiH(OCH(Me)(C₆F₅))₂ (75%) and PhSi(OCH(Me)(C₆F₅))₃ (25%) was observed after 3.5 h. Product ratio was determined from the integration of the methylene proton resonances at 5.26 ppm (*PhSiH(OCH(Me)(C₆F₅))₂*) and 5.42 ppm (*PhSi(OCH(Me)(C₆F₅))₃*).

PhSiH(OCH(Me)(C₆F₅))₂: ¹H NMR (benzene-*d₆*): δ = 7.54 (m, 2H, *phenyl*), 7.12-7.09 (m, 3H, *phenyl*), 5.26 (m, 2H, C*H*), 5.09 (s, 1H, Si*H*), 1.38 (d, *J*H-H = 6.4 Hz, 6H, C*H₃*).

PhSi(OCH(Me)(C₆F₅))₃: ¹H NMR (benzene-*d₆*): 7.59 (m, 2H, *phenyl*), 7.15-7.12 (m, 3H *phenyl*), 5.42 (m, 3H, C*H*), 1.33 (d, *J*H-H = 6.4 Hz, 9H, C*H₃*).

Semimicro scale hydrosilylation of 2,2,2-trifluoroacetophenone: In the glovebox, a benzene-*d₆* (0.7 mL) solution of PhSiH₃ (64.6 μL, 0.523 mmol) and 2,2,2-trifluoroacetophenone (71.2 μL, 0.523 mmol) was added to a vial containing 3.5 mg (0.00523 mmol) of complex **2**. The solution, which had turned blue in color, was transferred into a J. Young tube. No reaction was observed within 6 h, after which time the solution became brown in color. A ¹H NMR spectrum collected after 12 h revealed complete conversion to an enantiomeric mixture of PhSi(OCH(CF₃)(Ph))₃. Unreacted

PhSiH$_3$ was found at 7.38, 7.07, and 4.23 ppm. Complete conversion was detected by comparing the aromatic peaks with the starting material.

PhSi(OCH(CF$_3$)(Ph))$_3$: ^{1}H NMR (benzene-d_6): δ = 7.62 (m, 2H, *phenyl*), 7.24 (m, 4H, *phenyl*), 7.03 (m, 8H, *phenyl*), 6.96 (m, 6H, *phenyl*), 5.20 (m, 3H, OC*H*, enantiomeric mixture).

Semimicro scale hydrosilylation of benzophenone: In the glovebox, a benzene-d_6 (0.7 mL) solution of PhSiH$_3$ (36.9 μL, 0.299 mmol) and benzophenone (54.5 mg, 0.299 mmol) was added to a vial containing 2 mg (0.00299 mmol) of complex **2**. The brown solution was then transferred into a J. Young tube and the progress of the reaction was monitored. ^{1}H NMR spectroscopy revealed complete conversion after 20 min at room temperature to a mixture of PhSiH(OCH(Ph)$_2$)$_2$ (87%) and PhSi(OCH(Ph)$_2$)$_3$ (13%). Product ratio was determined from the integration of the methylene proton resonances at 5.94 ppm (PhSi(OCH(Ph)$_2$)$_3$) and 6.05 ppm (PhSi(OCH(Ph)$_2$)$_3$). Unreacted PhSiH$_3$ was found at 7.38, 7.07, and 4.23 ppm.

PhSiH(OCH(Ph)$_2$)$_2$: ^{1}H NMR (benzene-d_6): δ = 7.68 (d, $J_{\text{H-H}}$ = 7.1 Hz, 2H, *phenyl*), 7.30 (d, $J_{\text{H-H}}$ = 7.1 Hz, 8H, *phenyl*), 7.11-7.08 (m, 8H, *phenyl*), 7.05-7.08 (m, 3H, *phenyl*), 7.03 (m, 4H, *phenyl*) 5.94 (s, 2H, C*H*), 5.36 (s, 1H, Si*H*).

PhSi(OCH(Ph)$_2$)$_3$: ^{1}H NMR (benzene-d_6, selected resonance): δ = 6.05 (s, 3H, C*H*).

Semimicro scale hydrosilylation of 2',4',6'-trimethylacetophenone: In the glovebox, a benzene-d_6 (0.7 mL) solution of PhSiH$_3$ (40.6 μL, 0.329 mmol) and 2',4',6'-trimethylacetophenone (54.7 μL, 0.329 mmol) was added to a vial containing 2.2 mg (0.00329 mmol) of complex **2**. The brown solution was then transferred into a J. Young tube and the progress of reaction was monitored over time. After 5 d at room

temperature, analysis by ^{1}H NMR spectroscopy revealed 80% conversion along with the formation of PhSiH(OCH(Me)(Mes))$_2$ as the only product. Unreacted PhSiH$_3$ was observed at 4.23 ppm.

PhSiH(OCH(Me)(Mes))$_2$: ^{1}H NMR (benzene-*d$_6$*): δ = 7.69 (m, 2H, *phenyl*), 7.14-7.09 (m, 3H, *phenyl*), 6.68 (s, 4H, *Mes*), 5.51 (m, 2H, C*H*), 5.21 (s, 1H, Si*H*), 2.30 (m, 12H, *o*-C*H$_3$*), 2.11 (m, 6H, *p*-C*H$_3$*), 1.45 (d, $J_{H\text{-}H}$ = 6.6 Hz, 6H, C*H$_3$*).

Semimicro scale hydrosilylation of 2,4-dimethyl-3-pentanone (1 mol% catalyst): In the glovebox a benzene-*d$_6$* (0.7 mL) solution of PhSiH$_3$ (47.9 µL, 0.389 mmol) and 2,4-dimethyl-3-pentanone (33.9 µL, 0.389 mmol) was added to a vial containing 2.6 mg (0.00389 mmol) of complex **2**. The brown solution was transferred to a J. Young tube and sealed. ^{1}H NMR spectroscopy revealed complete conversion to form PhSiH$_2$(OCH(^{i}Pr)$_2$) (82%) and PhSiH(OCH(^{i}Pr)$_2$)$_2$ (18%) after 36 min at room temperature. Product ratio was determined form the integration of methylene proton resonances at 3.14 ppm (PhSiH$_2$(OCH(^{i}Pr)$_2$) and 3.36 ppm (PhSiH(OCH(^{i}Pr)$_2$)$_2$). Unreacted PhSiH$_3$ was identified at 7.38, 7.07, and 4.23 ppm.

^{1}H NMR (benzene-*d$_6$*): δ = 7.76 (m, 2H, *phenyl*), 7.66 (m, 2H, *phenyl*), 7.20 (m, 3H, *phenyl*), 7.18 (m, 3H, *phenyl*), 5.37 (s, 1H, PhSi*H*(OCH(^{i}Pr)$_2$)$_2$), 5.33 (s, 2H, PhSi*H$_2$*(OCH(^{i}Pr)$_2$)), 3.36 (t, $J_{H\text{-}H}$ = 5.4 Hz, 2H, PhSiH(OC*H*(^{i}Pr)$_2$)$_2$), 3.14 (t, $J_{H\text{-}H}$ = 5.4 Hz, 1H, PhSiH$_2$(OC*H*(^{i}Pr)$_2$), 1.80 (m, 2H, C*H*), 1.74 (m, 4H, C*H*), 1.09 (d, $J_{H\text{-}H}$ = 6.5 Hz, 6H, C*H$_3$*), 0.94 (m, 18H, C*H$_3$*), 0.81 (m, 12H, C*H$_3$*).

Atom-efficient hydrosilylation of 2,4-dimethyl-3-pentanone: In the glovebox, a benzene-*d$_6$* (0.7 mL) solution of PhSiH$_3$ (44.3 µL, 0.359 mmol) and 2,4-dimethyl-3-pentanone (101.7 µL, 0.718 mmol) was added to a vial containing 2.4 mg (0.00359

57

mmol) of complex **2**. The resulting brown solution was transferred to a J. Young tube and the progress of the reaction was monitored over time by NMR spectroscopy. Complete conversion to a mixture of PhSiH(OCH(^{i}Pr)$_2$)$_2$ (90%) and PhSiH$_2$(OCH(^{i}Pr)$_2$) (10%) was observed after 42 min at room temperature. Product ratio was determined from the integration of silane proton resonances at 5.36 ppm (PhSiH(OCH(^{i}Pr)$_2$)$_2$) and 5.33 ppm (PhSiH$_2$(OCH(^{i}Pr)$_2$)).

PhSiH(OCH(^{i}Pr)$_2$)$_2$: ^{1}H NMR (benzene-d_6): δ = 7.76 (m, 2H, *phenyl*), 7.20 (m, 3H, *phenyl*), 5.36 (s, 1H, Si*H*), 3.36 (t, J_{H-H} = 5.6 Hz, 2H, O*CH*), 1.80 (m, 4H, C*H*), 1.08 (d, J_{H-H} = 7.0 Hz, 6H, C*H$_3$*), 0.94 (m, 12H, C*H$_3$*), 0.80 (d, J_{H-H} = 7.0 Hz, 6H, C*H$_3$*).

Semimicro scale hydrosilylation of dicyclohexyl ketone: In the glovebox, a benzene-d_6 (0.7 mL) solution of PhSiH$_3$ (18.5 µL, 0.149 mmol) and dicyclohexyl ketone (30.3 µL, 0.149 mmol) was added to a vial containing 1 mg (0.00149 mmol) of complex **2**. The brown solution was transferred into a J. Young tube, which was sealed under N$_2$. ^{1}H NMR spectroscopy revealed complete conversion to a mixture of PhSiH(OCH(Cy)$_2$)$_2$ (75%) and PhSiH$_2$(OCH(Cy)$_2$) (25%) after 24 h at room temperature. Product ratio was determined form the integration of the methylene proton resonances at 3.47 ppm (PhSiH(OCH(Cy)$_2$)$_2$) and 3.25 ppm (PhSiH$_2$(OCH(Cy)$_2$)). Unreacted PhSiH$_3$ was observed at 7.38, 7.07, and 4.23 ppm.

^{1}H NMR (benzene-d_6): δ = 7.83 (m, 2H, *phenyl*), 7.71 (m, 2H, *phenyl*), 7.24 (m, 3H, *phenyl*), 7.19 (m, 3H, *phenyl*), 5.42 (s, 1H, PhSi*H*(OCH(Cy)$_2$)$_2$), 5.36 (s, 2H, PhSi*H$_2$*(OCH(Cy)$_2$)), 3.47 (t, J_{H-H} = 5.0 Hz, 2H, PhSiH(OC*H*(Cy)$_2$)$_2$), 3.25 (t, J_{H-H} = 5.0 Hz, 1H, PhSiH$_2$(OC*H*(Cy)$_2$)), 2.12 (m), 1.96 (m), 1.84 (m), 1.76-1.68 (broad m), 1.61 (m), 1.52 (m), 1.28-1.18 (m).

Semimicro scale hydrosilylation of cyclohexanone: In the glovebox, a benzene-d_6 (0.7 mL) solution of PhSiH$_3$ (18.5 μL, 0.149 mmol) and cyclohexanone (15 μL, 0.149 mmol) was added to a vial containing 1 mg (0.00149 mmol) of complex **2**. The brown solution was stirred for 4 min and then exposed to air to deactivate the catalyst. The resulting colorless solution was then filtered through a Celite column directly into an NMR tube. After 4 min at room temperature, analysis by ^{1}H NMR spectroscopy revealed complete conversion along with the formation of PhSiH(OCy)$_2$.[7] Unreacted PhSiH$_3$ was observed at 7.38, 7.07, and 4.23 ppm.

PhSiH(OCy)$_2$: ^{1}H NMR (benzene-d_6): δ = 7.86 (m, 2H, *phenyl*), 7.22 (m, 3H, *phenyl*), 5.38 (s, 1H, Si*H*), 3.99 (m, 2H, C*H*), 1.88 (m, 4H, C*H$_2$*), 1.65 (m, 4H, C*H$_2$*), 1.53 (m, 4H, C*H$_2$*), 1.32 (m, 2H, C*H$_2$*), 1.12 (m, 6H, C*H$_2$*).

Neat hydrosilylation of cyclohexanone (0.01 mol% catalyst loading): In the glovebox, a mixture of PhSiH$_3$ (6.46 mL, 52.34 mmol) and cyclohexanone (5.42 mL, 52.34 mmol) was added to a 250 mL round-bottom flask containing 3.5 mg (0.00523 mmol) of complex **2**. Heat generation was noticed during the addition. The mixture was stirred vigorously for 5 minutes, after which time the solution was exposed to air to deactivate the catalyst. The resulting colorless organic was filtered through Celite and the excess silane was removed from the product by rotary evaporation. PhSiH(O(Cy))$_2$[7] (64%) was isolated as the only hydrosilylated product as confirmed by ^{1}H and ^{13}C NMR spectroscopy.

PhSiH(OCy)$_2$: ^{1}H NMR (benzene-d_6): δ = 7.86 (m, 2H, *phenyl*), 7.22 (m, 3H, *phenyl*), 5.38 (s, 1H, Si*H*), 3.99 (m, 2H, C*H*), 1.88 (m, 4H, C*H$_2$*), 1.65 (m, 4H, C*H$_2$*), 1.53 (m, 4H, C*H$_2$*), 1.32 (m, 2H, C*H$_2$*), 1.12 (m, 6H, C*H$_2$*). ^{13}C NMR: δ: 135.48 (*C*, *phenyl*), 134.93

(C*H*, *phenyl*), 130.99 (C*H*, *phenyl*), 128.59 (C*H*, *phenyl*), 72.44 (OC*H*, *Cy*), 36.24 (C*H*$_2$, *Cy*), 26.22 (C*H*$_2$, *Cy*), 24.49 (C*H*$_2$, *Cy*).

Atom-efficient hydrosilylation of cyclohexanone: In the glovebox, a benzene-d_6 (0.7 mL) solution of PhSiH$_3$ (35.1 μL, 0.284 mmol) and cyclohexanone (85.9 μL, 0.852 mmol) was added to a vial containing 1.9 mg (0.00284 mmol) of complex **2**. The resulting brown solution was transferred into a J. Young tube and the progress of the reaction was monitored by NMR spectroscopy. Complete conversion to PhSi(OCy)$_3$[7] was observed after 4 h at room temperature.

Semimicro scale hydrosilylation of 2-hexanone (1 mol% catalyst): In the glovebox, a benzene-d_6 (0.7 mL) solution of PhSiH$_3$ (60.9 μL, 0.494 mmol) and 2-hexanone (60.9 μL, 0.494 mmol) was added to a vial containing 3.3 mg (0.00494 mmol) of complex **2**. The brown solution was stirred for 4 min and then exposed to air to deactivate the catalyst. The resulting colorless solution was then filtered through Celite directly into an NMR tube. ^{1}H NMR spectroscopy revealed complete conversion after 4 min along with the formation of PhSiH(OCH(Me)(^{n}Bu))$_2$ as the only product. Unreacted PhSiH$_3$ was found at 7.38, 7.07, and 4.23 ppm.

PhSiH(OCH(Me)(^{n}Bu))$_2$: ^{1}H NMR (benzene-d_6): δ = 7.81 (m, 2H, *phenyl*), 7.21 (m, 3H, *phenyl*), 5.32 (s, 1H, Si*H*), 4.08 (m, 2H, C*H*), 1.60 (m, 2H, C*H*$_2$), 1.40 (m, 4H, C*H*$_2$), 1.22 (m, 12H, C*H*$_3$), 0.87 (m, 6H, C*H*$_2$).

Neat hydrosilylation of 2-hexanone (0.01 mol% catalyst loading): In the glovebox, a mixture of PhSiH$_3$ (6.64 mL, 53.84 mmol), and cyclohexanone (6.65 mL, 53.84 mmol) was added to a 250 mL round-bottom flask containing 3.6 mg (0.00538 mmol) of complex **2**. The mixture was stirred vigorously for 5 min. During this time significant

60

heat generation was noticed. After 5 min, the mixture was exposed to air to deactivate the catalyst. The resulting colorless organic solution was filtered through Celite and the excess silane was removed from the product by rotary evaporation. PhSiH(OCHMe(^{n}Bu))$_2$ (62%) was isolated as the only hydrosilylated product, as confirmed by ^{1}H and ^{13}C NMR spectroscopy.

^{1}H NMR (benzene-d_6): δ = 7.81 (m, 2H, *phenyl*), 7.21 (m, 3H, *phenyl*), 5.32 (s, 1H, Si*H*), 4.08 (m, 2H, C*H*), 1.60 (m, 2H, C*H$_2$*), 1.40 (m, 4H, C*H$_2$*), 1.22 (m, 12H, C*H$_3$*), 0.87 (m, 6H, C*H$_2$*). ^{13}C NMR (benzene-d_6): δ = 135.40 (*C*, *phenyl*), 134.85 (*C*H, *phenyl*), 130.98 (*C*H, *phenyl*), 128.56 (*C*H, *phenyl*), 70.76 (O*C*H), 39.90 (*C*H$_2$), 28.53 (*C*H$_2$), 24.14 (*C*H$_2$), 23.43 (*C*H$_3$), 14.63 (*C*H$_3$).

Atom-efficient hydrosilylation of 2-hexanone: In the glovebox, a benzene-d_6 (0.7 mL) solution of PhSiH$_3$ (31.4 μL, 0.254 mmol) and 2-hexanone (94.1 μL, 0.762 mmol) was added to a vial containing 1.7 mg (0.00254 mmol) of complex **2**. The resulting brown solution was transferred into a J. Young tube and the progress of the reaction was monitored over time. ^{1}H NMR spectroscopy revealed 74% conversion of 2-hexanone to a mixture of PhSiH(OCH(Me)(^{n}Bu))$_2$ (75%) and PhSi(OCH(Me)(^{n}Bu))$_3$ (25%) after 24 h at room temperature. The conversion of PhSiH(OCH(Me)(^{n}Bu))$_2$ to PhSi(OCH(Me)(^{n}Bu))$_3$ appeared to be slow under these conditions.

Semimicro scale hydrosilylation of methyl acetate: In the glovebox, a benzene-d_6 solution (0.7 mL) of PhSiH$_3$ (73.8 μL, 0.598 mmol) and methyl acetate (47.5 μL, 0.598 mmol) was added to a 20 mL scintillation vial containing 4 mg (0.00598 mmol) of complex **2**. The resulting brown solution was then transferred into a J. Young tube and sealed under N$_2$. The progress of the reaction was monitored by ^{1}H NMR spectroscopy

over time at room temperature. Complete conversion was observed after 24 h, as judged by the disappearance of starting material resonances. A mixture of products containing PhSi(OEt)$_2$(OMe) (35%), PhSi(OMe)$_3$ (26%), PhSi(OEt)$_3$ (21%), and PhSi(OEt)(OMe)$_2$ (18%) was identified by ^{1}H NMR spectroscopy. Product ratio was determined from the integration of ethyl CH$_2$ resonances at 3.87 ppm (PhSi(OEt)$_3$), 3.86 ppm (PhSi(OEt)$_2$(OMe)), and 3.77 ppm (PhSi(OEt)(OMe)$_2$). The methyl proton resonances at 3.53 ppm, 3.51 ppm, and 3.50 ppm were also used.

^{1}H NMR (benzene-d_6): δ = 7.81 (m), 7.24 (m), 7.19-7.13 (m), 3.87 (q, J_{H-H} = 6.8 Hz, 6H, CH_2 for PhSi(OEt)$_3$), 3.86 (q, J_{H-H} = 6.8 Hz, 4H, CH_2 for PhSi(OEt)$_2$(OMe)), 3.77 (q, J_{H-H} = 6.8 Hz, 2H, CH_2 for PhSi(OEt)(OMe)$_2$), 3.53 (s, CH_3), 3.51 (s, CH_3), 3.50 (s, CH_3), 1.20-1.15 (m), 1.13 (m).

Unreacted phenylsilane was found at 7.38, 7.09 and 4.23 ppm. A trace of dihydrosilylated products PhSiH(OMe)$_2$ and PhSiH(OEt)$_2$ were also noticed.

Semimicro scale hydrosilylation of ethyl acetate: In the glovebox, a benzene-d_6 solution (1 mL) of PhSiH$_3$ (44.3 μL, 0.359 mmol) and ethyl acetate (35.2 μL, 0.359 mmol) was injected into a 20 mL scintillation vial containing 2.4 mg (0.00359 mmol) of complex **2**. The resulting brown solution was then transferred into a J. Young tube and the progress of the reaction was monitored by ^{1}H NMR spectroscopy at room temperature. Complete conversion was observed after 5.5 h, as judged by the disappearance of ethyl acetate resonances and the identification of PhSi(OCH$_2$CH$_3$)$_3$ as the lone product.

PhSi(OCH$_2$CH$_3$)$_3$: ^{1}H NMR 400 MHz (benzene-*d*$_6$): δ = 7.87 (m, 2H, *phenyl*), 7.23 (m, 3H, *phenyl*), 3.85 (q, *J*$_{H-H}$ = 7.1 Hz, 6H, C*H*$_2$), 1.17 (t, *J*$_{H-H}$ = 7.0 Hz, 9H, C*H*$_3$). A small amount of PhSiH$_3$ was found at 7.38, 7.07 and 4.23 ppm.

Semimicro scale hydrosilylation of isopropyl acetate: In the glovebox, a benzene-*d*$_6$ solution (1 mL) of PhSiH$_3$ (55.3 μL, 0.449 mmol) and isopropyl acetate (52.6 μL, 0.449 mmol) was added to a 20 mL scintillation vial containing 3 mg (0.00449 mmol) of complex **2**. The resulting brown solution was then transferred to a J. Young tube and sealed under N$_2$. The progress of the reaction was monitored by NMR spectroscopy over time while the tube was heated at 80 °C. Complete conversion was observed after 3 d, as judged by the disappearance of isopropyl acetate ^{1}H NMR resonances. A mixture of products including PhSi(OEt)$_3$ (36%), PhSiH(O^{i}Pr)$_2$ (28%), PhSiH(OEt)$_2$ (18%), and PhSi(O^{i}Pr)$_3$ (18%) was observed by ^{1}H NMR spectroscopy. ^{1}H NMR (benzene-*d*$_6$): δ = 7.86 (m), 7.77 (m), 7.21 (m), 5.26 (s, Si*H*), 5.23 (s, Si*H*), 4.32 (m, *CH,* O^{i}Pr), 4.19 (m, *CH,* O^{i}Pr), 3.84 (q, C*H*$_2$, OEt), 3.75 (m, , C*H*$_2$, OEt), 1.22-1.115 (m), 1.12 (m). Silane proton resonances at 5.26 ppm and 5.23 ppm along with ethyl peaks at 3.84 ppm and 3.75 ppm and the isopropyl CH peaks at 4.32 ppm and 4.19 ppm were used to determine the product ratio.

Semimicro scale hydrosilylation of phenyl acetate: In the glovebox, a benzene-*d*$_6$ solution (1 mL) of PhSiH$_3$ (44.3 μL, 0.359 mmol) and phenyl acetate (45.7 μL, 0.359 mmol) was added to a 20 mL scintillation vial containing 2.4 mg (0.00359 mmol) of complex **2**. The resulting brown solution was then transferred into a J. Young tube and the progress of the reaction was monitored by NMR spectroscopy over time at room temperature. After 10 d, 95% of the phenyl acetate had been hydrosilylated to form a

mixture of products including PhSi(OPh)$_3$ (36%), PhSi(OEt)$_3$ (36%), and PhSi(OEt)$_2$(OPh) (28%). Ethyl CH$_2$ resonances at 3.87 ppm (PhSi(OEt)$_3$) and 3.86 ppm (PhSi(OEt)$_2$(OPh)) were used to determine the product ratio. In addition, aromatic peaks (*Ph*Si) at 7.15 ppm, 7.13 ppm and 7.03 ppm were also used.

^{1}H NMR (benzene-d_6): δ = 7.88 (m, *phenyl*), 7.15 (m, *phenyl*), 7.13 (m, *phenyl*), 7.03 (m, *phenyl*), 6.80 (m, *phenyl*), 3.87 (q, J_{H-H} = 7.1 Hz, 6H, C*H$_2$* for PhSi(OEt)$_3$), 3.86 (q, J_{H-H} = 7.1 Hz, 4H, C*H$_2$* for PhSi(OEt)$_2$(OPh)), 1.12 (t, J_{H-H} = 6.8 Hz, 9H, C*H$_3$* for PhSi(OEt)$_3$), 1.06 (t, J_{H-H} = 6.8 Hz, 6H, C*H$_3$* for PhSi(OEt)$_2$(OPh)).

Semimicro scale hydrosilylation of *tert*-butyl acetate: In the glovebox, a benzene-d_6 solution (1 mL) of PhSiH$_3$ (36.9 μL, 0.299 mmol) and *tert*-butylacetate (40.4 μL, 0.299 mmol) was added to a 20 mL scintillation vial containing 2 mg (0.00299 mmol) of complex **2**. The resulting brown solution was then transferred to a J. Young tube. The progress of the reaction was monitored by NMR spectroscopy over time while it was heated at 80 ^{o}C. After heating for 10 d, 85% of the *tert*-butylacetate had been transformed into mixture of products including PhSiH(O^{t}Bu)$_2$ (36%), PhSiH(OEt)(O^{t}Bu) (36%), and PhSi(OEt)$_3$ (28%). Silane proton resonances at 5.46 ppm (PhSiH(O^{t}Bu)$_2$) and 5.35 ppm (PhSiH(OEt)(O^{t}Bu)) along with the ethyl CH$_2$ resonances at 3.85 ppm (PhSi(OEt)$_3$) and 3.73 ppm (PhSiH(OEt)(O^{t}Bu)) were used to determine the product ratio.

^{1}H NMR (benzene-d_6): δ = 7.88 (m, 2H, *phenyl*), 7.82 (m, 2H, *phenyl*), 7.79 (m, 2H, *phenyl*), 7.25-7.20 (m, 9H, *phenyl*), 5.46 (s, 1H, Si*H* for PhSiH(O^{t}Bu)$_2$), 5.35 (s, 1H, Si*H* for PhSiH(OEt)(O^{t}Bu)), 3.85 (q, J_{H-H} = 6.8 Hz, 6H, C*H$_2$* for PhSi(OEt)$_3$), 3.73 (q, J_{H-H} = 6.8 Hz, 2H, C*H$_2$* for PhSiH(OEt)(O^{t}Bu)), 1.37 (s, 9H, C*H$_3$*), 1.31 (s, 18H, C*H$_3$*), 1.17 (t,

J_{H-H} = 7.1 Hz, 9H, CH_3), 1.13 (t, J_{H-H} = 7.1 Hz, 3H, CH_3). Unreacted phenylsilane was found at 7.39, 7.09 and 4.23 ppm.

Semimicro scale deuterosilylation of methyl acetate using PhSiD$_3$ in benzene-d_6: In the glovebox, a benzene-d_6 solution (1 mL) of PhSiD$_3$ (16.63 mg, 0.149 mmol) and methyl acetate (11.8 μL, 0.149 mmol) was added to a 20 mL scintillation vial containing 5 mg (0.00748 mmol) of complex **2**. The resulting brown solution was then transferred to a sealed J. Young tube. The progress of the reaction was monitored by ^{1}H NMR spectroscopy over time at room temperature and complete conversion was detected after 24 h. A mixture of products including PhSi(OCD$_2$CH$_3$)$_3$, PhSi(OMe)$_3$, PhSi(OCD$_2$CH$_3$)$_2$(OMe), and PhSi(OCD$_2$CH$_3$)(OMe)$_2$ were identified by ^{1}H NMR spectroscopy. ^{1}H NMR (benzene-d_6): δ = 7.83 (m), 7.23 (m), 7.19-7.13 (m), 3.87 (q, J_{H-H} = 6.8 Hz, 6H, CH_2 for PhSi(OEt)$_3$), 3.86 (q, J_{H-H} = 6.8 Hz, 4H, CH_2 for PhSi(OEt)$_2$(OMe)), 3.77 (q, J_{H-H} = 6.8 Hz, 2H, CH_2 for PhSi(OEt)(OMe)$_2$), 3.51 (s, CH_3), 3.50 (s, CH_3), 3.48 (s, CH_3), 1.15 (broad m), 1.13 (m). Unreacted phenylsilane-d_3 was observed at 7.38, and 7.08 ppm.

Semimicro scale deuterosilylation of methyl acetate using PhSiD$_3$ in benzene: In the glovebox, a benzene solution (1 mL) of PhSiD$_3$ (16.63 mg, 0.149 mmol) and methyl acetate (11.8 μL, 0.149 mmol) was added to a 20 mL scintillation vial containing 5 mg (0.00748 mmol) of complex **2**. The resulting brown solution was then transferred into a J. Young tube and a drop of benzene-d_6 wad added. The progress of the reaction was monitored by ^{2}H NMR spectroscopy over time at room temperature and complete conversion was detected after 24 h. ^{2}H NMR (benzene): δ: 3.78 (broad m). Unreacted phenylsilane-d_3 was found at 4.22 ppm.

Homogeneity Test: In the glovebox, a mixture of PhSiH$_3$ (0.369 mL, 2.991 mmol) and acetophenone (0.349 mL, 2.991 mmol) was injected into a 100 mL round bottom flask containing Hg (29.99 g, 149.55 mmol). To this mixture complex **2** (2 mg, 0.002991 mmol) was added and the resulting brownish mixture was stirred vigorously for 4 min. After 4 min it was exposed to air to deactivate the catalyst. The resulting colorless organic was pipetted out carefully and filtered through Celite column. ^{1}H NMR spectroscopy in benzene-d_6 revealed complete conversion of acetophenone into a mixture of PhSiH(OCH(Me)(Ph))$_2$ (82%) and PhSi(OCH(Me)(Ph))$_3$ (18%).

General method of hydrosilylation of aldehydes using 0.1 mol% catalyst: In the glove box a 20 mL scintillation vial was charged with 0.0022 g of (^{Ph_2PPr}PDI)Mn **(2)** (0.00329 mmol). An equimolar mixture of PhSiH$_3$ and the aldehyde was injected to it. The resulting solution was stirred for 2 min while it was vigorously bubbling and generating heat. Then the solution was exposed to oxygen to deactivate the catalyst. The colorless solution obtained was filtered through Celite and subjected to ^{1}H NMR to determine the conversion. It was followed by hydrolysis upon stirring with 2 mL of 10% aqueous NaOH solution for 2 h. Organic layer was extracted with diethyl ether (5 x 2 mL) and dried over anhydrous Na$_2$SO$_4$ and diethyl ether was evaporated in a rotary evaporator at 40 °C to isolate the corresponding alcohol. The alcohols were characterized by ^{1}H and ^{13}C NMR spectroscopy.

General method of hydrosilylation of aldehydes using 0.01 mol% catalyst: In the glove box a 100 mL round bottom flask was charged with 0.0022 g of (^{Ph_2PPr}PDI)Mn **(2)** (0.00329 mmol). To the catalyst, an equimolar mixture of PhSiH$_3$ and the aldehyde was added. The resulting solution was stirred for 2 min while it was intensely bubbling and

generating heat. Then the solution was exposed to oxygen to deactivate the catalyst. The colorless solution obtained was filtered through Celite and subjected to ^{1}H NMR to determine the conversion. It was followed by hydrolysis upon stirring with 2 mL of 10% aqueous NaOH solution for 2 h. Organic layer was extracted with diethyl ether (5 x 2 mL) and dried over anhydrous Na_2SO_4 and diethyl ether was evaporated in a rotary evaporator at 40 °C to isolate the corresponding alcohol. The alcohols were characterized by ^{1}H and ^{13}C NMR spectroscopy.

General method of hydrosilylation of formates using 0.02 mol% catalyst: In the glove box a 100 mL round bottom flask was charged with 0.002 g of (^{Ph_2PPr}PDI)Mn (0.00329 mmol). To the catalyst, an equimolar mixture of PhSiH$_3$ and formate was added. The resulting solution was stirred for 15 min while it was bubbling and generating heat. Then the solution was exposed to oxygen to deactivate the catalyst. The colorless solution obtained was filtered through Celite and subjected to ^{1}H NMR to determine the conversion. Then the siloxane mixture was hydrolyzed using 2 mL 10% aq. NaOH for 2 h. The organic fraction was extracted with Et$_2$O (3 x 2 mL) and dried over anhydrous Na$_2$SO$_4$. Finally dried in a rotavap to isolate the corresponding heavy alcohols.

Hydrosilylation of benzaldehyde catalyzed by 0.1 mol% of 2: In the glove box, a mixture of PhSiH$_3$ (0.369 mL, 2.991 mmol) and benzaldehyde (0.304 mL, 2.991 mmol) was added to 0.002 g (0.002991 mmol) of **2** pre-weighed in a 20 mL vial. The resulting brown solution was vigorously bubbling and became hot. It was stirred for 2 min and then exposed to air to deactivate the catalyst. The colorless solution was filtered through Celite and ^{1}H NMR was recorded to determine the percent conversion. It was followed by a hydrolytic work up while the mixture was stirred with 2 mL aqueous 10% NaOH

solution at room temperature for 2 h. The organic fraction was extracted with diethylether (4 x 3 mL) and dried over anhydrous Na_2SO_4. Removal of the diethylether on a rotavap at 35-38 °C afforded colorless oil identified as benzyl alcohol (0.381 g, 94%).

Hydrosilylation of 4-fluorobenzaldehyde catalyzed by 0.1 mol% of 2: In the glove box, a mixture of $PhSiH_3$ (0.277 mL, 2.243 mmol) and 4-fluorobenzaldehyde (0.242 mL, 2.243 mmol) was added to 0.0015 g (0.002243 mmol) of **2** pre-weighed in a 20 mL vial. The resulting brown solution was vigorously bubbling and became hot. It was stirred for 2 min and then exposed to air to deactivate the catalyst. The colorless solution was filtered through Celite and ^{1}H NMR was recorded to determine the percent conversion. It was followed by a hydrolytic work up while the mixture was stirred with 2 mL aqueous 10% NaOH solution at room temperature for 2 hours. The organic fraction was extracted with diethylether (4x3 mL) and dried over anhydrous Na_2SO_4. Removal of the diethylether on a rotavap at 35-38 °C afforded colorless oil identified as 4-fluorobenzyl alcohol (0.253 g, yield = 89%).

Hydrosilylation of 4-chlorobenzaldehyde catalyzed by 0.1 mol% of 2: In the glove box, a mixture of $PhSiH_3$ (0.369 mL, 2.991 mmol) and 4-chlorobenzaldehyde (0.420 g, 2.991 mmol) in 0.5 mL of toluene was added to 0.002 g (0.002991 mmol) of **2** pre-weighed in a 20 mL vial. The resulting brown solution was vigorously bubbling and became hot. It was stirred for 2 min and then exposed to air to deactivate the catalyst. The colorless solution was filtered through Celite and ^{1}H NMR was recorded to determine the percent conversion. It was followed by a hydrolytic work up while the mixture was stirred with 2 mL aqueous 10% NaOH solution at room temperature for 2 h. The organic fraction was extracted with diethylether (4 x 3 mL) and dried over anhydrous Na_2SO_4.

Removal of the diethylether on a rotavap at 35-38 °C afforded white solid identified as 4-chlorobenzyl alcohol (0.379 g, 88%).

Hydrosilylation of 4-bromobenzaldehyde catalyzed by 0.1 mol% of 2: In the glove box, a mixture of $PhSiH_3$ (0.369 mL, 2.991 mmol) and 4-bromobenzaldehyde (0.553 g, 2.991 mmol) in 0.5 mL toluene was added to 0.002 g (0.002991 mmol) of **2** pre-weighed in a 20 mL vial. The resulting brown solution was vigorously bubbling and became hot. It was stirred for 2 min and then exposed to air to deactivate the catalyst. The colorless solution was filtered through Celite and ^{1}H NMR was recorded to determine the percent conversion. It was followed by a hydrolytic work up while the mixture was stirred with 2 mL aqueous 10% NaOH solution at room temperature for 2 h. The organic fraction was extracted with diethylether (4 x 3 mL) and the organic layer was dried over anhydrous Na_2SO_4. Removal of the diethylether on a rotavap at 35-38 °C afforded white solid identified as 4-bromoobenzyl alcohol (0.461 g, 92%).

Hydrosilylation of 4-iodobenzaldehyde catalyzed by 0.1 mol% of 2: In the glove box, a mixture of $PhSiH_3$ (0.369 mL, 2.991 mmol) and 4-iodobenzaldehyde (0.694 g, 2.991 mmol) in 0.5 mL toluene was added to 0.002 g (0.002991 mmol) of **2** pre-weighed in a 20 mL vial. The resulting brown solution became slightly warm. It was stirred for 2 min and then exposed to air to deactivate the catalyst. The colorless solution was filtered through Celite and ^{1}H NMR was recorded, which showed only 32% conversion.

Hydrosilylation of 4-cyanobenzaldehyde catalyzed by 0.1 mol% of 2: In the glove box, a mixture of $PhSiH_3$ (0.369 mL, 2.991 mmol) and 4-cyanobenzaldehyde (0.392 g, 2.991 mmol) in 0.5 mL of diethylether was added to 0.002 g (0.002991 mmol) of **2** pre-weighed in a 20 mL vial. The resulting brown solution was vigorously bubbling and

became hot. It was stirred for 2 min and then exposed to air to deactivate the catalyst. The colorless solution was filtered through Celite and ^{1}H NMR was recorded to determine the percent conversion. It was followed by a hydrolytic work up while the mixture was stirred with 2 mL aqueous 10% NaOH solution at room temperature for 2 h. The organic fraction was extracted with diethylether (4 x 3 mL) and dried over anhydrous Na_2SO_4. Removal of the diethylether on a rotavap at 35-38 °C afforded white solid identified as 4-cyanobenzyl alcohol (0.376 g, 79%).

Hydrosilylation of *p*-tolualdehyde catalyzed by 0.1 mol% of 2: In the glove box, a mixture of PhSiH$_3$ (0.369 mL, 2.991 mmol) and *p*-tolualdehyde (0.353 mL, 2.991 mmol) was added to 0.002 g (0.002991 mmol) of **2** pre-weighed in a 20 mL vial. The resulting brown solution was vigorously bubbling and became hot. It was stirred for 2 min and then exposed to air to deactivate the catalyst. The colorless solution was filtered through Celite and ^{1}H NMR was recorded to determine the percent conversion. It was followed by a hydrolytic work up while the mixture was stirred with 2 mL aqueous 10% NaOH solution at room temperature for 2 h. The organic fraction was extracted with diethylether (4 x 3 mL) and dried over anhydrous Na_2SO_4. Removal of the diethylether on a rotavap at 35-38 °C afforded white solid identified as 4-methylbenzyl alcohol (0.395 g, 90%).

Hydrosilylation of *p*-anisaldehyde catalyzed by 0.1 mol% of 2: In the glove box, a mixture of PhSiH$_3$ (0.369 mL, 2.991 mmol) and *p*-anisaldehyde (0.342 mL, 2.991 mmol) was added to 0.002 g (0.002991 mmol) of **2** pre-weighed in a 20 mL vial. The resulting brown solution was vigorously bubbling and became hot. It was stirred for 2 min and then exposed to air to deactivate the catalyst. The colorless solution was filtered through Celite and ^{1}H NMR was recorded to determine the percent conversion. It was followed

by a hydrolytic work up while the mixture was stirred with 2 mL aqueous 10% NaOH solution at room temperature for 2 h. The organic fraction was extracted with diethylether (4 x 3 mL) and dried over anhydrous Na_2SO_4. Removal of the diethylether on a rotavap at 35-38 °C afforded colorless oil identified as 4-methoxybenzyl alcohol (0.337 g, 81%).

Hydrosilylation of 2-nitrobenzaldehyde catalyzed by 0.1 mol% of 2: In the glove box, a mixture of $PhSiH_3$ (0.369 mL, 2.991 mmol) and 2-nitrobenzaldehyde (0.452 g, 2.991 mmol) in 0.5 mL of toluene was added to 0.002 g (0.002991 mmol) of **2** pre-weighed in a 20 mL vial. The resulting brown solution was vigorously bubbling and became hot. It was stirred for 2 min and then exposed to air to deactivate the catalyst. The colorless solution was filtered through Celite and ^{1}H NMR was recorded to determine the percent conversion. It was followed by a hydrolytic work up while the mixture was stirred with 2 mL aqueous 10% NaOH solution at room temperature for 2 h. The organic fraction was extracted with diethylether (4 x 3 mL) and dried over anhydrous Na_2SO_4. Removal of the diethylether on a rotavap at 35-38 °C afforded pale yellow solid identified as 2-nitrobenzyl alcohol (0.330 g, 72%).

Hydrosilylation of 2-naphthaldehyde catalyzed by 0.1 mol% of 2: In the glove box, a mixture of $PhSiH_3$ (0.369 mL, 2.991 mmol) and 2-naphthaldehyde (0.467 g, 2.991 mmol) in 0.5 mL of diethylether was added to 0.002 g (0.002991 mmol) of **2** pre-weighed in a 20 mL vial. The resulting brown solution was vigorously bubbling and became hot. It was stirred for 2 min and then exposed to air to deactivate the catalyst. The colorless solution was filtered through Celite and ^{1}H NMR was recorded to determine the percent conversion. It was followed by a hydrolytic work up while the mixture was stirred with 2 mL aqueous 10% NaOH solution at room temperature for 2 h. The organic fraction was

extracted with diethylether (4 x 3 mL) and dried over anhydrous Na_2SO_4. Removal of the diethylether on a rotavap at 35-38 °C afforded white solid identified as 2-naphthol (0.364 g, 77%).

Hydrosilylation of pyridine-3-carbaldehyde catalyzed by 0.1 mol% of 2: In the glove box, a mixture of $PhSiH_3$ (0.369 mL, 2.991 mmol) and pyridine-3-carbaldehyde (0.281 mL, 2.991 mmol) was added to 0.002 g (0.002991 mmol) of **2** pre-weighed in a 20 mL vial. The resulting brown solution was vigorously bubbling and became hot. It was stirred for 2 min and then exposed to air to deactivate the catalyst. The colorless solution was filtered through Celite and ^{1}H NMR was recorded to determine the percent conversion. It was followed by a hydrolytic work up while the mixture was stirred with 2 mL aqueous 10% NaOH solution at room temperature for 2 h. The organic fraction was extracted with diethylether (4 x 3 mL) and dried over anhydrous Na_2SO_4. Removal of the diethylether on a rotavap at 35-38 °C afforded yellow oil identified as pyridine-3-carbinol (0.065 g, 27%).

Hydrosilylation of furfural catalyzed by 0.1 mol% of 2: In the glove box, a mixture of $PhSiH_3$ (0.369 mL, 2.991 mmol) and furfural (0.248 mL, 2.991 mmol) was added to 0.002 g (0.002991 mmol) of **2** pre-weighed in a 20 mL vial. The resulting brown solution was vigorously bubbling and became hot. It was stirred for 2 min and then exposed to air to deactivate the catalyst. The colorless solution was filtered through Celite and ^{1}H NMR was recorded to determine the percent conversion. It was followed by a hydrolytic work up while the mixture was stirred with 2 mL aqueous 10% NaOH solution at room temperature for 2 h. The organic fraction was extracted with diethylether (4 x 3 mL) and

dried over anhydrous Na_2SO_4. Removal of the diethylether on a rotavap at 35-38 °C afforded yellow oil identified as furfuryl alcohol (0.234 g, 89%).

Hydrosilylation of 3-cyclohexene-1-carboxaldehyde catalyzed by 0.1 mol% of 2: In the glove box, a mixture of $PhSiH_3$ (0.369 mL, 2.991 mmol) and 3-cyclohexene-1-carboxaldehyde (0.339 mL, 2.991 mmol) was added to 0.002 g (0.002991 mmol) of **2** pre-weighed in a 20 mL vial. The resulting brown solution was vigorously bubbling and became hot. It was stirred for 2 min and then exposed to air to deactivate the catalyst. The colorless solution was filtered through Celite and ^{1}H NMR was recorded to determine the percent conversion. It was followed by a hydrolytic work up while the mixture was stirred with 2 mL aqueous 10% NaOH solution at room temperature for 2 h. The organic fraction was extracted with diethylether (4 x 3 mL) and dried over anhydrous Na_2SO_4. Removal of the diethylether on a rotavap at 35-38 °C afforded pale yellow oil identified as 3-cyclohexene-1-carbinol (0.291 g, 87%).

Hydrosilylation of citral catalyzed by 0.1 mol% of 2: In the glove box, a mixture of $PhSiH_3$ (0.369 mL, 2.991 mmol) and citral (0.0.509 mL, 2.991 mmol) was added to 0.002 g (0.002991 mmol) of **2** pre-weighed in a 20 mL vial. The resulting brown solution was vigorously bubbling and became hot. It was stirred for 2 min and then exposed to air to deactivate the catalyst. The colorless solution was filtered through Celite and ^{1}H NMR was recorded to determine the percent conversion. It was followed by a hydrolytic work up while the mixture was stirred with 2 mL aqueous 10% NaOH solution at room temperature for 2 h. The organic fraction was extracted with diethylether (4 x 3 mL) and dried over anhydrous Na_2SO_4. Removal of the diethylether on a rotavap at 35-38 °C afforded pale yellow oil identified as geraniol (0.381 g, 82%).

Benzyl alcohol: ^{1}H NMR (400 MHz, benzene-d_6): δ = 7.24 – 7.12 (m, 4H), 7.08 (m, 1H), 4.32 (s, 2H). ^{13}C NMR (101 MHz, benzene-d_6): δ = 128.90, 127.80, 127.29, 110.79, 65.24.

4-Fluorobenzyl alcohol: ^{1}H NMR (400 MHz, benzene-d_6): δ = 6.94 (d, J = 2.1, 2H), 6.79 (t, J = 8.7, 2H), 4.21 (s, 2H). ^{13}C NMR (101 MHz, benzene-d_6): δ = 164.16, 161.69, 137.52, 115.78, 64.25.

4-Chlorobenzyl alcohol: ^{1}H NMR (400 MHz, benzene-d_6): δ = 7.09 (d, J = 8.3, 2H), 6.84 (d, J = 8.1, 2H), 4.09 (d, J = 5.3, 2H), 1.06 (s, 1H). ^{13}C NMR (101 MHz, benzene-d_6): δ = 140.58, 133.44, 129.02, 128.56, 64.27.

4-Bromobenzyl alcohol: ^{1}H NMR (400 MHz, benzene-d_6): δ = 7.24 (d, J = 8.3, 2H), 6.77 (d, J = 8.2, 2H), 4.07 (s, 2H), 1.36 (s, 1H). ^{13}C NMR (101 MHz, benzene-d_6): δ = 140.94, 131.98, 128.90, 121.66, 64.41

4-Cyanobenzyl alcohol: ^{1}H NMR (500 MHz, benzene-d_6): δ = 7.00 (d, J = 8.2, 2H), 6.77 (d, J = 7.9, 2H), 4.05 (d, J = 16.6, 2H), 1.23 (s, 1H). ^{13}C NMR (126 MHz, benzene-d_6): δ = 147.07, 132.37, 127.02, 119.45, 111.73, 64.08.

4-Methylbenzyl alcohol: ^{1}H NMR (400 MHz, benzene-d_6): δ = 7.12 (d, J = 7.8, 2H), 6.99 (d, J = 7.8, 2H), 4.35 (d, J = 4.9, 2H), 2.12 (s, 3H), 1.49 (s, 1H). ^{13}C NMR (101 MHz, benzene-d_6): δ = 139.35, 137.20, 129.62, 127.52, 65.29, 21.46.

4-Methoxybenzyl alcohol: ^{1}H NMR (400 MHz, benzene-d_6): δ = 7.21 – 7.07 (m, 2H), 6.85 – 6.68 (m, 2H), 4.38 (s, 2H), 3.32 (s, 3H), 2.56 (s, 1H). ^{13}C NMR (101 MHz, benzene-d_6): δ = 159.85, 134.35, 129.05, 114.44, 65.01, 55.15.

2-Nitrobenzyl alcohol: ^{1}H NMR (400 MHz, benzene-d_6): δ = 7.63 (d, J = 8.2, 1H), 7.36 (d, J = 7.8, 1H), 6.93 (t, J = 7.6, 1H), 6.66 (t, J = 7.8, 1H), 4.54 (s, 2H), 1.51 (s, 1H). ^{13}C NMR (101 MHz, benzene-d_6): δ = 137.98, 133.68, 129.20, 127.99, 124.95, 62.27.

2-Naphthol: ^{1}H NMR (400 MHz, benzene-d_6): δ = 7.99 – 7.95 (m, 1H), 7.68 (s, 1H), 7.58 (d, J = 8.7, 1H), 7.53 (dd, J = 5.8, 3.6, 1H), 7.40 (dd, J = 8.4, 1.5, 1H), 7.25 – 7.21 (m, 3H), 5.06 (d, J = 9.7, 2H), 4.45 (s, 0H). ^{13}C NMR (101 MHz, benzene-d_6): δ = 138.37, 135.86, 134.27, 133.78, 131.46, 131.10, 128.80, 128.77, 128.66, 126.61, 126.31, 126.08, 125.75, 66.03.

Pyridine-3-carbinol: ^{1}H NMR (400 MHz, benzene-d_6): δ = 8.47 (d, J = 1.4, 1H), 8.22 (d, J = 4.8, 1H), 7.36 (d, J = 7.8, 1H), 6.72 (dd, J = 7.7, 4.9, 1H), 5.28 (s, 1H), 4.41 (s, 2H). ^{13}C NMR (101 MHz, benzene-d_6): δ = 148.70, 148.52, 138.35, 135.29, 123.94, 62.29.

Furfuryl alcohol: ^{1}H NMR (400 MHz, benzene-d_6): δ = 7.08 – 7.02 (m, 1H), 6.05 – 6.01 (m, 1H), 5.96 (t, J = 3.6, 1H), 4.22 (d, J = 5.2, 2H), 1.28 (s, 1H). ^{13}C NMR (126 MHz, benzene-d_6): δ = 155.39, 142.64, 110.84, 107.71, 57.73.

3-Cyclohexene-1-methanol: ^{1}H NMR (500 MHz, benzene-d_6) δ = 5.74 – 5.57 (m, 2H), 3.26 (s, 2H), 2.12 – 1.82 (m, 4H), 1.78 – 1.54 (m, 3H), 1.36 (s, 1H), 1.18 (dq, J = 11.9, 8.0, 1H). ^{13}C NMR (126 MHz, benzene-d_6): δ = 127.60, 126.74, 67.92, 37.03, 28.81, 25.91, 25.39.

Geraniol: ^{1}H NMR (400 MHz, benzene-d_6): δ = 5.52 – 5.33 (m, 1H), 5.25 – 5.06 (m, 1H), 4.05 (dd, J = 3.8, 2.8, 2H), 2.11 (dd, J = 15.0, 7.1, 1H), 2.00 (dd, J = 14.2, 4.9, 3H), 1.68 – 1.60 (m, 4H), 1.53 (s, 2H), 1.51 (d, J = 3.8, 3H). ^{13}C NMR (101 MHz, benzene-d_6): δ = 138.45, 131.97, 126.38, 125.42, 59.66, 40.40, 32.67, 27.39, 26.18, 24.01, 17.7.

Hydrosilylation of benzyl formate using 0.02 mol% of 2: In an inert atmosphere, a 100 mL round bottom flask was charged with 0.0021 g (0.00314 mmol) of **2**. A neat mixture of PhSiH$_3$ (1.94 mL, 15.70 mmol) and benzyl formate (1.96 mL, 15.70 mmol) was added to the flask and stirred at ambient temperature for 15 min during which time vigorous bubbling and heat generation was noticed. After 15 min the reaction mixture was exposed to air to deactivate the catalyst. ^{1}H NMR after filtration through Celite showed complete consumption of starting material. Then 2 mL of 10% aq. NaOH was added to the colorless solution to hydrolyze the siloxane mixture. The organic fraction was then extracted with Et$_2$O (3 x 2 mL) and the combined organic layers were dried over anhydrous Na$_2$SO$_4$. Solvent was removed using a rotavap to isolate pure benzyl alcohol (1.49 g, 13.81 mmol, yield = 88%).

PhCH$_2$OH: ^{1}H NMR, benzene-*d$_6$*, δ = 7.20-7.14 (m, 4H, *Ph*), 7.08 (m, 1H, *Ph*), 4.35 (s, 2H, C*H$_2$*).

Hydrosilylation of phenyl ethyl formate using 0.02 mol% of 2: In an inert atmosphere, a 100 mL round bottom flask was charged with 0.0014 g (0.00209 mmol) of **2**. A neat mixture of PhSiH$_3$ (1.3 mL, 10.47 mmol) and phenyl ethyl formate (149 mL, 10.47 mmol) was added to the flask and stirred at ambient temperature for 15 min during which time vigorous bubbling and heat generation was noticed. After 15 min the reaction mixture was exposed to air to deactivate the catalyst. ^{1}H NMR after filtration through Celite showed complete consumption of starting material. Then 2 mL of 10% aq. NaOH was added to the colorless solution to hydrolyze the siloxane mixture. The organic fraction was then extracted with Et$_2$O (3 x 2 mL) and the combined organic layers were

dried over anhydrous Na_2SO_4. Solvent was removed using a rotavap to isolate pure 2-phenyl ethanol (1.1 g, 9.004 mmol, yield = 86%).

PhCH2CH$_2$OH: ^{1}H NMR, benzene-d_6, δ = 7.13-7.11 (m, 2H, *Ph*), 7.08-7.00 (m, 3H, *Ph*), 3.48 (t, 2H, C*H$_2$*), 2.54 (t, 2H, C*H$_2$*). ^{13}C NMR, benzene-d_6: δ = 129.69, 129.03, 128.46, 126.86, 63.67, 40.36.

Hydrosilylation of *p*-anisyl formate using 0.02 mol% of 2: In an inert atmosphere, a 100 mL round bottom flask was charged with 0.0024 g (0.00359 mmol) of **2**. A neat mixture of PhSiH$_3$ (2.21 mL, 17.95 mmol) and *p*-anisyl formate (2.88 mL, 17.95mmol) was added to the flask and stirred at ambient temperature for 1 h. ^{1}H NMR after filtration through Celite showed < 2% conversion.

Hydrosilylation of hexyl formate using 0.02 mol% of 2: In an inert atmosphere, a 100 mL round bottom flask was charged with 0.0026 g (0.00389 mmol) of **2**. A neat mixture of PhSiH$_3$ (2.4 mL, 19.44 mmol) and hexyl formate (2.8 mL, 19.44 mmol) was added to the flask and stirred at ambient temperature for 15 min during which time vigorous bubbling and heat generation was noticed. After 15 min the reaction mixture was exposed to air to deactivate the catalyst. ^{1}H NMR after filtration through Celite showed complete consumption of starting material. Then 2 mL of 10% aq. NaOH was added to the colorless solution to hydrolyze the siloxane mixture. The organic fraction was then extracted with Et$_2$O ()3 x 2 mL) and the combined organic layers were dried over anhydrous Na2SO4. Solvent was removed using a rotavap to isolate pure 1-hexanol (1.23 g, 12.03 mmol, yield = 62%).

CH$_3$(CH$_2$)$_4$CH$_2$OH: ^{1}H NMR, benzene-d_6, δ = 3.41 (t, 2H, C*H$_2$*), 1.94 (bs, 1H, *OH*), 1.38 (m, 2H, C*H$_2$*), 1.20 (s, 6H, C*H$_2$*), 0.88 (t, 3H, C*H$_3$*). ^{13}C NMR, benzene-d_6: δ =

Hydrosilylation of isoamyl formate using 0.02 mol% of 2: In an inert atmosphere, a 100 mL round bottom flask was charged with 0.0021 g (0.00314 mmol) of **2**. A neat mixture of PhSiH$_3$ (1.937 mL, 15.70 mmol) and isoamyl formate (2.07 mL, 15.70 mmol) was added to the flask and stirred at ambient temperature for 15 min during which time vigorous bubbling and heat generation was noticed. After 15 min the reaction mixture was exposed to air to deactivate the catalyst. ^{1}H NMR after filtration through Celite showed complete consumption of starting material. Then 2 mL of 10% aq. NaOH was added to the colorless solution to hydrolyze the siloxane mixture. The organic fraction was then extracted with Et$_2$O (3 x 2 mL) and the combined organic layers were dried over anhydrous Na$_2$SO$_4$. Solvent was removed using a rotavap to isolate pure isoamyl alcohol (0.788 g, 8.93 mmol, yield = 57%).

(CH$_3$)$_2$CHCH$_2$CH$_2$OH: ^{1}H NMR, benzene-d_6, δ = 3.44 (m, 2H, C*H$_2$*), 1.62 (m, 1H, C*H*), 1.31 (m, 2H, C*H$_2$*), 0.83 (d, 6H, C*H$_3$*). ^{13}C NMR, benzene-d_6: δ = 61.23 (*CH$_2$*OH), 42.36 (*CH$_2$*), 25.26 (*CH*), 23.21 (*CH$_3$*).

Hydrosilylation of geranyl formate using 0.02 mol% of 2: In an inert atmosphere, a 100 mL round bottom flask was charged with 0.002 g (0.002991 mmol) of **2**. A neat mixture of PhSiH$_3$ (1.845 mL, 14.96 mmol) and geranyl formate (2.98 mL, 14.96 mmol) was added to the flask and stirred at ambient temperature for 1 h. After 1 h the reaction mixture was exposed to air to deactivate the catalyst. ^{1}H NMR after filtration through Celite showed < 2% conversion.

Procedure for the determination of maximum TON for aldehyde hydrosilylation: In the glove box, a round bottom flask was charged with 0.0015 g (0.002243 mmol) of **1**. A mixture of 2.768 mL (22.43 mmol) of PhSiH$_3$ and 2.280 mL (22.43 mmol) of

benzaldehyde was added to the flask and stirred for 2 min. The mixture became hot and a brown solution was formed. The solution was cooled to room temperature. Similiarly, another four consecutive additions of 10000 equivalents of PhSiH$_3$ and benzaldehyde were done over 80 minutes. Finally, the pale brown mixture was exposed to air to deactivale the catalyst. ^{1}H NMR spectrum of the mixture revealed a 63% conversion of the total 50000 equivalents of substrates resulting in a TON of 31500.

2.10. References:

1. (a) Marciniec, B. *Hydrosilylation: A Comprehensive review on recent advances*. Springer, Berlin, Germany, **2010**. (b) Marciniec, B.; Guliñski, J. *J. Orgmet. Chem.* **1993**, *446*, 15-23. (c) Shaikh, N. S.; Junge, K.; Beller, M. *Org. Lett.* **2007**, *9*, 5429-5432.

2. (a) Enthaler, S.; Junge, K.; Beller, M. *Angew. Chem. Int. Ed.* **2008**, *47*, 3317-3321. (b) Troegel, D.; Stohrer, J. *Coord. Chem. Rev.* **2011**, *255*, 1440-1450. (c) Díez-González, S.; Nolan, S. P. *Org. Prep. Proc. Int.* **2007**, *39*, 523-529. (d) Shaikh, N. S.; Enthaler, S.; Junge, K.; Beller, M. *Angew. Chem. Int. Ed.* **2008**, *47*, 2497-2501.

3. (a) Speier, J. L. *Adv. Orgmet. Chem.* **1979**, *17*, 407-447. (b) Chatterjee, B.; Gunanathan, C. *Chem. Commun.* **2014**, *50*, 888-890. (c) Lewis, L. N.; Stein, J.; Gao, Y. Colborn, R. E.; Hutchins, G. *Platinum Metals Rev.* **1997**, *41*, 66-75. (d) Karstedt, B. D. *Platinum Complexes of Unsaturated Siloxanes and Platinum Containing Organopolysiloxanes*. **1973**.

4. For leading Fe catalysts see: (a) Ruddy, A. J.; Kelly, C. M.; Crawford, S. M.; Wheaton, C. A.; Sydora, O. L.; Small, B. L.; Stradiotto, M.; Turculet, L. *Organometallics* **2013**, *32*, 5581−5588. (b) Yang, J.; Tilley, T. D. *Angew. Chem., Int. Ed.* **2010**, *49*, 10186−10188. (c) Blom, B.; Enthaler, S.; Inoue, S.; Irran, E.; Driess, M. *J. Am. Chem. Soc.* **2013**, *135*, 6703−6713. (c) Bhattacharya, P.; Krause, J. A.; Guan, H. *Organometallics* **2011**, *30*, 4720−4729. (e) Kandepi, V. V. K. M.; Cardoso, J. M. S.; Peris, E.; Royo, B. *Organometallics* **2010**, *29*, 2777−2782. (f) Tondreau, A. M.; Darmon, J. M.; Wile, B. M.; Floyd, S. K.; Lobkovsky, E.; Chirik, P. J. *Organometallics* **2009**, *28*, 3928− 3940. (g) Tondreau, A. M.; Lobkovsky, E.; Chirik, P. J. *Org. Lett.* **2008**, *10*, 2789−2792.

5. For leading Co examples, see: (a) Zhou, H.; Sun, H.; Zhang, S.; Li, X. *Organometallics* **2015**, *34*, 1479−1486. (b) Niu, Q.; Sun, H.; Li, X.; Klein, H.-F.; Flörke, U. *Organometallics* **2013**, *32*, 5235−5238. (c) Sauer, D. C.; Wadepohl, H.; Gade, L. H. *Inorg. Chem.* **2012**, *51*, 12948−12958. (d) Yu, F.; Zhang, X.-C.; Wu, F.-F.; Zhou, J.-N.; Fang, W.; Wu, J.; Chan, A. S. C. *Org. Biomol. Chem.* **2011**, *9*, 5652. (e) Brunner, H.;

Amberger, K. J. *Organomet. Chem*. **1991**, *417*, C63− C65. (f) Nesbit, M. A.; Suess, D. L. M.; Peters, J. C. *Organometallics* **2015**, *34*, 4741.

6. For leading Ni examples, see: (a) Porter, T. M.; Hall, G. B.; Groy, T. L.; Trovitch, R. J. *Dalton Trans*. **2013**, *42*, 14689−14692. (b) Bheeter, L. P.; Henrion, M.; Brelot, L.; Darcel, C.; Chetcuti, M. J.; Sortais, J.-B.; Ritleng, V. *Adv. Synth. Catal*. **2012**, *354*, 2619−2624. (c) Postigo, L.; Royo, B. *Adv. Synth. Catal*. **2012**, *354*, 2613−2618. (d) Tran, B. L.; Pink, M.; Mindiola, D. J. *Organometallics* **2009**, *28*, 2234−2243. (e) Chakraborty, S.; Krause, J. A.; Guan, H. *Organo- metallics* **2009**, *28*, 582−586 and references cited therein. (f) MacMil- lan, S. N.; Hill Harman, W.; Peters, J. C. *Chem. Sci*. **2014**, *5*, 590−597. (g) Steiman, T. J.; Uyeda, C. *J. Am. Chem. Soc*. **2015**, *137*, 6104−6110.

7. For leading Cu examples, see: (a) Roy, S. R.; Sau, S. C.; Mandal, S. K. *J. Org. Chem*. **2014**, *79*, 9150−9160. (b) Albright, A.; Gawley, R. E. *J. Am. Chem. Soc*. **2011**, *133*, 19680−19683. (c) Yu, F.; Zhou, J.-N.; Zhang, X.-C.; Sui, Y.-Z.; Wu, F.-F.; Xie, L.-J.; Chan, A. S. C.; Wu, J. *Chem. - Eur. J*. **2011**, *17*, 14234−14240. (d) Zhang, X.-C.; Wu, F.-F.; Li, S.; Zhou, J.-N.; Wu, J.; Li, N.; Fang, W.; Lam, K. H.; Chan, A. S. C. *Adv. Synth. Catal*. **2011**, *353*, 1457−1462. (e) Díez-Gonzaĺez, S.; Escudero-Adań,E.;Benet-Buchholz,J.;Stevens,E.D.;Slawin,A.M. Z.; Nolan, S. P. *Dalton Trans*. **2010**, *39*, 7595−7606. (f) Fujihara, T.; Semba, K.; Terao, J.; Tsuji, Y. *Angew. Chem., Int. Ed*. **2010**, *49*, 1472− 1476. (g) Mostefaï, N.; Sirol, S.; Courmarcel, J.; Riant, O. *Synthesis* **2007**, 1265−1271.(h) Díez-Gonzaĺez, S.;Scott, N.M.;Nolan, S. P. Organometallics **2006**, 25, 2355−2358. (i) Lipshutz, B. H.; Lower, A.; Kucejko, R. J.; Noson, K. *Org. Lett*. **2006**, *8*, 2969−2972. (j) Díez- Gonzaĺez, S.; Kaur, H.; Zinn, F. K.; Stevens, E. D.; Nolan, S. P. *J. Org. Chem*. **2005**, *70*, 4784−4796. (k) Wu, J.; Ji, J.-X.; Chan, A. S. C. *Proc. Natl. Acad. Sci. U. S. A*. **2005**, *102*, 3570−3575. (l) Lee, D.; Yun, J. *Tetrahedron Lett*. **2004**, *45*, 5415−5417. (m) Kaur, H.; Zinn, F. K.; Stevens, E. D.; Nolan, S. P. *Organometallics* **2004**, *23*, 1157−1160. (n) Lipshutz, B. H.; Noson, K.; Chrisman, W.; Lower, A. *J. Am. Chem. Soc*. **2003**, *125*, 8779−8789. (o) Lipshutz, B. H.; Noson, K.; Chrisman, W. *J. Am. Chem. Soc*. **2001**, *123*, 12917−12918. (p) Sirol, S.; Courmarcel, J.; Mostefai, N.; Riant, O. *Org. Lett*. **2001**, *3*, 4111−4113. (q) Brunner, H.; Miehling, W. *J. Organomet. Chem*. **1984**, *275*, C17− C21.

8. For leading Zn catalysts, see: (a) Rit, A.; Zanardi, A.; Spaniol, T. P.; Maron, L.; Okuda, J. *Angew. Chem., Int. Ed*. **2014**, *53*, 13273− 13277. (b) Lummis, P. A.; Momemi, M. R.; Lui, M. W.; McDonald, R.; Ferguson, M. J.; Miskolzie, M.; Brown, A.; Rivard, E. *Angew. Chem., Int. Ed*. **2014**, *53*, 9347−9351. (c) Łowicki, D.; Bezłada, A.; Mlynarski, J. *Adv. Synth. Catal*. **2014**, *356*, 591−595. (d) Boone, C.; Korobkov, I.; Nikonov, G. I. *ACS Catal*. **2013**, *3*, 2336−2340. (e) Pang, S.; Peng, J.; Li, J.; Bai, Y.; Xiao, W.; Lai, G. *Chirality* **2013**, *25*, 275−280. (f) Enthaler, S.; Schröder, K.; Inoue, S.; Eckhardt, B.; Junge, K.; Beller, M.; Drieβ, M. *Eur. J. Org. Chem*. **2010**, *2010*, 4893−4901. (g) Gajewy, J.; Kwit, M.; Gawroński, J. *Adv. Synth. Catal*. **2009**, *351*, 1055−1063. (h)Geŕard, S.; Pressel, Y.; Riant, O. *Tetrahedron: Asymmetry* **2005**, *16*, 1889−1891. (i) Bette, V.; Mortreux, A.; Savoia, D.; Carpentier, J.-F. *Adv. Synth. Catal*. **2005**, *347*, 289−302. (j) Bette, V.; Mortreux, A.; Savoia, D.; Carpentier, J.-F. *Tetrahedron* **2004**, *60*, 2837−2842.

(k) Mastranzo, V. M.; Quintero, L.; Anaya de Parrodi, C. A.; Juaristi, E.; Walsh, P. J. *Tetrahedron* **2004**, *60*, 1781−1789. (l) Mimoun, H. *J. Org. Chem*. **1999**, *64*, 2582−2589. (m) Sattler, W.; Ruccolo, S.; Rostami Chaijan, M.; Nasr Allah, T.; Parkin, G. *Organometallics* **2015**, *34*, 4717.

9. (a) R. I. Khusnutdinov, A. R. Bayguzina, U. M. Dzhemilev, *Russ. J. Org. Chem.* **2012**, *48*, 309-348. (b) R. J. Trovitch, *Synlett* **2014**, *25*, 1638-1642. (c) Valyaev, D. A.; Lavigne, G.; Lugan, N. *Coord. Chem. Rev.* **2016**, *308*, 191-235.

10. B. T. Gregg, P. K. Hanna, E. J. Crawford, A. R. Cutler, *J. Am. Chem. Soc.* **1991**, *113*, 384-385.

11. (a) M. B. Cavanaugh, B. T. Gregg, A. R. Cutler, *Organometallics* **1996**, *15*, 2764-2769. (b) Z. Mao, B. T. Gregg, A. R. Cutler, *J. Am. Chem. Soc.* **1995**, *117*, 10139-10140.

12. S. U. Son, S-J. Paik, I. S. Lee, Y-A. Lee, Y. K. Chung, *Organometallics* **1999**, *18*, 4114-4118.

13. S. U. Son, S-J. Paik, Y. K. Chung, *J. Mol. Catal. A: Chem.* **2007**, *151*, 87-90.

14. V. K. Chidara, G. Du, *Organometallics* **2013**, *32*, 5034-5037.

15. Mukhopadhyay, T. K.; Flores, M.; Groy, T. L.; Trovitch, R. J. *J. Am. Chem. Soc.* **2014**, *136*, 882-885.

16. Ghosh, C; Mukhopadhyay, T. K.; Flores, M.; Groy, T. L.; Trovitch, R. J. *Inorg. Chem.* **2015**, *54*, 10398-10406.

17. Mukhopadhyay, T. K.; Groy, T. L.; Trovitch, R. J. *J. Am. Chem. Soc. (manuscript in preparation)*.

18. LeBlanc, F. A.; Piers, W.; Parvez, M. *Angew. Chem., Int. Ed*. **2014**, *53*, 789−792.

19. Berk, S. C.; Kreutzer, K. A.; Buchwald, S. L. *J. Am. Chem. Soc*. **1991**, *113*, 5093−5095.

20. Le Bideau, F.; Henique, J.; Samuel, E.; Elschenbroich, C. *Chem. Commun*. **1999**, 1397−1398.

CHAPTER 3

MECHANISTIC INVESTIGATION OF BIS(IMINO)PYRIDINE MANGANESE

CATALYZED CARBONYL AND CARBOXYLATE HYDROSILYLATION

3.1. Abstract:

We recently reported a bis(imino)pyridine (or pyridine diimine, PDI) manganese precatalyst, (^{Ph2PPr}PDI)Mn (**2**), which is active for the hydrosilylation of ketones and dihydrosilylation of esters. It was also shown in Chapter 2 that **2** can hydrosilylate aldehydes and formates with unprecedented TOFs. In this chapter, we describe concurrent mechanisms of **1**-mediated hydrosilylation through which catalysis is achieved. Under stoichiometric and catalytic conditions, addition of PhSiH$_3$ to (^{Ph2PPr}PDI)Mn was found to result in partial conversion to the diamagnetic hydride complex, (^{Ph2PPr}PDI)MnH (**2-H**), which was independently prepared in Chapter 1. When 2,2,2-trifluoroacetophenone was added to **2**, radical transfer yielded (^{Ph2PPr}PDI·)Mn(OC·(Ph)(CF$_3$)) (**4**), which undergoes intramolecular C-C formation to form the respective Mn(II) dimer, [(μ-O,N_{py}-4-OC(CF$_3$)(Ph)-4-H-^{Ph2PPr}PDI)Mn]$_2$ (**5**). Upon finding **4** to be inefficient and **5** to be inactive, kinetic trials were conducted to elucidate the mechanisms of **2**- and **2-H**-mediated hydrosilylation. Varying precatalyst (**2** or **2-H**), substrate, and PhSiH$_3$ concentrations revealed a first order dependence on each reagent. A kinetic isotope effect (KIE) of 2.2 was observed for **2** when conducting the hydrosilylation of 2,4-dimethyl-3-pentanone, suggesting Si-H(D) bond activation precludes the rate determining step. Although kinetic trials revealed **2** to be the more active precatalyst for carbonyl hydrosilylation, a concurrent **2-H**-mediated pathway is

more efficient for ester hydrosilylation. A higher KIE of 4.2 was noticed in the case of **2-H** catalyzed hydrosilylation of 2,4-dimethyl-3-pentanone. Considering our experimental and computational observations, **2**-catalyzed hydrosilylation is believed to proceed through a modified Ojima mechanism, while **2-H**-mediated hydrosilylation occurs via insertion. The first order kinetic profile for each pathway affords an additive rate expression and the role of PDI chelate non-innocence throughout catalysis is discussed.

3.2. Introduction:

Hydrosilylation catalysts have long been used to mediate Si-C and Si-O bond formation in an atom-efficient fashion.[1] Since Speier's initial report of chloroplatinic acid-catalyzed olefin hydrosilylation,[2] precious metal catalysts have been relied upon for the production of silicone adhesives, rubbers, and release coatings.[3] Olefin hydrosilylation is known to proceed through the Chalk-Harrod mechanism, which features Si-H oxidative addition, alkene insertion into M-H, and reductive elimination of the respective alkylsilane.[4] A modified Chalk-Harrod mechanism featuring alkene insertion into M-SiR$_3$ has also been documented to account for the formation of unsaturated biproducts.[5] Conversely, Si-O formation by way of carbonyl hydrosilylation has emerged as a mild route to alcohols that can be conducted in a stereoselective manner.[6] In the presence of monohydrosilanes, precious metal catalysts including Wilkinson's catalyst[7] are believed to mediate carbonyl hydrosilylation via the Ojima Mechanism (Fig. 3.1), whereby Si-H oxidative addition, carbonyl insertion into M-SiR$_3$, and reductive elimination yields the respective silyl ether.[8] Recent investigations have

suggested that electrophilic silylene intermediates are responsible for Rh-catalyzed carbonyl reduction in the presence of dihydro- and trihydrosilanes.[9] Similarly, σ-silane complexes of Ru and Ir are believed to mediate carbonyl hydrosilylation by promoting substrate nucleophilic attack at Si.[10]
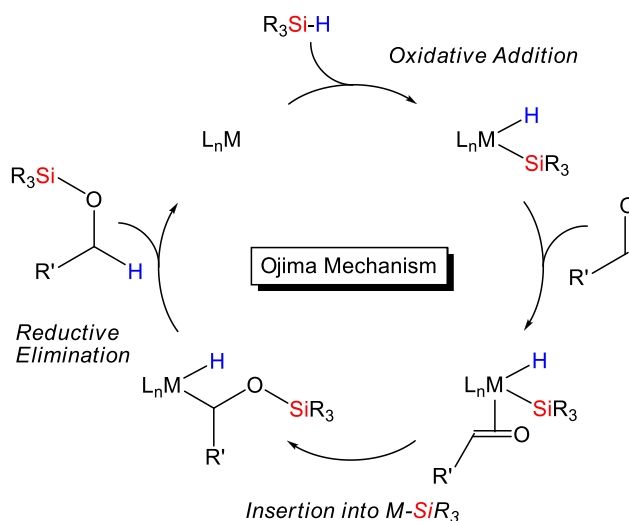
Figure 3.1. Ojima mechanism for carbonyl hydrosilylation.

As precious metal catalyzed hydrosilylation pathways have been extensively studied, efforts to develop low-cost 1st row metal hydrosilylation catalysts have only recently started to intensify.[11-16] Base metal catalysts are advantageous from a cost and toxicity perspective;[17] however, they can be difficult to study since they tend to engage in one electron reaction pathways and often adopt high-spin electronic configurations.[18] This has led to a relative dearth of mechanistic information regarding 1st row metal carbonyl hydrosilylation, while the catalysts which have been thoroughly investigated are believed to operate through widely varied mechanisms.[19] For example, although a fair number of Mn-based hydrosilylation catalysts have been reported,[20] their mechanisms

84

have either not been described or are poorly understood. Furthermore, it is unclear whether low-valent Mn^0,[21] Mn^I,[22] and Mn^{II} catalysts[23] proceed via similar or different mechanisms than each other or the lone high-valent Mn catalyst that has been described, $(3,5\text{-}^tBu_2\text{-salen})MnN$.[24]

In 2014, we reported that formally zerovalent ($^{Ph2PPr}PDI$)Mn (**2**) achieves ketone hydrosilylation TOFs of up to 76,800 h^{-1} (more accurately expressed as 1,280 min^{-1}) and ester dihydrosilylation TOFs of up to 18 h^{-1} under ambient conditions.[25] Also, in Chapter 2, an expanded scope with higher activities for **2**-mediated aldehyde (TOF up to 4950 min^{-1}) and formate (TOF up to 330 min^{-1}) hydrosilylation have been shown. This chapter will describe the details of the operable mechanism via a comprehensive kinetic analysis that suggests concurrent modified Ojima and Mn-H insertion mechanisms are responsible for catalysis. With an updated understanding of catalyst electronic structure and reactivity, the role of PDI chelate redox non-innocence throughout catalysis is also discussed.

3.3. Possible pathways:

Achieving such higher efficiencies for carbonyl and carboxylate hydrosilylation, determination of the operative mechanism has been sought. Knowing that **1** possesses one unpaired electron ($S = 1/2$) on the Mn center, it is reasonable to think of either (i) a radical chain mechanism or (ii) a radical transfer mechanism. Also, a Si-H oxidative addition pathway as proposed by Ojima *et al.*, can not be excluded. Although it seems difficult in this case to attain a Mn(IV) intermediate after Si-H oxidative addition,

considering the redox non-innocence of our ligand this is a potential possibility. In order to gain insight a set of controlled catalytic and stoichiolmetric reactions were conducted. When a radical initiator AIBN ($t_{1/2}$ = 1 h at 85 °C) was employed as catalyst for the hydrosilylation of benzaldehyde and 2,4-dimethyl-3-pentanone no conversion was observed even after 2 h at 90 °C, which argues against a radical initiated pathway. This fact was further confirmed by the absence of any silyl coupled dimer after catalysis, which is supposed to be the termination product of silyl radical.

3.4. Stoichiometric silane addition:

The next controlled experiment was performed by adding one equivalent of PhSiH$_3$ to complex **2** in benzene-d_6 solution (Scheme 3.1), which resulted in 20% conversion to a hydride complex **(2-H)** as monitored by ^{1}H NMR in 24 h, identified from a typical triplet resonance at -2.98 ppm. Independent synthesis and characterization of complex **2-H** have already been described in Chapter 1 (Scheme 1.5).
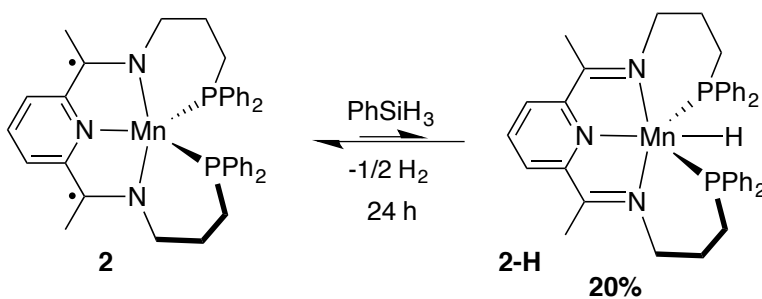
Scheme 3.1. Observation of (^{Ph2PPr}PDI)MnH (**2-H**) from silane addition to **2**.

The qualitative electronic structures of **2** and **2-H** indicate low spin Mn(II) and Mn(III) center respectively that feature a doubly reduced PDI^{2-} chelate. Density functional theory (DFT) calculations reveal that **2** and **2-H** feature atypical electronic

structures arising from triplet PDI chelate antiferromagnetic coupling to intermediate spin Mn. Our preliminary electronic structure investigation of **2** suggested that this complex possesses a low-spin Mn(II) center (S_{Mn} = ½) that is supported by a singlet ^{Ph_2PPr}PDI dianion. Furthermore, we proposed that the unpaired spin on Mn might allow catalysis to occur following electron transfer to the incoming carbonyl substrate. Based on exhaustive DFT, reactivity, and kinetic studies related to **1**-mediated carbonyl and carboxylate hydrosilylation, we are humbled to report that our preliminary electronic structure and mechanistic predictions are no longer preferred.

3.5. Stoichiometric ketone addition:

During ketone hydrosilylation screening, an unusual blue color formation was noticed when 2,2,2-trifluoroacetophenone is added to a benzene-d_6 solution of **2**.[25] Interestingly, when one equivalent of 2,2,2-trifluoroacetophenone was added to a benzene solution of **2**, an instantaneous color change from brown to deep blue occurred. The blue complex **(4)** was found to feature paramagnetically broadened resonances in ^{1}H NMR spectroscopy. A solution state magnetic moment of 4.4 μ_B was obtained for **4**, which implies three unpaired spins on Mn that is antiferromagnetically coupled to ligand based electrons. An electronic spectrum was collected for complex **4**, which shows two absorption maxima at 360 nm (ε = 3504 $M^{-1}cm^{-1}$) and 612 nm (ε = 3573 $M^{-1}cm^{-1}$) as a result of charge transfer transitions. Complex **4** can be proposed as a radical transfer alkoxide complex (^{Ph_2PPr}PDI·)Mn(OC·(Ph)(CF$_3$)) with κ^4-*N,N,N,*P-chelated Mn as shown in Scheme 3.2. A lack of informative spectroscopic data for **4** called for crystallographic characterization. Surprisingly, in an attempt to crystallize **4** from a concentrated THF

87

solution at -35 °C, amber crystals suitable for X-ray diffraction were obtained. The solid-state structure of the amber complex [(μ-O,N_{py}-4-OC(CF$_3$)(Ph)-4-H-^{Ph_2PPr}PDI)Mn]$_2$ (**5**) is shown in Figure 3.2, revealed a dimeric Mn complex with a new C-C bond formed via intramolecular coupling of ketone based radical anion and the *p*-pyridine of adjacent molecule. Complex **5** features a distorted trigonal bipyramid geometry with a κ^4-*N,N,N,P*-chelate around Mn, which further supports the presumed description of **4** as (^{Ph_2PPr}PDI·)Mn(OC·(Ph)(CF$_3$)).
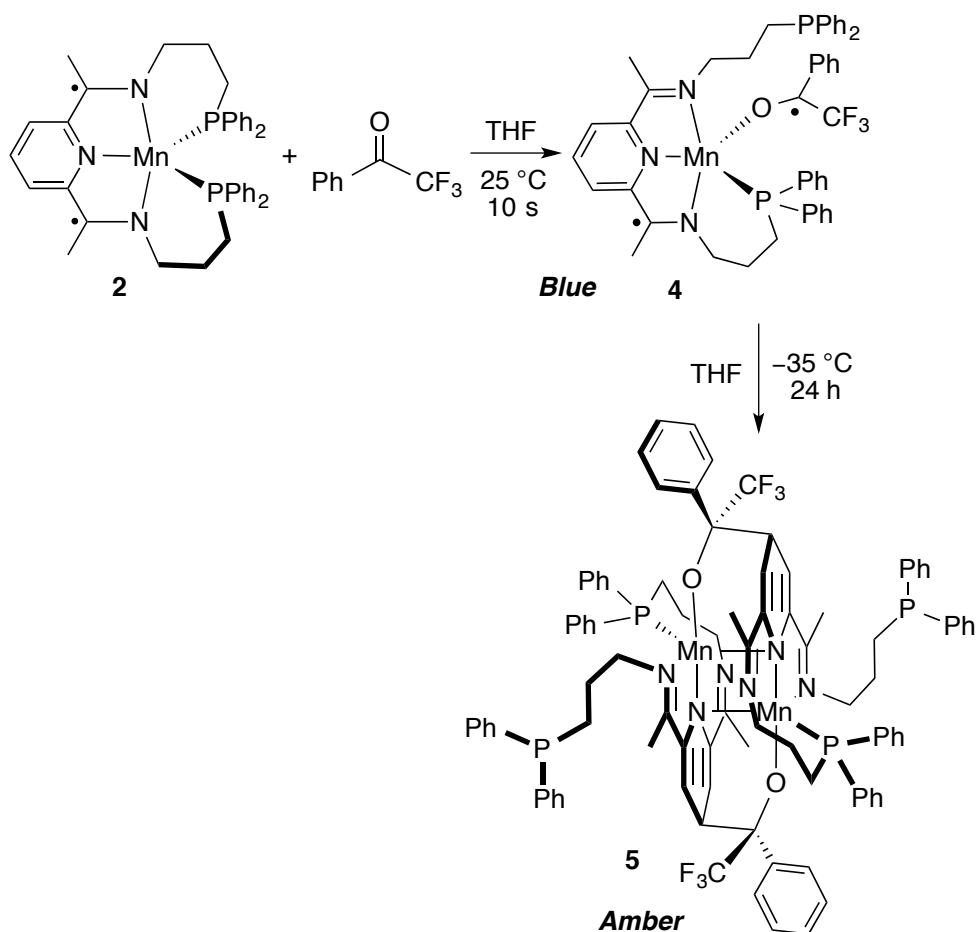
Scheme 3.2. Stoichiometric addition of 2,2,2-trifluoroacetophenone to **2** and subsequent formation of radical coupled dimer (**5**).
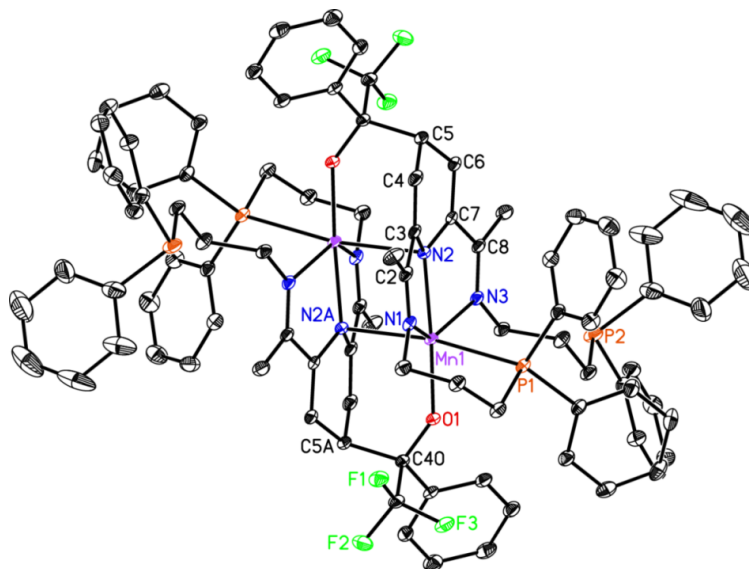
Figure 3.2. The solid-state structure of **5** shown at 30% probability ellipsoids. Hydrogen atoms and co-crystallized solvent molecules are omitted for clarity.

Table 3.1. Relevant bond lengths (Å) and angles (°) for **5**.

Mn(1)-N(1)	2.302(3)	C(7)-N(2)	1.388(3)
Mn(1)-N(2)	2.161(3)	C(3)-C(4)	1.348(3)
Mn(1)-N(3)	2.270(3)	C(4)-C(5)	1.506(4)
Mn(1)-P(1)	2.805(4)	C(5)-C(6)	1.503(3)
Mn(1)-N(2A)	2.428(3)	C(6)-C(7)	1.354(4)
Mn(1)-O(1)	2.023(4)	N(2)-Mn(1)-O(1)	174.28(4)
C(2)-N(1)	1.289(4)	N(2)-Mn(1)-P(1)	103.19(4)
C(8)-N(3)	1.290(3)	N(1)-Mn(1)-N(3)	139.34(3)
C(2)-C(3)	1.486(3)	N(1)-Mn(1)-P(1)	73.26(4)
C(7)-C(8)	1.483(3)	N(1)-Mn(1)-O(1)	111.79(4)
C(3)-N(2)	1.388(3)	P(1)-Mn(1)-O(1)	82.21(4)

Since this radical coupling required electron transfer from the imine π^* bonds to the central pyridine ring to generate a new C-C bond, the imine bonds (average C=N bond distance is 1.29 Å, Table 3.1) retain double bond character and the C_{imine}-$C_{pyridine}$ bonds become single bonds (average distance is 1.48 Å). Notably, the aromaticity of the central pyridine ring is also destroyed as a consequence as the C(3)-C(4), C(4)-C(5), C(5)-C(6), and C(6)-C(7) distances are 1.348(3), 1.506(4), 1.503(3), and 1.354(4) Å

respectively. The Mn(1)-N$_{PDI}$ and Mn(1)-P(1) distances are consistent with a high spin Mn center. Although there is not sufficient spectroscopic information for **5** due to its extreme insolubility, it is believed that this complex possesses a high spin Mn(II) center with five unpaired spin.

3.6. Kinetic analysis:

3.6.1. Catalyst comparison:

With the exclusion of radical chain mechanism and the observations of **2-H**, **4**, and **5** it is obvious to question whether the operative pathway consists of a radical transfer to the ketone or Si-H oxidative addition. Similar radical transfer from Co/Zr heterobimetallic complex to benzophenone was reported by Zhou *et al.* and it was also shown that the mechanism involves a ketyl radical which undergoes concerted homolytic cleavage in presence of silane to generate silyl ethers.[26] However, in our case it has been found that **4** requires more than 48 h to react with PhSiH$_3$ to produce the corresponding silyl ether and the diimer **5** does not react to PhSiH$_3$, which are strong evidences against a radical transfer process. Moreover, when **4**-catalyzed hydrosilylation of 2,4-dimethyl-3-pentanone was carried out under identical condition as **2**, a 12-fold smaller rate (Figure 3.3) has been noticed compared to **2**-catalyzed reaction. Extreme insolubility of **5** did not allow to obtain a concentration profile for this reaction. These facts clearly rule out the involvement of a radical transfer complex in the catalytic cycle.
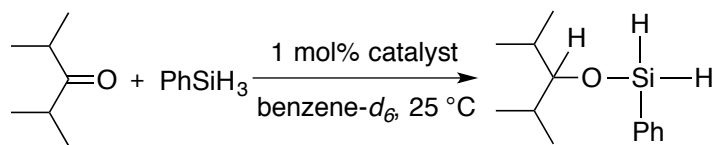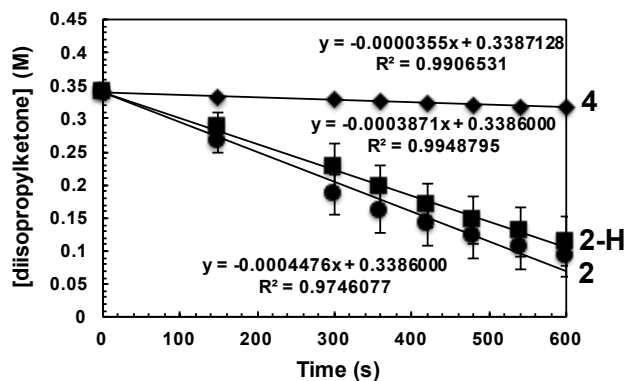
Figure 3.3. Catalyst comparison plot for the hydrosilylation of 2,4-dimethyl-3-pentanone catalyzed by 1 mol% of **2** (●), **2-H** (■), and **4** (◆).

3.6.2. Rate law determination for 2-catalyzed hydrosilylation:

With the exclusion of radical catalyzed pathway and radical transfer mechanism, a rigorous kinetic analysis was performed on **2**-catalyzed hydrosilylation to establish a rate law. The hydrosilylation of 2,4-dimethyl-3-pentanone was studied using 1 mol% of **2** at varying concentration of ketone while fixing the concentration of other reagents and catalyst. The rate of ketone consumption was monitored by ^{1}H NMR data collection over time for six different concentrations with respect to anisole as an internal standard and every reaction was run in triplicate. A first order rate dependence on the ketone concentration has been found and shown in Figure 3.4 A. Variation of silane concentration and catalyst concentration also displayed a linear dependence to the observed rate (Figure 3.4 B and C respectively). In a similar method **2**-catalyzed ester hydrosilylation was investigated. When isopropyl formate was hydrosilylated using 1 mol% of **2** under varying concentrations of formate, $PhSiH_3$, and **2**, exactly same trend has been noticed (Figure 3.4. D, E, and F). Therefore, the rate expressions for **2**-catalyzed ketone and formate hydrosilylation can be formulated as:

$$\text{Rate} = k_{obs}[\textbf{2}][\text{ketone}][PhSiH_3] \quad \text{and} \quad \text{Rate} = k_{obs}[\textbf{2}][\text{formate}][PhSiH_3]$$

91
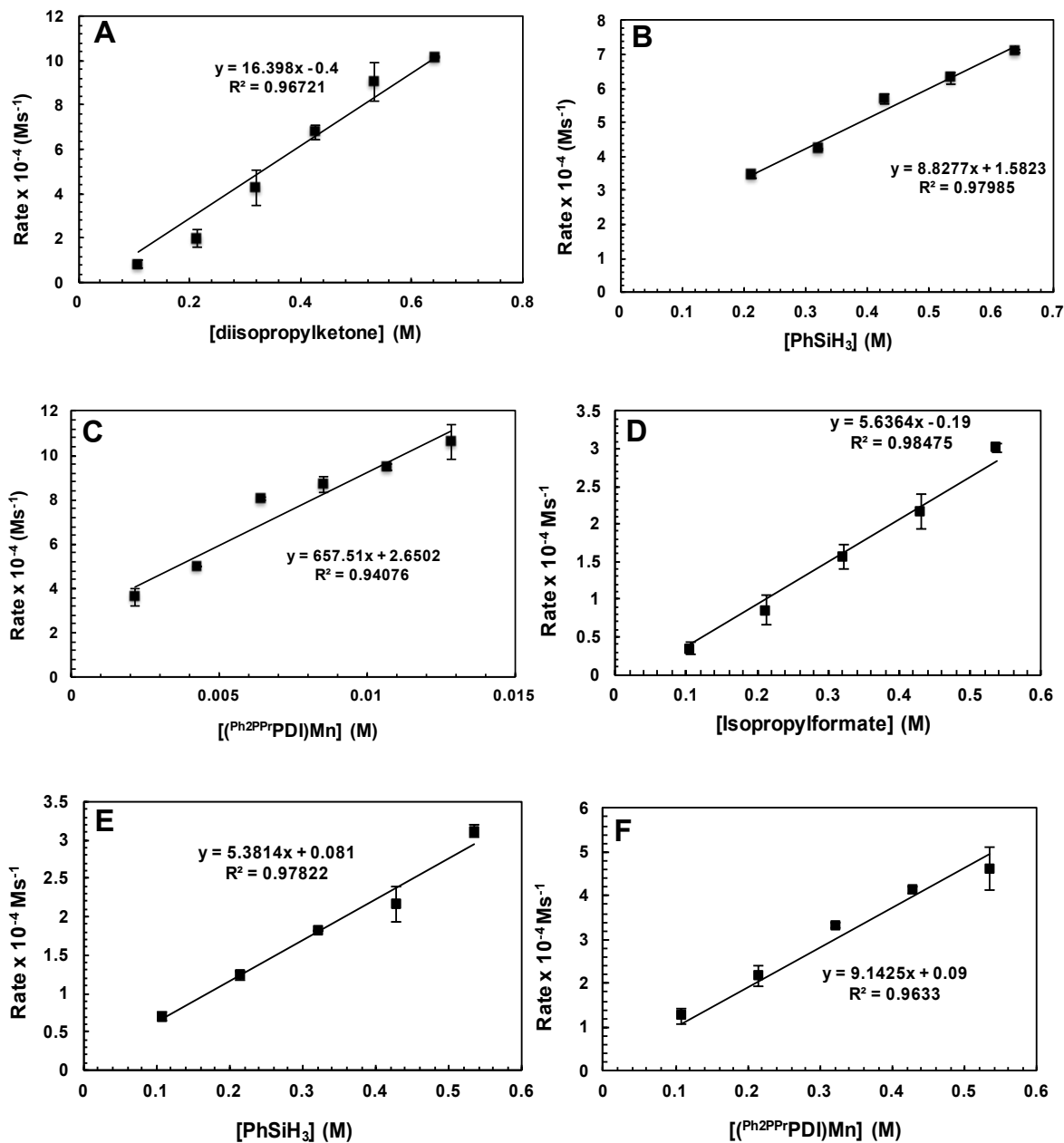
Figure 3.4. Dependence of ketone (A), silane (B), and **2** (C) on the rate of 1 mol% of **2**-catalyzed hydrosilylation of 2,4-dimethyl-3-pentanone. Rate = k_{obs}[ketone][PhSiH$_3$][**2**]. Dependence of formate (D), silane (E), and **2** (C) on the rate of 1 mol% of **2**-catalyzed hydrosilylation of isopropyl formate. Rate = k$_{obs}$ [formate][PhSiH$_3$][**2**].

92

3.6.3. Kinetic Isotope Effect:

In view of the stoichiometric silane addition reaction (Scheme 3.1), it can be hypothesized that the catalysis may involve a Si-H oxidative addition. Although one equivalent PhSiH$_3$ addition to **2** resulted in the slow formation **2-H**, it did not allow for the isolation of a silane adduct. It is believed that the conversion of **2** to **2-H** occurs either via a homolytic or a heterolytic Si-H bond cleavage. Since we did not observe any coupled silyl dimer in any catalytic reaction, it is reasonable to postulate that this conversion takes place through a heterolysis of Si-H bond.[27, 28] Heterolytic Si-H breaking was reported for Mo[27] and Re[28] catalyzed hydrosilylation. While there is no experimental evidence in case of Mo except theoretical modeling, the Re catalyzed reaction were shown to proceed via an ionic Si-H bond breaking. Another pathway was proposed by Blom *et al.*, where a 1,2-hydride migration from Si to Fe in a silylene-iron (NHSi-Fe) complex was proposed,[12g] which is unlikely in our case. It is possible that the first step involves an oxidative addition of Si-H bond along with partial Si-H heterolysis. The oxidative adduct reacts faster when ketone is around in the catalytic reactions. This observation is in good agreement with the fact that hydrosilylation using more substituted monohydrosilanes are slower[25] compared to phenylsilane, because the monohydrosilanes will generate sterically demanding adducts. The Si-H oxidative addition was further bolstered by a kinetic isotope effect (KIE) of 2.2 obtained by comparing the rates in presence of PhSiH$_3$/PhSiD$_3$ (Figure 3.5).
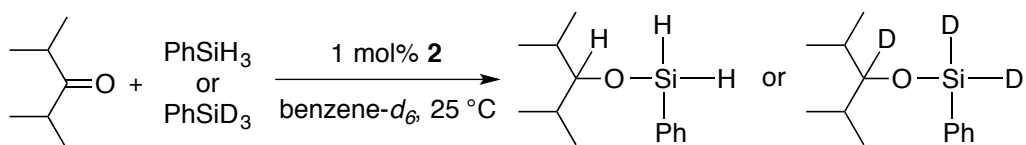
Rate (PhSiH$_3$) = 5.654 x 10^{-4} Ms^{-1}

Rate (PhSiD$_3$) = 2.534 x 10^{-4} Ms^{-1}
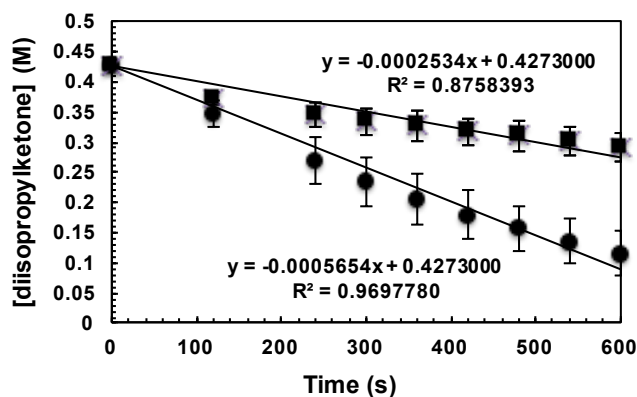
Figure 3.5. Graph comparing the disappearance of 2,4-dimethyl-3-pentanone for PhSiH$_3$ (●) and PhSiD$_3$ (■) catalyzed by 1 mol% of **2**. (KIE = 2.2 ± 0.11 after triplicate runs).

3.7. Proposed mechanism:

3.7.1. (^{Ph2PPr}PDI)Mn (2) mediated mechanism:

Taken into consideration the first order dependence of ketone, silane and catalyst on the rate and a significant KIE value, a mechanism can be proposed. However, a question still remains whether it is Ojima mechanism or modified Ojima mechanism (Figure 3.6). In the Ojima mechanism oxidative addition of silane follows ketone insertion into the M-SiR$_3$ bond resulting in the formation of a sterically-demanding intermediate **(A)**. On the other hand, modified Ojima mechanism involves insertion of ketone into the M-H bond to form sterically-favored intermediate **(B)**. It is believed that ketone insertion into the M-H bond (modified Ojima mechanism) is more likely since **2** can easily hydrosilylate bulky substrates such as 2,4-dimethyl-3-pentanone and dicyclohexyl ketone.[25] Therefore, the operative mechanism of **2**-catalyzed carbonyl hydrosilylation (Figure 3.7) starts with a reversible oxidative addition of PhSiH$_3$ across

94

the Mn center with presumed phosphine dissociation.[26] Phosphine arm dissociation may not be involved in the operative cycle as no influence on the rate has been found when 2,4-dimethyl-3-pentanone was hydrosilylated using in presence of 20, 40, or 80 equivalents of exogenous PPh$_3$ using 1 mol% of **1**. In all three cases the initial rate has been found to be $(6.07 \pm 0.035) \times 10^{-4}$ Ms^{-1}. The resulting adduct **A** now coordinates to the incoming ketone and subsequent insertion into the Mn-H bond to generate an alkoxide intermediate **C**, which is believed to be the rate determining step. In case of ketone hydrosilylation, **C** undergoes a fast reductive elimination to furnish the monohydrosilylated product while regenerating catalyst **2**. This resulting siloxane is now more reactive than PhSiH$_3$ and undergoes oxidative addition of Si-H bond across the metal center resulting di- and trihydrosilylated products, which explains the observation of unreacted PhSiH$_3$ after each catalytic reaction.
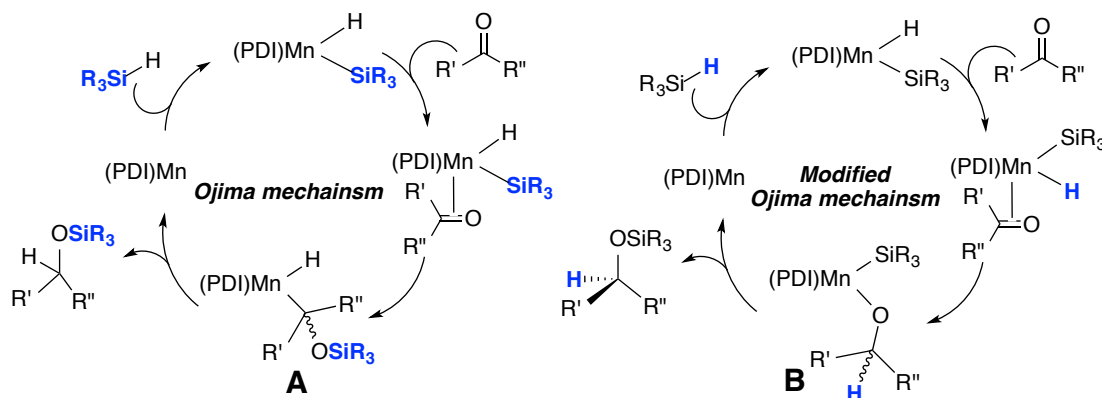
Figure 3.6. Ojima mechanism and modified Ojima mechanism for ketone hydrosilylation.

However, in case of esters or formates, a fast β-alkoxide elimination is believed to occur, which produces another alkoxide intermediate **D** and an aldehyde. Although efforts have been made to isolate the aldehyde in order to support the mechanism, high

95

reactivity of the aldehyde and relatively smaller time scale of the hydrosilylation reaction did not allow for the observation of aldehyde by ^{1}H NMR spectroscopy. The mechanism completes a cycle by fast reductive elimination of siloxane product from **D** and regeneration of the catalyst. This has also been confirmed by the established rate law (rate = k_{obs} [formate][PhSiH$_3$][**2**], Figure 3.4 D, E, F), which shows first order dependence of each reagent on the rate of **2**-catalyzed isopropyl formate hydrosilylation. Notably, the redox activity of PDI-chelate maintains a divalent Mn center throughout the catalytic cycle, which is an excellent coherence to the proposition of chelate design to impart stability to low valent fist row metals.
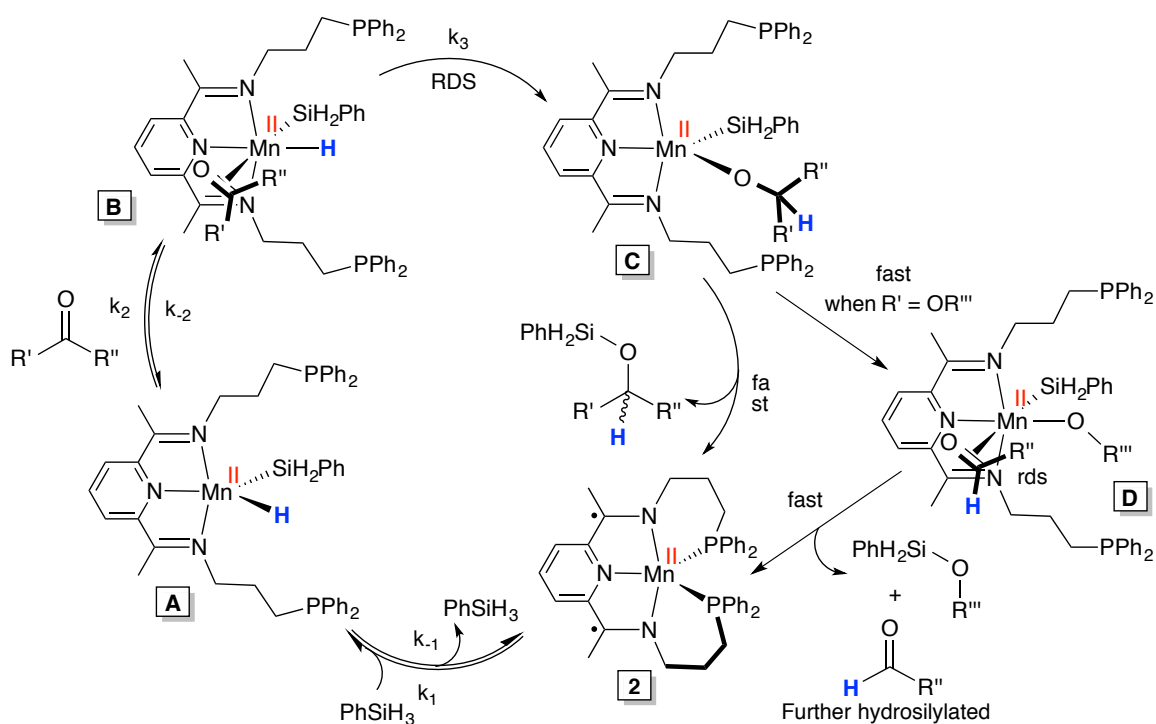
Figure 3.7. Modified Ojima mechanism for **2**-catalyzed aldehyde (R', R'' = H), ketone (R', R'' = alkyl or aryl), formate (R' = H, R'' = OR'''; where R''' = alkyl), and ester (R' = alkyl, R'' = OR'''; where R''' = alkyl or aryl) hydrosilylation.

3.7.2 Role of (^{Ph2PPr}PDI)MnH in the catalytic cycle:

Having proposed the modified Ojima mechanism based on experimental and kinetic evidences, we sought to investigate the post catalysis reaction mixture to gather supportive information. Surprisingly, while analyzing the hydrosilylation reactions in ^{1}H NMR, a mixture of **2** and **2-H** was observed after reaction completion for every substrate. This crucial observation raises the possibility of (^{Ph2PPr}PDI)MnH **(2-H)** mediated pathways that contribute to the observed rate. This hypothesis was further supported by the previous observation of **2-H** from reaction of **2** and PhSiH$_3$ (Scheme 3.1). Therefore, a complete kinetic analysis for **2-H**-catalyzed hydrosilylation has been implemented. Hydrosilylation of 2,4-dimethyl-3-pentanone has been conducted using 1 mol% of **2-H** with varying concentrations of ketone, silane, and **2-H** separately. Analysis of the concentration profiles for all these reactions displays a linear change in the observed rate for each substrate. The plot of rate against concentrations are shown in Figure 3.8 (A, B, and C), which manifests a first order dependence of each concentration on the rate. Additionally, a KIE of 4.1 ± 0.57 (Figure 3.8 D) was obtained by performing the hydrosilylation of 2,4-dimethyl-3-pentanone in presence of PhSiH$_3$ and PhSiD$_3$. It is also to be noted that **2-H**-catalyzed ketone hydrosilylation rate is comparable to that of **2**-mediated reaction (Figure 3.2) with the former reaction being slightly slower.
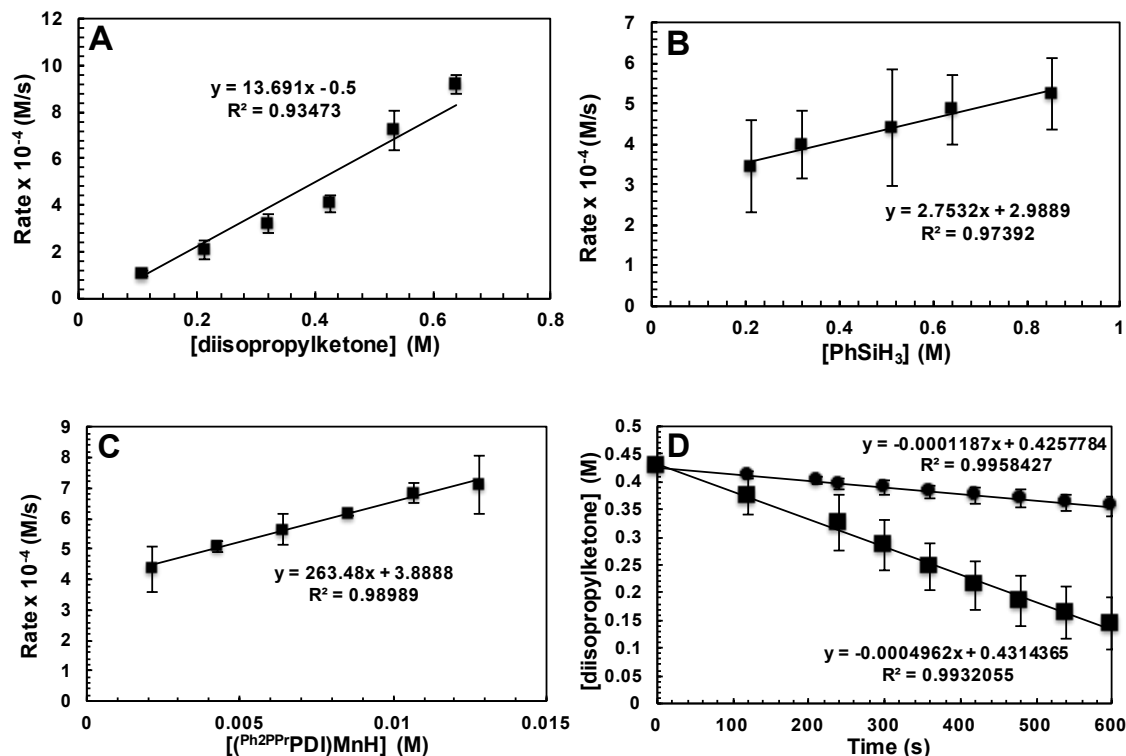
Figure 3.8. Dependence of ketone (A), silane (B), and **2-H** (C) on the rate of 1 mol% of **2-H**-catalyzed hydrosilylation of 2,4-dimethyl-3-pentanone. Rate = k_{obs}[**2-H**][ketone][PhSiH$_3$]. KIE is shown in D for 1 mol% **2-H**-catalyzed reaction using PhSiH$_3$ (■) and PhSiD$_3$ (●).

Surprisingly, **2-H** has been found to exhibit a faster rate of ester hydrosilylation when compared to **2** as it is evident from the hydrosilylation of ethyl acetate and isopropyl formate (Figure 3.9). At this point the rate expression can be formulated as a function of additive pathways that each have a dependence on substrate and PhSiH$_3$, which is shown in equation 1.

$$\text{Rate} = k_{\text{Ojima}}[\mathbf{2}][\text{substrate}][\text{PhSiH}_3] + k_{\text{Insert}}[\mathbf{2\text{-}H}][\text{substrate}][\text{PhSiH}_3] \qquad (\text{eq. 1})$$

$$\text{where } k_{\text{Ojima}} = k_1 k_2 k_3 / k_{-1} k_{-2} \text{ and } k_{\text{Insert}} = k_4 k_5 k_6 / k_{-4} k_{-5}$$
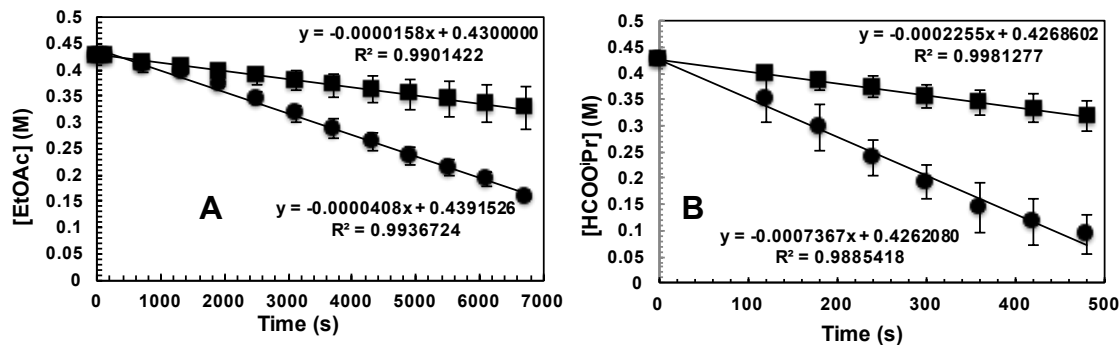
Figure 3.9. Concentration profiles for 1 mol% of **2** (■) and **2-H** (●) catalyzed ethyl acetate (A) and isopropyl formate (B) hydrosilylations.

Based on the 1st order dependence on each reagent for both **2**- and **2-H**-catalyzed reactions and the observation of hydride **2-H** after every catalytic reaction, a secondary insertion pathway[12h, 13d, 14a,b, 15e,h] has been proposed (Figure 3.10). This mechanism begins with the conversion of **2** into **2-H** in presence of $PhSiH_3$, albeit the actual mechanism for this step is still unknown. Then the resulting hydride complex **2-H** binds the incoming ketone which follows insertion of ketone into the Mn-H bond to generate an alkoxide intermediate **F**. During the ketone and aldehyde hydrosilylation **F** undergoes σ-bond metathesis with silane in a rate-determining step to release siloxane products and **2**, hence completes a catalytic cycle. The enhanced KIE of 4.2 for **2-H**-catalyzed hydrosilylation supports this step because σ-bond metathesis requires additional reorganizational energy when compared to oxidative addition in the case of **1**. In the case of ester hydrosilylation, a fast *β*-alkoxide elimination from **F** occurs to form another alkoxide **G**, which via σ-bond metathesis produces the siloxane products and catalyst. The aldehyde released in the elimination step is hydrosilylated under the reaction condition to yield silyl ethers.

99
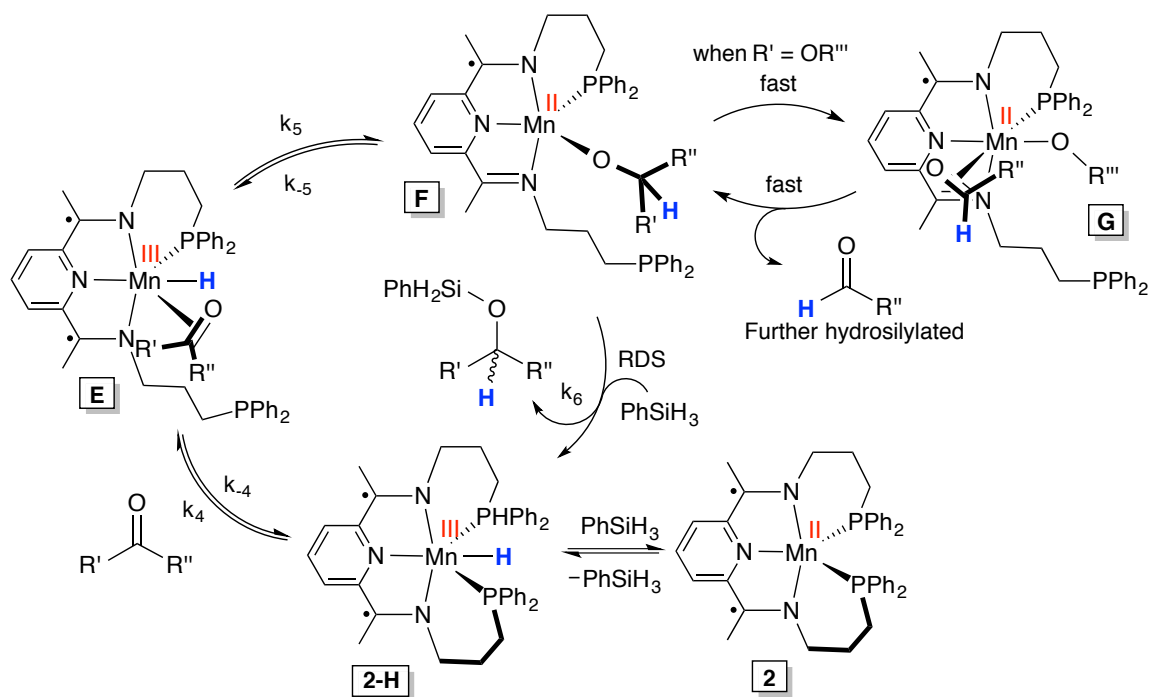
Figure 3.10. Secondary insertion pathways mediated by **2-H** accounting for aldehyde (R', R'' = H), ketone (R', R'' = alkyl or aryl), formate (R' = H, R'' = OR'''; where R''' = alkyl), and ester (R' = alkyl, R'' = OR'''; where R''' = alkyl or aryl) hydrosilylation.

Given the long due debate on actual mechanism of Mn catalyzed carbonyl hydrosilylations[20-23] due to instability caused by one electron redox processes, this comprehensive mechanism presented here bears high significance. Although there are a number carbonyl hydrosilylation mechanism proposed in the literature that are catalyzed by first row metals, namely Cu,[15e,h] Ni,[14a,b] Co,[13d] and Fe[12e,h] and Mn[24] based hydrides, most of these lack detailed mechanistic study, be it intermediate isolation or kinetic information. Nolan in 2005 postulated a (NHC)CuH complex to be the active catalyst and the mechanism was proposed to proceed via C=O insertion into the Cu-H bond to result an alkoxide species.[15h] This alkoxide then undergoes a σ-bond metathesis to release the silyl ether and the putative hydride complex. Guan showed a similar insertion mechanism, where a PCP-supported nickel hydride, [2,6-(^{t}Bu$_2$PO)$_2$C$_6$H$_3$]NiH complex

was observed to undergo a ketone insertion to form an alkoxide intermediate.[14a] Another putative Ni-H complex, $[(PN^{iPr3})Ni(\mu_2-H)]_2$ was hypothesized by Mindiola, which adapts the same insertion and σ-bond metathesis pathways during carbonyl hydrosilylation.[14b] Niu *et al.* also proposed an insertion pathway for a Co-H mediated carbonyl hydrosilylation based on experimental evidence.[13d] Similarly, Chidara suggested this carbonyl insertion pathway for $MnN(salen-3,5-^tBu_2)$, which is first converted into a hydride species as observed by NMR spectroscopy.[24] Although there is no further synthetic and kinetic study, this hydride was suggested to undergo an insertion and σ-bond metathesis pathway. Guan outlined the possibility of a similar insertion pathway for a PCP-based iron hydride complex, but there were insufficient evidences to further proof this hypothesis.[12e] Recently, a detailed mechanistic study on the Fe(boxmi) complexes has been documented by Gede, where the operative mechanism has been characterized by a σ-bond metathesis of an alkoxide intermediate with silane, resulting in a hydride species, which then undergoes ketone insertion and subsequent σ-bond metathesis to furnish the silyl ether product.[12h]

Taking into account these reports and based on our kinetic and stoichiometric experiments, it is very likely that the (^{Ph2PPr}PDI)Mn **(2)** complex operates through a modified Ojima pathway (Figure 3.7) along with contribution from a secondary insertion pathway mediated by (^{Ph2PPr}PDI)MnH **(2-H)** (Figure 3.10). These proposed pathways are bolstered by the isolation of relevant intermediates and kinetic analysis. The mechanism proved herein encompasses the role of pentacoordinate redox non-innocent chelate in stabilizing the low oxidation state of Mn. This study also encourages for further exploration of the insufficient reductive chemistry of Mn particularly in catalysis.

3.8. Concluding remarks:

In summary, for the first time, a definitive Mn catalyzed carbonyl hydrosilylation mechanism has been determined using a combination of stoichiometric substrate addition, isotopic labeling, and rigorous kinetic analysis. While Ojima mechanism has been observed for **1**-catalyzed carbonyl and carboxylate hydrosilylation a secondary insertion pathway mediated by **2** has also been found to contribute to the observed rate. Although both mechanisms proposed here are reasonable according to the experimental evidences, a detailed computational analysis to construct a reaction profile graph would be an excellent addition to further bolster these pathways.

3.9. Experimental procedures:

General Considerations. Unless otherwise stated all synthetic reactions were performed in an MBraun glovebox under an atmosphere of purified nitrogen. Aldrich or Acros anhydrous solvents were purified using a Pure Process Technology solvent system and stored in the glovebox over activated 4Å molecular sieves and sodium before use. Benzene-d_6 was purchased from Cambridge Isotope Laboratories and dried over 4Å molecular sieves and K^0 metal before use. (THF)$_2$MnCl$_2$ was purchased from Acros. 2,4-dimethyl-3-pentanone and 2,2,2-trifluoroacetophenone were bought from Sigma Aldrich. Phenylsilane was purchased from Oakwood chemicals. Phenylsilane-d_3 were prepared according to literature procedure.[28] ^{Ph2PPr}PDI ligand was prepared following reported procedure.[26,29] All the substrates, reagents and NMR solvents were scrupulously dried over 4 Å molecular sieves or distilled.

NMR spectroscopy: Solution ^{1}H nuclear magnetic resonance (NMR) spectra were recorded at room temperature on a Varian 400-MR 400 MHz NMR spectrometer. All ^{1}H and ^{13}C NMR chemical shifts (ppm) are reported relative to $Si(CH_3)_4$ using [1]H (residual) and ^{13}C chemical shifts of the solvent as secondary standards. ^{31}P NMR data is reported relative to H_3PO_4. Elemental analyses were performed at Robertson Microlit Laboratories Inc. (Ledgewood, NJ) and the Arizona State University CLAS Goldwater Environmental Laboratory (Tempe, AZ). Solution state magnetic susceptibility was determined from Evans method using Varian 400 MHz NMR spectrometer.

X-ray Crystallography. Diffraction data were collected and analyzed by Dr. Thomas L. Groy at Arizona State University. Single crystals suitable for X-ray diffraction were coated with polyisobutylene oil in the glovebox and transferred to glass fiber with Apiezon N grease, which was then mounted on the goniometer head of a Bruker APEX Diffractometer equipped with Mo K_α radiation. A hemisphere routine was used for data collection and determination of the lattice constants. The space group was identified and the data was processed using the Bruker SAINT+ program and corrected for absorption using SADABS. The structures were solved using direct methods (SHELXS) completed by subsequent Fourier synthesis and refined by full-matrix, least-squares procedures on $[F^2]$ (SHELXL).

Preparation of radical transferred complex (^{Ph_2PPr}PDI)Mn(OC•Ph(CF$_3$)) (4): Under an inert atmosphere, a 20 mL scintillation vial was charged with 0.108 g (0.162 mmol) of **2** in approximately 10 mL benzene. To the dark brown solution, 0.023 mL (0.162 mmol) of 2,2,2-trifluoroacetophenone was added. The solution had turned into deep blue color immediately. It was stirred for 1 h and then filtered through Celite. The filtrate was dried

under vacuum to isolate a blue residue. After repeated washing with diethylether (5x3mL) followed by drying in vacuo, 0.078 g (0.092 mmol, yield = 56%) of blue solid was isolated. Analysis for $C_{47}H_{46}N_3P_2MnOF_3$: Calcd. C, 66.77%; H, 5.48%; N, 4.96%. Found: C, 66.69%; H, 5.35%; N, 4.78%. ^{1}H NMR (benzene-d$_6$): δ (ppm) No resonances observed. Magnetic moment (Evans method): μ_{eff} = 4.4 μ_B. UV−vis: λ_{max} = 360 nm (ε = 2319 M^{-1} cm^{-1}), λ_{max} = 612 nm (ε = 2695 M^{-1} cm^{-1}).

Preparation of radical coupled dimer [(μ-O,N_{py}-4-OC(CF$_3$)(Ph)-4-H-^{Ph_2,PPr}PDI)Mn]$_2$ (5): A concentrated THF solution of **4** (0.078 g, 0.092 mmol) was placed at -35 °C for 24 h. Removal of blue solution followed by washing with toluene (3x2mL) and Et$_2$O (2 x 2 mL) followed by drying in vacuum yielded 0.027 g of amber crystals. Analyses for $C_{94}H_{92}N_6P_4Mn_2O_2F_6$: calcd. C, 66.77%; H, 5.48%; N, 4.96%. Found C, 66.02%; H, 5.66%; N, 4.75%. ^{1}H NMR (benzene-d$_6$): δ (ppm) No resonances observed.

Preparation of PhSiD$_3$: In glove box a 20 mL scintillation vial was charged with 0.401 g (9.54 mmol) of LiAlD$_4$ in approximately 10 mL dry Et$_2$O. To the suspension 2.624 g (12.40 mmol) of PhSiCl$_3$ was added dropwise over 2 min. The mixture was stirred at room temperature for 15 h. The resulting suspension was poured into 5 mL of ice-cold water to quench excess LiAlD$_4$. The organic fraction was extracted and washed twice with water (2x5 mL). The Et$_2$O layer was then dried over anhydrous Na$_2$SO$_4$ and dried on a rotary evaporator at ambient temperature to isolate 1.201 g (10.25 mmol) of PhSiD$_3$ as a colorless liquid. ^{1}H NMR (benzene/benzene-d_6), δ (ppm): 7.38 (m, 1H, p-phenyl), 7.13-7.02 (m, 4H, phenyl). ^{2}H NMR (benzene/benzene-d_6), δ (ppm): 4.22 (s, 3D).

General method of conducting kinetic experiments: In the glove box a J.Young tube was charged with a benzene-d_6 solution (0.7 mL) of 0.002 g of catalyst. The tube was then placed into a liquid N_2 jacketed cold well to freeze the catalyst solution. While the solution was frozen, $PhSiH_3$ was injected followed by the substrate (ketone or ester). Finally, 10 μL of anisole was added as an internal standard. The tube was sealed under N_2 atmosphere and promptly transferred into a dewar filled with liquid N_2. After warming the reaction mixture in the tube to room temperature, a ^1H NMR experiment was started quickly and it was set up for every 1 min (or 30 s) interval data collection. The substrate consumption rate was calculated by integrating the starting material and product with respect to a known concentration of anisole. Each experiment was either triplicated or duplicated to determine an average rate and standard deviation.

Procedure of KIE experiment using 1 as catalyst: In the glove box a J.Young tube was charged with a 0.7 mL benzene-d_6 solution of 0.002 g (0.002991 mmol) of **1** and placed into a liquid N_2 jacketed cold well. While the catalyst solution was frozen 0.0372 mL (0.2991 mmol) of $PhSiD_3$ and 0.0424 mL (0.2991 mmol) of 2,4-dimethyl-3-pentanone was injected. Then 0.010 mL (0.092 mmol) of anisole was added as an internal standard. The tube was sealed under N_2 atmosphere and quickly transferred into a dewar filled with liquid N_2. The mixture was warmed to room temperature and ^1H NMR data was collected at every 30 s time interval. Percent conversion was determined by integrating the reactant and product peaks with respect to unchanged anisole. This experiment was repeated two more times to obtain a standard deviation.

Procedure of KIE experiment using 2 as catalyst: In the glove box a J.Young tube was charged with a 0.7 mL benzene-d_6 solution of 0.002 g (0.002987 mmol) of **2** and placed

into a liquid N_2 jacketed cold well. While the catalyst solution was frozen 0.0371 mL (0.2987 mmol) of PhSiD$_3$ and 0.0423 mL (0.2987 mmol) of 2,4-dimethyl-3-pentanone was injected. Then 0.010 mL (0.092 mmol) of anisole was added as an internal standard. The tube was sealed under N_2 atmosphere and quickly transferred into a dewar filled with liquid N_2. The mixture was warmed to room temperature and ^{1}H NMR data was collected at every 30 s time interval. Percent conversion was determined by integrating the reactant and product peaks with respect to unchanged anisole. This experiment was repeated two more times to obtain a standard deviation.

Semimicro scale hydrosilylation of 2,4-dimethyl-3-pentanone in presence of 20 equiv. of triphenylphosphine: In glove box a J-Young tube was charged with a benzene-d_6 solution (0.7 mL) of 0.002 g of catalyst and 0.0156 g (0.0598 mmol) of triphenylphosphine. The tube was then placed into a liquid N_2 jacketed cold well to freeze the catalyst solution. While the solution was frozen, 0.0369 mL (0.2991 mmol) of PhSiH$_3$ was injected followed by 0.0424 mL (0.2991 mmol) of 2,4-dimethyl-3-pentanone. Finally, 10 μL of anisole was added as an internal standard. The tube was sealed under N_2 atmosphere and promptly transferred into a dewar filled with liquid N_2. After warming the reaction mixture in the tube to room temperature, a ^{1}H NMR experiment was started quickly and it was arrayed using the NMR instrument for 1 min interval data collection. The substrate consumption rate was calculated by integrating the starting material and product with respect to the known concentration of anisole. Each experiment was either duplicated to determine an average rate and standard deviation. The rate has been found to be 6.07 x 10^{-4} Ms^{-1}.

Semimicro scale hydrosilylation of 2,4-dimethyl-3-pentanone in presence of 40 equiv. of triphenylphosphine: In glove box a J-Young tube was charged with a benzene-d_6 solution (0.7 mL) of 0.002 g of catalyst and 0.0314 g (0.1196 mmol) of triphenylphosphine. The tube was then placed into a liquid N_2 jacketed cold well to freeze the catalyst solution. While the solution was frozen, 0.0369 mL (0.2991 mmol) of $PhSiH_3$ was injected followed by 0.0424 mL (0.2991 mmol) of 2,4-dimethyl-3-pentanone. Finally, 10 μL of anisole was added as an internal standard. The tube was sealed under N_2 atmosphere and promptly transferred into a dewar filled with liquid N_2. After warming the reaction mixture in the tube to room temperature, a ^1H NMR experiment was started quickly and it was arrayed using the NMR instrument for 1 min interval data collection. The substrate consumption rate was calculated by integrating the starting material and product with respect to the known concentration of anisole. The rate has been found to be 6.11 x 10^{-4} Ms^{-1}.

Semimicro scale hydrosilylation of 2,4-dimethyl-3-pentanone in presence of 80 equiv. of triphenylphosphine: In glove box a J-Young tube was charged with a benzene-d_6 solution (0.7 mL) of 0.002 g of catalyst and 0.0628 g (0.2393 mmol) of triphenylphosphine. The tube was then placed into a liquid N_2 jacketed cold well to freeze the catalyst solution. While the solution was frozen, 0.0369 mL (0.2991 mmol) of $PhSiH_3$ was injected followed by 0.0424 mL (0.2991 mmol) of 2,4-dimethyl-3-pentanone. Finally, 10 μL of anisole was added as an internal standard. The tube was sealed under N_2 atmosphere and promptly transferred into a dewar filled with liquid N_2. After warming the reaction mixture in the tube to room temperature, a ^1H NMR experiment was started quickly and it was arrayed using the NMR instrument for 1 min

interval data collection. The substrate consumption rate was calculated by integrating the starting material and product with respect to the known concentration of anisole. The rate has been found to be 6.04 x 10^{-4} Ms^{-1}.

3.10. References:

1. For early hydrosilylation reviews see (a) Speier, J. L. *Adv. Organomet. Chem.* **1979**, *17*, 407-447. (b) Ojima, I. *Chem. Org. Silicon Compd.* **1989**, *2*, 1479-1526.

2. Speier, J. L.; Webster, J. A.; Barnes, G. H. *J. Am. Chem. Soc.* **1957**, *79*, 974-979.

3. Troegel, D.; Stohrer, J. *Coord. Chem. Rev.* **2011**, *255*, 1440-1459.

4. Chalk, A. J.; Harrod, J. F. *J. Am. Chem. Soc.* **1965**, *87*, 16-21.

5. Maruyama, Y.; Yamamura, K.; Nakayama, I.; Yoshiuchi, K.; Ozawa, F. *J. Am. Chem. Soc.* **1998**, *120*, 1421-1429, and references therein.

6. For leading examples see: (a) Deutsch, C.; Krause, N.; Lipshutz, B. H. *Chem. Rev.* **2008**, *108*, 2916-2927. (b) Morris, R. H. *Chem. Soc. Rev.* **2009**, *38*, 2282-2291. (c) Riener, K.; Högerl, M. P.; Gigler, P.; Kühn, F. E. *ACS Catal.* **2012**, *2*, 613-621. (d) Bleith, T.; Wadepohl, H.; Gade, L. H. *J. Am. Chem. Soc.* **2015**, *137*, 2456-2459.

7. Osborn, J. A.; Jardine, F. H.; Young, J. F.; Wilkinson, G. *J. Chem. Soc. A* **1966**, 1711-1732.

8. (a) Ojima, I.; Nihonyanagi, M.; Kogure, T.; Kumagai, M.; Horiuchi, S.; Nakatsugawa, K. *J. Organomet. Chem.* **1975**, *94*, 449-461. (b) Reyes, C.; Prock, A.; Giering, W. P. *Organometallics* **2002**, *21*, 546-554.

9. (a) Schneider, N.; Finger, M.; Haferkemper, C.; Bellemin-Laponnaz, S.; Hofmann, P.; Gade, L. H. *Angew. Chem. Int. Ed.* **2009**, *48*, 1609-1613. (b) Schneider, N.; Finger, M.; Haferkemper, C.; Bellemin-Laponnaz, S.; Hofmann, P.; Gade, L. H. *Chem.-Eur. J.* **2009**, *15*, 11515-11529.

10. (a) Gutsulyak, D. M.; Vyboishchikov, S. F.; Nikonov, G. I. *J. Am. Chem. Soc.* **2010**, *132*, 5950-5951. (b) Park, S.; Brookhart, M. *Organometallics* **2010**, *29*, 6057-6064. (c) Lipke, M. C.; Tilley, T. D. *J. Am. Chem. Soc.* **2014**, *136*, 16387-16398.

11. For first-row metal alkene hydrosilylation catalysts see: (a) Tondreau, A. M.; Atienza, C. C. H.; Weller, K. J.; Nye, S. A.; Lewis, K. M.; Delis, J. G. P.; Chirik, P. J. *Science*

2012, *335*, 567-570. (b) Atienza, C. C. H.; Tondreau, A. M.; Weller, K. J.; Lewis, K. M.; Cruse, R. W.; Nye, S. A.; Boyer, J. L.; Delis, J. G. P.; Chirik, P. J. *ACS Catal.* **2012**, *2*, 2169-2172. (c) Tondreau, A. M.; Atienza, C. C. H.; Darmon, J. M.; Milsmann, C.; Hoyt, H. M.; Weller, K. J.; Nye, S. A.; Lewis, K. M.; Boyer, J.; Delis, J. G. P.; Lobkovsky, E.; Chirik, P. J. *Organometallics* **2012**, *31*, 4886-4893. (d) Peng, D.; Zhang, Y.; Du, X.; Zhang, L.; Leng, X.; Walter, M. D.; Huang, Z. *J. Am. Chem. Soc.* **2013**, *135*, 19154-19166. (e) Srinivas, V.; Nakajima, Y.; Ando, W.; Sato, K.; Shimada, S. *Catal. Sci. Tech.* **2015**, *5*, 2081-2084. (f) Chen, J.; Cheng, B.; Cao, M.; Lu, Z. *Angew. Chem. Int. Ed.* **2015**, *54*, 4661-4664. (g) Steinman, T. J.; Uyeda, C. *J. Am. Chem. Soc.* **2015**, *137*, 6104-6110. (h) Sunada, Y.; Noda, D.; Soejima, H.; Tsutsumi, H.; Nagashima, H. *Organometallics* **2015**, *34*, 2896-2906. (i) Buslov, I.; Becouse, J.; Mazza, S.; Montandon-Clerc, M.; Hu, X. *Angew. Chem. Int. Ed.* **2015**, *54*, 14523-14526. (j) Chen, C.; Hect, M. B.; Kavara, A.; Brennessel, W. W.; Mercado, B. Q.; Weix, D. J.; Holland, P. L. *J. Am. Chem. Soc.* **2015**, *137*, 13244-13247. (k) Noda, D.; Tahara, A.; Sunada, Y.; Nagashima, H. *J. Am. Chem. Soc.* **2016**, *138*, 2480-2483.

12. For leading Fe carbonyl hydrosilylation catalysts see: (a) Tondreau, A. M.; Lobkovsky, E.; Chirik, P. J. *Org. Lett.* **2008**, *10*, 2789-2792. (b) Tondreau, A. M.; Darmon, J. M.; Wile, B. M.; Floyd, S. K.; Lobkovsky, E.; Chirik, P. J. *Organometallics* **2009**, *28*, 3928-3940. (c) Kandepi, V. V. K. M.; Cardoso, J. M. S.; Peris, E.; Royo, B. *Organometallics* **2010**, *29*, 2777-2782. (d) Yang, J.; Tilley, T. D. *Angew. Chem. Int. Ed.* **2010**, *49*, 10186-10188. (e) Bhattacharya, P.; Krause, J. A.; Guan, H. *Organometallics* **2011**, *30*, 4720-4729. (f) Ruddy, A. J.; Kelly, C. M.; Crawford, S. M.; Wheaton, C. A.; Sydora, O. L.; Small, B. L.; Stradiotto, M.; Turculet, L. *Organometallics* **2013**, *32*, 5581-5588. (g) Blom, B.; Enthaler, S.; Inoue, S.; Irran, E.; Driess, M. *J. Am. Chem. Soc.* **2013**, *135*, 6703-6713. (h) Bleith, T.; Gade, L. H. *J. Am. Chem. Soc.* **2016**, *ASAP*.

13. For leading Co carbonyl hydrosilylation catalysts see: (a) Brunner, H.; Amberger, K. *J. Organomet. Chem.* **1991**, *417*, C63-C65. (b) Yu, F.; Zhang, X.-C.; Wu, F.-F.; Zhou, J.-N.; Fang, W.; Wu, J.; Chan, A. S. C. *Org. Biomol. Chem.* **2011**, *9*, 5652. (c) Sauer, D. C.; Wadepohl, H.; Gade, L. H. *Inorg. Chem.* **2012**, *51*, 12948-12958. (d) Niu, Q.; Sun, H.; Li, X.; Klein, H.-F.; Flörke, U. *Organometallics* **2013**, *32*, 5235-5238. (e) Zhou, H.; Sun, H.; Zhang, S.; Li, X. *Organometallics* **2015**, *34*, 1479-1486. (f) Nesbit, M. A.; Suess, D. L. M.; Peters, J. C. *Organometallics* **2015**, *34*, 4741-4752.

14. For leading Ni carbonyl hydrosilylation catalysts see: (a) Chakraborty, S.; Krause, J. A.; Guan, H. *Organometallics* **2009**, *28*, 582-586, and references therein. (b) Tran, B. L.; Pink, M.; Mindiola, D. J. *Organometallics* **2009**, *28*, 2234-2243. (c) Postigo, L.; Royo, B. *Adv. Synth. Catal.* **2012**, *354*, 2613-2618. (d) Bheeter, L. P.; Henrion, M.; Brelot, L.; Darcel, C.; Chetcuti, M. J.; Sortais, J.-B.; Ritling, V. *Adv. Synth. Catal.* **2012**, *354*, 2619-2624. (e) Porter, T. M.; Hall, G. B.; Groy, T. L.; Trovitch, R. J. *Dalton Trans.* **2013**, *42*, 14689-14692. (f) MacMillan, S. N.; Harman, W. H.; Peters, J. C. *Chem. Sci.* **2014**, *5*, 590-597.

15. For leading Cu carbonyl hydrosilylation catalysts see: (a) Brunner, H.; Miehling, W. *J. Organomet. Chem.* **1984**, *275*, C17-C21. (b) Sirol, S.; Courmarcel, J.; Mostefai, N.; Riant, O. *Org. Lett.* **2001**, *3*, 4111-4113. (c) Lipshutz, B. H.; Noson, K.; Chrisman, W. *J. Am. Chem. Soc.* **2001**, *123*, 12917-12918. (d) Lipshutz, B. H.; Noson, K.; Chrisman, W.; Lower, A. *J. Am. Chem. Soc.* **2003**, *125*, 8779-8789. (e) Kaur, H.; Zinn, F. K.; Stevens, E. D.; Nolan, S. P. *Organometallics* **2004**, *23*, 1157-1160. (f) Lee, D.; Yun, J. *Tetrahedron Lett.* **2004**, 5415-5417. (g) Wu, J.; Ji, J.-X.; Chan, A. S. C. *Proc. Natl. Acad. Sci., U.S.A.* **2005**, *102*, 3570-3575. (h) Díez-González, S.; Kaur, H.; Zinn, F. K.; Stevens, E. D.; Nolan, S. P. *J. Org. Chem.* **2005**, *70*, 4784-4796. (i) Díez-González, S.; Scott, N. M.; Nolan, S. P. *Organometallics* **2006**, *25*, 2355-2358. (j) Lipshutz, B. H.; Lower, A.; Kucejko, R. J.; Noson, K. *Org. Lett.* **2006**, *8*, 2969-2972. (k) Mostefaï, N.; Sirol, S.; Courmarcel, J.; Riant, O. *Synthesis* **2007**, *8*, 1265-1271. (l) Fujihara, T.; Semba, K.; Terao, J.; Tsuji, Y. *Angew. Chem. Int. Ed.* **2010**, *49*, 1472-1476. (m) Díez-González, S.; Escudero-Adán, E.; Benet-Buchholtz, J.; Stevens, E. D.; Slawin, A. M. Z.; Nolan, S. P. *Dalton Trans.* **2010**, *39*, 7595-7606. (n) Zhang, X.-C.; Wu, F.-F.; Li, S.; Zhou, J.-N.; Wu, J.; Li, N.; Fang, W.; Lam, K. H.; Chan, A. S. C. *Adv. Synth. Catal.* **2011**, *353*, 1457-1462. (o) Yu, F.; Zhou, J.-N.; Zhang, X.-C.; Sui, Y.-Z.; Wu, F.-F.; Xie, L.-J.; Chan, A. S. C.; Wu, J. *Chem. Eur. J.* **2011**, *17*, 14234-14240. (p) Albright, A.; Gawley, R. E. *J. Am. Chem. Soc.* **2011**, *133*, 19680-19683. (q) Roy, S. R.; Sau, S. C.; Mandal, S. K. *J. Org. Chem.* **2014**, *79*, 9150-9160.

16. For leading Zn carbonyl hydrosilylation catalysts see: (a) Mimoun, H. *J. Org. Chem.* **1999**, *64*, 2582-2589. (b) Mastranzo, V. M.; Quintero, L.; de Parrodi, C. A.; Juaristi, E.; Walsh, P. J. *Tetrahedron* **2004**, *60*, 1781-1789. (c) Bette, V.; Mortreux, A.; Savoia, D.; Carpentier, J.-F. *Tetrahedron* **2004**, *60*, 2837-2842. (d) Bette, V.; Mortreux, A.; Savoia, D.; Carpentier, J.-F. *Adv. Synth. Catal.* **2005**, *347*, 289-302. (e) Gérard, S.; Pressel, Y.; Riant, O. *Tetrahedron: Asym.* **2005**, *16*, 1889-1891. (f) Gajewy, J.; Kwit, M.; Gawroński, J. *Adv. Synth. Catal.* **2009**, *351*, 1055-1063. (g) Enthaler, S.; Schröder, K.; Inoue, S.; Eckhardt, B.; Junge, K.; Beller, M.; Drieβ, M. *Eur. J. Org. Chem.* **2010**, 4893-4901. (h) Pang, S.; Peng, J.; Li, J.; Bai, Y.; Xiao, W.; Lai, G. *Chirality* **2013**, *25*, 275-280. (i) Boone, C.; Korobkov, I.; Nikonov, G. I. *ACS Catal.* **2013**, *3*, 2336-2340. (j) Łowicki, D.; Bezłada, A.; Mlynarski, J. *Adv. Synth. Catal.* **2014**, *356*, 591-595. (k) Lummis, P. A.; Momemi, M. R.; Lui, M. W.; McDonald, R.; Ferguson, M. J.; Miskolzie, M.; Brown, A.; Rivard, E. *Angew. Chem. Int. Ed.* **2014**, *53*, 9347-9351. (l) Rit, A.; Zanardi, A.; Spaniol, T. P.; Maron, L.; Okuda, J. *Angew. Chem. Int. Ed.* **2014**, *53*, 13273-13277. (m) Sattler, W.; Ruccolo, S.; Chaijan, M. R.; Allah, T. N.; Parkin, G. *Organometallics* **2015**, 34, 4717-4731.

17. (a) Enthaler, S.; Junge, K; Beller, M. *Angew. Chem. Int. Ed.* **2008**, *47*, 3317-3321. (b) Plietker, B. *Iron Catalysis in Organic Chemistry*; Wiley-VCH: Weinheim, Germany, **2008**.

18. Collman, J. P.; Hegedus, L. S.; Norton, J. R.; Finke, R. G. In *Principles and Applications of Organotransition Metal Chemistry*. University Science Books, Sausalito, CA, 1987, pp. 306-333.

19. In Metsänen, T. T.; Gallego, D.; Szilvási, T.; Driess, M.; Oestreich, M. *Chem Sci.* **2015**, *6*, 7143-7149, a peripheral mechanism which does not involve iron mediated organometallic pathways has been proposed. While the Ni and Zn catalysts described in refs 14a and 16m are believed to catalyze carbonyl hydrosilylation via insertion into M-H followed by Si-H σ-bond metathesis, the leading Co catalyst for this transformation (ref 13f) relies on borane-assisted Si-H activation and carbonyl insertion into the resulting Co-Si bond.

20. (a) Valyaev, D. A.; Lavigne, G.; Lugan, N. *Coord. Chem. Rev.* **2016**, 308, 191-235. (b) Trovitch, R. J. *Synlett* **2014**, *25*, 1638-1642.

21. (a) Igarashi, M.; Fuchikami, T. *Tetrahedron Lett.* **2001**, *42*, 1945-1947. (b) Zheng, J.; Chevance, S.; Darcel, C.; Sortais, J.-B. *Chem. Commun.* **2013**, *49*, 10010-10012.

22. (a) Mao, Z.; Gregg, B. T.; Cutler, A. R. *J. Am. Chem. Soc.* **1995**, *117*, 10139-10140. (b) Cavanaugh; M. D.; Gregg, B. T.; Cutler, A. R. *Organometallics* **1996**, *15*, 2764-2769. (c) Son, S. U.; Paik, S.-J.; Lee, I. S.; Lee, Y.-A.; Chung, Y. K.; Seok, W. K.; Lee, H. N. *Organometallics* **1999**, *18*, 4114-4118. (d) Son, S. U.; Paik, S.-J.; Chung, Y. K. *J. Mol. Catal. A: Chem.* **2000**, *151*, 87-90.

23. Ghosh, C.; Mukhopadhyay, T. K.; Flores, M.; Groy, T. L.; Trovitch, R. J. *Inorg. Chem.* **2015**, *54*, 10398-10406.

24. Chidara, V. K.; Du, G. *Organometallics* **2013**, *32*, 5034-5037.

25. Mukhopadhyay, T. K.; Flores, M.; Groy, T. L.; Trovitch, R. J. *J. Am. Chem. Soc.* **2014**, *136*, 882-885.

26.Zhou, W.; Marquard, S. L.; Bezpalko, M. W.; Foxman, B. M.; Thomas, C. M. *Organometallics* **2013,** *32*, 1766-1772.

27. Wang, Y.; Gu, P; Wang, W. Wei, H. *Catal. Sci. Technol.* **2014**, *4*, 43-46.

28. (a) Du, G.; Fanwick, P. E.; Abu-Omar, M. M. **2007**, *129*, 5180-5187. (b) Ison, E. A.; Trivedi, E. R.; Corbin, R. A.; Abu-Omar, M. M. **2005**, *127*, 15374-15375.

29. Pal, R.; Groy, T. L.; Bowman, A. C.; Trovitch, R. J. *Inorg. Chem.* 2014, *53*, 9357-9365.

30. Benkeser, R. A.; Landesman, H.; Foster, D. J. *J. Am. Chem. Soc.* **1952**, *74*, 648-650.

31. Ben-Daat, H.; Hall, G. B.; Groy, T. L.; Trovitch, R. J. *Eur. J. Inorg. Chem.* **2013**, 4430-4442.

CHAPTER 4

CARBON DIOXIDE PROMOTED PROTON REDUCTION USING A

BIS(IMINO)PYRIDINE MANGANESE COMPLEX AND INVESTIGATION OF

MECHANISTIC PATHAWAYS

4.1. Abstract:

Heating a 1:1 mixture of $(CO)_5MnBr$ and the phosphine-substituted pyridine diimine ligand, $^{Ph2PPr}PDI$, in THF at 65 °C for 24 h afforded the diamagnetic complex $[(^{Ph2PPr}PDI)Mn(CO)][Br]$ **(6)**. Higher temperatures and longer reaction times resulted in bromide displacement of the remaining carbonyl ligand and the formation of paramagnetic $(^{Ph2PPr}PDI)MnBr$ **(7)**. The molecular structure of **6** was determined by single crystal X-ray diffraction, and density functional theory (DFT) calculations indicate that this complex is best described as low-spin Mn(I) bound to a neutral $^{Ph2PPr}PDI$ chelating ligand. The redox properties of **6** and **7** were investigated by cyclic voltammetry (CV), and each complex was tested for electrocatalytic activity in the presence of both CO_2 and Brønsted acids. Although electrocatalytic response was not observed when CO_2, H_2O, or MeOH was added to **6** individually, the addition of H_2O or MeOH to CO_2-saturated acetonitrile solutions of **6** afforded voltammetric responses featuring increased current density as a function of proton source concentration (i_{cat}/i_p up to 2.4 for H_2O or 4.2 for MeOH at scan rates of 0.1 V/s). Bulk electrolysis using 5 mM **6** and 1.05 M MeOH in acetonitrile at -2.2 V vs $Fc^{+/0}$ over the course of 47 min gave H_2 as the only detectable product with a Faradaic efficiency of 96.7%. Electrochemical experiments indicate that CO_2 promotes **6**-mediated H_2 production by lowering apparent

pH. While evaluating **7** for electrocatalytic activity, this complex was found to decompose rapidly in the presence of acid. Reduction of **6** using Na/Hg allowed for the isolation of a formal Mn(0) complex (^{Ph2PPr}PDI)Mn(CO) **(8)**. Stronger reducing conditions resulted in the formation of formal Mn(-I) complexes relevant to catalytic proton reduction. Preliminary electronic structure of these reduced intermediates have been investigated thoroughly using spectroscopy and X-ray diffraction analysis. Although modest H$^+$ reduction reactivity was realized, the experiments described herein indicate that care must be taken when evaluating Mn complexes for electrocatalytic CO_2 reduction.

4.2. Introduction:

Storing solar energy by using it to convert abundant low-energy molecules into high-energy commodity chemicals that may be used as fuel is a critical future technology.[1-2] A key component of such technology is a reduction catalyst that acts in concert with an oxidation catalyst and a light harvesting device to efficiently drive an uphill reaction. To be economically viable and deployable on a large scale, the catalyst material should only use inexpensive and highly abundant elements.[3] Recent efforts have produced a number of interesting first-row metal complexes[4-6] capable of reducing, for example, H$^+$ to hydrogen gas.[7] Whereas hydrogen gas could be used directly as a fuel, the inconveniences of storage and transport[8] render CO_2 reduction products much more interesting targets.[9] The electrocatalytic reduction of carbon dioxide may give a variety of products,[10] of which carbon monoxide and formic acid are most frequently encountered.

Recently, several remarkable CO_2 reduction catalysts based on first-row metals have been reported.[11-13] Chardon-Noblat and Deronzier[14] showed that Mn complexes of the general formula (bpy-R_2)(CO)$_3$MnX (bpy-R_2 = 4,4'-disubstituted-2,2'-bipyridine, X = halide) can convert CO_2 to CO electrocatalytically with selectivities that are comparable to their widely investigated Re congeners.[15] Subsequently, Kubiak demonstrated that (bpy-$^tBu_2$)(CO)$_3$MnBr catalyzes the reduction of CO_2 to CO with a turnover frequency (TOF) of 340 s^{-1} at -2.2 V *vs*. SCE in the presence of 1 M 2,2,2-trifluoroethanol.[16] The 6,6'-dimesityl-substituted bpy ligand is thought to prevent catalyst dimerization, increasing the TOF of CO_2 reduction to 5,000 s^{-1}.[17] When employed with a Ru(II) photosensitizer, (bpy)(CO)$_3$MnBr was shown to convert CO_2 to formic acid with a turnover number (TON) of 149, while producing minor amounts of CO and H_2 with TONs of 12 and 14, respectively.[18] When cast in a Nafion film on a glassy carbon electrode, (bpy)(CO)$_3$MnBr mediated CO_2 reduction resulted in the simultaneous formation of CO and H_2 approximately in a ratio of 1:2.[19]

Many Mn-complexes capable of reducing CO_2 carry bpy ligands,[20] but some α-diimine[21-22] and 2-pyridyl-*N*-heterocyclic carbene[23] complexes of Mn have also been reported to be catalytically active. Redox non-innocence of the bpy[24] and α-diimine[25] ligands is believed to be the key to CO_2 reduction: by storing electrons not only on the metal, but also on the ligands during the formation of the catalytically competent intermediates,[15d,22] these complexes are thought to access formal oxidation states that are unusually low with relatively small energetic penalties. Thus, we hypothesized by analogy that redox non-innocent 2,6-bis(imino)pyridine (or pyridine diimine, PDI) ligands[26] may form electrocatalytically active complexes, as indicated in Figure 4.1.

Having previously discovered that $(k^5\text{-}N,N,N,P,P\text{-}^{Ph2PPr}PDI)Mn^{27}$ exhibits carbonyl hydrosilylation activities that are 180 times greater than those reported for $(Ph_3P)(CO)_4MnC(O)CH_3$ (Fig. 4.1, **B** and **A**, respectively),[28,29] herein we describe a (PDI)Mn complex[37] that mimics the $(bpy)(CO)_3MnBr$ system (Fig. 4.1) but prevents the unproductive catalyst dimerization side reaction observed for the prominent $(bpy)(CO)_3MnBr$ catalyst.[14] The (PDI)Mn system has been shown to be capable of producing H_2 with modest rate. Additionally, relevant intermediates are isolated to obtain insight into the operable mechanism.

Ketone Hydrosilylation
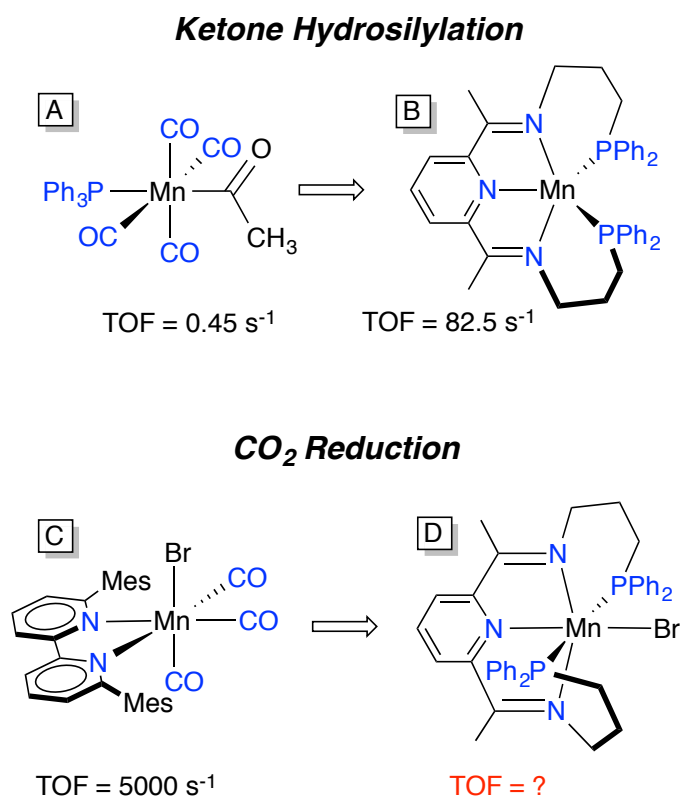
CO$_2$ Reduction

Figure 4.1. Considering a pentadentate PDI chelate for Mn-based electrocatalytic CO_2 reduction. Formally neutral ligands are shown in blue. By analogy, we speculate that **D** may be an active CO_2 reduction catalyst, as indicated by the question marks for TOF in red.

4.3. Synthesis and characterization of [(^{Ph2PPr}PDI)Mn(CO)]Br and (^{Ph2PPr}PDI)MnBr:

A stoichiometric quantity of the ^{Ph2PPr}PDI ligand was added to a THF solution of (CO)$_5$MnBr (Scheme 4.1). Although no immediate change was observed at ambient temperature, heating the reaction in a thick-walled glass vessel to 65 °C for 24 h resulted in a dark solution and a significant amount of purple precipitate. Isolation of the precipitate and analysis by ^{31}P NMR spectroscopy revealed a single resonance at 55.42 ppm, suggesting that the chelating phosphine substituents are equivalent and attached to Mn. Infrared spectroscopy revealed a single CO stretch at 1825 cm^{-1}, identifying this product as the monocarbonyl complex, [(^{Ph2PPr}PDI)Mn(CO)][Br] (Scheme 4.1, **6**).[37] This formulation is further supported by the poor solubility of **6** in non-polar solvents. The UV-vis spectrum of **6** (Figure 4.5, left) shows two intense absorption maxima at 368 nm (e = 4049 M^{-1}cm^{-1}) and 528 nm (e = 6837 M^{-1}cm^{-1}) along with a weak band at 672 nm (e = 826 M^{-1}cm^{-1}).
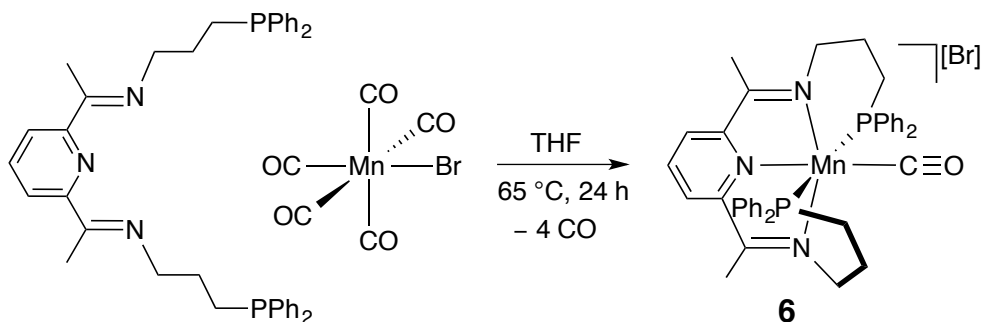
Scheme 4.1. Synthesis of [(^{Ph2PPr}PDI)Mn(CO)][Br] (**6**).

The composition of **6** was confirmed by single crystal X-ray diffraction (Fig. 4.3) and the metrical parameters determined for this complex are provided in Table 4.1. The geometry about the Mn center of **6** can best be described as distorted octahedral with N(1)-Mn(1)-N(3) and P(1)-Mn(1)-P(2) angles of 155.14(19) and 162.95(7)°,

respectively. The Mn-N [1.981(5), 1.931(4), and 1.996(5) Å] and Mn-P [2.2777(17) and 2.2974(18) Å] distances are relatively short, indicative of a low-spin Mn electronic configuration.[27,31] Importantly, inspection of the PDI chelate imine C=N distances reveals moderate elongation [1.311(7) and 1.310(8) Å] relative to those determined for unreduced PDI ligands (1.28 Å).[26b] The C(2)-C(3) and C(7)-C(8) distances determined for **6** of 1.456(8) and 1.446(8) Å, respectively, are significantly contracted from the C_{imine}-$C_{pyridine}$ distances found for unreduced chelates (1.50 Å).[26b] Taken together, these parameters suggest that **6** might possess a PDI chelate monoanion that is antiferromagnetically coupled to a low-spin Mn(II) center.
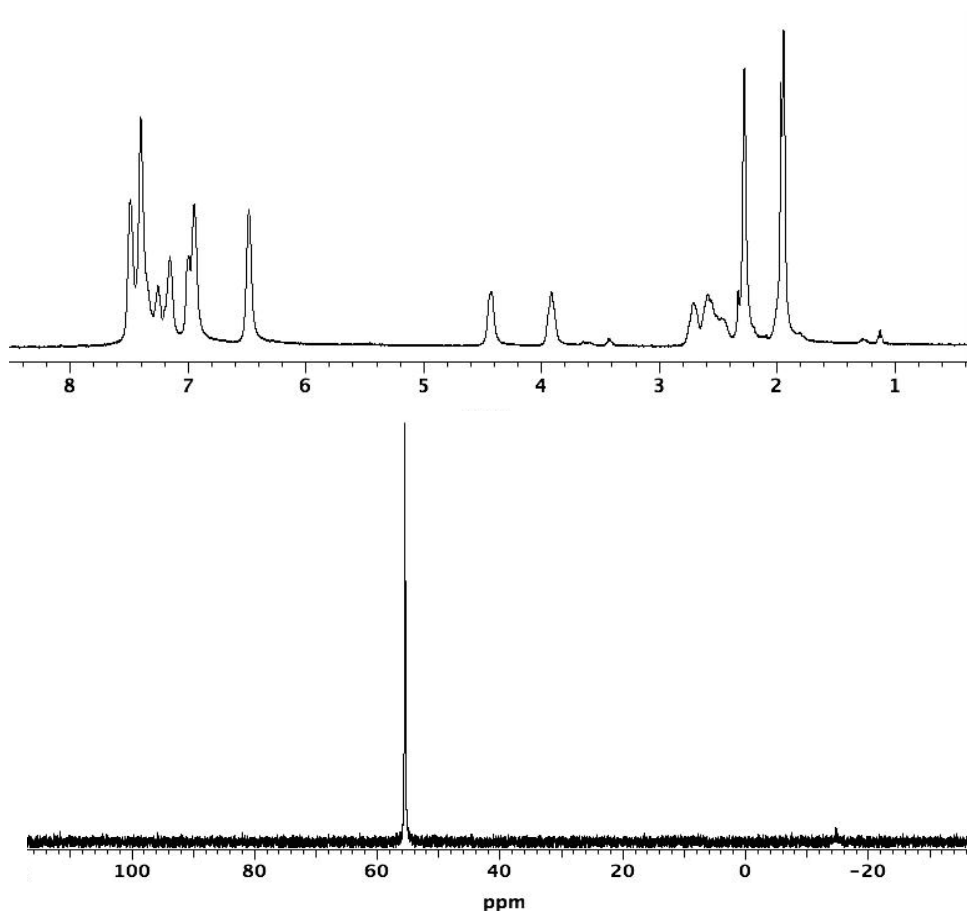
Figure 4.2. ^{1}H NMR (**top**) and ^{31}P NMR (bottom) spectra of **6**.

117
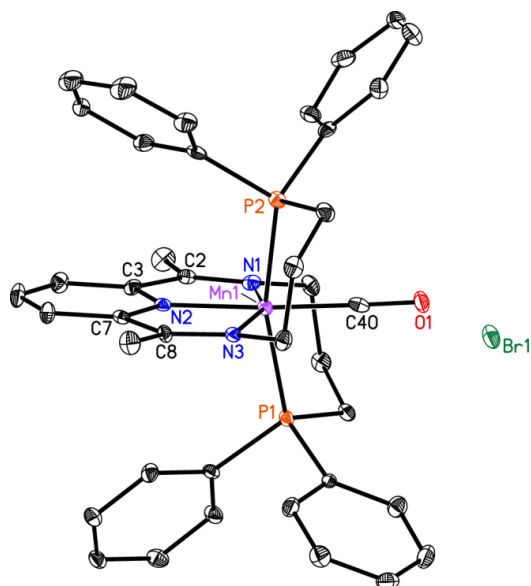
Figure 4.3. The solid-state structure of **6** shown at 30% probability ellipsoids. Hydrogen atoms and a co-crystallized pentane molecule are omitted for clarity.

Table 4.1. Relevant bond lengths (Å) and angles (°) for **6**.

Mn(1)-N(1)	1.981(5)	C(8)-N(3)	1.310(3)
Mn(1)-N(2)	1.931(4)	C(7)-C(8)	1.446(8)
Mn(1)-N(3)	1.996(5)	C(3)-N(2)	1.354(6)
Mn(1)-P(1)	2.2777(17)	C(7)-N(2)	1.370(7)
Mn(1)-P(2)	2.2974(18)	N(1)-Mn(1)-N(3)	155.14(19)
Mn(1)-C(40)	1.773(7)	N(2)-Mn(1)-C(40)	176.2(2)
C(40)-O(1)	1.177(7)	Mn(1)-C(40)-O(1)	92.16(4)
C(2)-N(1)	1.311(7)	P(1)-Mn(1)-P(2)	162.95(7)
C(2)-C(3)	1.456(8)		

To further clarify the electronic structure, density functional theory (DFT) calculations were performed on **6**. Ongoing unpublished work in our laboratory on [(κ^5-*N,N,N,P,P*-^{Ph2PPr}PDI)Mn] (Fig. 4.1, **B**) showed that the PBE functional provided good agreement with the experimental crystal structure and ground spin state. Therefore, we started by employing this method. Our calculations confirmed that **6** is a ground-state singlet, with the triplet state lying 17.3 kcal/mol higher in energy. This singlet converged

to a closed-shell state that is well-formulated as a Mn(I) state as shown in the qualitative molecular orbital diagram in Figure 4.4. The triplet involved promotion of an electron from the d_{xy} orbital into one of the PDI-based ligand orbitals (L1). A broken-symmetry orbital solution could be found for the triplet geometry, but attempts to perform a geometry optimization resulted in collapse to the closed-shell state. It is a reasonable assumption that the triplet and broken-symmetry singlet have similar geometries if the coupling between the electrons is weak, so we evaluated the energy of the broken-symmetry singlet at this geometry. As is typically the case, the broken-symmetry singlet was essentially isoenergetic with the triplet. This relative stability of the closed-shell configuration is likely due to the stabilizing effect of the π-acidic CO ligand, which lowers the energy of the metal-based (pseudo)-t_{2g} orbitals by removing electron density from the metal center and therefore increasing the energetic penalty for exciting an electron into a PDI-based orbital.
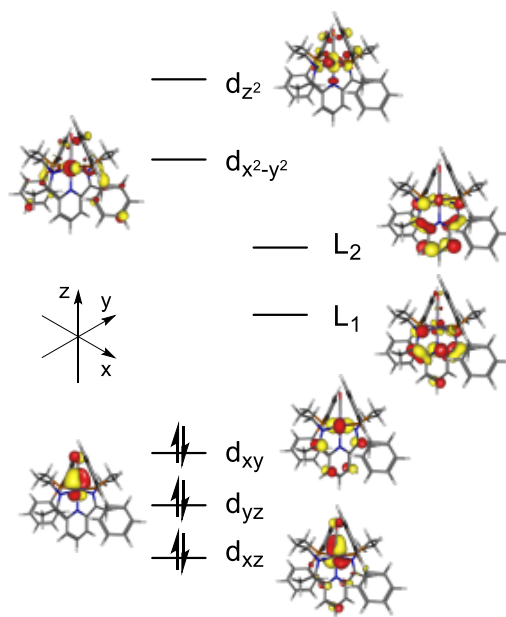
Figure 4.4. Energy-level diagram illustrating the calculated frontier orbitals of **6**.

As pure-GGA functionals such as PBE have a tendency to overestimate the stability of low-spin states we decided to perform single-point energy evaluations on our PBE geometries using the hybrid-GGA B3LYP to see if spin-state ordering would be significantly functional dependent. Using B3LYP, the triplet state is 8.2 kcal/mol higher in energy than the closed-shell singlet. The broken-symmetry singlet is still effectively isoenergetic with the triplet. Despite the large change in the magnitude of the spin-state energetics the closed-shell singlet is still predicted to be lower in energy than spin-states that invoked a reduced PDI-ligand.

While the optimized structures of both the triplet and singlet states for **6** agreed reasonably well with the crystallographic bond lengths for the PDI ligand, the Mn–P bond lengths show significant differences for the two spin states. The Mn–P bond lengths are significantly longer than the crystal structure for the triplet (both are 2.41 Å) whereas the singlet Mn–P bond lengths are a closer match (both are 2.34 Å). As mentioned earlier, it is likely that the broken-symmetry singlet geometry is very similar to the triplet, and hence this structural difference further confirms the assignment of the ground state as a closed shell singlet. These computational results suggest that **6** possesses an unreduced PDI chelate and that crystallographically observed N_{imine}–C_{imine} bond elongation and C_{imine}–$C_{pyridine}$ bond contraction are due to Mn-to-PDI backbonding rather than one-electron reduction of the chelate.

During preparations of **6**, small quantities of a bright blue toluene-soluble product were collected from reactions allowed to stir at 65 °C for longer than 24 h. To characterize this side product, an equimolar mixture of ^{Ph2PPr}PDI and $(CO)_5MnBr$ in toluene was intentionally heated to 80 °C for 72 h. The removal of CO and solvent

allowed for the isolation of a bright blue paramagnetic solid which has been identified as (^{Ph2PPr}PDI)MnBr (Scheme 4.2, **7**).[37] When analyzed by infrared spectroscopy, stretching frequencies consistent with CO coordination were absent, suggesting that complete carbonyl ligand displacement had occurred. The ^{1}H NMR spectrum exhibited a predominant paramagnetically shifted resonance at 74.68 ppm while signals attributable to **7** were not observed by ^{13}C NMR spectroscopy. The magnetic susceptibility of this complex was determined to be 4.4 μ_B at 297 K (Evans Method), suggestive of a high spin Mn(II) center that is antiferromagnetically coupled to a κ^4-N,N,N,P-^{Ph2PPr}PDI radical monoanion. Complex **7** has also been prepared by heating isolated samples of **6** under vacuum.
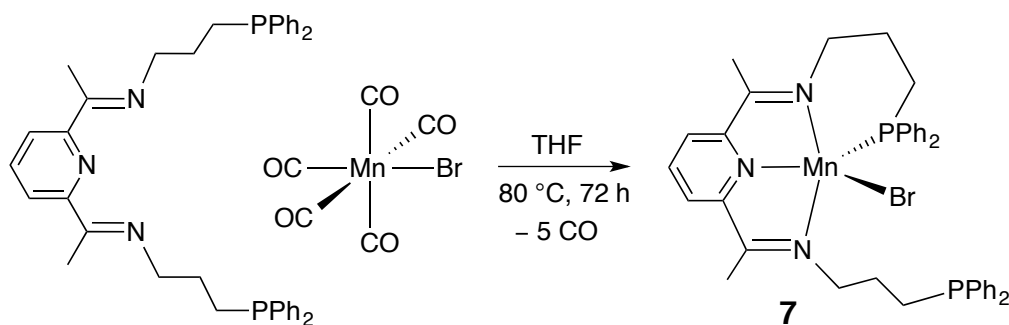
Scheme 4.2. Synthesis of (^{Ph2PPr}PDI)MnBr **(7)**.
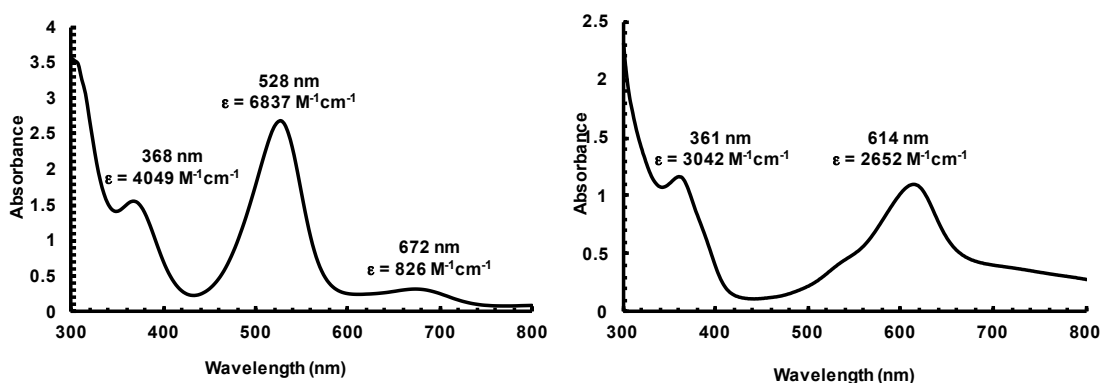
Figure 4.5. The UV-vis spectra of **6** (left) and **7** (right). The concentration used for both complexes is 3.86 x 10^{-4} M.

4.4. Electrochemical analysis:

4.4.1. Cyclic voltammetry of 6 and 7:[37]

The redox properties of **6** and **7** were analyzed by cyclic voltammetry. In 0.1 M [Bu$_4$N][PF$_6$] acetonitrile solution, cyclic voltammograms of **6** were found to feature two reversible waves with midpoint potentials of -0.30 V and -1.92 $vs.$ Fc$^{+/0}$ (all potentials are quoted relative to Fc$^{+/0}$ as an internal standard, Figure 4.6 A). The smaller wave at -0.30 V is attributed to the one electron oxidation of **6** to form the Mn(II) complex, whereas the second two-electron reduction wave at -1.92 V is associated with the formation of the formal Mn(-I) complex. Bulk electrolysis experiments revealed that the wave at -1.92 V becomes irreversible after passing more than 2.0 F/mol of charge, supporting the assignment of a two-electron reduction. The observation of a two-electron reduction, instead of a pair of successive one-electron reductions suggests that **6** does not dimerize upon reduction, as has been reported for (bpy-^{t}Bu$_2$)(CO)$_3$MnBr.[16] Although reduction of **6** occurs at a potential 370 mV more negative than the reversible two-electron reduction reported for (bpy-Mes$_2$)(CO)$_3$MnBr (1.55 V),[17] the latter does not exhibit electrocatalytic CO$_2$ to CO reduction until approximately -2.0 V (overpotential = 0.7 V), rendering the redox properties of **6** promising for analogous activity. In contrast, cyclic voltammograms of **7** show only irreversible waves at -2.70 and -3.11 V, corresponding to complex reduction (Figure 4.6 B).

4.4.2. Evidence for electrocatalysis:

To investigate the possibility that **6** is a CO$_2$ reduction precatalyst, cyclic voltammograms of this complex were collected in dry and wet CO$_2$-saturated

acetonitrile.[32] As shown in Figure 4.7, the reduction at -2.03 V becomes irreversible upon

saturation of the solution with CO_2, but an increase in current was not detected. Data

collected from a CO_2-saturated acetonitrile solution of **6** including 3.0 M H_2O showed a

significant increase in reductive current, indicating that **6** performs reductive catalysis in

the presence of CO_2 and H_2O at approximately -1.9 V. Similar experiments were

conducted using **7**, but H_2O addition resulted in immediate decomposition of the

complex.
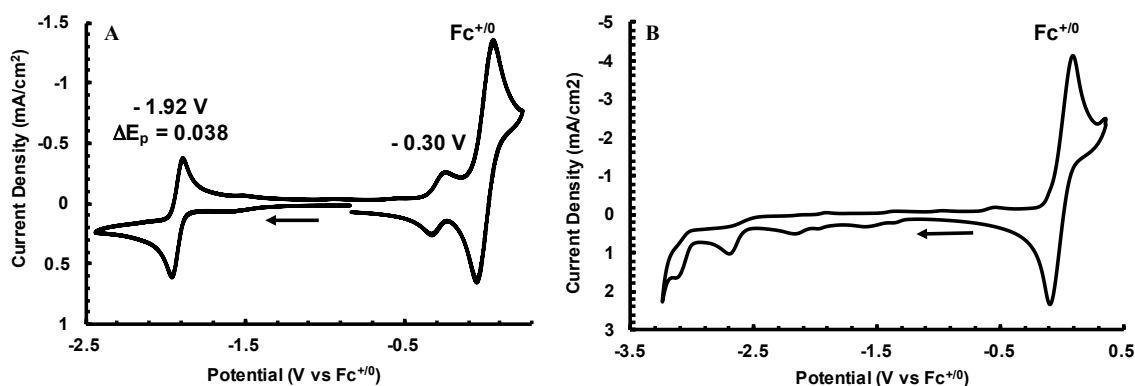
Figure 4.6. Cyclic voltammogram of **6** (A) and **7** (B) in 0.1 M [Bu$_4$N][PF$_6$] acetonitrile. Ferrocene used as an internal standard (wave centered at 0.0 V). Potential scan rate = 0.1 V/s. Arrow indicates the direction of cycling.
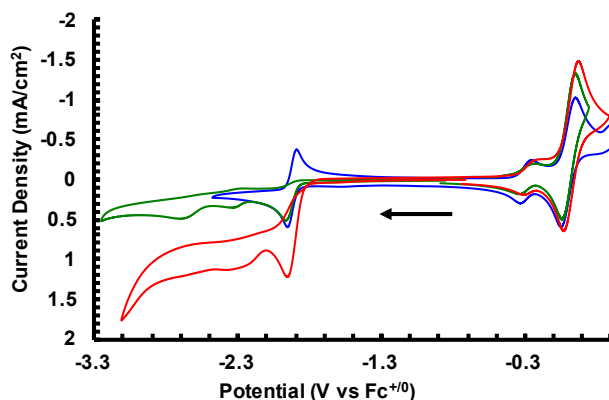
Figure 4.7. Cyclic voltammograms of **6** (blue), a solution of **6** saturated with CO_2 (green), and a CO_2 saturated solution of **6** containing 3.0 M H_2O (red). All

voltammograms collected in 0.1 M [Bu$_4$N][PF$_6$] acetonitrile using ferrocene as an internal standard (scan rate = 0.1 Vs^{-1}). Complex **6** is present at 1 mM concentration in all three experiments.

4.4.3. Electrocatalysis and controlled experiments:

To characterize electrocatalysis by **6**, voltammograms were collected with varying quantities of Brønsted acid in CO_2-saturated 1 mM solutions of complex. The current density in dry solvent at -1.98 V was 0.5 mA/cm^2; increasing water concentration from 0.55 M to 3.15 M H_2O displayed a rise in current density up to 1.2 mA/cm^2 with i_{cat}/i_p = 2.4 (Figure 4.8 A). To ensure that the catalyst remains homogenous, the "rinse test" was employed. The electrode was removed from a catalytically active solution containing 2.15 M H_2O in acetonitrile, rinsed with dry acetonitrile, and placed in a CO_2-saturated water/acetonitrile solution without catalyst. No activity was observed (Figure 4.8 B), suggesting that electrode-deposits and the electrode itself are not likely to be responsible for catalysis. Although this data is suggestive of CO_2 reduction, a lowering in apparent pH from 9.3 (no H_2O) to 7.7 (3.15 M H_2O) was observed for H_2O/acetonitrile solutions of **6** under a continuous CO_2 purge. The pH values determined under CO_2 were reproduced for each of the H_2O concentrations in Figure 4.9 A using Good's buffer, and comparable catalytic current was observed at -1.99 V in the absence of CO_2 (Figure 4.10). This control experiment suggests that CO_2 is likely reacting with H_2O to form carbonic acid, which lowers the apparent pH of the catalyst solution enough to promote **6**-mediated H_2 production.
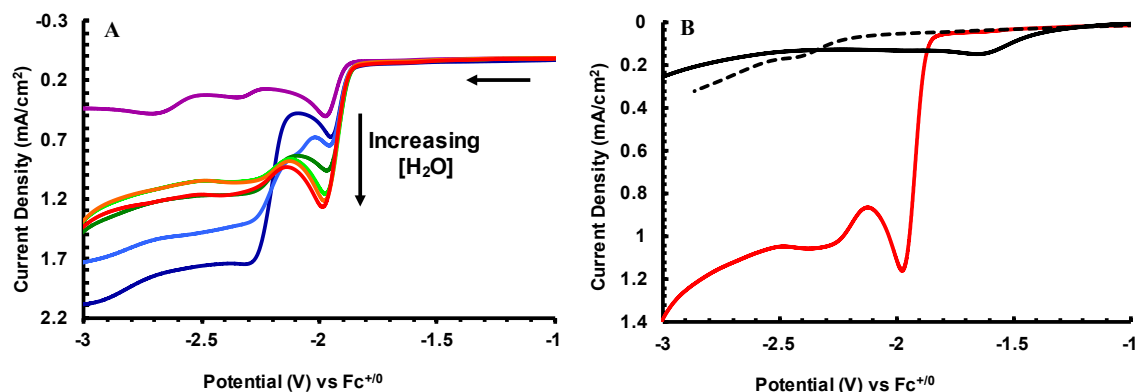
Figure 4.8. (A) Partial cyclic voltammograms of **6** showing electrocatalytic reduction as a function of increasing H_2O concentration in CO_2-saturated 0.1 M [Bu$_4$N][PF$_6$] acetonitrile solution. In absence of manganese (dotted black), post electrolysis electrode in absence of manganese (solid black), no water (purple), 0.55 M H_2O (dark blue), 1.10 M H_2O (light blue), 1.65 M H_2O (dark green), 2.15 M H_2O (bright green), 2.65 M H_2O (orange), 3.15 M H_2O (red). **(B)** Partial cyclic voltammograms demonstrating that the post electrolysis electrode is not responsible for catalysis. The experiments were conducted at a scan rate of 0.1 V s^{-1} following CO_2 saturation: (a) 1 mM [(**^{Ph2PPr}PDI)Mn(CO)][Br**] in the presence of 2.15 M H_2O (green). (b) 2.15 M H_2O using post catalysis electrode without [(**^{Ph2PPr}PDI)Mn(CO)][Br**] (solid black). (c) 2.15 M H_2O using clean electrode without [(**^{Ph2PPr}PDI)Mn(CO)][Br**] (dotted black).
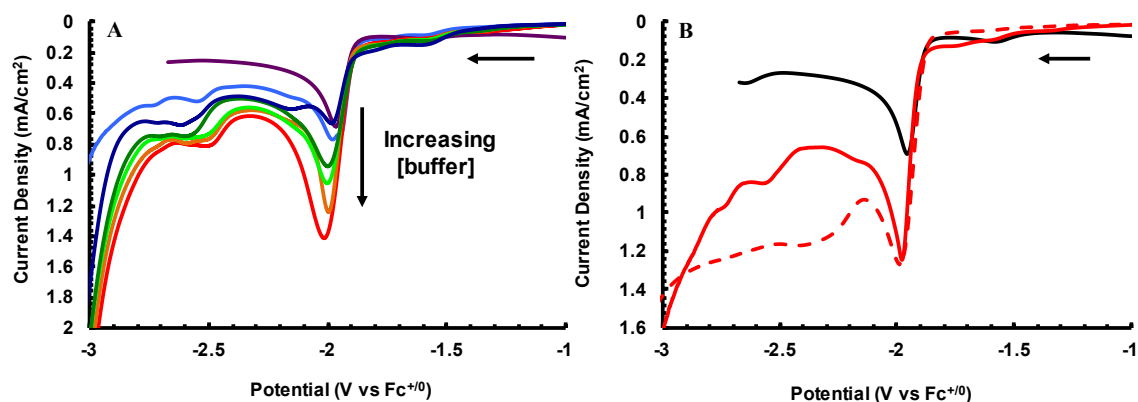
Figure 4.9. (A) The apparent pH values of CO_2 saturated solutions of 1 mM [(**^{Ph2PPr}PDI)Mn(CO)][Br**] in 0.1 M [Bu$_4$N][PF$_6$] possessing different concentrations of water were measured: no water (9.3), 0.55 M (8.9), 1.10 (8.4), 1.65 M (8.2), 2.15 M (8.0), 2.65 M (7.9), 3.15 (7.7). These apparent pH values were mimicked using Good's buffer (MES-TAP-HEPS-CHES; 0.15 M in water) and partial cyclic voltammograms were collected in acetonitrile in the absence of CO_2: 0 M (purple), 0.55 M (deep blue), 1.10 M (light blue), 1.65 M (deep green), 2.15 M (bright green), 2.65 M (orange), 3.15 M (red). Scan rate of 0.1 V/s. Complex **6** is present at 1 mM concentration in all experiments. **(B)** Partial cyclic voltammograms of 1 mM [(**^{Ph2PPr}PDI)Mn(CO)][Br**] in acetonitrile (black),

1 mM **[(^{Ph2PPr}PDI)Mn(CO)][Br]** in a 3.15 M H_2O/acetonitrile solution containing Good's buffer (pH = 7.8) in absence of CO_2 (solid red), and 1 mM **[(^{Ph2PPr}PDI)Mn(CO)][Br]** in CO_2-saturated 3.15 M H_2O/acetonitrile solution (pH = 7.8, dotted line). 0.1 M [Bu_4N][PF_6] was used as electrolyte. Scan rate of 0.1 V/s.
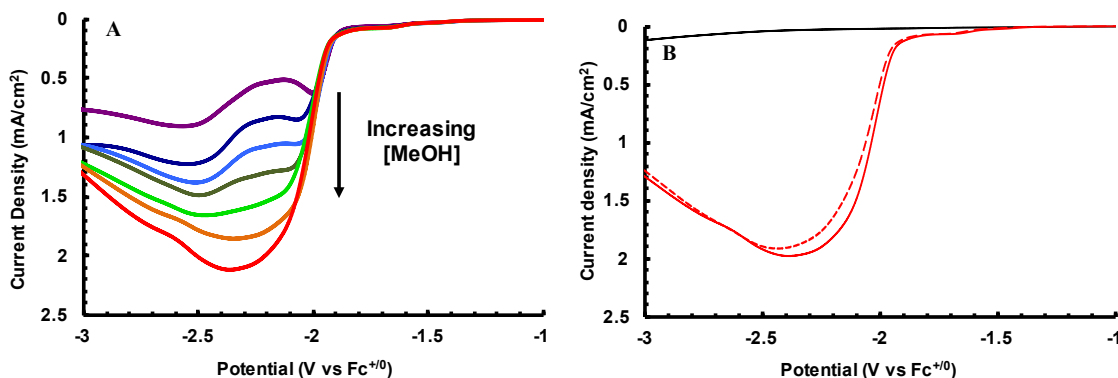
Figure 4.10. Partial cyclic voltammograms of **6** showing electrocatalytic reduction as a function of increasing methanol concentration in CO_2-saturated 0.1 M [Bu_4N][PF_6] acetonitrile. **(A)** 0.15 M MeOH (purple), 0.30 M MeOH (dark blue), 0.45 M MeOH (light blue), 0.60 M MeOH (dark green), 0.75 M MeOH (bright green), 0.90 M MeOH (orange), 1.05 M MeOH (red). All voltammograms collected using ferrocene as an internal standard at a scan rate = 0.1 Vs^{-1}. Complex **6** is present at 1 mM concentration in all experiments. **(B)** Partial cyclic voltammograms demonstrating that light is not required for catalysis. The following experiments were conducted in 0.1 M [NBu_4][PF_6]/MeCN at a scan rate of 0.1 V s^{-1} following CO_2 saturation: (a) 1 mM **[(^{Ph2PPr}PDI)Mn(CO)][Br]** and 1.05 M MeOH in light (solid red). (b) 1 mM **[(^{Ph2PPr}PDI)Mn(CO)][Br]** and 1.05 M MeOH in the absence of light (dotted red). (c) 1.05 M MeOH using post catalysis electrode without **[(^{Ph2PPr}PDI)Mn(CO)][Br]** (solid black).

To circumvent carbonic acid formation, analogous electrochemical experiments were conducted in anhydrous MeOH. The addition of MeOH to CO_2-saturated 1 mM solutions of **6** resulted in even greater current densities of up to 2.1 mA/cm^2 at -2.33 V (i_{cat}/i_p = 4.2 for 1.05 M MeOH, Figure 4.10 A). Control experiments conducted on catalyst free CO_2-saturated MeOH solutions showed no evidence for electrode promoted H_2 production (Figure 4.10 B). Since metal carbonyls are often light sensitive,

voltammograms with 1.05 M MeOH were obtained in the dark and a minimal decrease in catalytic current was noted (1.9 vs. 2.1 mA/cm^2, Figure 4.10 B).

4.4.4. Controlled potential electrolysis:

Bulk electrolysis was then conducted to determine the products formed during reductive catalysis using **6**. Notably, bulk electrolysis of a CO_2-saturated solution of 5 mM **6** and 1.05 M MeOH in acetonitrile at -2.2 V over 47 min produced H_2 as the sole product as determined by gas chromatography (there was no evidence for CO formation). Quantifying the H_2 produced as a function of time yielded a Faradaic efficiency of 96.7% and a modest TOF of 0.176 h^{-1} (Figure 4.11).[37] Analysis of the post electrolysis solution by multinuclear NMR, infrared, and UV-visible spectroscopy revealed that **6** remained unmodified following electrolysis. This observation demonstrates that the catalyst does not scavenge newly generated CO and that the catalyst is stable beyond 47 min of active reduction.
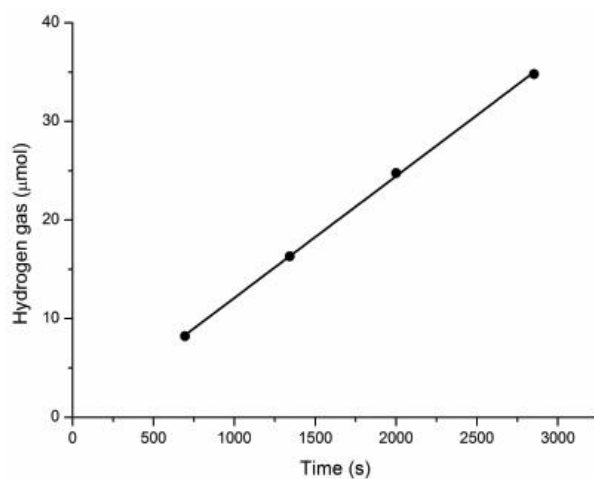
Figure 4.11. The evolution of H_2 during bulk electrolysis on a CO_2-saturated solution of 5 mM [(^{Ph2PPr}**PDI)Mn(CO)][Br]** and 1.05 M MeOH in acetonitrile at -2.2 V, as measured by GC.

127

The exclusive formation of H_2 in the bulk electrolysis raised an important question whether CO_2 has an active role in the proton reduction process. This encouraged us to perform additional control experiments. Cyclic voltammograms of **6** in the presence of 1.1 M MeOH without CO_2 was collected, which showed virtually unchanged values of current density from the noncatalytic voltammogramms obtained without MeOH. There was only a very subtle increase in current density relative to MeOH free experiments at low potentials (0.8 to 0.9 mA/cm^2 at -1.95 V, Figure 4.12 A). In contrast cyclic voltammograms obtained with MeOH under CO_2-saturated conditions afforded a drastically increased cathodic current density (2.6 mA/cm^2, Figure 4.12 A), suggesting that CO_2 plays a role in the observed catalysis. At this point it is reasonable to think that the observed H_2 production may be a result of lowering of pH of the medium caused by CO_2 saturation. The pseudo pH of an acetonitrile solution containing 1 mM **6** and 1.05 M MeOH was found to be 9.8 and purging with a continuous flow of CO_2 resulted in a reduced pseudo pH value of 8.4. Separately, benzoic acid was added to an acetonitrile solution containing 1 mM **6** and 1.05 M MeOH to achieve a pseudo pH of 8.1 in the absence of CO_2, and linear sweep voltammetry towards reducing potentials was found to result in a current density of 1.5 mA/cm^2 at -1.96 V (Figure 4.12 B). This current density is lower than the current density observed under CO_2 (2.5 mA/cm^2 at -2.05 V, Figure 4.12 B).

128
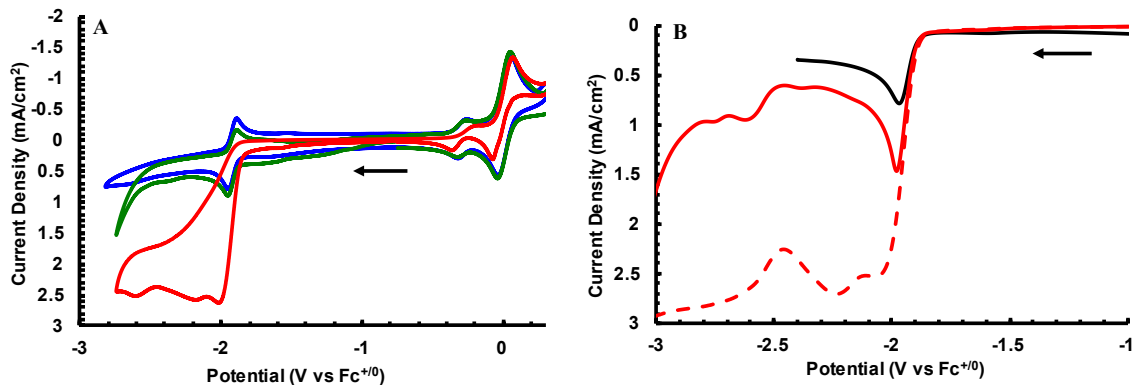
Figure 4.12. (A) Cyclic voltammograms of **1** (blue), **1** in the presence of 1.1 M MeOH (no CO_2, green), and a CO_2 saturated solution of **1** containing 1.1 M MeOH (red). All voltammograms collected in 0.1 M [Bu$_4$N][PF$_6$] acetonitrile solution using ferrocene as an internal standard (scan rate = 0.1 Vs^{-1}). Complex **1** is present at 1 mM concentration in all three experiments. **(B)** Linear sweep voltammograms of **1** (black), **1** in the presence of 1.05 M MeOH and 2mM PhCOOH (solid red), and **1** in a CO_2 saturated acetonitrile solution containing 1.05 MeOH (dashed red). All voltammograms collected in 0.1 M [Bu$_4$N][PF$_6$] acetonitrile solution using ferrocene as an internal standard (scan rate = 0.1 Vs^{-1}). Complex **1** is present at 1 mM concentration in all three experiments.

While the observation of catalytic current in the presence of benzoic acid is indicative of H^+ reduction, it was hypothesized that the lower than anticipated current density is due to concurrent **6**-mediated reduction of CO_2 to formic acid. Formic acid is a common product of photocatalytic[18] and membrane-supported[19] CO_2 reduction, and H_2 is a familiar side product in these reactions. To determine whether *in situ* generated formic acid would be further transformed under these conditions, cyclic voltammograms of 1 mM **6** in the presence of 0.2 M HCOOH were obtained in N_2-saturated solution. Compared to the voltammograms of **6** in the absence of acid, an increased cathodic current density of 1.2 mA/cm^2 was observed (*vs.* 0.6 mA/cm^2 at -2.0 V), suggesting that **6** is capable of producing hydrogen from formic acid. Voltammograms collected using a catalyst-free solution revealed that the working electrode would also be capable of

generating H_2 from HCOOH at potentials more negative than -1.75 V if generated during electrolysis.

A second attempt was made to conduct the bulk electrolysis a different working electrode a smaller cell in order to track whether small amount of CO are formed. The working electrode used in this case was a 3 mm diameter glassy carbon electrode. The controlled potential electrolysis was then performed using a CO_2-saturated solution of 5 mM **6** and 1.05 M MeOH in acetonitrile at -2.2 V over 3 h. Along with similar H_2 production (95.4 ± 4 %, rate = 3.3 s^{-1}), a trace amount of CO has been observed while analyzing the head space in GC. This electrolysis was performed again under identical conditions and in absence of CO_2 and similar CO formation was still noticed, which suggested partial decomposition of **6** under the experimental conditions. This was also confirmed by the decreased intensity in the electronic spectrum of **6** after electrolysis.

Taken together, the CV and bulk electrolysis experiments suggest that complex **6** is capable of producing H_2 from CO_2-acidified acetonitrile solutions of H_2O and MeOH, albeit with modest efficiency and minimal catalyst decomposition. Although a six-coordinate inner-sphere bromide complex mimicking (bpy)(CO)$_3$MnBr was initially targeted as an electrocatalyst (Figure 4.1, **D**), the inactivity of **7** in the presence of H_2O or MeOH suggests that the CO ligand of **6** is required for complex stabilization. The observed H^+ reduction is believed to take place following the reduction of **6** and concurrent dissociation of a ^{Ph2PPr}PDI phosphine group.[33] Although H_2 was not the desired electrolysis product, this study demonstrates that high-denticity chelates can prevent undesired electrocatalyst dimerization. Dimerization during Mn-catalyzed CO_2 reduction has recently been prevented with a 6,6'-dimesityl-substituted bpy ligand;[17]

however, terdentate and tetradentate 2,2'-bypridine and α-diimine supporting chelates represent intriguing alternatives to incorporating steric bulk, as they offer an opportunity to simultaneously tune the electronic properties of the metal.

4.5. Isolation of reduced intermediates:

4.5.1. Synthesis of (^{Ph2PPr}PDI)Mn(CO) (8):

In order to obtain further insight on the fate of complex **6** under reducing potentials, the chemical reduction of **6** has been attempted. It is apparent from the cyclic voltammetry of **6** (Figure 4.6 A) that the $2e^-$ reversible wave at -1.92 V vs $Fc^{+/0}$ is due to reduction of Mn(I) complex to a putative Mn(-I) species, which is likely to possess a reduced PDI chelate, such that (PDI$^-$)Mn(0) is a more appropriate representation of the electronic structure. Upon reacting with excess K/Hg for 6 h ^{1}H NMR and ^{31}P NMR spectroscopic analysis of the mixture revealed the formation of two complexes, one featuring broadened ^{1}H NMR resonances and the other featuring diamagnetic resonances indicative of a formal Mn(-I) complex. Due to the difficulty in isolating each product from the mixture, milder conditions were used. Upon reducing **6** with excess Na/Hg for 6 h a purple formal Mn(0) complex was isolated (Scheme 4.3), which displays broadened resonances in the ^{1}H NMR spectrum. This complex showed an IR stretching frequency at 1812 cm^{-1} for the lone CO ligand, which is lower than the value for **6** suggesting complex reduction.
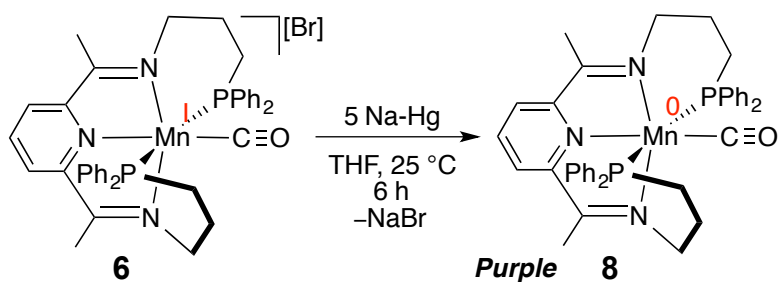
Scheme 4.3. Synthesis of (^{Ph2PPr}PDI)Mn(CO) **(8)**.
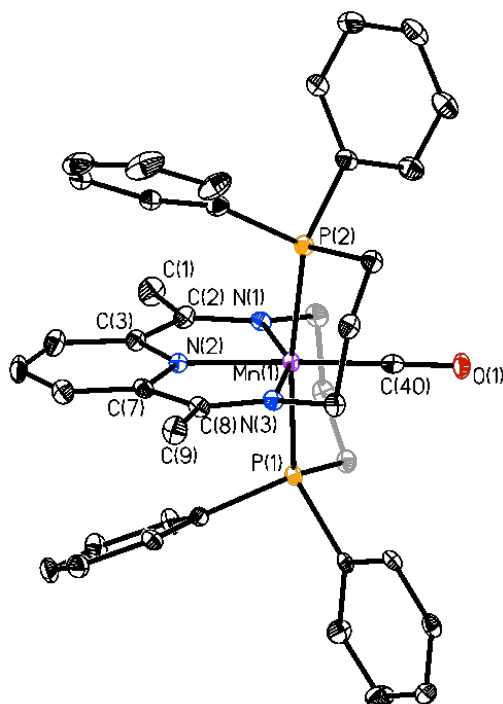
Figure 4.13. Solid-state structure of **8** shown at 30% probability ellipsoid. Hydrogen atoms and co-crystallized solvent molecules are omitted for clarity.

Table 4.2. Relevant bond lengths (Å) and angles (°) for **8**.

Mn(1)-N(1)	1.992(3)	C(8)-N(3)	1.356(3)
Mn(1)-N(2)	1.950(3)	C(7)-C(8)	1.429(3)
Mn(1)-N(3)	1.980(3)	N(1)-Mn(1)-N(3)	156.02(3)
Mn(1)-P (ave)	2.309(4)	N(2)-Mn(1)-C(40)	178.18(2)
Mn(1)-C(40)	1.759(4)	N(2)-Mn(1)-P(1)	92.16(4)
C(2)-N(1)	1.352(3)	P(1)-Mn(1)-P(2)	173.05(4)
C(2)-C(1)	1.428(3)		

This complex was also crystallized from concentrated toluene solution layered with diethylether and analysis by single crystal X-ray diffraction data revealed a six coordinate distorted octahedral complex κ^5-(^{Ph2PPr}PDI)Mn(CO) (Figure 4.13, **8**) with P(1)-Mn(1)-P(2), N(2)-Mn(1)-C(40), N(1)-Mn(1)-N(3), and N(2)-Mn(1)-P(1) angles of 173.05(4)°, 178.18(2)°, 156.02(3)°, and 92.16(4)° respectively (Table 4.2). The Mn(1)-N(1), Mn(1)-N(2), and Mn(1)-N(3) distances of 1.992(3), 1.950(3), and 1.980(3) Å, respectively, are shorter than that of **6** and suggest a low spin Mn center. The imine bonds, C(2)-N(1) and C(8)-N(3) are significantly elongated to 1.352(3) and 1.356(3) Å, while C(2)-C(3) and C(7)-C(8) bonds are shortened from C-C single bond lengths to 1.428(3) and 1.429(3) Å, respectively, which is an indicative of chelate reduction.[26b] Although these bond lengths strongly suggest a doubly reduced PDI chelate, the backbonding cannot be ignored, which was already seen in the case of **6**.
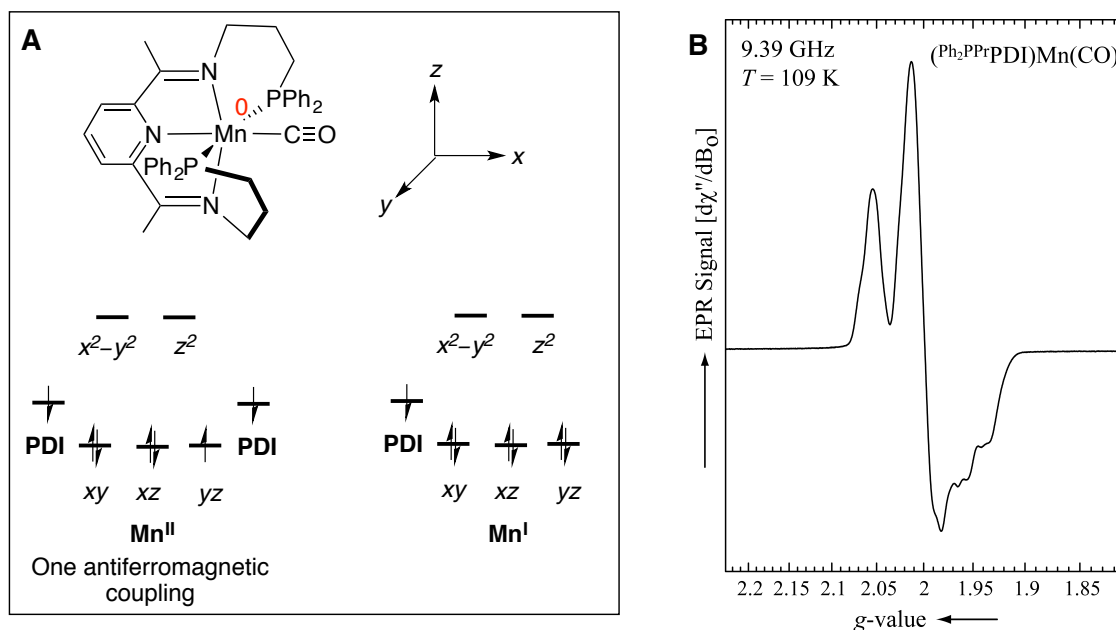
Figure 4.14. Qualitative d-orbital splitting **(A)**. The X-band EPR spectrum of **8** (g = 2.054, 1.999, and 1.95) collected in a toluene glass at 109 K. The microwave power was 4 mW, the modulation frequency 100 kHz and the modulation amplitude 0.2 mT.

133

Considering these facts and comparing these lengths to the reported values of PDI-chelate reduction,[26b] the electronic structure of **8** can be described by either cases shown in Figure 4.14 A. In both possibilities a ligand-centered radical exists, which has been confirmed by electron paramagnetic resonance (EPR) spectra. The X-band (9.39 GHz) EPR spectrum of **8** (Figure 4.14 B) resulted in a rhombic signal with 'g' values of 2.054, 1.999, and 1.959 that are consistent to organic ligand centered radical. The observed spectrum does not resemble those measured for Mn compounds, i.e. the spectrum does not show the hyperfine splitting corresponding to the nuclear spin of Mn. Although these electronic descriptions are supported by experimental parameters without a theoretical calculation it is difficult to depict the actual oxidation state of Mn in **8**.

4.5.2. Synthesis of formal Mn(-I) intermediates:

Isolation of a formal Mn(0) intermediate demanded further efforts towards the formally anionic manganese complexes. Complex **6** was reduced using excess K/Hg for 12 h, which yielded a dark green complex. A diethylether solution of this product produced dark green crystals at -35 °C, which were identified as $\{[\kappa^4\text{-}(^{Ph2PPr}PDI)Mn(CO)]K(Et_2O)]\}_2$ **(9)**. ^{1}H NMR of this complex displays resonances in the diamagnetic region and ^{31}P NMR contains two singlets at 83.24 and -15.63 ppm. The CO stretching frequency in **9** has been found at a surprisingly low wavenumber at 1698 cm^{-1} by IR spectroscopy. Single crystal X-ray diffraction of **9** (Figure 4.14) confirmed the dimeric structure with κ^4-*N,N,N,P*-PDI coordination, albeit the data was not of sufficient quality for publication. Each Mn center has distorted trigonal bipyramid geometry with

N(2)-Mn(1)-N(3), N(3)-Mn(1)-P(3), N(1)-Mn(1)-C(59) and N(1)-Mn(1)-P(3) angles of 157.84(2)°, 91.96(8)°, 138.61(2)°, and 131.78(8)° respectively.
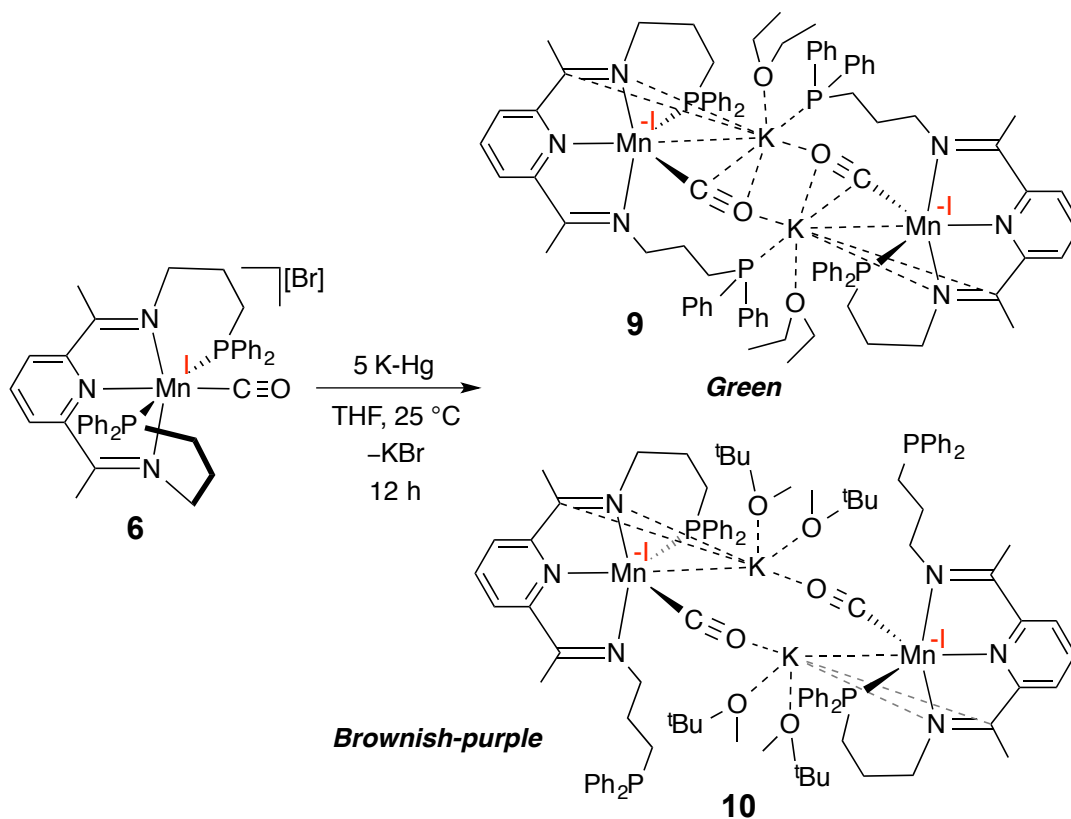
Scheme 4.4. Synthesis of formal Mn(-I) intermediates.
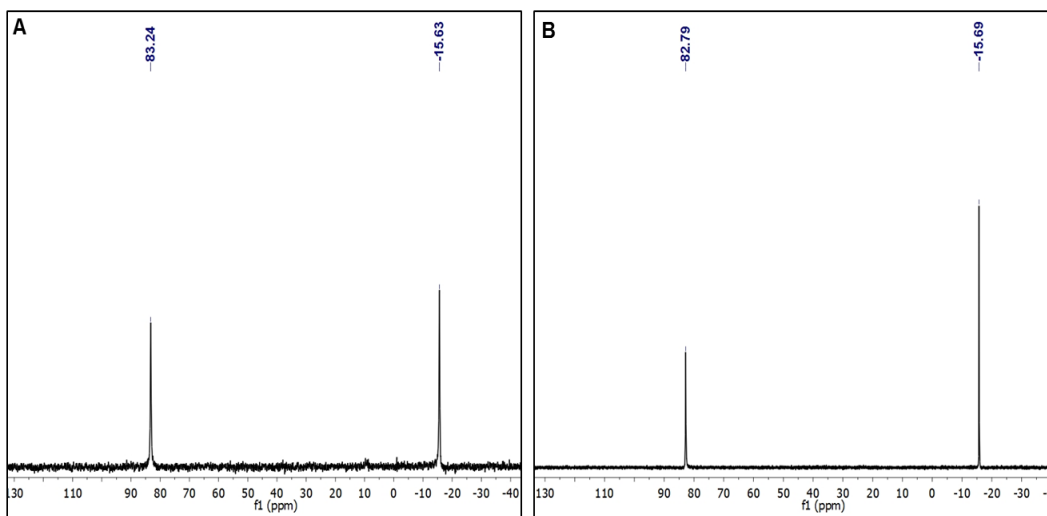
Figure 4.15. ^{31}P NMR spectra of **9** (A) and **10** (B) in benzene-d_6.

The Mn(1)-N(1), Mn(1)-N(2), Mn(1)-N(3), and Mn(1)-P(3) bond distances are 1.871(4), 1.942(3), and 1.929(3), and 2.194(8) Å respectively are shorter than **1** and **3** and suggesting a low spin Mn center. The chelate has been reduced significantly as the imine bonds C(25)-N(2) and C(27)-N(3) are elongated to 1.371(3) and 1.364(3) Å while C(25)-C(20) and C(27)-C(24) bonds contracted to 1.418(3) and 1.404(3) Å. Interestingly an unusual K-PDI coordination mode has been observed in the solid-state structure of **9**.
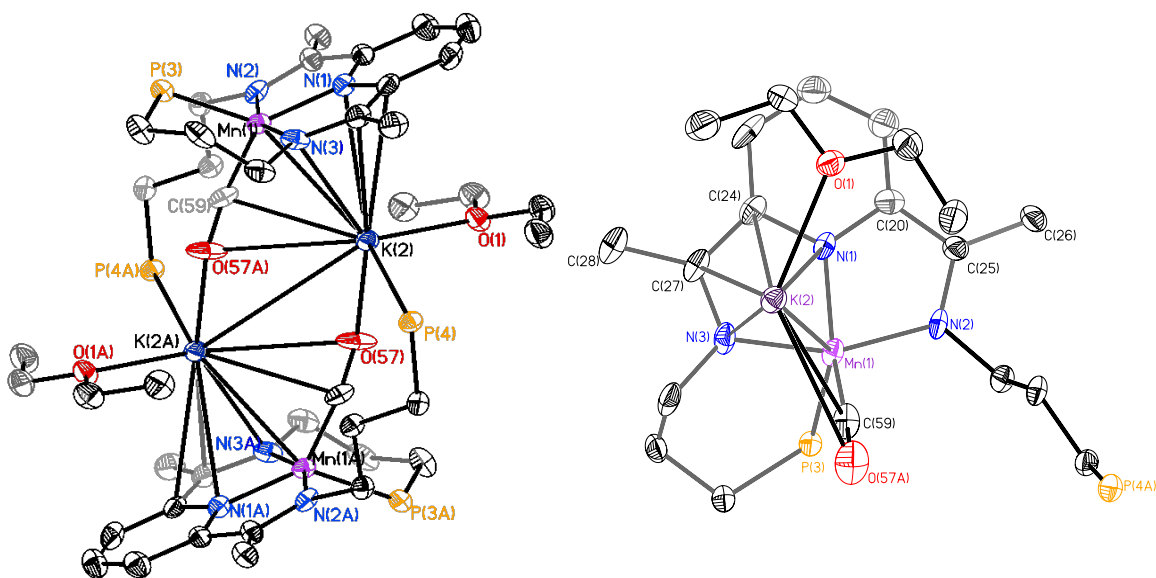
Figure 4.16. Solid-state structure of **9** (left) shown at 30% probability ellipsoids. In the right the monomeric moiety has been shown. Hydrogen atoms and co-crystallized solvent molecules are omitted for clarity.

Table 4.3. Relevant bond lengths (Å) and angles (°) for **9**.

Mn(1)-N(1)	1.871(4)	C(27)-C(24)	1.404(3)
Mn(1)-N(2)	1.942(3)	N(2)-Mn(1)-N(3)	157.84(2)
Mn(1)-N(3)	1.929(3)	N(1)-Mn(1)-P(3)	131.78(8)
Mn(1)-P(3)	2.194(8)	N(1)-Mn(1)-C(59)	138.61(2)
Mn(1)-C(59)	1.736(3)	P(3)-Mn(1)-C(59)	89.07(8)
C(25)-N(2)	1.371(3)	N(3)-Mn(1)-C(59)	95.63(2)
C(25)-C(20)	1.418(3)	N(3)-Mn(1)-P(3)	91.96(8)
C(27)-N(3)	1.364(3)		

When this dark green product was crystallized from *tert*-butyl methyl ether it afforded dark purple crystals which were identified as $\{[\kappa^4$-($^{Ph2PPr}PDI)Mn(CO)]K(^tBuOMe)_2]\}_2$ **(10)**. The ^1H NMR of **10** also features resonances in diamagnetic region and two singlets at 82.79 and -15.69 ppm were noticed in the ^{31}P NMR spectra. As in **9**, the IR spectrum of **10** also showed a highly shifted CO stretching frequency at 1697 cm^{-1} suggesting increased backbonding due to reduction. The crystal structure of **10** revealed a dimeric structure with κ^4-*N,N,N,P*-PDI coordination around each Mn. However, unlike **9** it does not contain the K-PDI coordination. The Mn(1)-N$_{PDI}$ and Mn(1)-P(1) [2.180(4) Å] bonds (Table 4.4) are consistent to a low spin Mn center. Each manganese atom lies at the center of a distorted trigonal bipyramid containing a highly reduced chelate with C(2)-N(1), C(8)-N(3), C(2)-C(3), and C(7)-C(8) bond lengths of 1.359(3), 1.360(3), 1.393(3), and 1.398(3) Å respectively.
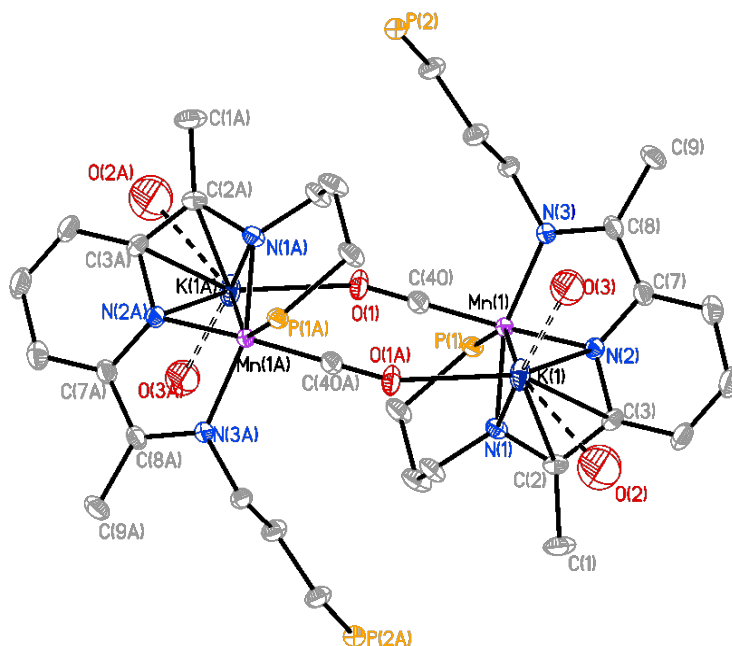
Figure 4.17. Solid-state structure of **10** shown at 30% probability ellipsoids. Hydrogen atoms, tert-butyl groups, and co-crystallized solvent molecules are omitted for clarity.

Table 4.4. Relevant bond lengths (Å) and angles (°) for **10**.

Mn(1)-N(1)	1.931(3)	C(3)-N(2)	1.396(3)
Mn(1)-N(2)	1.885(3)	C(7)-N(2)	1.401(3)
Mn(1)-N(3)	1.934(3)	C(40)-O(1)	1.201(3)
Mn(1)-P(1)	2.180(4)	N(1)-Mn(1)-N(3)	157.84(3)
Mn(1)-C(40)	1.743(2)	N(2)-Mn(1)-C(40)	151.32(2)
C(2)-N(1)	1.359(3)	N(2)-Mn(1)-P(1)	122.22(3)
C(2)-C(3)	1.393(3)	P(1)-Mn(1)-C(40)	86.13(4)
C(8)-N(3)	1.360(3)	N(1)-Mn(1)-C(40)	99.26(2)
C(7)-C(8)	1.398(3)	N(1)-Mn(1)-P(1)	88.79(4)

Having synthesized and characterized these dinuclear complexes, the reduction of **6** was attempted again under slightly different conditions in order to isolate a monomeric Mn(-I) product. Similar reduction in presence of stoichiometric 18-Crown-6 afforded an olive-green anionic complex identified as [κ^4-(^{Ph2PPr}PDI)Mn(CO)][K(18-Crown-6)] **(11)**, which is analogous to the reported [Mn(mesbpy)(CO)$_3$][K(18-Crown-6)].[17] This compound also features a diamagnetic ^{1}H NMR (Figure 4.18 top) and two singlet resonances were observed in the ^{31}P NMR spectrum (86.27 and -15.62 ppm, Figure 4.18 bottom). The CO stretching frequency of **11** was observed at 1730 cm^{-1} in the IR spectrum. A concentrated diethylether solution of **11** furnished single crystals suitable for X-ray diffraction.
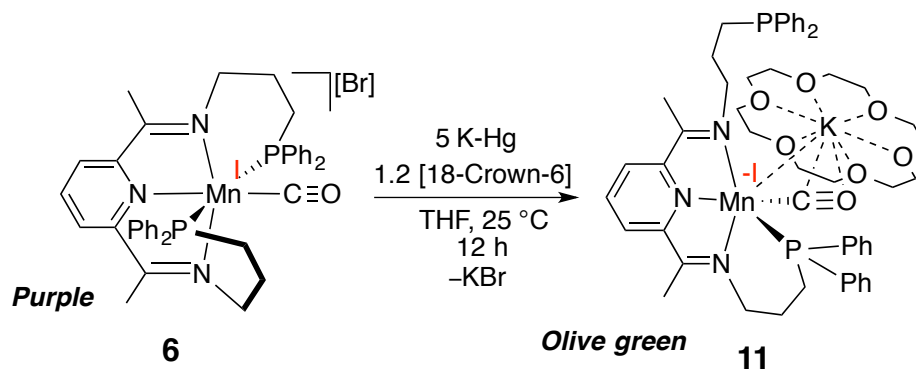
Scheme 4.5. Synthesis of moneric Mn(-I) complex **11**.

138
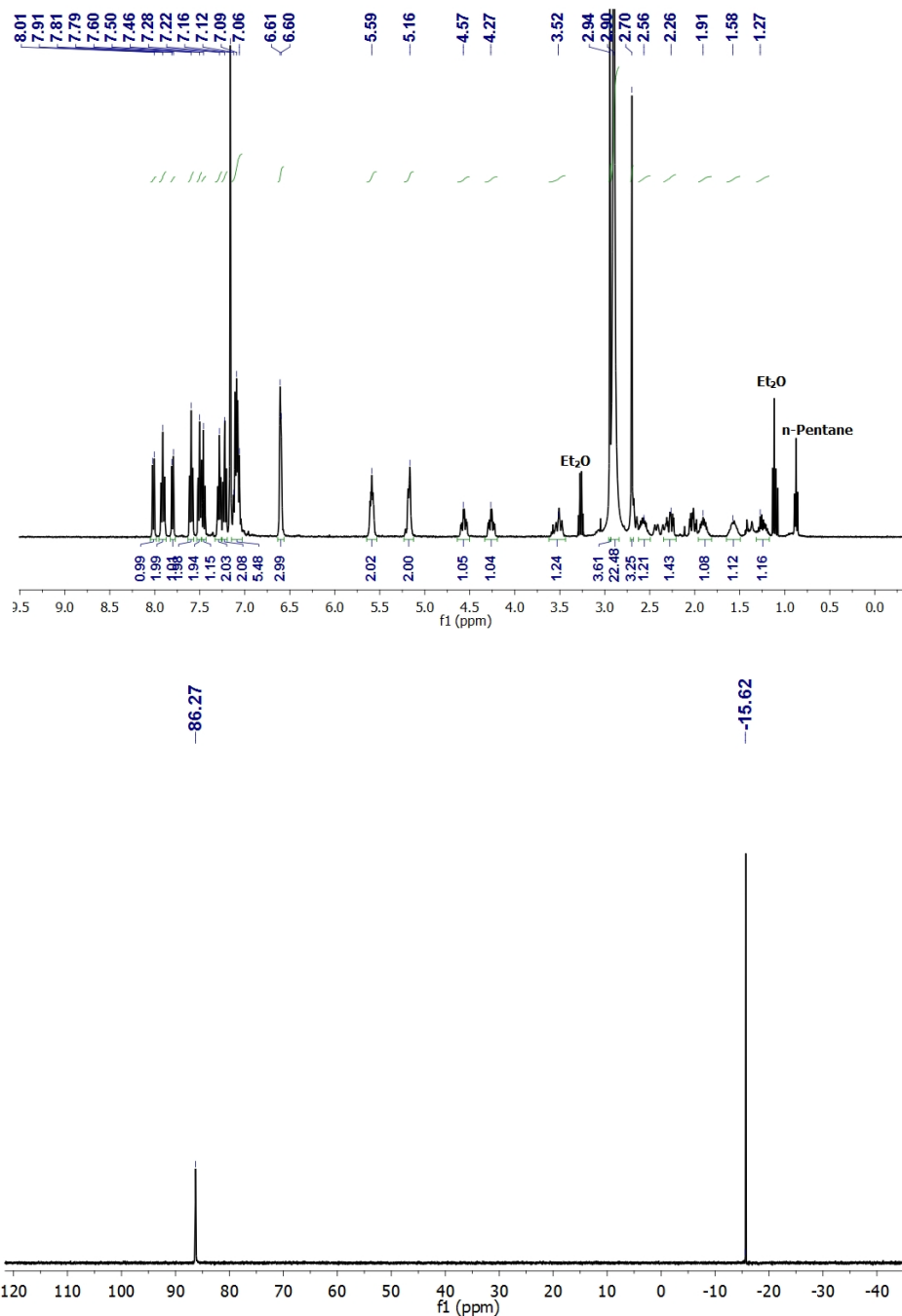
Figure 4.18. ^{1}H NMR (tobottom) and ^{31}P NMR (B) spectra of **11** in benzene-d_6.

The solid-state structure of **11** is shown in Figure 4.19, which possesses a distorted trigonal bipyramidal geometry about the Mn center with N(1)-Mn(1)-N(3), N(2)-Mn(1)-P(1), N(1)-Mn(1)-P(1) angles of 157.38(3)°, 120.43(4)°, and 88.70(4)°

respectively. A κ^4-*N,N,N,P*-chelate was also seen in the crystal structure, which is the reason for the presence of two different resonances in the ^{31}P NMR of **11**. The Mn(1)-N$_{PDI}$ distances (Table 4.5) are indicative of a low spin metal center. The elongated imine bonds C(2)-N(1) (1.357(3) Å), and C(8)-N(3) (1.356(3) Å) and contracted C(2)-C(3) (1.404(3) Å) and C(7)-C(8) (1.412(3) Å) bonds suggested a doubly reduced PDI chelate. A detailed analysis of these spectroscopic data and crystallographic information was then sought to describe the electronic structure of all of these monoanionic Mn complexes. When the imine C=N bond and the C$_{imine}$-C$_{pyridine}$ bonds were compared to the literature values of neutral, radical monoanionic, and dianionic PDI[26b] (Table 4.6), it has been found that the complexes **4**, **5**, and **6** possess a doubly reduced chelate (PDI^{2-}) with minimal back donation to CO π^* orbitals. The increase in back donation upon reduction is also clearly reflected in the low energy CO stretching frequencies for all three complexes.
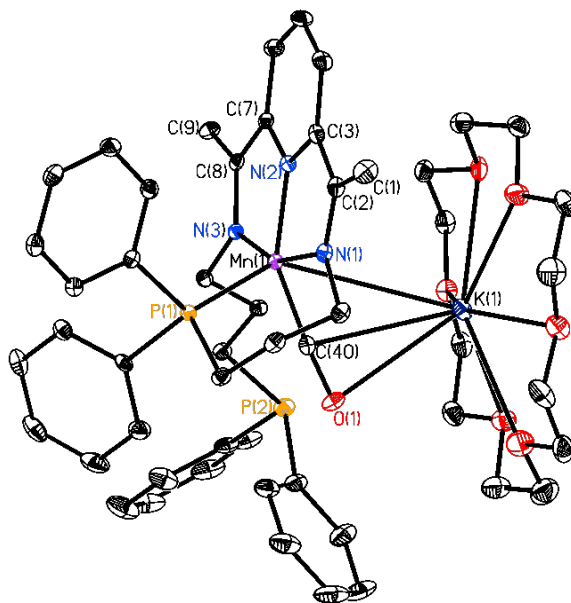

Figure 4.19. Solid-state structure of **11** shown at 30% probability ellipsoids. Hydrogen atoms and co-crystallized solvent molecules are omitted for clarity.

140

Table 4.5. Relevant bond lengths (Å) and angles (°) for **11**.

Mn(1)-N(1)	1.935(3)	C(3)-N(2)	1.400(3)
Mn(1)-N(2)	1.884(3)	C(7)-N(2)	1.394(3)
Mn(1)-N(3)	1.942(3)	C(40)-O(1)	1.201(3)
Mn(1)-P(1)	2.188(4)	N(1)-Mn(1)-N(3)	157.38(3)
Mn(1)-C(40)	1.754(4)	N(2)-Mn(1)-C(40)	150.61(8)
C(2)-N(1)	1.357(3)	N(2)-Mn(1)-P(1)	120.43(4)
C(2)-C(3)	1.404(3)	P(1)-Mn(1)-C(40)	88.30(8)
C(8)-N(3)	1.356(3)	N(1)-Mn(1)-C(40)	97.44(3)
C(7)-C(8)	1.412(3)	N(1)-Mn(1)-P(1)	88.70(4)

Table 4.6. Chelate bond length (Å) comparison.

Bond (average)	4	5	6	Lit. PDI^{2-}
C=N	1.368(3)	1.360(3)	1.357(3)	1.36[26b]
C_{imine} - C_{imine}	1.411(3)	1.396(3)	1.408(3)	1.40[26b]
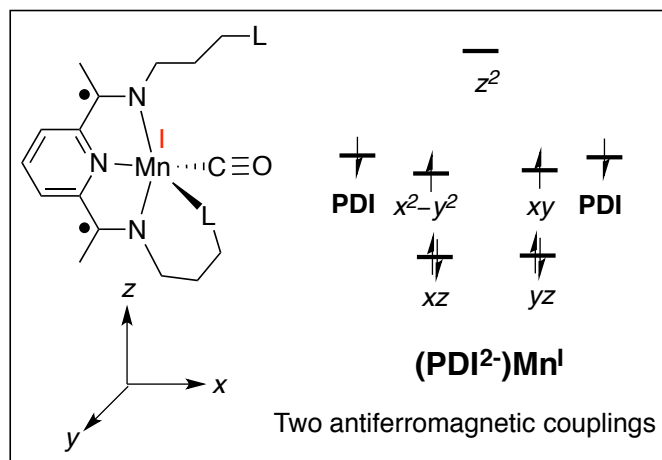
Figure 4.20. Qualitative *d*-orbital splitting of formal Mn(-I) complexes

Considering these facts, it can be proposed that these formally monoanionic Mn complexes feature low spin Mn(I) center that is antiferromagnetically coupled to triplet dianionic PDI^{2-} chelate. Although this electronic structure description is reasonable and

satisfying the diamagnetism observed in these complexes, a supportive DFT analysis would be greatly desired to further bolster this theory.

Having synthesized these reduced intermediates, the initial mechanistic hypothesis of complex reduction and phosphine dissociation have been proved. To obtain further insight of the CO_2 assisted H^+ reduction mechanism, a set of controlled experiments were carried out in order to isolate any reactive intermediates. Upon adding one atmosphere of CO_2 to a benzene-d_6 solution of **11** in a J-Young tube an instantaneous color change to bright purple was noticed. However, spectroscopic analysis of the resulting solution remained inconclusive as the product showed paramagnetically broadened resonances. Similarly, addition of stoichiometric quantity of benzoic acid and phenol separately produced paramagnetic products with identical color change. Attempts to crystallize these new complexes using various solvent combinations were unsuccessful, which is presumably due to the fluxional phosphine arms that are dissociated upon substrate addition. Unfortunately employing stoichiometric amount of stronger acids such as formic acid or $HBF_4.OEt_2$ resulted in slow complex decomposition. Although these intermediates are highly reactive, lack of proper mechanistic evidences and difficulties in isolating relevant intermediates indicate towards the instability of these highly reduced PDIMn complexes and requires major synthetic modifications to improve the robustness for electrocatalytic applications.

4.6. Concluding remarks:

In summary, PDI-supported manganese complexes have been investigated for eletrocatalytic fuel production processes. A modest activity for H_2 production from a CO_2

acidified acetonitrile solution (pseudo pH = 8.4) has been achieved along with minimal complex decomposition at the experimental reduction potential (-2.2 V vs $Fc^{+/0}$). Although the relevant intermediates are isolated following chemical reduction of **1** under differing conditions, an insightful reactivity study remained unattainable due to the fluxional phosphine arm and the paramagnetic nature of resulting products. Further synthetic manipulation to generate more robust and efficient manganese electrocatalysts using redox non-innocence ligands are currently ongoing in our laboratory.

4.7. Experimental Procedure:

General Considerations: All synthetic manipulations were performed within an MBraun glovebox under an atmosphere of purified nitrogen. Anhydrous solvents were purified using a Pure Process Technology solvent system and stored in the glovebox over activated 4Å molecular sieves and sodium before use. Benzene-d_6 was purchased from Cambridge Isotope Laboratories and acetone-d_6 was purchased from Acros Organics and dried over 4Å molecular sieves before use. Precursors $(CO)_5MnBr$ and 3-(diphenylphosphino)-1-propylamine were used as received from Strem Chemicals. Acetonitrile was purchased from Sigma-Aldrich and dried over 4Å molecular sieves before use. Tetrabutylammonium hexafluorophosphate was purchased from Sigma-Aldrich and used as received. Ferrocene was purchased from Acros Organics while MeOH was purchased from EMD and dried over 4Å molecular sieves before use. ^{Ph2PPr}PDI was prepared according to the published procedure.[30]

Solution ^1H nuclear magnetic resonance (NMR) spectra were recorded at room temperature on a Varian 400-MR 400 MHz NMR spectrometer. All ^1H and ^{13}C NMR

chemical shifts (ppm) are reported relative to $Si(CH_3)_4$ using ^1H (residual) and ^{13}C chemical shifts of the solvent as secondary standards. ^{31}P NMR data is reported relative to H_3PO_4. UV-vis measurements were conducted using a Hitachi U-2010 spectrophotometer in quartz cuvettes with a path length of 1 cm. Infrared spectroscopy was performed using KBr pellets on a Bruker VERTEX 70 spectrophotometer with an MCT detector. Elemental analyses were performed at Robertson Microlit Laboratories Inc. (Ledgewood, NJ). Solid state magnetic susceptibilities were determined at 23 °C using a Johnson Matthey magnetic susceptibility balance calibrated with $HgCo(SCN)_4$ and $K_3Fe(CN)_6$. Solution state magnetic susceptibility was determined via Evans method.

X-ray crystallography: Diffraction data were collected and analyzed by Dr. Thomas L. Groy at Arizona State University. Single crystals suitable for X-ray diffraction were coated with polyisobutylene oil in the glovebox and transferred to glass fiber with Apiezon N grease before mounting on the goniometer head of a Bruker APEX Diffractometer equipped with Mo Kα radiation. A hemisphere routine was used for data collection and determination of the lattice constants. The space group was identified and the data was processed using the Bruker SAINT+ program and corrected for absorption using SADABS. The structures were solved using direct methods (SHELXS) completed by subsequent Fourier synthesis and refined by full-matrix, least-squares procedures on $[F^2]$ (SHELXL).

Preparation of [(^{Ph2PPr}PDI)Mn(CO)][Br] (6): A 100 mL thick walled glass tube was charged with 0.150 g (0.245 mmol) of $^{Ph2PPr}PDI$ in 5 mL THF. A 5 mL THF solution of 0.067 g (0.245 mmol) of $(CO)_5MnBr$ was added to the tube. The clear orange solution was sealed under nitrogen and heated at 65 °C for 24 h while stirring. After 24 h, the

reaction mixture was purple with a large amount of insoluble purple material in suspension. The headspace of the flask was evacuated on a Schlenk line using two freeze-pump-thaw cycles. The mixture was filtered through Celite and the Celite pad was washed with 1 mL of THF to remove byproducts. Then it was washed with 20 mL of acetone to obtain a deep purple filtrate, which was dried under vacuum. The resulting purple solid was washed twice with 2 mL portions of diethyl ether and further dried under vacuum. Recrystallization from acetonitrile at -35 °C afforded 0.0489 g (0.0629 mmol, 26% yield) of purple crystals identified as **6**. Elemental analysis for $C_{40}H_{41}N_3P_2MnOBr$: Calcd. C, 61.87%; H, 5.32%; N, 5.41%. Found: C, 62.01%; H, 5.40%; N, 5.53%. ^1H NMR (acetonitrile-d_3): δ (ppm) = 7.49 (m, 4H, *phenyl*), 7.39 (m, 6H, *phenyl*), 7.25 (m, 1H, *Py*), 7.14 (m, 2H, *Py*), 6.96 (m, 6H, *phenyl*), 6.48 (m, 4H, *phenyl*), 4.42 (m, 2H, CH_2), 3.91 (m, 2H, CH_2), 2.71 (m, 2H, CH_2), 2.58 (m, 4H, CH_2), 2.27 (m, 6H, CH_3), 1.96 (m, 2H, CH_2). ^{13}C NMR (acetonitrile-d_3): δ (ppm) = 165.1 (t, 2.3 Hz, *CO*), 157.4 (*imine C*), 137.3 (*phenyl*), 137.0 (*phenyl*), 132.8 (*phenyl*), 132.6 (*phenyl*), 132.5 (*phenyl*), 131.6 (*phenyl*), 131.3 (*phenyl*), 130.3 (*phenyl*), 129.7 (*phenyl*), 129.3 (*phenyl*), 58.9 (NCH_2), 28.6 (*CH$_3$*), 24.6 (m, PCH_2), 15.3 (*CH$_2$*). $^{31}P\{^1H\}$ NMR (acetonitrile-d_3): δ (ppm) = 55.42 (s, PPh$_2$). IR (KBr): ν_{CO} = 1825 cm^{-1}. UV-vis (from 9 independent concentrations in acetonitrile): λ_{max} = 368 nm (ε = 4050 M^{-1}cm^{-1}), 528 nm (ε = 6840 M^{-1}cm^{-1}), 672 nm (ε = 830 M^{-1}cm^{-1}).

Preparation of (^{Ph2PPr}PDI)MnBr (7): A thick walled glass tube was charged with 0.151 g (0.247 mmol) of ^{Ph2PPr}PDI in approximately 4 mL of THF. A 10 mL THF solution of 0.068 g (0.247 mmol) of (CO)$_5$MnBr was added and the tube was sealed under N$_2$ atmosphere. The resulting orange solution was stirred at 80 °C for 72 h. An intense blue

solution, with a small amount of insoluble purple material was formed. The headspace of the flask was evacuated on a Schlenk line using two freeze-pump-thaw cycles to remove carbon monoxide. The blue solution was vacuum filtered through Celite, and THF was removed *in vacuo* to obtain a deep blue solid. This solid was washed three times with 4 mL portions of pentane and further dried to afford 0.140 g (0.187 mmol, 76% yield) of **7**. Elemental analysis for $C_{39}H_{41}N_3P_2MnBr$: Calcd. C, 62.58%; H, 5.52%; N, 5.61%. Found: C, 62.37%; H, 5.81%; N, 5.38%. Magnetic Susceptibility: μ_{eff} = 4.4 μ_B (benzene-d_6, 25 °C). ^1H NMR (benzene-d_6, 25 °C): δ (ppm) = 74.68 (peak width at ½ height = 4224 Hz). ^{13}C NMR (benzene-d_6, 25 °C): No resonances located. UV-vis (from 9 independent concentrations in THF): λ_{max} = 361 nm (ε = 3040 $M^{-1}cm^{-1}$), 614 nm (ε = 2650 M^{-1} cm^{-1}).

Preparation of (^{Ph2PPr}PDI)Mn(CO) (8): In an inert atmosphere, a 20 mL scintillation vial was charged with 0.109 g (0.1403 mmol) of **6** in approximately 15 mL of dry THF. Then 0.0161 g (0.702 mmol) of freshly cut Na^0 metal was added to the vial and stirred for 6 h at ambient temperature. A dark purple solution was generated, which was then vacuum filtered through Celite and THF was removed in vacuo. The resulting solid was dissolved in 10 mL of toluene and filtered through Celite. The filtrate was concentrated and layered with Et_2O and placed at -35 °C. After drying 0.043 g (0.0616 mmol, 44% yield) of purple crystals were obtained, which was identified as (^{Ph2PPr}PDI)Mn(CO) **(8)**

Preparation of {[κ^4-(^{Ph2PPr}PDI)Mn(CO)]K(Et$_2$O)]}$_2$ (9): In an inert atmosphere, a 20 mL scintillation vial was charged with 2.26 g (11.33 mmol) of Hg^0 and approximately 5 mL dry THF was added to it. 0.0221 g of freshly cut K^0 metal was then added to the vial and vigorously stirred for 30 min. To the resulting amalgam, a 10 mL THF slurry of 0.0.088 g (0.1133 mmol) of **6** was added and stirred at ambient temperature for 6 h. A

dark solution was generated, which was then vacuum filtered through Celite and THF was removed *in vacuo*. The resulting solid was dissolved in 10 mL of toluene and filtered through Celite. The filtrate was concentrated and layered with Et_2O and placed at -35 °C. Green crystals were obtained after 24 h, which were identified as **{[κ⁴-(Ph2PPrPDI)Mn(CO)]K(Et₂O)]}₂ (9)**. ^1H NMR (benzene-d_6, 25 °C): δ (ppm) 8.01 (m, 4H), 7.61 (m, 6H), 7.37 (m, 10H), 7.12-7.05 (m, 20H), 6.52 (m, 6H), 5.49 (m, 4H), 5.09 (m, 2H), 4.71 (m, 4H), 4.50 (m, 2H), 3.97 (m, 2H), 3.37 (q, 8H, OC*H₂*CH₃), 3.05 (m, 2H), 2.80 (s, 3H, C*H₃*), 2.64 (s, 3H, C*H₃*), 1.38 (m, 6H, C*H₂*), 1.15 (t, 12H, OCH₂C*H₃*). ^{31}P NMR (benzene-d_6, 25 °C): δ (ppm) 83.24 (s, Ph₂*P*), -15.63 (s, Ph₂*P*).

Preparation of {[κ⁴-(Ph2PPrPDI)Mn(CO)]K(ᵗBuOMe)₂]}₂ (10): In an inert atmosphere, a 20 mL scintillation vial was charged with 3.10 g (15.60 mmol) of Hg^0 and approximately 5 mL dry THF was added to it. 0.304 g (0.779 mmol) of freshly cut K^0 metal was then added to the vial and vigorously stirred for 30 min. To the resulting amalgam, a 10 mL THF slurry of 0.121 g (0.156 mmol) of **6** was added and stirred at ambient temperature for 14 h. A dark solution was generated, which was then vacuum filtered through Celite and THF was removed in vacuo. The resulting solid was dissolved in 10 mL of toluene and filtered through Celite. Toluene was evacuated and the residue was dissolved in 2-3 mL of ᵗBuOMe and placed at -35 °C. Brownish-purple crystals (0.095 g, 0.052 mmol, 33% yield) were obtained after 24 h, which were identified as **{[κ⁴-(Ph2PPrPDI)Mn(CO)]K(ᵗBuOMe)₂]}₂ (10)**. ^1H NMR (benzene-d_6, 25 °C): δ (ppm) 8.05 (m, 2H, *pyridine*), 7.93 (m, 2H, *pyridine*), 7.60 (m, 6H, *phenyl*), 7.34 (m, 8H, p-*pyridine and phenyl*), 7.20 (m, 4H, *phenyl*), 7.08-6.97 (m, 15H, *phenyl*), 6.53 (m, 6 H, *phenyl*), 5.46 (m, 4H, C*H₂*), 5.08 (m, 2H, C*H₂*), 4.67 (m, 2H, C*H₂*), 4.46 (m, 2H, C*H₂*), 3.93 (m,

2H, CH_2), 3.03 (s, 6H, ^{t}BuOMe), 2.99 (m, 2H, CH_2), 2.80 (s, 6H, CH_3), 2.55 (s, 6H, CH_3), 2.37 (m, 2H, CH_2), 2.30 (m, 2H, CH_2), 1.93 (m, 8H, CH_2), 1.38 (m, 2H, CH_2), 1.07 (s, 18H, ^{t}BuOMe). ^{31}P NMR (benzene-d_6, 25 °C): δ (ppm) 82.79 (s, Ph$_2$$P$), -15.69 (s, Ph$_2$$P$).

Preparation of [κ^4-(^{Ph2PPr}PDI)Mn(CO)][K(18-Crown-6)] (11): In an inert atmosphere, a 20 mL scintillation vial was charges with 4.76 g (23.82 mmol) of Hg^0 and approximately 5 mL dry THF was added to it. 0.0465 g (1.191 mmol) of freshly cut K^0 metal was then added to the vial and vigorously stirred for 30 min. To the resulting amalgam, a 10 mL THF slurry of 0.185 g (0.238 mmol) of **6** was added followed by 0.079 g of 18-Crown-6 (0.298 mmol). The mixture was stirred at ambient temperature for 12 h. A dark greenish-brown solution was generated, which was then vacuum filtered through Celite and THF was removed *in vacuo*. The resulting solid was dissolved in 10 mL of toluene and filtered through Celite. The filtrate was concentrated and layered with Et$_2$O and placed at -35 °C for 24 h. After removing Et$_2$O and drying, 0.190 g (0.189 mmol, 79% yield) of olive-green crystals were obtained, which were identified as **[κ^4-(^{Ph2PPr}PDI)Mn(CO)][K(18-Crown-6)] (11)**. ^{1}H NMR (benzene-d_6, 25 °C): δ (ppm) 8.02 (d, *J* = 7.5 Hz, 1H, *pyridine*), 7.91 (t, *J* = 7.9 Hz, 2H, *phenyl*), 7.80 (d, *J* = 7.5 Hz, 1H, *pyridine*), 7.60 (t, *J* = 6.9 Hz, 2H, *phenyl*), 7.50 (t, *J* = 6.9 Hz, 2H, *phenyl*), 7.46 (t, *J* = 7.9 Hz, 1H, *p-pyridine*), 7.28 (t, *J* = 7.7 Hz, 2H, *phenyl*), 7.22 (t, *J* = 7.5 Hz, 2H, *phenyl*), 7.12-7.06 (m, 6H, *phenyl*), 6.61 (m, 3H, *phenyl*), 5.59 (m, 2H, CH_2), 5.16 (m, 2H, CH_2), 4.57 (m, 1H, CH_2), 4.27 (m, 1H, CH_2), 3.52 (m, 1H, CH_2), 2.94 (s, 3H, CH_3), 2.90 (s, 24H, CH_2 from 18-Crown-6), 2.70 (s, 3H, CH_3), 2.56 (m, 1H, CH_2), 2.26 (m, 1H, CH_2), 1.91 (m, 1H, CH_2), 1.58 (m, 1H, CH_2), 1.27 (m, 1H, CH_2). ^{31}P NMR (benzene-d_6, 25 °C):

δ (ppm) 245.31 (CO), 145.36, 145.10, 140.89, 139.11, 136.53, 134.76, 133.92, 133.73, 133.66, 133.52, 133.28, 133.11, 131.75, 129.06, 128.99, 127.77, 127.68, 128.27, 111.98, 104.28, 103.76, 70.08 (18-Crown-6), 66.26, 64.06, 59.16, 33.12, 29.54, 27.04, 22.97, 15.95, 14.50. ^{31}P NMR (benzene-d_6, 25 °C): δ (ppm) 86.27 (s, Ph_2P), -15.62 (s, Ph_2P).

Cyclic voltammetry: All experiments were conducted using a three-electrode system with a glassy carbon working electrode (3 mm diameter with a surface area of 0.0707 cm^2), a silver wire pseudo-reference electrode, and a platinum counter electrode. The working electrode was cleaned with diamond paste (0.1 μm Glennel UB Formulation, from Electron Microscopy Sciences) and washed with water and acetonitrile (MeCN) before use. The reference electrode was dipped into 1M HCl and air-dried prior to use. All voltammograms are reported relative to ferrocene, which was used as an internal standard.

Bulk Electrolysis: Bulk electrolysis experiments were undertaken either in a sealed BASi bulk electrolysis cell or in a four necked screw capped hand made cell prepared in a glove box, and gas chromatography was used to quantify the H_2 and CO produced. The working electrode was either a reticulated vitreous carbon electrode (cylinder of 40 mm diameter, 50 mm height, and 5 mm depth) or a 3 mm diameter glassy carbon electrode. A non-aqueous (MeCN) Ag/AgCl reference electrode was placed in a separate compartment and connected via a fine porosity glass frit. A platinum wire was used as counter electrode. A 50 mL soluton of 5 mM **1** in 0.1M [NBu_4][PF_6]/MeCN was used with 1.05 M MeOH and saturated with CO_2. The cell had a head space of 38.75 mL. Gas withdrawals from the headspace were made with a Hamilton 1750 SL locking gastight syringe and were compensated with an equal addition of argon. Following calibration

149

with known concentrations of H_2 and CO over the region 0-3.0% (volume %), a Varian CP-3800 gas chromatograph (thermal conductivity detector, Alltech Porapak Q 80/100 column, Argon as carrier gas) was used to determine the concentrations of CO and H_2 in the headspace. The CO concentration remained below detection limits. The Faradaic efficiency for the electrolytic production of H_2 was 95.4 ± 4 % with a rate of 3.3 s^{-1} (calculated from $i_{cat}/i_p = (n/0.4463)(k_{cat}RT/F\nu)^{1/2}$).

4.8. References:

1. Walter, M. G.; Warren, E. L.; McKone, J. R.; Boettcher, S. W.; Mi, Q.; Santori, E. A.; Lewis, N. S. *Chem. Rev.* **2010**, *110*, 6446-6473.

2. (a) Gust, D.; Moore, T. A.; Moore, A. L. *Acc. Chem. Res.* **2009**, *42*, 1890-1898. (b) Gust, D.; Moore, T. A.; Moore, A. L. *Acc. Chem. Res.* **2001**, *34*, 40-48. (c) Gust, D.; Moore, T. A.; Moore, A. L. *Acc. Chem. Res.* **1993**, *26*, 198-205.

3. Nocera, D. G. *Acc. Chem. Res.* **2012**, *45*, 767-776.

4. For representative Fe catalysts see: (a) Roy S.; Mazinani, S. K. S.; Groy, T. L.; Gan, L.; Tarakeshwar, P.; Mujica, V.; Jones, A. K. *Inorg. Chem.* **2014**, *53*, 8919-8929. (b) Darmon, J. M.; Raugei, S.; Liu, T.; Hulley, E. B.; Weiss, C. J.; Bullock, R. M.; Helm, M. L. *ACS Catal.* **2014**, *4*, 1246-1260. (c) Gloaguen, F.; Rauchfuss, T. B. *Chem. Soc. Rev.* **2009**, *38*, 100-108.

5. For representative Co catalysts see: (a) McCrory, C. C. L.; Uyeda, C.; Peters, J. C. *J. Am. Chem. Soc.* **2012**, *134*, 3164-3170. (b) Dempsey, J. L.; Brunschwig, B. S.; Winkler, J. R.; Gray, H. B. *Acc. Chem. Res.* **2009**, *42*, 1995-2004. (c) Jacques, P.-A.; Artero, V.; Pécaut, J.; Fontecave, M. *Proc. Natl. Acad. Sci. U.S.A.* **2009**, *106*, 20627-20632. (d) Hu, X.; Brunschwig, B. S.; Peters, J. C. *J. Am. Chem. Soc.* **2007**, *129*, 8988-8998. (e) Artero, V.; Fontecave, M. *Coord. Chem. Rev.* **2005**, *249*, 1518-1535.

6. For representative Ni catalysts see: (a) Gan, L.; Groy, T. L.; Tarakeshwar, P.; Mazinani, S. K. S.; Shearer, J.; Mujica, V.; Jones, A. K. *J. Am. Chem. Soc.* **2015**, 137, 1109-1115. (b) Helm, M. L.; Stewart, M. P.; Bullock, R. M.; DuBois, M. R.; DuBois, D. L. *Science* **2011**, *333*, 863-866. (c) Kilgore, U. J.; Roberts, J. A. S.; Pool, D. H.; Appel, A. M.; Stewart, M. P.; DuBois, M. R.; Dougherty, W. G.; Kassel, W. S.; Bullock, R. M.; DuBois, D. L. *J. Am. Chem. Soc.* **2011**, *133*, 5861-5872. (d) Wilson, A. D.; Shoemaker, R. K.; Miedaner, A.; Muckerman, J. T.; DuBois, D. L.; DuBois, M. R. *Proc. Natl. Acad.*

Sci. U.S.A. **2007**, *104*, 6951-6956. (e) Wilson, A. D.; Newell, R. H.; McNevin, M. J.; Muckerman, J. T.; DuBois, M. R.; DuBois, D. L. *J. Am. Chem. Soc.* **2006**, *128*, 358-366.

7. Lewis, N. S.; Nocera, D. G. *Proc. Natl. Acad. Sci. U.S.A.* **2006**, *103*, 15729-15735.

8. Crabtree, G. W.; Dresselhaus, M. S; Buchanan, M. V. *Phys. Today* **2004**, *57*, 39-44.

9. (a) Benson, E. E.; Kubiak, C. P.; Sathrum, A. J.; Smieja, J. M. *Chem. Soc. Rev.* **2009**, *38*, 89-99. (b) Kumar, B.; Llorente, M.; Froehlich, J.; Dang, T.; Sathrum, A.; Kubiak, C. P. *Annu. Rev. Phys. Chem.* **2012**, *63*, 541-69.

10. (a) Schneider, J.; Jia, H.; Muckerman, J. T.; Fujita, E. *Chem. Soc. Rev.* **2012**, *41*, 2036-2051. (b) Doherty, M. D.; Grills, D. C.; Muckerman, J. T.; Polyansky, D. E.; Fujita, E. *Coord. Chem. Rev.* **2010**, *254*, 2472-2482. (c) Fujita, E. *Coord. Chem. Rev.* **1999**, *185-186*, 373-384.

11. For Fe catalysts see: (a) Costentin, C.; Passard, G.; Robert, M.; Savéant, J.-M. *Proc. Natl. Acad. Sci. U.S.A.* **2014**, *111*, 14990-14994. (b) Costentin, C.; Passard, G.; Robert, M.; Savéant, J.-M. *J. Am. Chem. Soc.* **2014**, *136*, 11821-11829. (c) Costentin, C.; Drouet, S.; Robert, M.; Savéant, J.-M. *Science* **2012**, *338*, 90-94. (d) Thammavongsy, Z.; Seda, T.; Zakharov, L. N.; Kaminsky, W.; Gilbertson, J. D. *Inorg. Chem.* **2012**, *51*, 9168-9170. (e) Chen, J.; Szalda, D. J.; Fujita, E.; Creutz, C. *Inorg. Chem.* **2010**, *49*, 9380-9391. (f) Grodkowski, J.; Neta, P. *J. Phys. Chem. A* **2000**, *104*, 4475-4479. (g) Dhanasekaran, T.; Grodkowski, J.; Neta, P.; Hambright, P.; Fujita, E. *J. Phys. Chem. A* **1999**, *103*, 7742-7748. (h) Grodkowski, J.; Behar, D.; Neta, P. Hambright, P. *J. Phys. Chem. A* **1997**, *101*, 248-254. (i) Bhugun, I.; Lexa, D.; Savéant, J.-M. *J. Am. Chem. Soc.* **1996**, *118*, 1769-1776. (j) Bhugun, I.; Lexa, D.; Savéant J.-M. *J. Am. Chem. Soc.* **1994**, *116*, 5015-5016. (k) Hammouche, M.; Lexa, D.; Momenteau, M.; Savéant J.-M. *J. Am. Chem. Soc.* **1991**, *113*, 8455-8466. (l) Hammouche, M.; Lexa, D.; Savéant J.-M. *J. Electroanal. Chem.* **1988**, *249*, 347-351.

12. For Co catalysts see: (a) Ogata, T.; Yamamoto, Y.; Wada, Y.; Murakoshi, K.; Kusaba, M.; Nakashima, N.; Ishida, A.; Takamuku, S.; Yanagida, S. *J. Phys. Chem.* **1995**, *99*, 11916-11922. (b) Ogata, T.; Yanagida, S.; Brunschwig, B. S.; Fujita, E. *Energy Convers. Manage.* **1995**, *36*, 669-672. (c) Matsuoka, S.; Yamamoto, K.; Ogata, T.; Kusaba, M.; Nakashima, N.; Fujita, E.; Yanagida, S. *J. Am. Chem. Soc.* **1993**, *115*, 601-609. (d) Fujita, E.; Szalda, D. J.; Creutz, C.; Sutin, N. *J. Am. Chem. Soc.* **1988**, *110*, 4870-4871. (e) Fisher, B.; Eisenberg, R. *J. Am. Chem. Soc.* **1980**, *102*, 7363-7365.

13. For Ni catalysts see: (a) Thoi, V. S.; Chang, C. J. *Chem. Commun.* **2011**, *47*, 6578-6580. (b) Simón-Manso, E.; Kubiak, C. P. *Organometallics* **2005**, *24*, 96-102. (c) Fujita, E.; Brunschwig, B. S.; Ogata, T.; Yanagida, S. *Coord. Chem. Rev.* **1994**, *132*, 195-200. (d) Craig, C. A.; Spreer, L. O.; Otvos, J. W.; Calvin, M. *J. Phys. Chem.* **1990**, *94*, 7957-7960. (e) Daniele, S.; Ugo, P.; Bontempelli, G.; Fiorani, M. *J. Electroanal. Chem.* **1987**, *219*, 259-271. (f) Beley, M.; Collin, J.-P.; Ruppert, R.; Sauvage, J.-P. *J. Am. Chem. Soc.*

151

1986, *108*, 7461-7467. (g) Meshitsuka, S.; Ichikawa, M.; Tamaru, K. *J. Chem. Soc., Chem. Commun.* **1974**, 158-159.

14. Bourrez, M.; Molton, F.; Chardon-Noblat, S.; Deronzier, A. *Angew. Chem. Int. Ed.* **2011**, *50*, 9903-9906.

15. (a) Smieja, J. M.; Benson, E. E.; Kumar, B.; Grice, K. A.; Seu, C. S.; Miller, A. J. M.; Mayer, J. M.; Kubiak, C. P. *Proc. Natl. Acad. Sci. U.S.A.* **2012**, *109*, 15646-15650. (b) Smieja, J. M.; Kubiak, C. P. *Inorg. Chem.* **2010**, *49*, 9283-9289. (c) Kumar, B.; Smieja, J. M.; Kubiak, C. P. *J. Phys. Chem. C* **2010**, *114*, 14220-14223. (d) Johnson, F. P. A.; George, M. W.; Hartl, F.; Turner, J. J. *Organometallics* **1996**, *15*, 3374-3387. (e) Sullivan, B. P.; Bolinger, C. M; Conrad, D.; Vining, W. J.; Meyer, T. J. *J. Chem. Soc., Chem. Commun.* **1985**, 1414-1416. (f) Hawecker, J.; Lehn, J.-M.; Ziessel, R. *J. Chem. Soc., Chem. Commun.* **1984**, 328-330.

16. Smieja, J. M.; Sampson, M. D.; Grice, K. A.; Benson, E. E.; Froehlich, J. D.; Kubiak, C. P. *Inorg. Chem.* **2013**, *52*, 2484-2491.
17. Sampson, M. D.; Nguyen, A. D.; Grice, K. A.; Moore, C. E.; Rheingold, A. L.; Kubiak, C. P. *J. Am. Chem. Soc.* **2014**, *136*, 5460-5471.

18. Takeda, H.; Koizumi, H.; Okamoto, K.; Ishitani, O. *Chem. Commun.* **2014**, *50*, 1491-1493.

19. Walsh, J. J.; Neri, G.; Smith, C. L.; Cowan, A. J. *Chem. Commun.* **2014**, *50*, 12698-12701.

20. For an example of Mn-catalyzed proton reduction see: (a) Valyaev, D. A.; Peterleitner, M. G.; Semeikin, O. V.; Utegenov, K. I.; Ustynyuk, N. A.; Sournia-Saquet, A.; Lugan, N.; Lavigne, G. *J. Organomet. Chem*. **2007**, *692*, 3207–3211. (b) Hou, K.; Poh, T.; Fan, W. Y. *Chem. Commun.* **2014**, *50*, 6630

21. For recent contributions see: (a) Riplinger, C.; Sampson, M. D.; Ritzmann, A. M.; Kubiak, C. P. *J. Am. Chem. Soc.* **2014**, *136*, 16285-16298. (b) Bourrez, M.; Orio, M.; Molton, F.; Vezin, H.; Duboc, C.; Deronzier, A.; Chardon-Noblat, S. *Angew. Chem. Int. Ed.* **2014**, *53*, 240-243. (c) Grills, D. C.; Farrington, J. A.; Layne, B. H.; Lymar, S. V.; Mello, B. A.; Preses, J. M.; Wishart, J. F. *J. Am. Chem. Soc.* **2014**, *136*, 5563-5566.

22. (a) Zeng, Q.; Tory, J. Hartl, F. *Organometallics* **2014**, *33*, 5002-5008. (b) Vollmer, M. V.; Machan, C. W.; Clark, M. L.; Antholine, W. E.; Agarwal, J.; Schaefer III, H. F.; Kubiak, C. P.; Walensky, J. R. *Organometallics* **2015**, *34*, 3-12.

23. (a) Agarwal, J.; Stanton III, C. J.; Shaw, T. W.; Vandezande, J. E.; Majetich, G. F.; Bocarsly, A. B.; Schaefer III, H. F. *Dalton Trans.* **2015**, 44, 2122-2131. (b) Agarwal, J.; Shaw, T. W; Stanton III, C. J.; Majetich, G. F.; Bocarsly, A. B.; Schaefer III, H. F. *Angew. Chem. Int. Ed.* **2014**, *53*, 5152-5155.

24. (a) Mukhopadhyay, T. K.; Feller, R. K.; Rein, F. N.; Henson, N. J.; Smythe, N. C.; Trovitch, R. J.; Gordon, J. C. *Chem. Commun.* **2012**, *48*, 8670-8672. (b) Scarborough, C. C.; Wieghardt, K. *Inorg. Chem*. **2011**, *50*, 9773-9793, and references therein. (c) Irwin, M.; Jenkins, R. K.; Denning, M. S.; Krämer, T.; Grandjean, F.; Long, G. J.; Herchel, R.; McGrady, J. E.; Goicoechea, J. M. *Inorg. Chem*. **2010**, *49*, 6160-6171. (d) Kraft, S. J.; Fanwick, P. E.; Bart, S. C. *Inorg. Chem*. **2010**, *49*, 1103-1110. (e) Roitershtein, D.; Domingos, Ã.; Pereira, L. C.; J.; Ascenso, J. R.; Marques, N. *Inorg. Chem*. **2003**, *42*, 7666-7673. (f) Schultz, M.; Boncella, J. M.; Berg, D. J.; Tilley, T. D.; Anderson, R. A.; *Organometallics* **2001**, *21*, 460-472. (g) Evans, W. J.; Drummond, D. K. *J. Am. Chem. Soc*. **1989**, *111*, 3329-3335.

25. (a) Porter, T. M.; Hall, G. B.; Groy, T. L.; Trovitch, R. J. *Dalton Trans.* **2013**, *42*, 14689-14692. (b) Khusniyarov, M. M.; Weyhermüller, T. Bill, E.; Wieghardt, K. *J. Am. Chem. Soc.* **2009**, *131*, 1208-1221, and references therein. (c) Muresan, N.; Lu, C. C.; Ghosh, M.; Peters, J. C.; Abe, M.; Henling, L. M.; Weyhermöller, Bill, E.; Wieghardt, K. *Inorg. Chem.* **2008**, *47*, 4579-4590. (d) Muresan, N.; Chlopek, K.; Weyhermüller, T.; Neese, F.; Wieghardt, K. *Inorg. Chem*. **2007**, *46*, 5327-5337. (e) Khusniyarov, M. M.; Harms, K.; Burghaus, O.; Sundermeyer, J. *Eur. J. Inorg. Chem*. **2006**, 2985-2996.

26. (a) Bart, S. C.; Chlopek, K.; Bill, E.; Bouwkamp, M. W.; Lobkovsky, E.; Neese, F.; Wieghardt, K.; Chirik, P. J. *J. Am. Chem. Soc.* **2006**, *128*, 13901-13912. (b) Knijnenburg, Q.; Gambarotta, S.; Budzelaar, P. H. M. *Dalton Trans*. **2006**, 5442-5448. (c) de Bruin, B.; Bill, E.; Bothe, E.; Weyhermüller, T.; Wieghardt, K. *Inorg. Chem*. **2000**, *39*, 2936-2947.

27. Mukhopadhyay, T. K.; Flores, M.; Groy, T. L.; Trovitch, R. J. *J. Am. Chem. Soc*. **2014**, *136*, 882-885.

28. Cavanaugh, M. D.; Gregg, B. T.; Cutler, A. R. *Organometallics* **1996**, *15*, 2764-2769.

29. Trovitch, R. J. *Synlett* **2014**, 25, 1638-1642.

30. Ben-Daat, H.; Hall, G. B.; Groy, T. L.; Trovitch, R. J. *Eur. J. Inorg. Chem.* **2013**, 4430-4442.

31. Russell, S. K.; Bowman, A. C.; Lobkovsky, E.; Wieghardt, K.; Chirik, P. J. *Eur. J. Inorg. Chem.* **2012**, 535-545.

32. Gennaro, A.; Isse, A. A.; Vianello, E. *J. Electroanal. Chem.* **1990**, *289*, 203-215.

33. Hydrosilylation reactions using (^{Ph2PPr}PDI)Mo(CO) have recently been found to proceed following phosphine donor dissociation. Please see: Pal, R.; Groy, T. L.; Bowman, A. C.; Trovitch, R. J. *Inorg. Chem.* **2014**, *53*, 9357-9365.

34. Jaguar, version 8.1, Schrodinger, LLC, New York, NY, 2013.

35. (a) Perdew, J. P.; Burke, K.; Ernzerhof, M. *Phys. Rev. Lett.* **1996**, *77*, 3865-3868. (b) Perdew, J. P.; Burke, K.; Ernzerhof, M. *Phys. Rev. Lett.* **1997**, *78*, 1396.

36. Rassolov, V.; Pople, J. A.; Ratner, M.; Windus, T. L. *J. Chem. Phys.* **1998**, *109*, 1223-1229.

37. Mukhopadhyay, T. K.; MacLean, N. L.; Gan, L.; Ashley, D. C.; Groy, T. L.; Baik, M.-H.; Jones, A. K.; Trovitch, R. J. *Inorg. Chem.* **2015**, *54*, 4475.

CHAPTER 5

SYNTHESES AND ELECTRONIC STRUCTURE EVALUATION OF

TRIPHOS SUPPORTED LOW VALENT IRON COMPLEXES

5.1. Abstract:

A series of Triphos [$PhP(CH_2CH_2PPh_2)_2$] and Triphos* [$CH_3C(CH_2PPh_3)_3$] supported iron di- and tri-halide complexes have been prepared by mixing Triphos and FeX_n (X = Br, Cl; n = 2, 3) in tetrahydrofuran. The reduction of (Triphos)$FeBr_2$ with excess Na^0 produced a bis(ligand) complex (κ^3-Triphos)Fe(κ^2-triphos), while reduction in presence of excess 2,2'-bipyridine (Bpy) allowed for the isolation of (κ^3-Triphos)Fe(bpy). Although, in both of these complexes Fe is formally zerovalent, a combined study of X-ray diffraction data, cyclic voltammetry and density functional theory on (κ^3-Triphos)Fe(Bpy), revealed a low spin Fe(I) center that is antiferromagnetically coupled to π-radical monoanionic Bpy chelate. Thus it implies that the redox non-innocence nature of Bpy ligand directly influences the electronics of the metal center. Furthermore, reducing (Triphos)$FeBr_2$ and (Triphos*)$FeBr_2$ in presence of excess 1,3,5,7-cyclooctatetraene (COT), resulted in the formation of (κ^3-Triphos)Fe(COT) complexes. These complexes have also been prepared by adding the corresponding ligand to (COT)$_2$Fe. The solid state structure of each complex was determined by single crystal X-ray diffraction and close inspection of the metrical parameters revealed significant COT ligand reduction, independent of the coordination geometry about iron. While the neutral and dianionic forms of the COT ligand have historically received a great deal of attention, a dearth of information regarding the often

evoked radical monoanion form of this ligand prompted the full electronic structure investigation of these complexes using a range of techniques. Comparing the Mössbauer spectroscopic data collected for both $(Triphos)Fe(\eta^4-COT)$ complexes with data obtained for two appropriate reference compounds $((\kappa^3-Triphos)Fe(bpy))$ and $(\kappa^3-Triphos)Fe(\kappa^2-triphos))$ indicated that they possess a low-spin Fe(I) metal center that is antiferromagnetically coupled to a COT radical monoanion. Further evidence for this electronic structure determination by EPR spectroscopy has also been collected. Comparing the solid-state metrical parameters determined in this study to related first row transition metal complexes has provided significant insight into the electronic structure analysis of related organometallic complexes. Also, on the other hand, addition of CO to $(Triphos)FeBr_2$ afforded $(Triphos)FeBr_2(CO)$ with a *mer*-Triphos chelate. $(Triphos)FeBr_2(CO)$ upon reaction with stoichiometric $NaEt_3BH$ allowed for the isolation *trans*-$(Triphos)Fe(H)(Br)(CO)$, while two equiv. of $NaEt_3BH$ resulted in the formation of $(Triphos)Fe(CO)_2$ via a transient putative intermediate $(Triphos)Fe(H)_2(CO)$. Also, adding 2.2 equiv. of $NaBH_4$ to $(Triphos)FeBr_2(CO)$ led to the formation of diamagnetic $(Triphos)Fe(H)(\eta^2-BH_4)$ via CO dissociation, which was confirmed by deuterium substitution using $NaBD_4$. Notably, efforts to prepare $(Triphos)FeH(\eta^2-BH_4)$ following 2.2 eq. $NaBH_4$ addition to $(Triphos)FeBr_2$ were unsuccessful. The importance of these observations as they relate to previously reported (Triphos)Fe reactivity and recent developments in Fe catalysis is discussed.

5.2. Introduction:

Low-valent iron complexes have gained great attention over the past decade due to their tremendous application in atmospheric N_2 reduction[1] as well as in catalytic organic transformations.[2] Moreover, the abundance, low cost, and biologically benign nature of Fe has tempted researchers to develop sustainable alternatives to precious metal catalysts. Nonetheless, the choice of suitable ligand has a crucial role in stabilizing the low oxidation state of iron. While the use of redox non-innocence ligands[3] is presently disseminating, much iron chemistry has relied upon phosphine-based ligands. Notably, phosphine chelated iron complexes have a rich coordination chemistry[4,1h,i] due to the strong σ-donating and good π-accepting ability of phosphine. Particularly, iron complexes supported by tridentate pincer type ligands such as PNP,[5] and PCP,[6] have achieved enormous success in homogeneous catalysis due to their stability, activity and variability.[6g] On the other hand, the coordination chemistry and catalytic applications of (Triphos)Fe (FePPP) complexes[7] have yet to be explored. Two important PPP type ligands that have been utilized to some extent to synthesize well defined iron complexes are $PhP(CH_2CH_2PPh_2)_2$ (Triphos)[7a,b,f,g,m] and $MeC(CH_2PPh_2)_3$ (Triphos*).[7c,d,e,h,j,l] Triphos is known to coordinate a metal center either in a *facial*- or a *meridonial*-fashion[7g] in an octahedral geometry. On the other hand, Triphos* is a relatively rigid chelate.[7h,j,l] Although, initially we sought to develop iron-dinitrogen complexes with these two ligands under reducing condition, failure to prepare such complexes led us to use ancillary ligands (such as 2,2'-bipyridine, 1,3,5,7-cyclooctatetraene, and CO) and isolate well-defined iron(0) complexes.

The electronic structure description of low-valent transition metal complexes containing 2,2'-bipyridine (Bpy), has been an interesting debate in recent years.[8] After the insightful electronic structure discussion of 18 different Bpy-supported transition metal complexes published by Scarborough and Wieghardt,[8e] we determined to investigate the detailed electronic structure of our Bpy-supported reduced iron complexes.[8j]

Also, η^4-diene coordination mode of 1,3,5,7-cyclooctatetraene (COT) to low-valent first row metal is of particular interest due to the lack of complete electronic structure description of such complexes. With a continuum of backbonding into the linear combinations of diene π^*-orbitals possible, transition metal complexes featuring η^4-COT can adopt an electronic configuration that lies anywhere between a neutral L_2 type or reduced XL type bonding.[9] Accurate electronic structure descriptions can often be reached following close inspection of crystallographically-determined diene metrical parameters. While this approach to electronic structure assignment remains appropriate for many η^4-diene complexes of low-spin second and third row metals, this methodology remains a drastic oversimplification for complexes of the first transition series due to the ambiguity of one electron reduction of ligand and π-backbonding. In addition, while poor single crystal X-ray diffraction data has undoubtedly contributed to the inability of researchers to develop clean-cut η^4-COT complex electronic structure divisions, there happen to be no crystallographically characterized reference compounds that feature an η^4-COT radical monoanion or dianion. Due to the fact that COT tends to be reduced to its dianionic form upon addition of an alkali metal reagent (typically resulting in μ-η^8,η^8-coordination),[10] isolating and determining the solid-state structure of a compound

158

featuring η^4-COT radical anion coordination to a single alkali metal atom would be considered an extraordinary achievement. More than 50 years after Dickens and Lipscomb hinted at the possibility of achieving η^4-COT coordination that lies somewhere between a neutral diolefin and a dianion (COT⁻),[11a] thoroughly-understood examples of a transition metal complex featuring an η^4-COT radical monoanion ligand have yet to be formulated.[12] Herein, two positively identified and structurally characterized complexes of this type are presented with detailed electronic structure investigation. The potential of this research is to provide insight into the electronic structure formulation of other low-valent η^4-COT supported transition metal complexes is also discussed.

Moreover, phosphine supported carbonyl hydride complexes have an important role in a handful of industrially important transformations such as the water-gas shift reaction, Fischer-Tropsch synthesis, hydroformylation, and hydrogenation.[7j,13] With the hypothesis that CO binding to (Triphos)Fe halides may assist in the isolation of stable low oxidation state iron complexes, we sought to develop Triphos supported carbonyl hydride complexes of iron similar to the catalytically active PNP[5a,b,d,e,i,l] and PPP[7c,j] iron complexes.

5.3. Preparation of Triphos iron halide complexes:

The study began with metalation of Triphos using stoichiometric FeX_n salts (n = 2, 3; X = Cl, Br).[8j] Notably, (Triphos)FeCl$_2$ was already reported by Davies *et al.* in 1980 with limited structural identification either in solid state or in solution.[7a] Later in 1981, Di Vaira *et al.* found the solid state structure of (κ^2-Triphos)$_2$FeCl$_2$, which possesses a distorted trans-octahedral geometry.[7b] Similarly, reacting tetrahydrofuran (THF) solution

159

of Triphos with equimolar quantity of $FeBr_2$, $FeCl_3$, and $FeBr_3$ separately, allowed for the isolation of (Triphos)$FeBr_2$ (**12-Br₂**), (Triphos)$FeCl_3$ (**12-Cl₃**), and (Triphos)$FeBr_3$ (**12-Br₃**) respectively (Scheme 5.1).
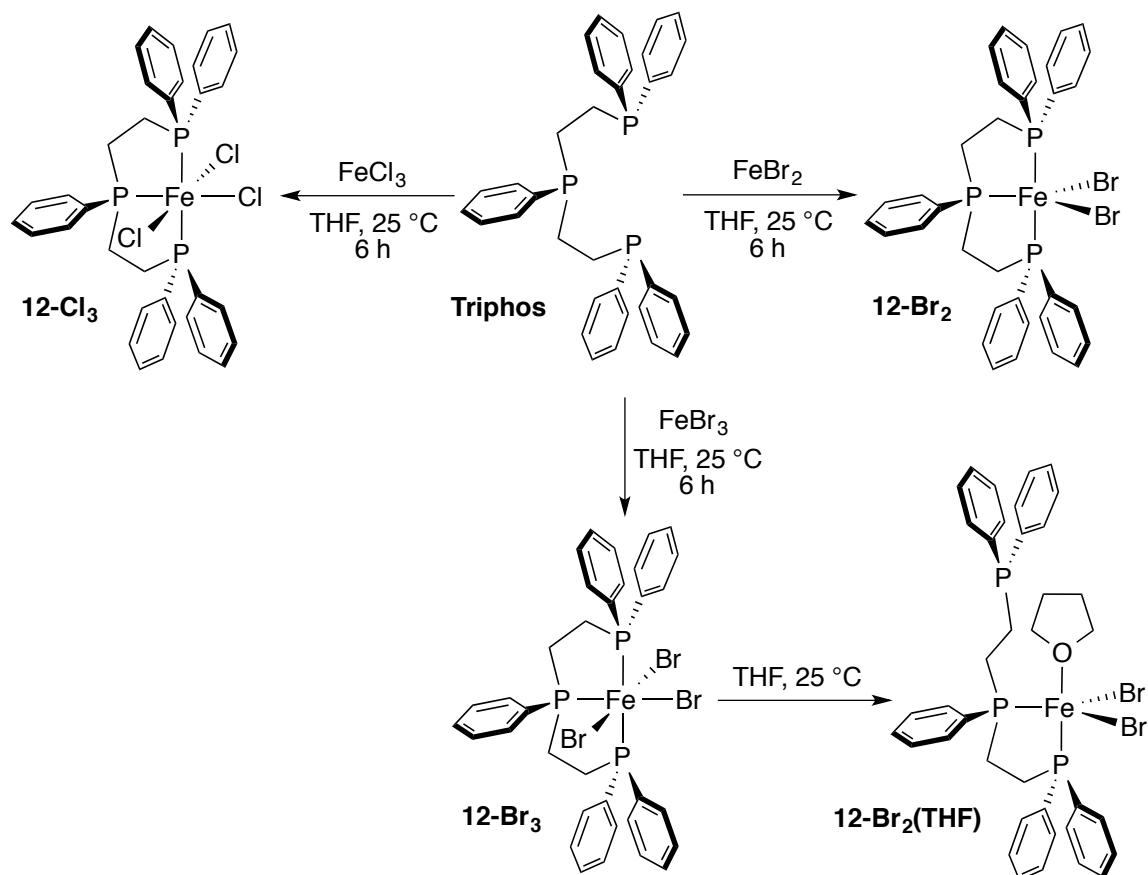
Scheme 5.1. Synthesis of (Triphos)FeX$_n$ complexes.

Attempts to crystallize these three complexes were unsuccessful. Spectroscopic characterization using NMR revealed broadened resonances for **12-Br₂** and **12-Cl₃** ranging over 110 ppm and 70 ppm respectively. Triphos methylene resonances are also shifted from the values observed for unbound ligand. None of the two complexes produced any signals in the ^{31}P NMR spectra. On the other hand, only one significant broad peak at 27.51 ppm was observed for **12-Br₃**. Interestingly, this complex showed a

broad signal at -22.10 ppm (peak width at half height = 449.9 Hz) in the ^{31}P spectrum collected in THF-d$_8$. Knowing that the ^{31}P resonances for free Triphos are at -16.47 and -20.43 ppm, it is believed that the weaker ligand field imparted by bromide ligands in **12-Br$_3$** causes dissociation of one phosphine arm in solution. Solid-state magnetic moments collected for **12-Br$_2$** (μ_{eff} = 4.8 μ_B), **12-Cl$_3$** (μ_{eff} = 4.3 μ_B), and **12-Br$_3$** (μ_{eff} = 5.6 μ_B) are indicative of high spin iron centers.

5.4. Reduction of (Triphos)FeX$_n$ complexes:

Having these halide starting materials synthesized, Fe-N$_2$ complexes were targeted by reducing with alkali metals under N$_2$ atmosphere. When **12-Br$_2$** was reduced with 5 eq. of Na^0 metal in THF a bis(ligand) complex, (κ^3-Triphos)Fe(κ^2-Triphos) **[12-(κ^2-Triphos)]** was isolated (Scheme 5.2).[8j] Performing this reduction in presence of one additional equivalent of Triphos ligand afforded **[12-(κ^2-Triphos)]** and excess free ligand. The result remained same when 2.5 eq. of K^0 was used as reductant. The ^{1}H NMR spectrum of this complex showed all four methylene resonances clearly, which are close to their diamagnetic reference values. Also, six distinct phosphorus peaks have been observed in the ^{31}P spectrum among which, five peaks are shifted downfield (119.23, 99.11, 82.74, 76.95, and 68.24 ppm, Figure 5.1) indicating attachment to the Fe-center. The remaining phosphorus shift was observed at -12.08 ppm, which is attributed to a free phosphine arm. The multinuclear NMR spectra and the lack of a magnetic moment is an implication of a low spin Fe(0) center in **[12-(κ^2-Triphos)]**. Crystallization of this complex in diethylether produced single crystals suitable for X-ray diffraction, which confirmed the ligation. The electronic spectrum of **[12-(κ^2-Triphos)]** has a maximum

absorption at 441 nm ($\varepsilon = 4471$ M^{-1}cm^{-1}). Similarly, reduction of **1-Br$_3$** and **1-Cl$_3$** also produced **[12-(κ^2-Triphos)]**. However, in the case of **12-Cl$_3$** a stronger reducing agent (5 eq. of K^0) was required to drive the reaction.
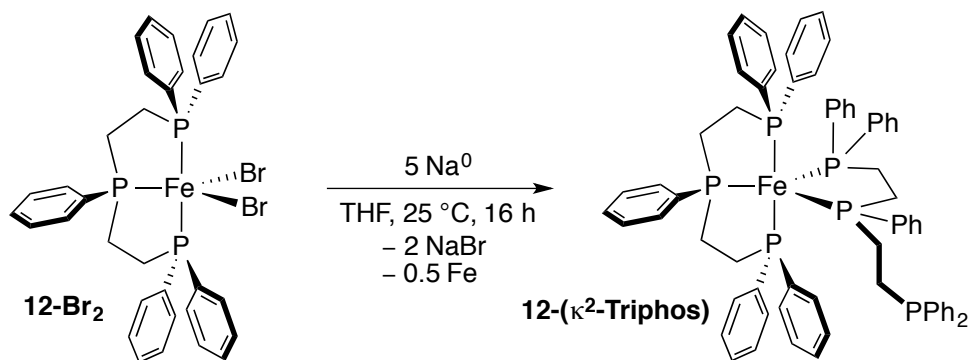
Scheme 5.2. Reduction of **12-Br$_2$** to **[12-(κ^2-Triphos)**.
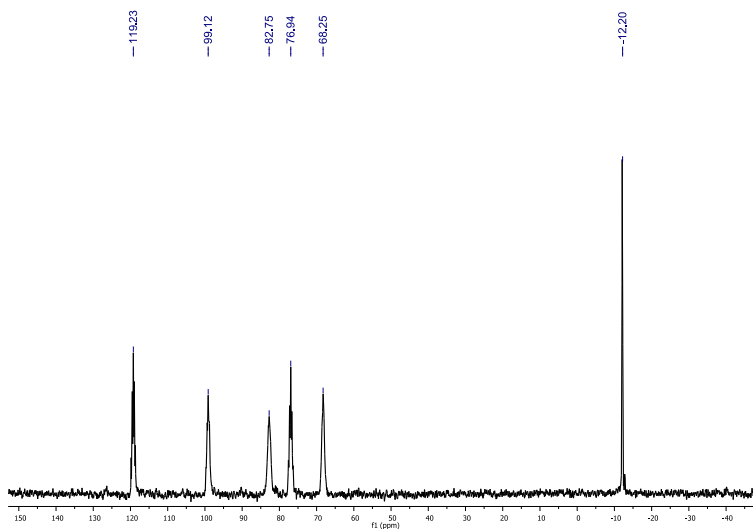
Figure 5.1. ^{31}P NMR spectrum of **[12-(κ^2-Triphos)]** in benzene-d_6.

Unfortunately, none of these Fe(II) salts furnished Fe^0-N$_2$ complexes upon reduction. Analogous Fe(0) complexes with tetradentate tripodal phosphine ligands ([κ^4-P(CH$_2$CH$_2$PMe$_2$)$_3$]Fe(N$_2$) and [κ^4-P(CH$_2$CH$_2$PMe$_2$)$_3$(μ^2-N$_2$)) were reported by Field *et*

162

al., which are structurally related to Triphos.[1h] The point to be noted that, although these complexes were spectroscopically identified, attempts to isolate them by solvent evaporation led to the dissociation of N_2 and formation of a dendritic $Fe(0)(PP_3)$ tetramer.[1h]

5.5. Reduction of (Triphos)FeBr$_2$ in presence of 2,2'-bipyridine:

After the failure to isolate N_2-bound iron complexes, we sought to reduce the (Triphos)Fe halide complexes in presence of trapping ligands. Reducing **12-Br$_2$** with excess Na^0 and one equivalent of 2,2'-bipyridine (Bpy) in diethylether produced a mixture of **[12-(κ^2-Triphos)]** and a new Bpy bound complex, $[\kappa^3$-Triphos]Fe(κ^2-2,2'-bipyridine) **(12-Bpy)**. When the amount of Bpy was increased to five equivalents in the reduction, pure **12-Bpy** was isolated as the only product. Multinuclear NMR spectroscopy on **12-Bpy** suggested it to be a diamagnetic complex. The ^{31}P NMR spectrum displayed a triplet at 112.93 ppm (J_{PP} = 8.1 Hz) and a doublet at 91.59 ppm (J_{PP} = 9.5 Hz) (Figure 5.2) indicating κ^3-chelation of Triphos. Crystallization of this complex in diethylether at -35 °C yielded red crystals suitable for X-ray diffraction, which further confirmed Bpy coordination. The crystal structure also showed a distorted square pyramidal geometry about the Fe-center.

The Bpy ligand has been a ubiquitous bidentate ligand in coordination chemistry literature.[8a] It was also found that this ligand can behave as a weak π-acceptor ligand.[8b] Moreover, crystallographically characterized transition metal and alkali metal complexes of bpy are known to feature neutral (Bpy^0),[8f] π-radical monoanion (Bpy$^{\bullet-}$)[8g,h] and dianion (Bpy^{2-}).[8i] Traditionally, the deviation of bond distances of Bpy ligand in a complex from

its unbound form has remained a useful method for the quantification of ligand reduction. Nonetheless, in low-valent first row metal complexes, the bond distances may reflect ambiguous ligand oxidation state due to the indistinguishable π-backbonding.

Scheme 5.3. Synthesis of **12-Bpy**.
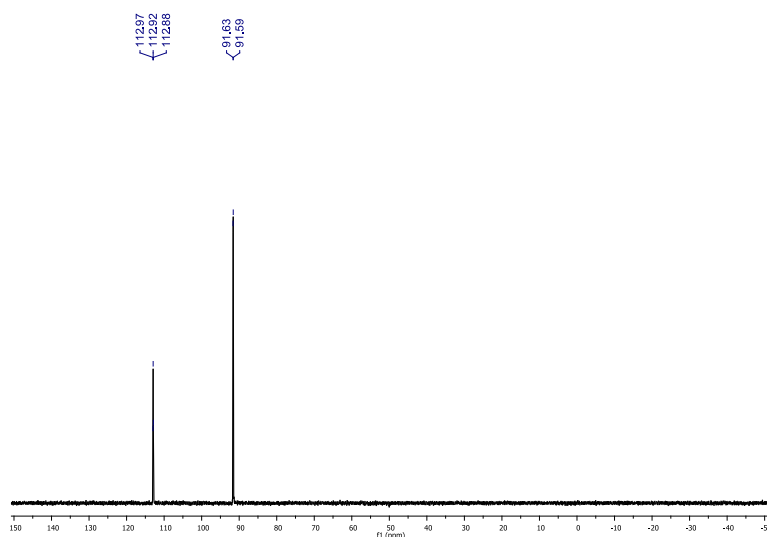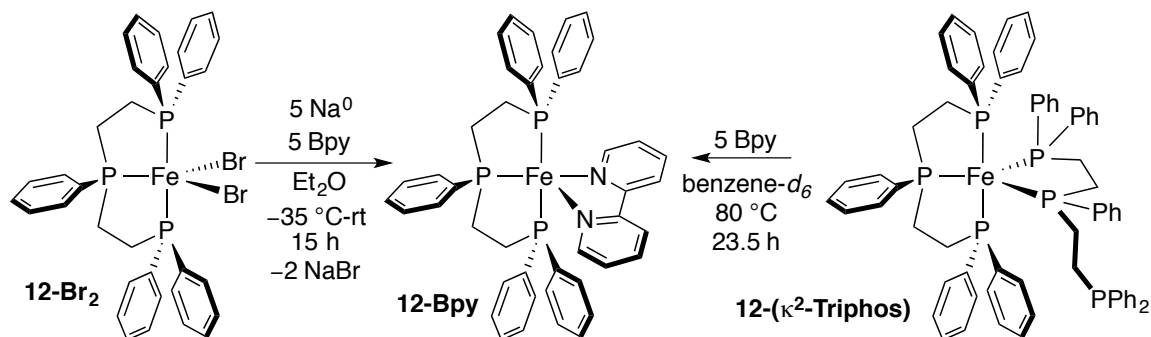
Figure 5.2. ^{31}P NMR spectrum of **(12-Bpy)** in benzene-d_6.

Recently, Scarborough *et al.* has shown excellent agreement between the experimental intraligand bond distances and the results from broken symmetry calculations of 18 Bpy supported complexes.[8e] Considering this fact, a thorough investigation of the metrical parameters of **12-Bpy** has been sought.[8j] The solid-state structure of **12-Bpy** (Figure 5.3) showed a distorted square pyramidal geometry about the

iron center as judged by P(1)-Fe(1)-P/N angles (Table 5.1.), which are close to 90°. The Fe(1)-P/N distances indicate the presence of a low spin iron center.
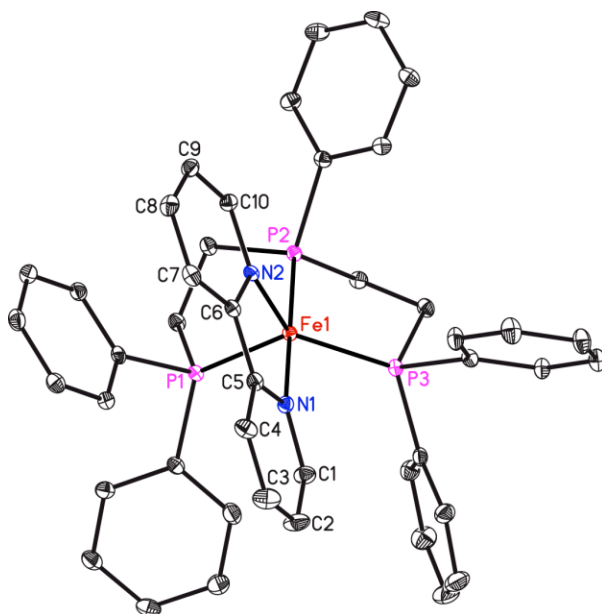
Figure 5.3. Solid-state structure of **12-Bpy** at 30% probability ellipsoids. Hydrogen atoms are omitted for clarity.

Table 5.1. Relevant bond lengths (Å) and angles (°) for **12-Bpy**.

Fe(1)-N(1)	1.956(2)	C(5)-N(1)	1.383(3)
Fe(1)-N(2)	1.936(2)	C(6)-N(2)	1.399(3)
Fe(1)-P(1)	2.1628(8)	P(1)-Fe(1)-P(2)	85.02(3)
Fe(1)-P(2)	2.1608(8)	P(1)-Fe(1)-P(3)	116.38(3)
Fe(1)-P(3)	2.2045(8)	P(1)-Fe(1)-N(1)	95.43(7)
C(5)-C(6)	1.420(4)	P(1)-Fe(1)-N(2)	104.83(7)

Interestingly, the C(5)-N(1) and C(6)-N(2) distances are 1.383(3) Å and 1.399(3) Å respectively, which are significantly elongated than the bond lengths observed for complexes featuring neutral Bpy.[8f] Concomitantly, the C(5)-C(6) bond is contracted to 1.420(4) Å. This bond distance is almost indistinguishable to the same observed for K(2,2'-bpy)(en).[8f] Notably, according to Scarborough and Wieghardt, complexes

featuring singly reduced Bpy ligands display atypical bond distances in the range of 1.41-1.43 Å. At this point it can be inferred that, the current complex **12-Bpy** features a π-radical monoanionic bpy (bpy$^{\bullet-}$).

However, **12-Bpy** has been found to be diamagnetic based on the spectroscopic analysis, which may not be expected for the Bpy$^{\bullet-}$ radical monoanion. Liu *et al.* reported a related π-radical monoanionic iminothione (o-(S)(NH)C$_6$H$_4$) (NS$^{\bullet-}$) supported iron complex, where formal Fe(0) is in fact a Fe(I) center that is antiferromagnetically coupled to a NS$^{\bullet-}$ ligand; hence resulting a diamagnetic complex.[14] Analogously, the observed diamagnetism in **12-Bpy** can be explained by antiferromagnetic coupling between Fe(I) and Bpy$^{\bullet-}$. To confirm this electronic description, electrochemical analysis on **12-Bpy** was performed.

5.5.1. Electrochemical analysis:

Cyclic voltammogram (Figure 5.4) of a solution of **12-Bpy** in 0.1 M [NBu$_4$][PF$_6$]/THF displays two reversible waves at E$_{1/2}$ = -1.61 V (vs Ag/Ag$^+$) and E$_{1/2}$ =
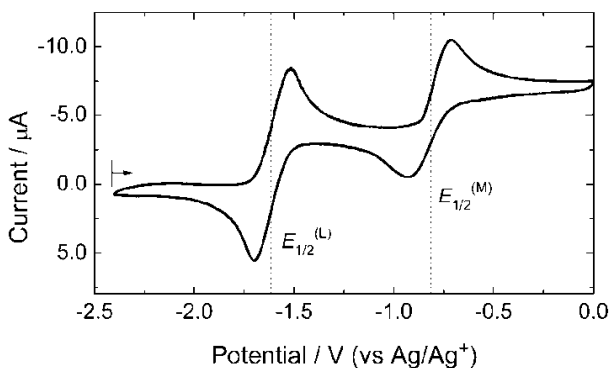
Figure 5.4. Cyclic voltammogram of **12-Bpy** in 0.1 M [NBu$_4$][PF$_6$]/THF (scan rate = 100 mV/s). E$_{1/2}^{L}$ = −1.61 V (vs Ag/Ag$^+$) and E$_{1/2}^{M}$ = −0.82 V (vs Ag/Ag$^+$).

166

−0.82 V (vs Ag/Ag$^+$). The more negative redox potential is a typical characteristic of Bpy$^{\bullet-}$/ Bpy^0 couple in non-aqueous solvents.[15] On the other hand, the second mid-potential can be ascribed to the Fe(I/II) redox couple, which is shifted to 0.4 V positive from the $E_{1/2}$ of **12-Br$_2$** (−1.20 V vs Ag/Ag$^+$).[15] This is attributed to the π-accepting ability of Bpy in contrast to the π-donating Br ligands.

5.5.2. Redox non-innocence of Bpy:

Additionally, a benzene-d_6 solution of **[12-(κ^2-Triphos)]** was heated at 80 °C in presence of 5 eq. of Bpy ligand for 23.5 hours. Continuous monitoring of the reaction mixture by ^{31}P NMR revealed slow conversion of **[12-(κ^2-Triphos)]** to **12-Bpy** (Scheme 5.3). The feasibility of this reaction can be explained by the π-accepting ability of Bpy ligand. In **[12-(κ^2-Triphos)]** the metal center is surrounded by strong σ-donating phosphines which results in an electron rich Fe(0) center. Although, phosphine ligands are weak π-acceptor, the poor delocalization of the electron density results in substitution of κ^2-Triphos chelate by Bpy, which possesses a delocalized LUMO and hence can act as an electron reservoir. This fact further supports the radical transfer from low-valent Fe(0) to Bpy. This observed redox non-innocence of Bpy inspired us to extend this study further towards other trapping chelates.

5.6. Reduction in presence of 1,3,5,7-cyclooctatetraene (COT):

The η^4-COT complex, [κ^3-Triphos]Fe(η^4-C$_8$H$_8$) (**12-COT**) had previously been synthesized by adding an equimolar quantity of Triphos to Fe(COT)$_2$ in benzene-d_6 solution.[16] However, knowing that the reduction of **12-Br$_2$** in presence of 5 equiv. of Bpy

can allow for the isolation of a well-defined Bpy-supported formal Fe(0) complex, similar reduction was carried out in presence of 10 equiv. of COT, which resulted in a 1:1 mixture of **12-κ²-Triphos** and **12-COT**. Increasing the amount of added COT to 20 equiv. and conducting the reaction at lower temperatures allowed for the isolation of **12-COT** as an analytically pure solid following solvent evaporation and recrystallization (Scheme 5.4). While it was initially reported that **12-COT** possesses a COT ligand that "is fluxional and presumably η^4-coordinated,"[16] the molecular structure of this complex was sought to verify the COT ligand coordination mode. Layering a concentrated toluene solution of **12-COT** with diethyl ether and allowing the solution to stand at −35 °C afforded single crystals suitable for X-ray diffraction. The solid-state structure determined for **12-COT** (Figure 5.5) and the relevant metrical parameters (Table 5.2) validate the initial assumption that this complex features η^4-COT coordination.
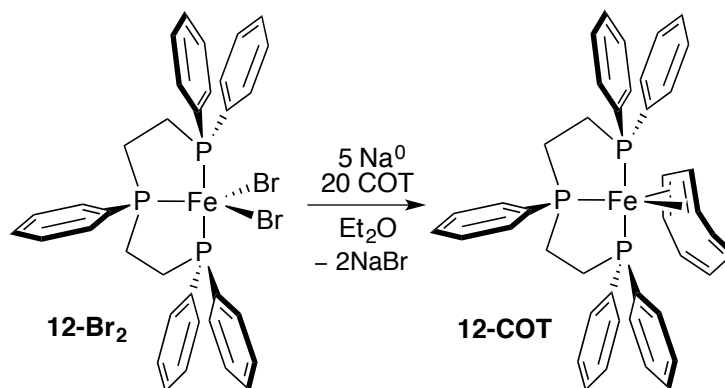
Scheme 5.4. Synthesis of **12-COT.**

As displayed in Figure 5.5, the molecular structure of **12-COT** possesses a distorted trigonal bipyramidal geometry about the iron center, with the COT ligand occupying one equatorial (C(1)−C(2)) and one axial coordination site (C(3)−C(4)). The P−Fe−P angles of 84.929(14), 86.625(15), and 98.432(15)° deviate from the idealized angles

of 90 and 120°, while the angle defined by P(2), the iron center, and the center of the C(3)−C(4) bond is far from linearity at 152.9°. Importantly, the metrical parameters determined for **12-COT** signify a substantial degree of η^4-COT ligand reduction, as elongation of the C(1)−C(2) and C(3)−C(4) double bonds to 1.432(2) Å each, along with concomitant shortening of the C(2)−C(3) single bond to 1.402(2) Å, is observed.
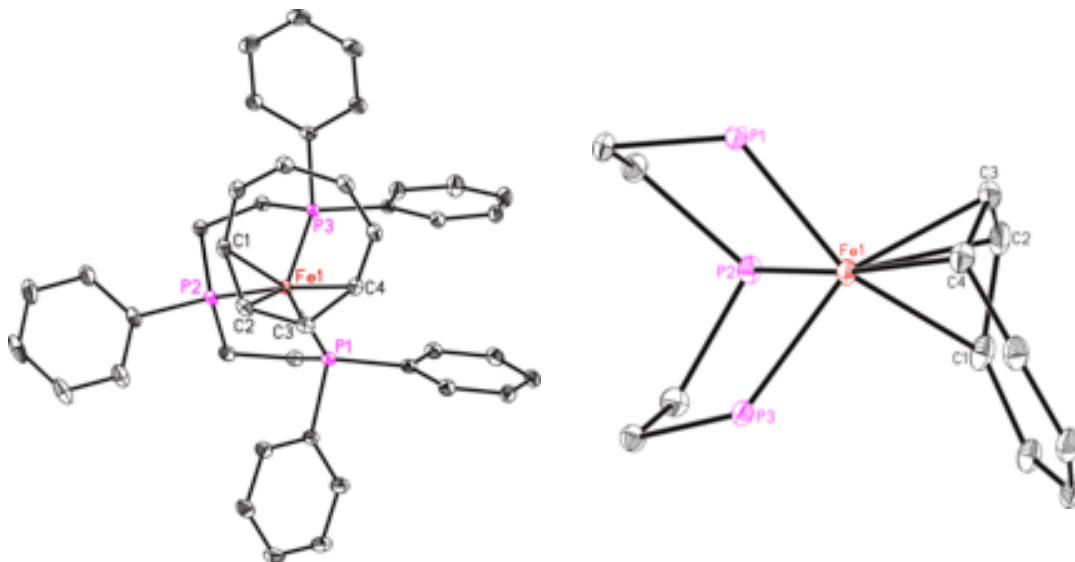
Figure 5.5 Solid-state structure of **12-COT** shown with 30% probability ellipsoids (left). At right, the core of **12-COT** is shown to highlight the overall geometry about iron. Hydrogen atoms and a co-crystallized toluene molecule have been omitted for clarity.

Table 5.2. Relevant bond lengths (Å) and angles (°) for **12-COT**.

Fe(1)-P(1)	2.1903(4)	P(1)-Fe(1)-P(2)	84.929(14)
Fe(1)-P(2)	2.1758(4)	P(1)-Fe(1)-P(3)	98.432(15)
Fe(1)-P(3)	2.1913(4)	P(2)-Fe(1)-P(3)	86.625(15)
Fe(1)-C(1)	2.1978(14)	P(2)-Fe(1)-C(4)	171.60(4)
Fe(1)-C(2)	2.0302(14)	P(2)-Fe(1)-C(3)	132.52(4)
Fe(1)-C(3)	2.0330(14)	P(2)-Fe(1)-C(2)	99.96(4)
Fe(1)-C(4)	2.2170(14)	P(2)-Fe(1)-C(1)	88.79(4)
C(1)-C(2)	1.432(2)	C(1)-C(2)-C(3)	125.22(13)
C(2)-C(3)	1.402(2)	C(2)-C(3)-C(4)	125.28(14)
C(3)-C(4)	1.432(2)		

It is also worth noting that the Fe(1)−C(2) and Fe(1)−C(3) bond distances of 2.0302(14) and 2.0330(14) Å found for the internal η^4-COT carbon atoms are much shorter than the Fe(1)−C(1) and Fe(1)−C(4) distances of 2.1978(14) and 2.2170(14) Å, respectively. The uncoordinated COT ligand carbon atoms feature a "localized butadiene" structure with C(5)−C(6), C(6)−C(7), and C(7)−C(8) bond distances of 1.359(2), 1.425(2), and 1.355(2) Å, respectively, a feature that has been observed for the unbound COT carbon atoms in related iron complexes.[11f]

Realizing that the geometry about the metal center in **12-COT** is somewhat atypical, the preparation of a second η^4-COT ligated complex featuring idealized trigonal bipyramidal geometry was targeted to gauge whether geometric considerations play a large role in the degree of crystallographically observed COT ligand reduction, as well as the overall electronic structure determination of such complexes. The Triphos ligand used to support **12-COT** is well-known for its coordinative flexibility and has been found to chelate in either a *fac-* or *mer-*fashion within an octahedral transition-metal environment.[7g] In order to keep the electronic influence of the chelate consistent, a tied-back variant of this ligand, $H_3CC(CH_2PPh_2)_3$, was chosen due to its rigidity and propensity to coordinate to iron in a *fac*-manner.[7h,j,l] This ligand is also known as Triphos throughout the literature; however, for the purposes of this manuscript, $H_3CC(CH_2PPh_2)_3$ will be denoted as Triphos* to differentiate it from the more flexible Triphos ligand, $PhP(CH_2CH_2PPh_2)_2$.

Following the methodology used to prepare and isolate **12-COT**,[16] the stoichiometric addition of Triphos* to Fe(COT)$_2$ in toluene solution allowed for the formation of (Triphos*)Fe(η^4-C$_8$H$_8$) (**13-COT**), as shown in Scheme 5.5. Alternatively, this complex

170

could be prepared in a reproducible fashion upon reducing (Triphos*)FeBr$_2$ **(13-Br$_2$)** in the presence 5 eq. of COT (see the Experimental Section). Like **12-COT**, **13-COT** was found to feature one broad ^{1}H NMR resonance for the freely rotating COT ligand at 5.53 ppm and one ^{31}P NMR resonance at 53.35 ppm, indicating that the phosphinoalkyl arms of the Triphos* ligand are equivalent in solution. Additionally, single crystals of **13-COT** suitable for X-ray diffraction were obtained and the solid-state structure determined for this complex is displayed in Figure 5.6.
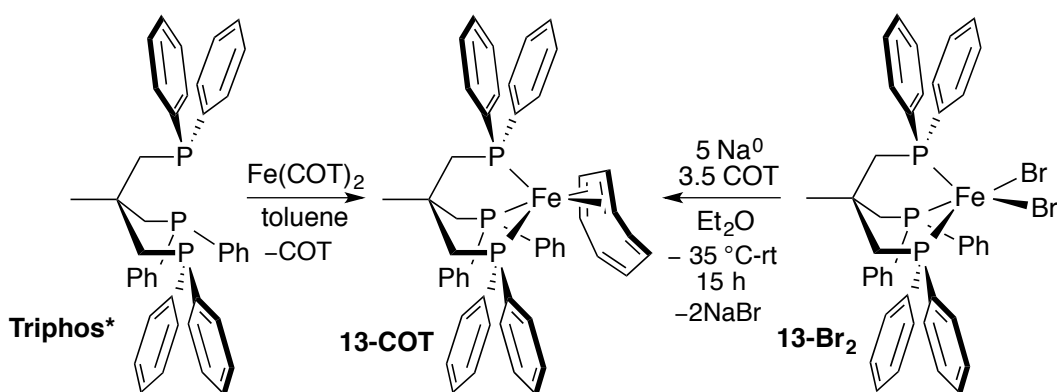
Scheme 5.5. Synthesis of **13-COT**.

The metrical parameters determined for **13-COT** (Table 5.3) reveal P-Fe-P bond angles of 88.44(3), 91.93(3), and 92.99(3)°, indicating that the geometry of the Triphos* chelate as it relates to iron is more representative of an idealized trigonal bipyramid than the angles found for **12-COT**. As with **12-COT**, the COT ligand in **13-COT** occupies one axial and one apical coordination site; however, it should be noted that **13-COT** features an angle defined by P(2), the metal, and the center of the C(1)-C(2) bond that is slightly further from linearity at 150.6°. Although the Fe-P distances determined for **2-COT** of 2.1759(8), 2.1909(8), and 2.2063(8) Å are similar to those found for **12-COT**, the former complex features even longer iron to external η^4-COT carbon atom bond

lengths of 2.233(3) [Fe(1)-C(1)] and 2.265(3) Å [Fe(1)-C(4)]. Importantly, the distances between the bound COT carbon atoms determined for **12-COT** and **13-COT** are statistically indistinguishable, suggesting that a significant amount of electron density is being transferred to the COT ligand from the formally zerovalent iron center in both cases (Table 5.2 and Table 5.3).
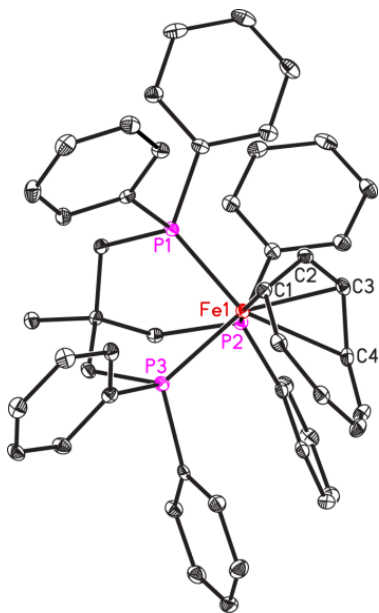
Figure 5.6. Solid-state structure of **13-COT** at 30% probability ellipsoids. Hydrogen atoms have been omitted for clarity.

Table 5.3. Relevant bond lengths (Å) and angles (°) for **13-COT**.

Fe(1)-P(1)	2.1759(8)	P(1)-Fe(1)-P(2)	88.44(3)
Fe(1)-P(2)	2.2063(8)	P(1)-Fe(1)-P(3)	91.93(3)
Fe(1)-P(3)	2.1909(8)	P(2)-Fe(1)-P(3)	92.99(3)
Fe(1)-C(1)	2.233(3)	P(2)-Fe(1)-C(4)	153.94(8)
Fe(1)-C(2)	2.047(3)	P(2)-Fe(1)-C(3)	97.89(8)
Fe(1)-C(3)	2.059(3)	P(2)-Fe(1)-C(2)	130.47(8)
Fe(1)-C(4)	2.265(3)	P(2)-Fe(1)-C(1)	168.79(7)
C(1)-C(2)	1.426(4)	C(1)-C(2)-C(3)	125.4(3)
C(2)-C(3)	1.391(4)	C(2)-C(3)-C(4)	125.6(3)
C(3)-C(4)	1.429(4)		

5.6.1. Survey of metrical parameters of all known η^4-COT complexes:

It has been known for over 50 years that backbonding into (or reduction of) an η^4-COT ligand leads to elongation of the olefin double bonds with concomitant shortening of the bridging C-C single bond as judged by single crystal X-ray diffraction,[11a] a feature which has been observed for numerous η^4-COT coordinated complexes (Table 5.4). At first glance, it is apparent that a wide range of X-ray diffraction data quality is presented in Table 5.4.[11,17] With the exception of $[(\eta^4\text{-COT})Cr]_2(\mu\text{-}\eta^5,\eta^5\text{-COT})$[17a] and $[(\eta^4\text{-COT})Mo]_2(\mu\text{-}\eta^5,\eta^5\text{-COT})$,[17f] most of the crystallographically verified η^4-COT complexes reported over 30 years ago, including $(\eta^4\text{-COT})Fe(CO)_3$,[11a] $[(CO)_3Fe]_2(\mu\text{-}\eta^4,\eta^4\text{-COT})$,[11a] $(\eta^4\text{-COT})Fe(PPh_3)(CO)_2$,[11c] $(\eta^4\text{-COT})Fe(\eta^4\text{-butadiene})(CO)$,[11d] $(\eta^4\text{-COT})Zr(\eta^8\text{-COT})(THF)$,[17d] $(\eta^4\text{-COT})Ru(CO)_3$,[17g] and $[(\eta^4\text{-COT})W]_2(\mu\text{-}\eta^5,\eta^5\text{-COT})$,[17k] feature C-C bond distances with estimated standard deviations that are inappropriate for detailed electronic structure discussion.[18] Additionally, the solid state structures determined for $(CO)_3Fe(\mu\text{-}\eta^4,\eta^4\text{-COT})Fe(CO)_2(=COEt(Ph))$,[11e] $(\eta^4\text{-COT})_2Fe(BAC)$,[11f] $(\eta^4\text{-COT})Zr(\eta^8\text{-COT})$,[17c] and $(\eta^5\text{-Cp*})Zr(\mu\text{-}\eta^8,\eta^2\text{-COT})(\eta^4\text{-COT})Zr(\eta^5\text{-Cp*})$[17e] possess a significant degree of C-C distance uncertainty within the COT ligand. The metrical parameters determined for $[(\eta^8\text{-COT})Ti]_2(\mu\text{-}\eta^4,\eta^4\text{-COT})$[19] and $[(2,6\text{-}(2,6\text{-}^iPr_2\text{-}C_6H_3)C_6H_3)Cr]_2(\mu\text{-}\eta^3,\eta^4\text{-COT})$[20] have been excluded from Table 5.4, since these complexes feature unusual $\mu\text{-}\eta^4,\eta^4$-COT and $\mu\text{-}\eta^3,\eta^4$-COT binding modes, respectively, in which one or more of the η^4-COT carbon atoms are coordinated to both metal centers. While population of the lowest lying COT π^*-orbital might not be achieved for the second and third row complexes shown in Table 5.4, it is important to note that several of the first row complexes listed feature significant C(1)-C(2)/C(3)-C(4) bond elongation with

173

concomitant C(2)-C(3) bond shortening, indicating that they could in fact have an electronic structure best described as having an η^4-COT radical monoanionic or dianionic ligand.

Table 5.4. Selected bond lengths (Å) for complexes featuring η^4-COT coordination. Distances shown in italics are excluded from electronic structure discussion throughout the text.[18]
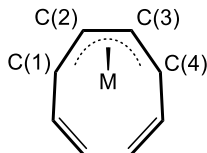
Complex	C(1)-C(2)	C(2)-C(3)	C(3)-C(4)	Ref.
[(η^4-COT)Cr]$_2$(μ-η^5,η^5-COT)	1.388(6)	1.398(5)	1.375(7)	17a
	1.387(5)	1.407(5)	1.427(5)	
(η^4-COT)Fe(CO)$_3$	1.42(1)	1.42(2)	1.42(1)	11a
[(η^4-COT)Fe(CO)$_3$]$_2$[((μ-η^1,η^1-(N,N)-2,4-(CF$_3$)$_2$N$_2$C$_3$)Ag]$_3$	1.446(8)	1.378(9)	1.421(8)	11b
	1443(9)	1.393(9)	1.399(9)	
[(CO)$_3$Fe]$_2$(μ-η^4,η^4-COT)	1.43(3)	1.39(4)	1.40(4)	11a
	1.48(4)	1.40(4)	1.44(3)	
(η^4-COT)Fe(PPh$_3$)(CO)$_2$	1.449(9)	1.417(10)	1.450(8)	11c
(η^4-COT)Fe(η^4-butadiene)(CO)	1.412(7)	1.388(16)	1.412(7)	11d
(CO)$_3$Fe(μ-η^4,η^4-COT)Fe(CO)$_2$(=COEt(Ph))	1.47(3)	1.36(3)	1.40(3)	11e
	1.48(3)	1.41(3)	1.43(3)	
(η^4-COT)Fe(BAC)$_2$^{a}	1.415(5)	1.382(6)	1.429(6)	11f
(η^4-COT)$_2$Fe(BAC)^a	1.387(13)	1.421(12)	1.419(13)	11f
	1.375(14)	1.430(14)	1.376(14)	
(η^4-COT)Fe(η^4,η^2-cyclooctatriene)$_2$^{b}	1.4201(16)	1.4049(16)	1.4224(15)	11f
(η^4-COT)Fe(μ-η^5,η^5-COT)Fe(R)^c	1.447(3)	1.400(3)	1.400(4)	11f
(Triphos)Fe(η^4-COT) (**12-COT**)	1.432(2)	1.402(2)	1.432(2)	11g
(Triphos*)Fe(η^4-COT) (**13-COT**)	1.426(4)	1.391(4)	1.429(4)	11g
[(η^4-COT)$_2$Co][K(2,2,2-crypt)]	1.429(4)	1.398(4)	1.437(4)	17b
(η^4-COT)Zr(η^8-COT)	1.40(2)	1.39(2)	1.40(2)	17c
(η^4-COT)Zr(η^8-COT)(THF)	1.36(3)	1.44(3)	1.45(2)	17d
(η^5-Cp*)Zr(μ-η^8,η^2-COT)(η^4-COT)Zr(η^5-Cp*)	1.42(1)	1.37(1)	1.41(1)	17e
[(η^4-COT)Mo]$_2$(μ-η^5,η^5-COT)	1.425(8)	1.416(8)	1.416(9)	17f
	1.432(9)	1.398(10)	1.427(10)	
(η^4-COT)Ru(CO)$_3$	1.443(8)	1.394(12)	1.443(8)	17g
[(η^5-Cp)Ru(μ-η^4,η^4-COT)(μ-H)Ru(η^5-Cp)][PF$_6$]	1.418(2)	1.428(4)	1.418(2)	17h

$[(\eta^5\text{-Cp})\text{Ru}]_2(\mu\text{-}\eta^4,\eta^4\text{-COT})$	1.455(4)	1.428(5)	1.430(5)	17h
	1.424(5)	1.425(5)	1.426(5)	
$[(\text{CO})_2\text{Ru}]_2(\mu\text{-}\eta^4,\eta^4\text{-COT})(\mu\text{-}\eta^1,\eta^1\text{-CO})$	1.401(6)	1.412(7)	1.409(8)	17i
$[(\eta^5\text{-Cp})\text{Rh}(\mu\text{-}\eta^4,\eta^4\text{-COT})\text{Rh}(\eta^2,\eta^2\text{-}$	1.423(5)	1.405(8)	1.423(5)	17j
norbornadiene)][BF$_4$]	1.425(5)	1.420(8)	1.425(5)	
$[(\eta^4\text{-COT})\text{W}]_2(\mu\text{-}\eta^5,\eta^5\text{-COT})$	1.38(3)	1.46(3)	1.41(3)	17k
	1.43(4)	1.37(4)	1.47(4)	

[a]BAC = *N,N*-bis(diisopropyl)aminocyclopropenylidene. [b]The 5- and 8-positions of the clyclooctatriene ring are bridged by a quaternary carbon atom that lies in the 2-position of an *N*-(2,6-diisopropylphenyl)-3,3,5,5-tetramethylpyrrolidine ring. [c]R = 2,4-(*N,N*)-bis(2,6-diisopropylphenyl-3,5-diphenylimidazole.

5.6.2. Mössbauer spectral parameters:

Since the crystallographically determined metrical parameters for **12-COT** and **13-COT** suggest that these complexes might have a reduced COT ligand with a non-zerovalent metal center, further spectroscopic study was sought before arriving at a final electronic structure description. Because the electronic structures of **12-κ²-Triphos** and **12-Bpy** are well-understood,[8j] it was believed that these complexes would serve as excellent reference compounds for the Mössbauer spectroscopic investigation of **12-COT** and **13-COT**. The Mössbauer spectrum of **12-κ²-Triphos** (Figure 5.7) was recorded at 77 K and was found to feature an equal abundance of geometrically distinct components characterized by isomer shift values (IS or δ) of 0.07 and 0.09 mm/s and quadrupole splitting parameters (ΔE_Q) of 2.00 and 2.13 mm/s, respectively (Table 5.5). The Mössbauer spectrum of **12-κ²-Triphos** was also found to feature a small amount of an iron containing impurity that grows in upon prolonged exposure to air. The values obtained for **12-κ²-Triphos** are comparable to those obtained for Fe(CO)$_5$ (δ = -0.09 mm/s, ΔE_Q = 2.57 mm/s),[21] such that the differences in isomer shift and quadrupole splitting between the complexes reflect the relative ligand field strength about iron.[22]

Like Fe(CO)$_5$,[23] **12-κ²-Triphos** was found to possess a near trigonal bipyramidal geometry in the solid state.
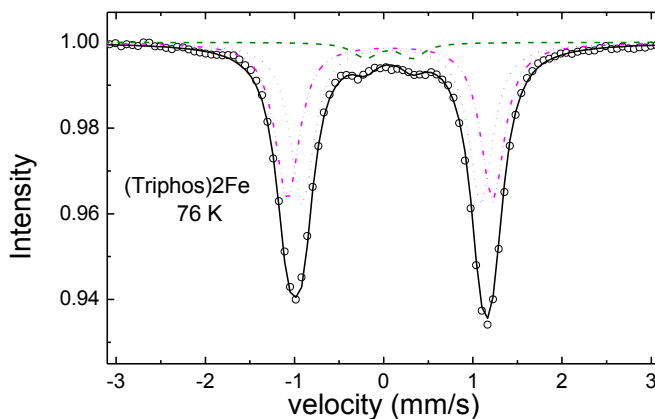
Figure 5.7. Mössbauer spectrum of **12-κ²-Triphos** at 76 K.

Table 5.5. Mössbauer parameters for complexes discussed in this study.

Complex	IS(1) (mm/s)	ΔE_Q (1) (mm/s)	IS(2) (mm/s)	ΔE_Q (1) (mm/s)	Fe(1)/Fe(2) Relative Abundance (%)
12-κ²-Triphos	0.09	2.00	0.07	2.31	50.5/49.5
12-Bpy	0.06	1.35	0.04	1.04	65.6/34.4
12-COT	0.11	1.08	-	-	100
13-COT	0.16	1.05	-	-	100
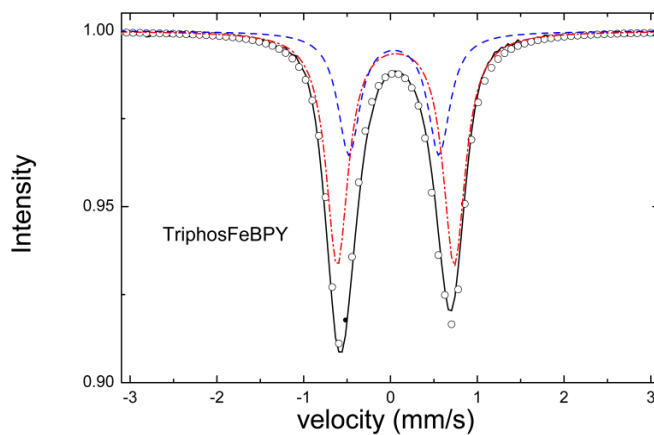
Figure 5.8. Mössbauer spectrum of **12-Bpy** at 76 K.

The Mössbauer spectrum of **12-Bpy** (Figure 5.8), which is known to have an electronic structure consistent with a monoreduced Bpy chelate that antiferromagnetically couples to an Fe(I) center,[8j] features two geometrically distinct components with isomer shifts (Table 5.5) that are similar to the ones determined for **12-κ²-Triphos**. Although the isomer shift parameter of high spin iron complexes often allows for an accurate oxidation state determination, this observation was not surprising because minimal isomer shift differences are known to exist between low-spin iron complexes with varying oxidation states.[22]
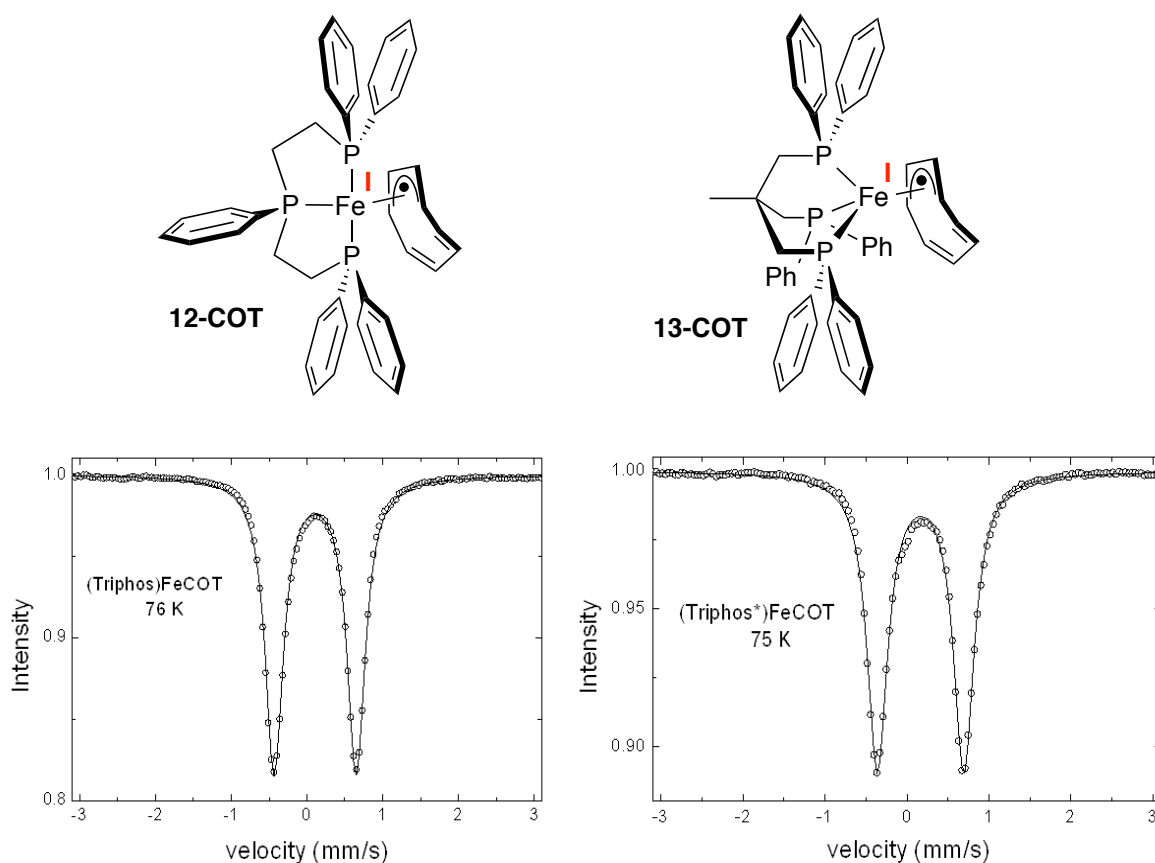
Figure 5.9. The electronic structure representations (top) and Mössbauer spectra (bottom) of **12-COT** (left) and **13-COT** (right).

177

On the other hand, the quadrupole splitting parameters determined for **12-Bpy** (1.04 and 1.35 mm/s) are significantly smaller than the values found for **12-κ²-Triphos** (2.00 and 2.31 mm/s), suggesting that the former complex has a diminished electric field gradient which arises from the removal of one iron-based electron. As with the reference compounds, the Mössbauer spectrum of **12-COT** (Figure 5.9, left) was found to feature an undistinguished isomer shift of 0.11 mm/s due to its low-spin configuration.[21]

However, the quadrupole splitting parameter of 1.08 mm/s determined for this complex is even smaller than the values found for **12-Bpy** (Table 5.5), consistent with a reduction in the iron d-electron count. Although a slightly higher isomer shift of 0.16 mm/s was found for **13-COT**, this complex also exhibited a diminished quadrupole splitting of 1.05 mm/s. For this reason, it is believed that the electronic structure of **12-COT** and **13-COT** is consistent with an η^4-COT radical monoanion that is antiferromagnetically coupled to a low-spin Fe(I) center, as displayed at the top of Figure 5.9.

5.6.3. Electron paramagnetic resonance spectra of 12-COT:

To obtain additional supporting evidence for the electronic structure determination of **12-COT**, the X-band (9.45 GHz) electron paramagnetic resonance (EPR) spectrum of this complex was recorded in a toluene glass over a range of cryogenic temperatures. The EPR spectrum of **12-COT** was found to contain a signal with seven-line splitting between 4 K and 130 K (Figure 5.10.b). Expectedly, this signal pattern deviates significantly from what would be expected for a single spin center ($S = \frac{1}{2}$) and the positions and relative amplitudes of the peaks are not consistent with those measured for a typical triplet state ($S = 1$). However, the EPR pattern observed for **12-**

COT is similar to those previously reported for systems with two $S = 1/2$ spins coupled by weak exchange and dipole-dipole interactions.[24] Within this model, both the triplet and singlet states are active (Figure 5.10.a). To ascertain whether the EPR spectrum of **12-COT** corresponds to such a spin system, the respective spin Hamiltonian was fit to the data (Figure 5.10.b, dashed line) while assuming that one spin belongs to the unpaired electron of a low-spin Fe(I) center and the second belongs to an unpaired electron located within the η^4-COT ligand (Fe^{1+}-COT$^{\cdot-}$).
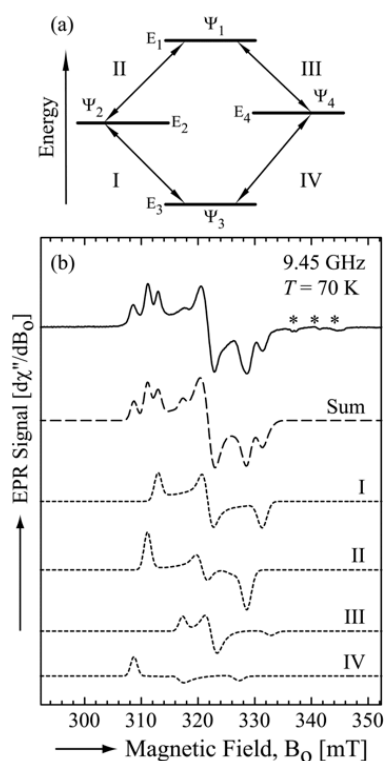
Figure 5.10. (a) Energy levels (E_i) of the eigenstates (Ψ_i) for the coupled metal-radical spin-dimer (Fe^{1+}-COT$^{\cdot-}$). The eigenstates of the triplet state are: $\Psi_1 = |+\,+\rangle$, $\Psi_2 = a|+\,-\rangle + b\,|-\,+\rangle$ and $\Psi_3 = |-\,-\rangle$, the one of the singlet state is: $\Psi_4 = -b|+\,-\rangle + a\,|-\,+\rangle$. The allowed transitions between these levels (I, II, III, and IV) are indicated by arrows. (b) Experimental (solid line) and simulated (dashed line) EPR spectra of **12-COT**. The small lines at higher field (marked with *) belong to minor impurities. Simulation of the spectral components corresponding to transitions I, II, III, and IV of randomly oriented

179

Fe^{1+}-COT^{-} spin-dimers (i.e., as obtained in frozen solutions) are also shown (dotted lines). The sum of the spectral components (dotted lines) results in the simulated spectrum (dashed line).

The spectral features observed for **12-COT** were well fit (σ = 2.3%, see Experimental Section for the definition of σ) when treating this complex as an Fe^{1+}-COT^{-} spin-dimer and the parameters that were obtained are summarized in Table 5.6. The magnitude of the isotropic exchange interaction J_o (-70.7 MHz) is small. This is consistent with the model used to fit the data and shows no significant overlapping between the wave functions corresponding to the unpaired electrons (two) within **12-COT**.

Table 5.6. Parameters used in fitting of the EPR spectrum of **12-COT** (Fe^{1+}-COT^{-}) in a toluene glass at 9.45 GHz and T = 70 K.

Parameter	Fe^{1+}-COT^{-}
J_o (MHz)	-70.7
$J_{x'}$ (MHz)	141.8
$J_{y'}$ (MHz)	-101.1
$J_{z'}$ (MHz)	-40.7
$\frac{1}{2}(g_{xA} + g_{xB})$	2.153
$\frac{1}{2}|g_{xA}-g_{xB}|^a$	0.016
$\frac{1}{2}(g_{yA} + g_{yB})$	2.115
$\frac{1}{2}|g_{yA}-g_{yB}|^a$	0.000
$\frac{1}{2}(g_{zA} + g_{zB})$	2.046
$\frac{1}{2}|g_{zA}-g_{zB}|^a$	0.009
ΔB_x (MHz)	39.0
ΔB_y (MHz)	58.1
ΔB_z (MHz)	54.1

[a]Specific g-values to either Fe^{1+} or COT^{-} cannot be assigned due to the multiple solutions obtained for these parameters. For this reason, Table 5.6 contains only the absolute values of the differences $|g_{iA}-g_{iB}|$.

5.6.4. Electrochemical analysis of 12-COT and 13-COT:

Cyclic voltammetry experiments were also performed on **12-COT** and **13-COT**. The voltammogram of **13-COT** in THF (0.1 M NBu$_4$PF$_6$ was used as electrolyte) displays three reversible redox processes (Figure 5.11 solid line), and differential pulse voltammetry confirmed that each of these reversible waves involves same number of electrons. Starting from the isolated electronic state of the complex (Fe^{1+}, COT$^{\cdot-}$), the first reduction with $E_{1/2}$ = -2.74 V vs Fc$^{+/0}$ (red region) is attributed to the metal based Fe$^{I/0}$ couple.
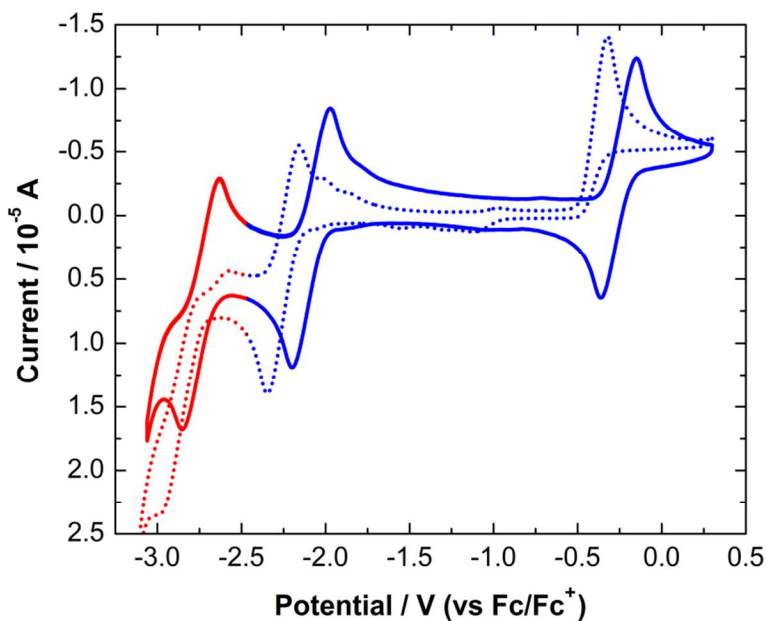
Figure 5.11. Cyclic voltammograms of **13-COT** (solid line) and **12-COT** (dotted line) in THF (electrolyte 0.1 M [NBu4][PF6]; scan rate = 20 mV/s). The red and blue regions indicate the reduction and oxidation processes, respectively, from the starting redox state of the neutral complexes.

The first oxidation at $E_{1/2}$ = -2.09 V vs Fc$^{+/0}$ (blue region) corresponds to ligand based COT$^{-I/0}$ couple. The second oxidation wave at $E_{1/2}$ = 0.25 V vs Fc$^{+/0}$ (blue region) is assigned to the metal based Fe$^{I/II}$ couple. Although the reverse redox process (Fe$^{II/I}$) is

observed on the time scale of voltammetry, sustained application of a voltage greater than -0.2 V showed that the oxidized Fe^{II}, COT^0 species is chemically unstable. Cyclic voltammetry on **12-COT** showed a similar pattern of three redox processes, but with a more complicated electrochemical behavior. As shown in Figure 5.11 (dotted line), only the first oxidation wave ($COT^{-I/0}$) is fully reversible with a mid potential of -2.24 V vs $Fc^{+/0}$, while both the first reduction ($Fe^{I/0}$) and second oxidation ($Fe^{I/II}$) waves are irreversible.

5.6.5. Density functional theory calculations:

The electronic structures of **12-Bpy** and **12-COT** were also investigated by conducting density functional theory (DFT) calculations on the optimized molecular structure of each complex. For **12-Bpy**, attempts to perform spin stability calculations on the closed shell, non-broken symmetry singlet revealed that this electronic structure did not appear to be the lowest energy state. Further analysis allowed for the identification of a broken symmetry (1,1) minimum that was approximately 20 kJ/mol lower in energy (Figure 5.12, left) than the closed shell singlet. We performed two calculations to assess the relative spin state stability of **12-COT** complex for the closed-shell singlet and triplet spin states. The singlet was predicted to be the ground state by 51 kJ/mol, with the optimized geometry being a close match to the experimental crystal structure. In the ground state solution, the COT ligand was bound in an η^4-fashion and the unbound planar COT carbon atoms were found to possess alternating bond lengths, as found for the [COT·]- radical anion gas phase geometry.[25] In contrast, the high spin structure was found to possess a planar, η^2-COT ligand with some spin delocalization (~0.3e). Although several calculations were performed with a broken symmetry wavefunction as a starting

182

point with antiferromagnetic spin delocalization onto the COT ligand, the results all returned to the closed shell singlet as the converged solution and therefore offer no support to the experimental spin measurements. A TDDFT calculation[26] was performed to explore any low energy singlet excited states, but the closest state calculated was 2.5 eV higher in energy.

12-Bpy   **12-COT**
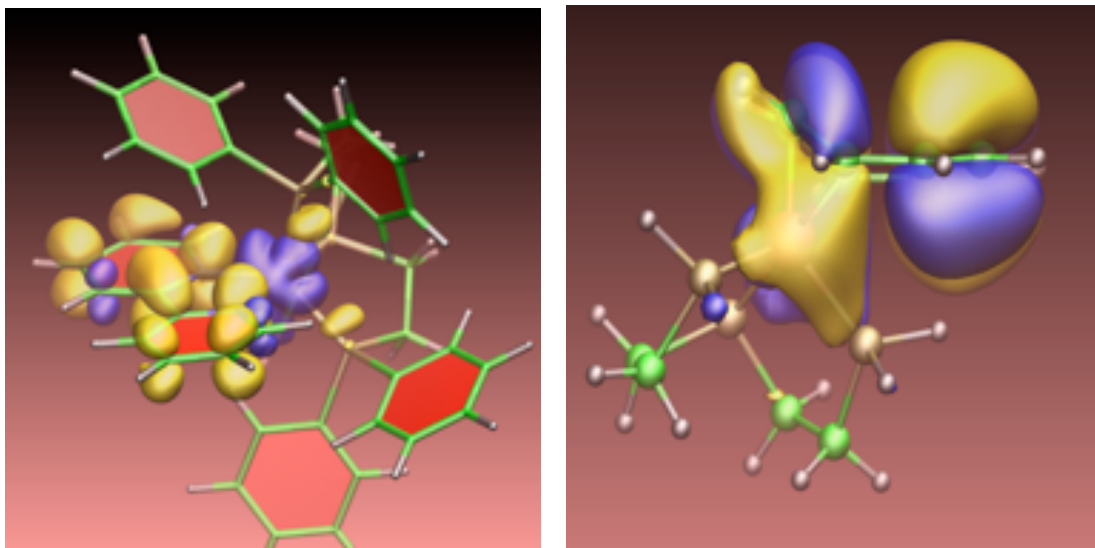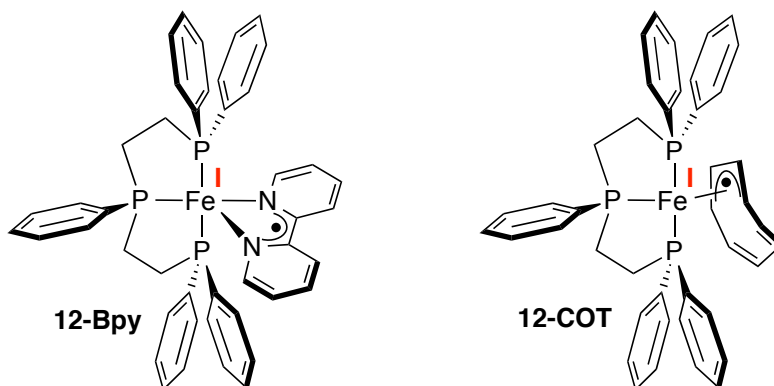
Figure 5.12. The calculated spin density for the broken symmetry solution found for **12-Bpy** (left). Calculated highest occupied molecular orbital for **12-COT** showing overlap between Fe *d*-orbitals and COT π* orbitals (right).

A simple Mulliken population analysis revealed a small amount of charge transfer between Fe and the COT ligand (~0.17e), with the highest occupied molecular orbitals showing considerable overlap between the Fe d-orbitals and an orbital that resembles the HOMO of the [COT$\cdot$]$^-$ radical anion in the gas phase (Figure 5.12, right).[25] A calculation of the Mayer bond orders suggests that the unbound COT carbon atoms resemble those of the [COT$\cdot$]$^-$ radical anion; however, the bond order of the central η^4-COT C-C bond was found to be 1.30, supporting the contention of charge transfer into the anti-bonding orbitals of the COT ligands from Fe. The calculated Mössbauer parameters[27] for optimized **12-COT** were found to be $\delta = 0.09$ mm/s and $\Delta E_Q = 1.33$ mm/s and are in fairly good agreement with the measured values. It is possible that our inability to calculate the experimentally observed broken symmetry solution is related to the close proximity of the COT Ψ_3 orbital to the iron center.

5.6.6. Comparison of M-C bonds of relevant η^4-COT complexes:

Since Mössbauer and EPR spectroscopic evidence strongly suggests that the electronic structures of **12-COT** and **13-COT** are best described as containing low-spin Fe(I) centers that are antiferromagnetically coupled to an η^4-COT radical monoanion, the crystallographically determined C-C and M-C bond distances found for these complexes can be applied as metrics for assessing the degree of η^4-COT ligand reduction present in complexes throughout the d-block. The C(2)-C(3) bond distances determined for **12-COT** and **13-COT** of 1.402(2) and 1.391(4) Å, respectively, are significantly shorter than that of a single C-C bond, and it is believed that a similar bond distance in related complexes could indicate the presence of a COT radical monoanion. In fact, the C(2)-C(3) distances determined for these complexes are even shorter than the range of 1.41-

1.43 Å that has recently been described for the central C-C single bond distance associated with Bpy radical anion ligands.[8e,j] Although less convincing when considered independently, C(1)-C(2) and C(3)-C(4) bond distances of approximately 1.43 Å may also suggest that a given η^4-COT complex features the singly reduced form of this ligand.

Table 5.7. M-C bond lengths (Å) for complexes featuring η^4-COT coordination.[18]
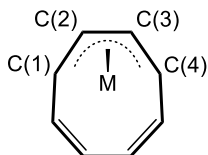
Complex	M-C(1)	M-C(2)	M-C(3)	M-C(4)	Ref.
(η^4-COT)Cr]$_2$(μ-η^5,η^5-COT)	2.369(5)	2.140(4)	2.104(3)	2.279(4)	17a
	2.341(3)	2.127(3)	2.112(3)	2.272(3)	
[(η^4-COT)Fe(CO$_3$)]$_2$[((μ-η^1,η^1-(N,N)-2,4-(CF$_3$)$_2$N$_2$C$_3$)Ag]$_3$	2.190(6)	2.046(5)	2.043(5)	2.187(5)	11b
	2.175(5)	2.045(5)	2.059(5)	2.184(6)	
(η^4-COT)Fe(BAC)$_2$^{a}	2.170(4)	2.066(4)	2.063(4)	2.406(4)	11f
(η^4-COT)Fe(η^4,η^2-cyclooctatriene)$_2$^{b}	2.1711(11)	2.0295(10)	2.0247(10)	2.2044(11)	11f
(η^4-COT)Fe(μ-η^5,η^5-COT)Fe(R)^c	2.177(2)	1.985(2)	2.025(3)	2.165(3)	11f
(Triphos)Fe(η^4-COT)(**12-COT**)	2.1978(14)	2.0302(14)	2.0330(14)	2.2170(14)	11g
(Triphos*)Fe(η^4-COT)(**13-COT**)	2.233(3)	2.047(3)	2.059(3)	2.265(3)	11g
[(η^4-COT)$_2$Co][K(2,2,2-crypt)]	2.152(3)	1.991(3)	1.989(3)	2.199(3)	17b
[(η^4-COT)Mo]$_2$(μ-η^5,η^5-COT)	2.327(5)	2.264(5)	2.271(5)	2.359(6)	17f
	2.355(5)	2.241(5)	2.242(6)	2.343(6)	
[(η^5-Cp)Ru(μ-η^4,η^4-COT)(μ-H)Ru(η^5-Cp)][PF$_6$]	2.219(2)	2.166(2)	2.166(2)	2.219(2)	17h
[(η^5-Cp)Ru]$_2$(μ-η^4,η^4-COT)	2.206(3)	2.157(3)	2.163(3)	2.228(3)	17h
	2.215(3)	2.164(3)	2.161(3)	2.214(3)	
[(CO)$_2$Ru]$_2$(μ-η^4,η^4-COT)(μ-η^1,η^1-CO)	2.345(4)	2.240(4)	2.238(4)	2.323(5)	17i
[(η^5-Cp)Rh(μ-η^4,η^4-COT)Rh(η^2,η^2-norbornadiene)][BF$_4$]	2.201(4)	2.219(4)	2.219(4)	2.201(4)	17j

^{a}BAC = N,N-bis(diisopropyl)aminocyclopropenylidene. ^{b}The 5- and 8-positions of the cyclooctatriene ring are bridged by a quaternary carbon atom that lies in the 2-position of an N-(2,6-diisopropylphenyl)-3,3,5,5-tetramethylpyrrolidine ring. ^{c}R = 2,4-(N,N)-bis(2,6-diisopropylphenyl-3,5-diphenylimidazole.

185

Likewise, the M-C bond distances determined for **12-COT** and **13-COT** might suggest the presence of a singly reduced COT ligand in analogous complexes. As shown in Table 5.7, the M-C(2) and M-C(3) distances found for **12-COT** [2.0302(14) and 2.0330(14) Å, respectively] and **13-COT** [2.047(3) and 2.059(3) Å, respectively] are 0.15-0.20 Å shorter than the distances determined for the neighboring M-C(1) and M-C(4) contacts. With the exception of $(\eta^4$-COT)Fe(BAC)$_2$, which features an abnormally long M-C(4) distance, this characteristic is shared with each of the other first row transition metal complexes displayed in Table 5.7.[18] While it is impractical to reassign the electronic structure of any of these complexes based on crystallographic metrical parameters alone, a particularly interesting comparison can be made between the M-C bond distances determined for **12-COT** or **13-COT** and the homoleptic COT supported Co(I-) complex, $[(\eta^4$-COT)$_2$Co][K(2,2,2-crypt)], prepared by Ellis and co-workers.[17b]

Along with the original publication of this complex, it was proposed that the COT ligands were serving as "superb acceptors" and may be regarded as one-electron oxidizing agents because the complex exhibits an overall square planar coordination geometry.[17b] Since the C-C (Table 6.4) and M-C (Table 5.7) bond distances determined for $[(\eta^4$-COT)$_2$Co][K(2,2,2-crypt)] are very similar to those determined for **12-COT** and **13-COT**,[17b] it is believed the electronic structure of $[(\eta^4$-COT)$_2$Co][K(2,2,2-crypt)] is likely best described as having a Co(I) center supported by two COT radical anions, rather than its formal Co(I-) designation.

In addition to its potential impact on fundamental electronic structure investigations, the research described herein may also hold implications for the mechanistic study of *N*-

heterocyclic carbene promoted COT ligand coupling reactions.[28] In a recent report by Grubbs and co-workers, it was found that the addition of *N*-heterocyclic carbene to two equivalents of $Fe(COT)_2$ allowed for the isolation of $(\eta^4\text{-COT})Fe(\mu\text{-}\eta^5,\eta^5\text{-COT})Fe(R)$ [R = 2,4-(*N,N*)-bis(2,6-diisopropylphenyl-3,5-diphenylimidazole], which further undergoes radical coupling of two η^4-COT ligands.[11f] Although a full electronic structure investigation of this complex with complimentary Mössbauer and EPR spectroscopic data has not been conducted, the solid state structure of $(\eta^4\text{-COT})Fe(\mu\text{-}\eta^5,\eta^5\text{-COT})Fe(R)$ has been reported to feature C(2)-C(3), Fe-C(2), and Fe-C(3) bond distances of 1.400(3), 1.985(2), and 2.025(3) Å, respectively, along with Fe-C(1) and Fe-C(4) distances of 2.177(2) and 2.165(3) Å, respectively (Table 5.7).[11f] Although the C(1)-C(2) and C(3)-C(4) distances of 1.447(3) and 1.400(4) Å appear to be somewhat unusual, the other COT and Fe-C distances suggest that this complex may feature an η^4-COT radical monoanion, rather than a neutral η^4-COT ligand.[11f] While it is impossible to tell which electronic structure assignment is correct without further spectroscopic study, it appears inappropriate to assume that this complex possesses a neutral η^4-COT ligand solely because it exhibits a "localized butadiene" structure within the unbound COT carbon atoms.

In moving beyond the first transition series examples shown in Table 5.7, it is clear that structurally characterized second row complexes featuring an η^4-COT ligand tend to have M-C(2) and M-C(3) distances that are much closer to their M-C(1) and M-C(4) counterparts. As recently discussed in the investigation of redox-active ligand supported Rh(I)[29] and Mo(0)[30] complexes, it is believed that each of the second row complexes in Table 5.7 likely feature electronic structures that are consistent with different degrees of

π-backbonding into the η^4-COT ligand rather than having a COT radical anion, since second row metals have d-orbitals that more efficiently overlap with ligand-based π-orbitals than their first row congeners.[30] This characteristic renders it unlikely that population of the COT π*-orbital[9] will be achieved, as the resulting π*-M(4d/5d) antibonding orbital would be highly destabilized relative to the filled orbital associated with π*-M(4d/5d) bonding.[31]

5.7. Carbonyl complexes of TriphosFe complexes and their reactivity:

5.7.1. CO addition to the halide complexes:

Knowing the diverse catalysis driven by PNP-supported iron complexes[5] and the importance of carbonyl hydride complexes in industrially valuable catalytic applications,[7j,13] preparations of well-defined (Triphos)Fe catalysts have been sought. To previously synthesized **12-Br₂**, one atmosphere of CO was added in acetone, which afforded a single diamagnetic complex identified as (Triphos)FeBr₂(CO) (**12-Br₂(CO)**, Scheme 5.6) as observed by multinuclear NMR spectroscopy.
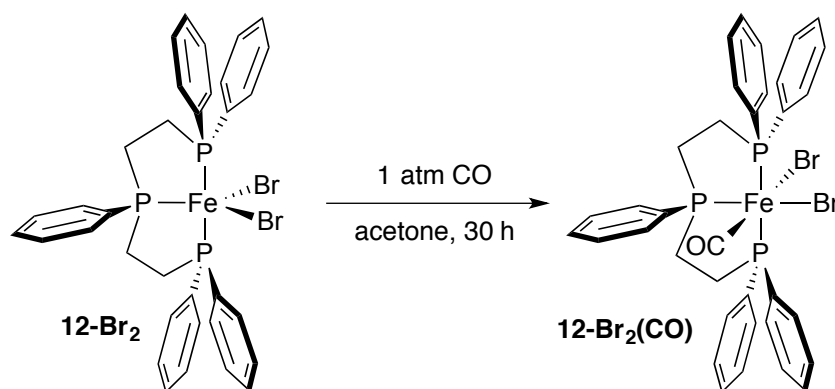
Scheme 5.6. Synthesis of **1-Br₂(CO)**.
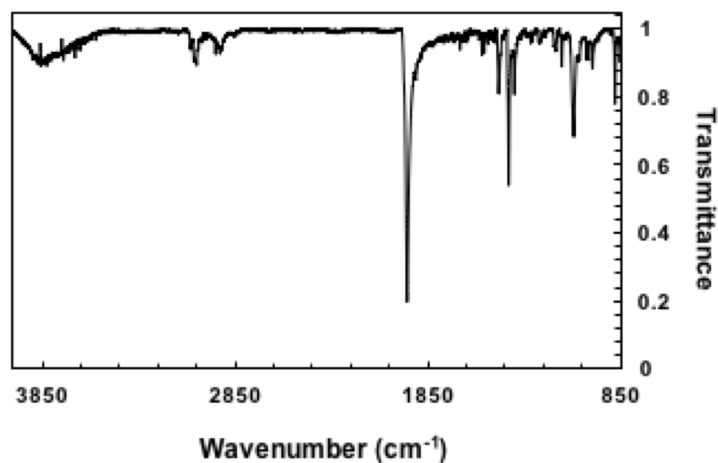
Figure 5.13. IR spectrum of **12-Br₂(CO)** in benzene-d_6.

The ^{31}P NMR spectrum of this complex was found to feature two resonances at 134.75(t) and 56.66(d) ppm, consistent with a terdentate and C_s-symmetric Triphos ligand. Furthermore, the ^{13}C NMR spectrum of **12-Br₂(CO)** was found to possess a multiplet at 219.76 ppm and infrared spectroscopy revealed a single CO stretch at 1957 cm^{-1} (Figure 5.13), further confirming the presence of one CO ligand.
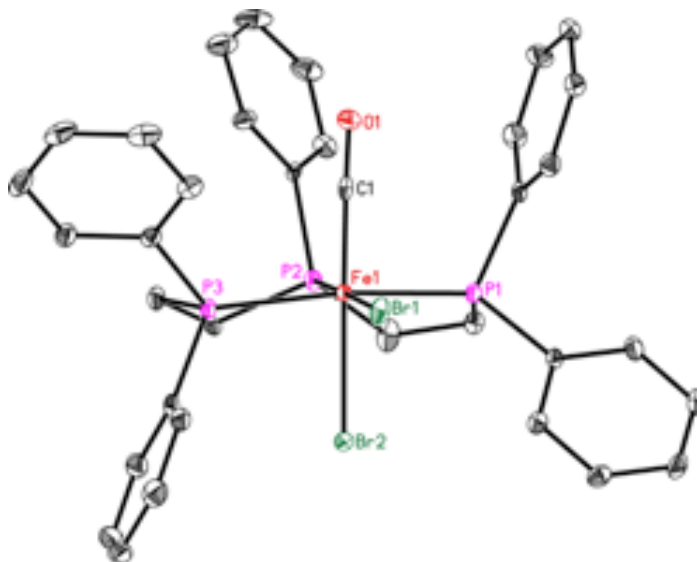
Figure 5.14. Solid state structure of **12-Br₂(CO)** shown at 30% probability ellipsoids. Hydrogen atoms and co-crystallized acetone molecule are omitted for clarity.

Table 5.8. Notable bond lengths (Å) and angles (°) determined for **12-Br$_2$(CO)**.

Fe(1)-P(1)	2.1903(4)	P(1)-Fe(1)-P(2)	84.929(14)
Fe(1)-P(1)	2.1758(4)	P(1)-Fe(1)-P(2)	98.432(15)
Fe(1)-P(1)	2.1913(4)	P(1)-Fe(1)-P(2)	86.625(15)
Fe(1)-P(1)	2.1978(14)	P(1)-Fe(1)-P(2)	171.60(4)
Fe(1)-P(1)	2.0302(14)	P(1)-Fe(1)-P(2)	132.52(4)
Fe(1)-P(1)	2.0330(14)	P(1)-Fe(1)-P(2)	99.96(4)
Fe(1)-P(1)	2.2170(14)		

The flexible coordination mode (*fac/mer*) of Triphos in an octahedral environment[7g] and the recent evidence of heat and light driven isomerization of (Triphos)FeCl$_2$(CO) described by Dzik and coworkers,[7m] demanded a detailed structural investigation of **12-Br$_2$(CO)**. Crystallization from a concentrated acetone solution at ambient temperature followed by X-ray diffraction analysis revealed a pseudo-octahedral geometry about Fe center with a *mer*-Triphos chelate and *cis*-bromide ligands (Figure 5.14). The bond distances determined for **12-Br$_2$(CO)** (Table 5.8) are largely consistent with those found for (Triphos)FeCl$_2$(CO); however, the Fe-P contacts of 2.2522(10), 2.1906(10), and 2.2697(10) Å are slightly longer than those of (Triphos)FeCl$_2$(CO) (2.2422(9), 2.1852(10), and 2.2547(9) Å).[7m] These minor differences can be attributed to enhanced π-donation from the bromide ligands to Fe(II) relative to that observed for chloride ligands. It should also be noted that the P(1)-Fe(1)-P(3) angle of 168.05(4)° determined for **12-Br$_2$(CO)** is slightly smaller than the angle of 169.17(4)° reported for (Triphos)FeCl$_2$(CO).

5.7.2. Reduction chemistry of carbonyl bromide complexes:

With **12-Br$_2$(CO)** in hand, its reduction in the presence of excess Na/Hg was attempted. After 18 h at 25 °C in THF, (Triphos)Fe(CO)$_2$ (**12-(CO)$_2$**, Scheme 5.7) was

observed by multinuclear NMR and IR spectroscopy along with an unidentified product mixture. Although early attempts to prepare this complex via Triphos substitution onto $Fe_2(CO)_9$ or $(COT)Fe(CO)_3$ did not allow for κ^3-Triphos coordination,[32a] **12-(CO)₂** has recently been prepared following the Na/Hg reduction of **12-Br₂** under 1 atm of CO.[32b] **12-(CO)₂** features two ^{31}P NMR resonances at 134.11 (t) and 96.43 (d) ppm and two sharp IR peaks at 1929 and 1873 cm^{-1} due to CO stretching. Interestingly, prolonged reduction resulted in a 1:1 mixture of **12-(CO)₂** and a new iron complex along with other unidentified products. The new complex displays two resonances at 131.16 and 101.70 ppm.

The ^{31}P NMR spectrum revealed a well-defined doublet of triplets at -10.8 ppm (J = 55.4 Hz, 6.9 Hz) in the ^1H NMR spectrum (Figure 5.15). The IR spectrum of this new species showed a broad signal at 1895 cm^{-1}. These evidences suggest it to be a carbonyl containing dihydride complex **12-(H)₂(CO)** (Scheme 5.7). Independent preparation of this complex was targeted by adding two equivalents of $NaEt_3BH$ to a cooled toluene slurry of **12-Br₂(CO)**. After 3 h stirring at room temperature a bright orange solid was isolated following workup and spectroscopic characterization of this product revealed a mixture of **12-(CO)₂** and **12-(H)₂(CO)**. Attempts to crystallize this dihydride were unsuccessful as it decomposes in solution within hours to form **12-(CO)₂**. Notably, an isostructural complex, $(Triphos^*)Fe(H)_2(CO)$ was reported by Guilera *et al.*,[7j] where rapid exchange of two hydrides was found to contribute to the fluxionality of the complex at ambient temperature in solution.
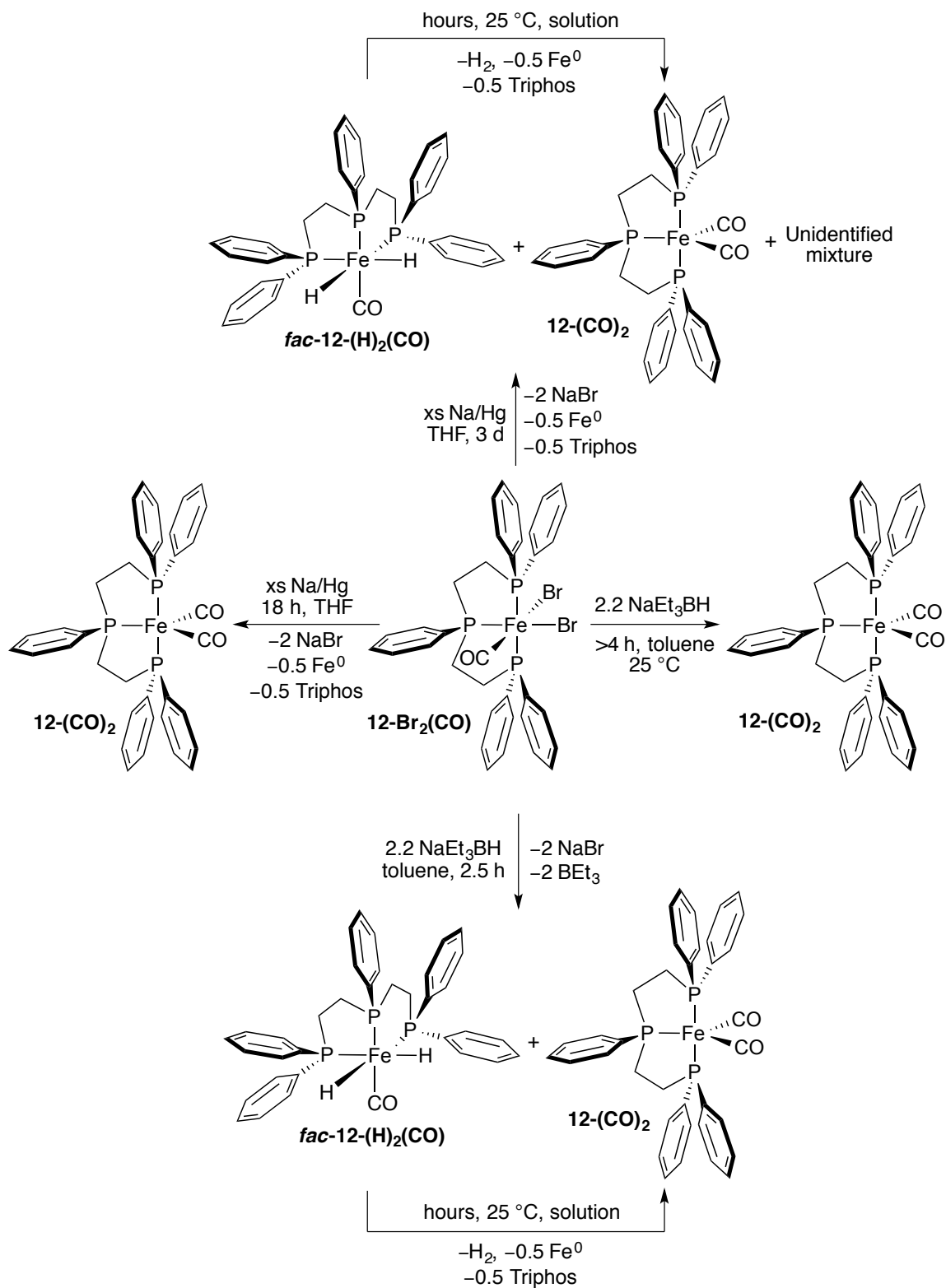
Scheme 5.7. Reduction of **12-Br₂(CO)** under different conditions.
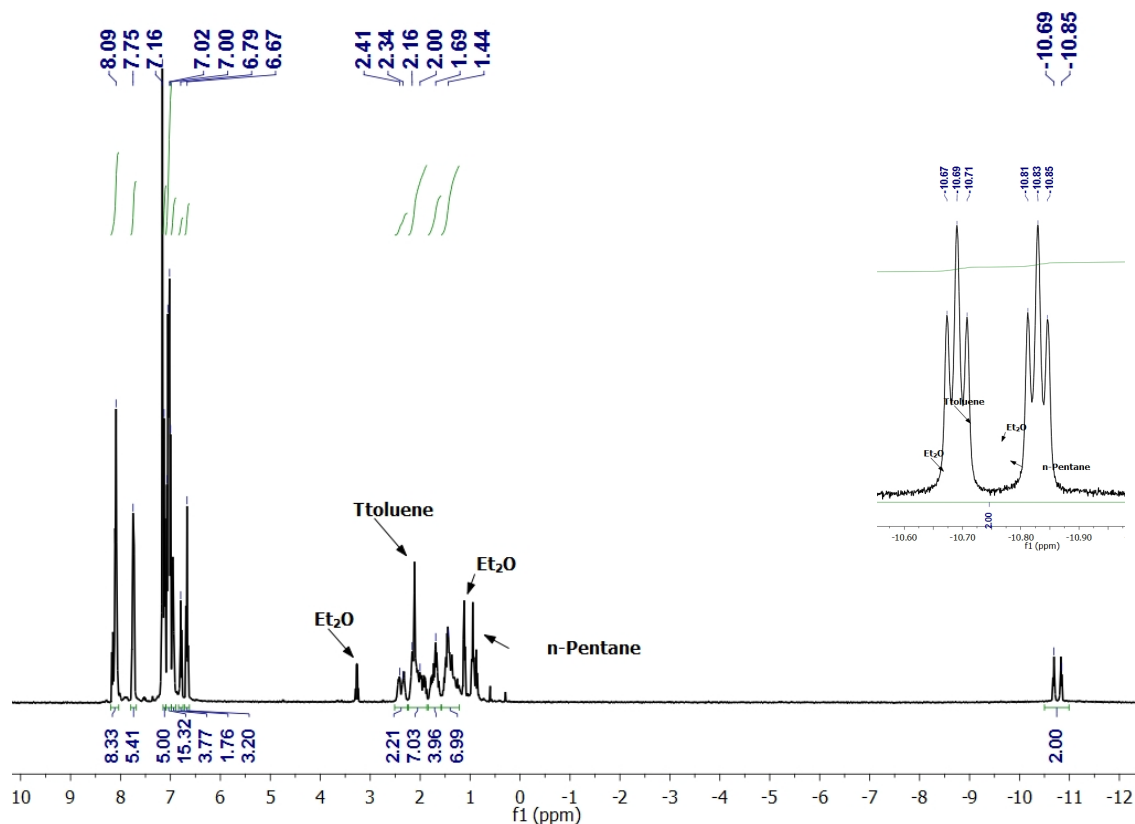
Figure 5.15. ^{1}H NMR of putative **12-(H)₂(CO)** in benzene-d_6. In the inset, a magnified view of the hydride resonance is shown.

Moreover, accounting for the flexibility of Triphos ligand,[7m] it is believed that this putative intermediate is very likely to be (Triphos)Fe(H₂)(CO) **(12-(H)₂(CO))**, with a *fac*-Triphos chelate (Scheme 5.7) and the chemical equivalence of the two hydrides are presumably due to fast exchange at room temperature. It is believed that this dihydride may be a result of C-H bond activation of THF followed by β-H elimination. Conducting the reduction in diethylether did not facilitate the reaction even after 5 days.

Knowing the instability of the "putative dihydride" complex, the amount of NaEt₃BH was reduced in order to isolate a stable monohydride complex analogous to the PNPFe monohydride complexes.[5a,d] The slow addition of stoichiometric NaEt₃BH to a

cold toluene solution of **12-Br$_2$(CO)** afforded an amber solid following workup and crystallization.
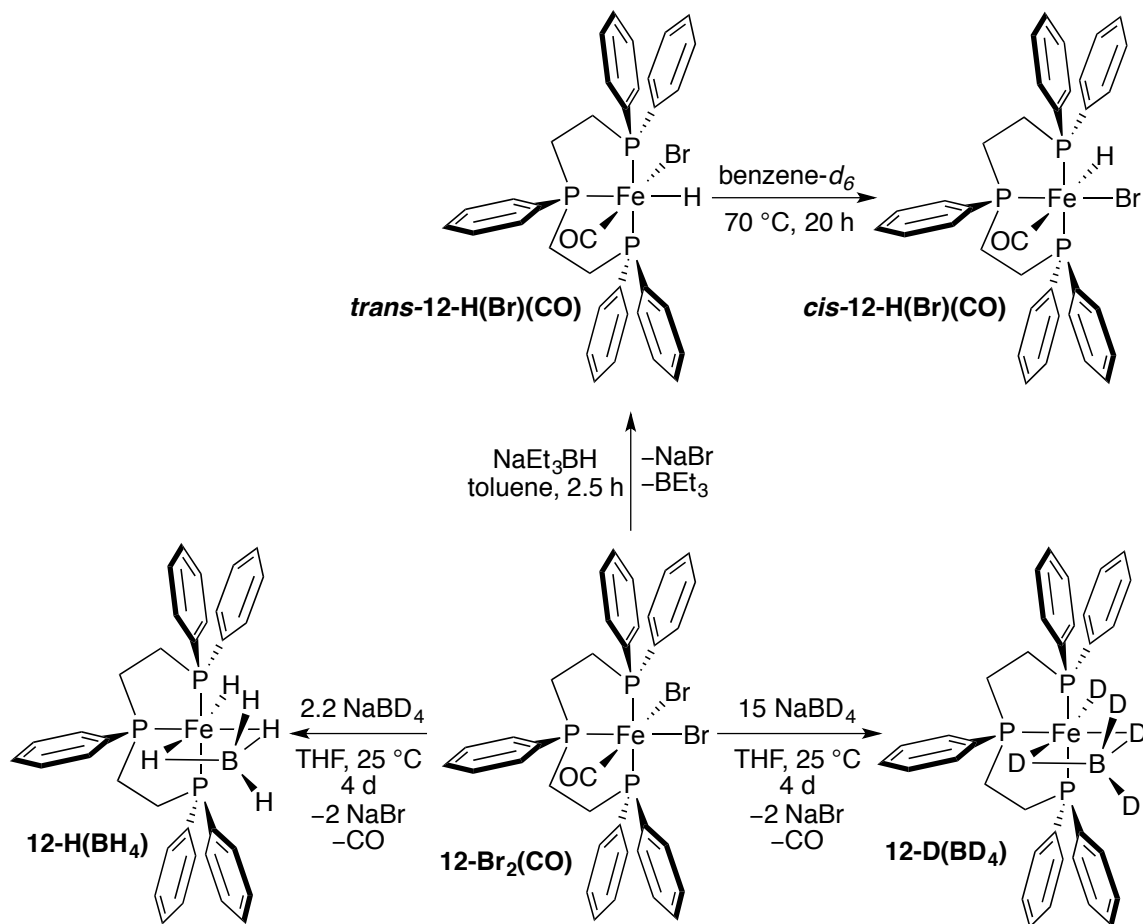
Scheme 5.8. Synthesis of **12-H(Br)(CO)** and **12-H(BH$_4$)**.

Analysis by ^{1}H NMR spectroscopy revealed an overlapping doublet of triplets centered at -7.06 ppm (J = 52.4 Hz, 63.0 Hz, Figure 5.15.).The doublet of triplets collapses to a singlet upon ^{31}P decoupling. The ^{31}P NMR spectrum exhibited resonances at 138.55 (t) and 82.31 (d) ppm. Infrared spectroscopy revealed a single stretch at 1950 cm^{-1}, indicating the formation of **12-H(Br)(CO)** (Scheme 5.8). Heating a benzene-d_6 solution of this product produced a new hydride resonance at -22.59 (dt, J = 44.7 Hz, 49.78 Hz). Although there is lack of X-ray diffraction data, the larger coupling constants

of the hydride signal at -7.06 ppm suggests it to be the *trans*-isomer, which upon heating

partially transforms to *cis*-isomer with smaller coupling constants.
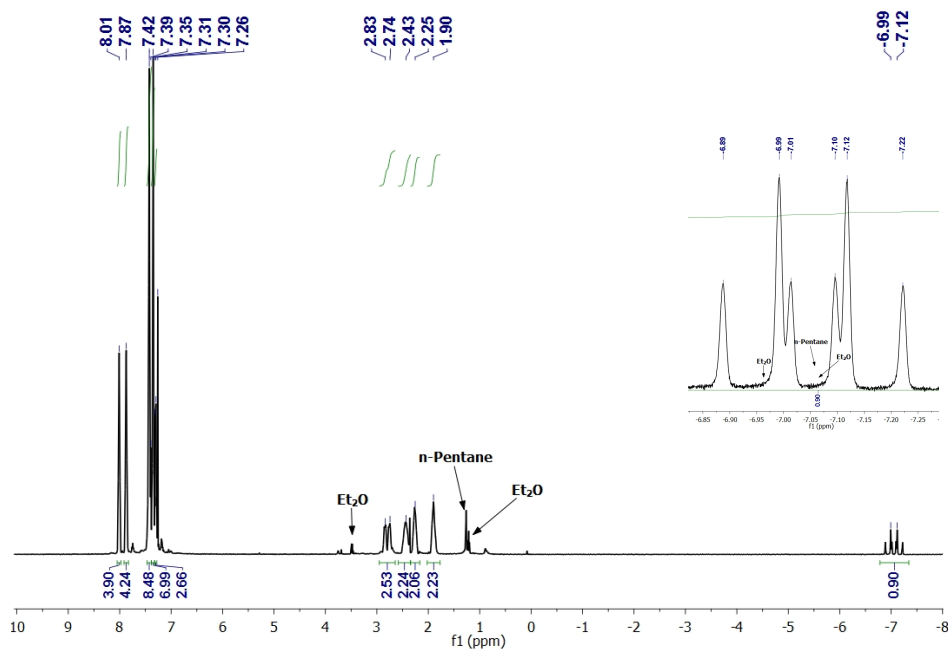
Figure 5.16. ^{1}H NMR of ***trans*-12-H(Br)(CO)** in chloroform-*d*. In the inset, a magnified
view of the hydride resonance is shown.
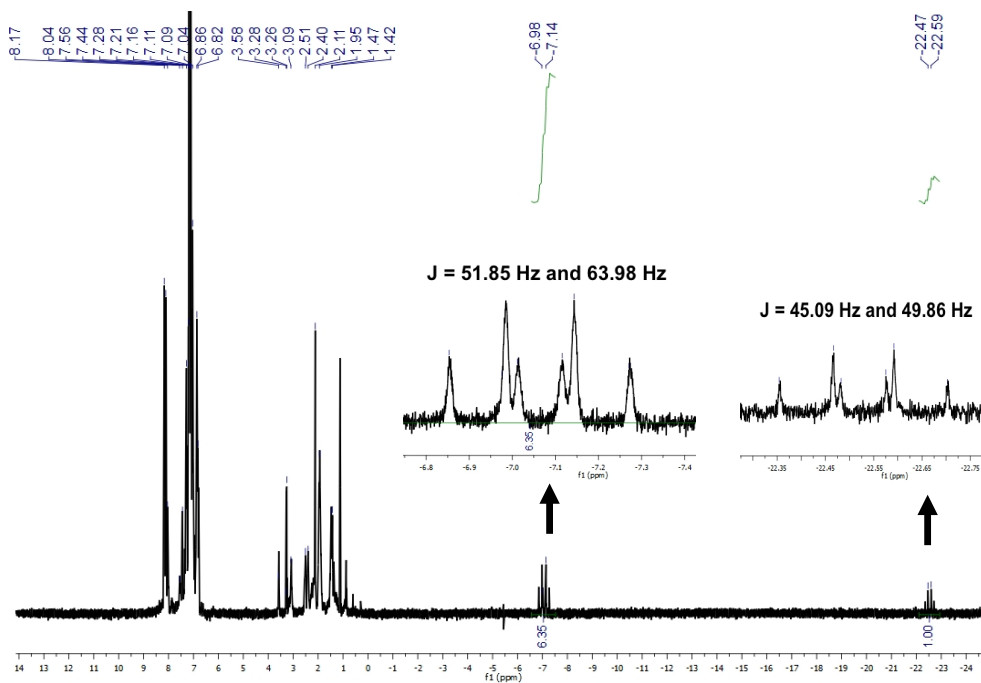
Figure 5.17. ^{1}H NMR spectrum of the mixture of ***cis*-** and ***trans*-12-H(Br)(CO)**.

Although the reaction outcomes in Scheme 5.7 suggest that dicarbonyl complex formation is favored following bromide ligand removal, efforts were made to prepare a persistent (Triphos)Fe hydride complex following NaBH$_4$ addition (Scheme 5.8). Fortunately, adding 2.2 eq. of NaBH$_4$ to **12-Br$_2$(CO)** rather than NaEt$_3$BH did not yield **12-(CO)$_2$**, rather a new diamagnetic complex featuring ^{31}P NMR resonances at 145.08 and 89.87 ppm (Scheme 5.8). The ^{1}H NMR spectrum of this product was found to possess an upfield-shifted pseudo quartet at -23.95 ppm along with two broad resonances at - 12.80 and -14.01 ppm (Figure 5.18, top). The pseudo quartet collapsed to a singlet upon ^{31}P-decoupling, indicating the presence of an Fe-H moiety. Since a broad resonance at 5.84 ppm that integrates to two hydrogen atoms was also observed, and no CO-derived stretches were detected by IR spectroscopy, this product was formulated to be (Triphos)FeH(η^2-BH$_4$) (**12-H(BH$_4$)**, Scheme 5.8). Preparation of **12-D(BD$_4$)** upon excess NaBD$_4$ addition to **12-Br$_2$(CO)** confirmed that the broad ^{1}H NMR resonances at -12.80 and -14.01 ppm are due to inequivalent borohydride(deuteride) positions that are bound to iron, while the resonance at 5.84 ppm corresponds to two equivalent and uncoordinated borohydride(deuteride) environments.
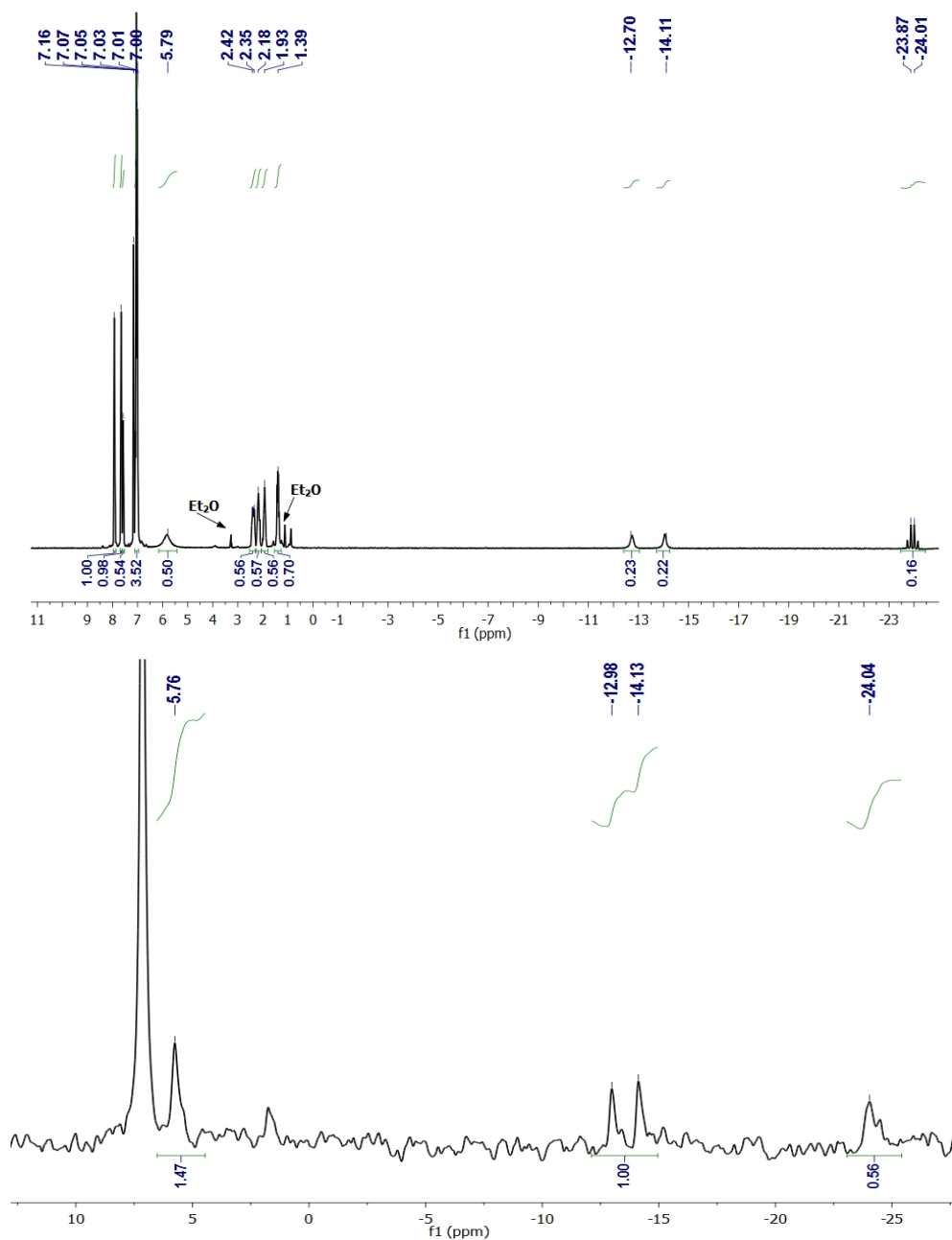
Figure 5.18. ^{1}H NMR (top) and ^{2}H NMR (bottom) of **12-H(BH$_4$)** in benzene-d_6 or benzene.

To confirm the borohydride coordination mode suggested in Scheme 5.8, single crystal X-ray diffraction data was collected. The solid state structure of **1-H(BH$_4$)** (Figure 5.19) reveals an η^2-BH$_4$ ligand that occupies coordination sites *cis* and *trans* to the located hydride, H1M. The Triphos chelate adopts a distorted *meridional* configuration with a

P(1)-Fe(1)-P(3) angle of 154.13(4)° and additional metrical parameters are provided in Table 5.9.
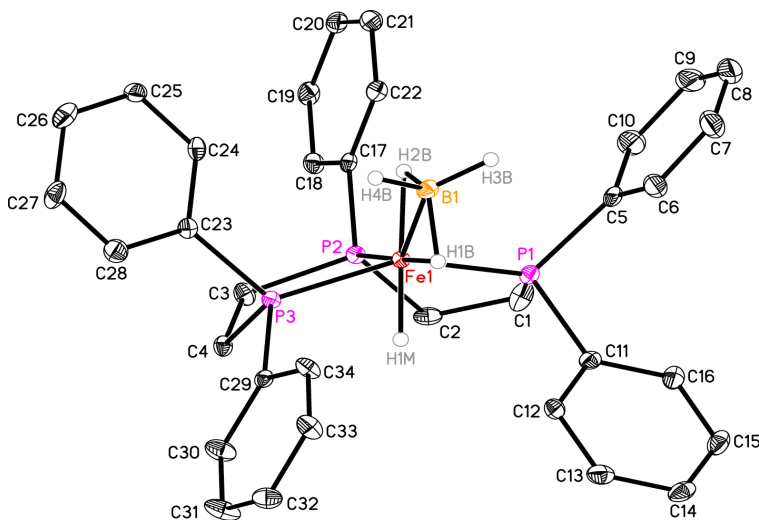
Figure 5.19. Solid state structure of **12-H(BH₄)** shown at 30% probability ellipsoids. Hydrogen atoms are omitted for clarity.

Table 5.9. Notable bond lengths (Å) and angles (°) determined for **12-H(BH₄)**.

Fe(1)-P(1)	2.1745(10)	B(1)-H(3B)	1.12(3)
Fe(1)-P(1)	2.1286(10)	B(1)-H(4B)	1.15(4)
Fe(1)-P(1)	2.1829(10)	P(1)-Fe(1)-P(2)	86.47(4)
Fe(1)-H(1M)	1.37(3)	P(2)-Fe(1)-P(3)	86.80(4)
Fe(1)-H(1B)	1.59(3)	P(1)-Fe(1)-P(3)	154.13(4)
Fe(1)-H(2B)	1.59(3)	P(2)-Fe(1)-H(1B)	177.9(12)
Fe(1)-B(1)	2.106(4)	P(2)-Fe(1)-P(2B)	108.2(12)
B(1)-H(1B)	1.24(3)	P(2)-Fe(1)-P(1M)	80.8(13)
B(1)-H(2B)	1.22(3)		

Considering the bound borohydride H-atoms, the geometry about the Fe center of **12-H(BH₄)** is distorted octahedral with P(2)-Fe(1)-H(1B) and P(2)-Fe(1)-H(2B) angles of 177.9(12) and 108.2(12) °, respectively. With an Fe(1)-B(1) distance of 2.106(4) Å (these atoms are within covalent bonding distance considering radii of 0.84 Å for B and 1.32 Å

for low-spin Fe), B-H σ-bond character is clearly being donated to the metal center. This is further demonstrated by the Fe-coordinated B-H bond distances of 1.24(3) and 1.22(3) Å relative to the unbound B-H distances of 1.12(3) and 1.15(4) Å. The BH_4 ligand can therefore be counted as an anionic 4-electron donor which helps to stabilize 18-electron **12-H(BH₄)**. It should be noted that **12-H(BH₄)** cannot easily undergo reductive elimination, the reason for its persistence in solution.

It is intriguing that B-H σ-bond donation is strong enough to allow for the isolation of low-spin **12-H(BH₄)** and that η^2-BH_4 coordination is responsible for CO dissociation. To further probe these issues, we attempted to synthesize **12-H(BH₄)** by adding 2.2 eq. $NaBH_4$ to **12-Br₂**. Surprisingly, this reaction did not afford **12-H(BH₄)**, suggesting that **12-H(BH₄)** is formed following salt metathesis between $NaBH_4$ and **12-H(Br)(CO)**. This observation also suggests that $NaBH_4$ addition to **12-Br₂** does not generate a monohydride intermediate that is sufficiently long-lived to yield **1-H(BH₄)**.

5.8. Concluding remarks:

In summary, a thorough electronic structure investigation on **12-Bpy** has been presented, which revealed redox non-innocence of Bpy ligand. Also, the first isolated and well-characterized organometallic complexes featuring an η⁴-COT radical monoanion ligand have been presented. Although DFT calculations were unable to predict a broken symmetry solution for **12-COT**, Mössbauer and EPR spectroscopic investigations, in combination with single crystal X-ray diffraction studies offered experimental support for this electronic structure designation. It is believed that the solid-state metrical parameters reported herein for both **12-COT** and **13-COT** provide a model for assessing the

electronic structure of other first row transition metal complexes that possess an η^4-COT ligand, and perhaps any first row complex that contains an η^4-diene ligand. In turn, revealing the fundamental electronic properties of these complexes may lead researchers to develop an advanced understanding of their reactivity. Furthermore, by incorporating CO into the (Triphos)Fe system and following reaction with hydride reagents, a series of catalytically relevant Fe-H complexes have been synthesized and rigorously characterized. The reactivity described herein[33] may prove valuable for future studies, which seek to develop thermally stable iron precatalysts for organic transformations. Researchers have had recent success in utilizing analogous isostructural (PNP)Fe precatalysts for *E*-selective semi-hydrogenation of alkynes,[5c] the reversible hydrogenation of ketones,[5p] the hydrogenation of CO_2 to formic acid,[5o] base-free hydrogenation of ketones,[5b] and the selective dehydrogenation of methanol.[5d] It is hoped that this study[33] will allow similar applications to be developed for iron complexes bearing PPP pincer scaffolds including Triphos.

5.9. Experimental Procedure

General Considerations: Unless otherwise stated, all synthetic reactions were performed in an MBraun or Vacuum Atmospheres glovebox under an atmosphere of purified nitrogen or argon. Aldrich or Acros anhydrous solvents were either sparged with argon or dried using a Pure Process Technology solvent purification system before being stored in the glovebox over activated 4Å molecular sieves (Fischer Scientific) and sodium (Alfa Aesar) before use. Benzene-d_6, chloroform-*d*, tetrahydrofuran-d_8, and sodium borodeuteride were purchased from Cambridge Isotope Laboratories and dried over 4Å

molecular sieves prior to use. Bis(cyclooctatetraene) iron(0), bis(2-diphenylphosphinoethyl)phenylphosphine (Triphos), and 1,1,1-Tris(diphenylphosphinomethyl)ethane (Triphos*), 2,2-bipyridine, and 1,3,5,7-cyclooctatetraene were purchased from Strem Chemicals while iron(II) dibromide was purchased from Acros. All of the gases used in this study were obtained from either Airgas or Praxair. Sodium borohydride, sodium triethylborohydride, and CO were purchased from Sigma-Aldrich.

Solution ^{1}H nuclear magnetic resonance (NMR) spectra were recorded at room temperature on either a Bruker AVANCE 400 MHz or Varian MR400 spectrometer. All ^{1}H and ^{13}C NMR chemical shifts are reported relative to SiMe$_4$ using ^{1}H (residual) and ^{13}C chemical shifts of the solvent as secondary standards. ^{31}P NMR data is reported relative to H$_3$PO$_4$. Elemental analyses were performed at either Robertson Microlit Laboratories Inc. (Ledgewood, NJ) or on a PerkinElmer 2400 Series elemental analyzer at the Goldwater Environmental Laboratory (Arizona State University). Solid state magnetic susceptibilities were determined at 23 ˚C using a Johnson Matthey magnetic susceptibility balance calibrated with HgCo(SCN)$_4$ and K$_3$Fe(CN)$_6$.

Single crystals suitable for X-ray diffraction were coated with polyisobutylene oil in a drybox and transferred to a nylon loop which was then mounted on the goniometer head of a Bruker APEX (University of Arizona) or APEX II (Los Alamos National Laboratory) diffractometer equipped with Mo K$_\alpha$ radiation. A hemisphere routine was used for data collection and determination of the lattice constants. The space group was identified and the data were processed using the Bruker SAINT+ program and corrected for absorption using SADABS. The structures were solved using direct methods

(SHELXS), completed by subsequent Fourier synthesis, and refined by full-matrix, least-squares procedures on $|F|^2$ (SHELXL).

Electron Paramagnetic Resonance Spectroscopy: *Instrumentation*. Data collection and analysis were performed at the EPR Facility of Arizona State University. Continuous wave EPR spectra were recorded at 70 K using a Bruker ELEXSYS E580 continuous wave X-band spectrometer (Bruker, Silberstreifen, Germany) equipped with an Oxford Model ESR900 liquid helium cryostat (Oxford Instruments, Oxfordshire, UK). The magnetic field modulation frequency was 100 kHz with a field modulation of 0.5 mT peak-to-peak. The microwave power was 4 mW, the microwave frequency was 9.45 GHz and the sweep time was 84 seconds.

Spin Hamiltonian. The EPR spectrum of two $S = 1/2$ spins coupled by isotropic and anisotropic interactions has been extensively discussed. So, we refer the reader to the main textbooks and reviews for a more comprehensive background.[34] The EPR spectrum of **12-COT** was analyzed considering that the molecule contains two $S = 1/2$ spins. One corresponding to the unpaired electron from the low-spin Fe(I) (denoted by $\mathbf{S_A}$) and the other belongs to the unpaired electron at the COT radical (denoted by $\mathbf{S_B}$). They interact with an external magnetic field (Zeeman interaction) and with each other, through exchange and dipole-dipole interactions. The spin Hamiltonian, $\mathcal{H}$, of this system is:

$$\mathcal{H} = \beta_e \mathbf{S_A} \cdot \boldsymbol{g_A} \cdot \mathbf{B_o} + \beta_e \mathbf{S_B} \cdot \boldsymbol{g_B} \cdot \mathbf{B_o} + hJ_o \mathbf{S_A} \cdot \mathbf{S_B} + h\mathbf{S_A} \cdot \boldsymbol{J} \cdot \mathbf{S_B}$$

(1)

Where $\boldsymbol{g_A}$ and $\boldsymbol{g_B}$ are the g-tensors of $\mathbf{S_A}$ and $\mathbf{S_B}$, respectively, and β_e is the Bohr magneton. The first two terms are the Zeeman interactions with the applied magnetic field $\mathbf{B_o}$. The

third and fourth terms are, respectively, the isotropic (Heisenberg) exchange and the dipole-dipole interactions that couple S_A with S_B.

Fitting of EPR spectra. To quantitatively compare experimental and simulated spectra, we divided the spectra into N intervals, i.e. we treated the spectrum as an N-dimensional vector **R**. Each component R_j has the amplitude of the EPR signal at a magnetic field B_j, with j varying from 1 to N. The amplitudes of the experimental and simulated spectra were normalized so that the span between the maximum and minimum values of R_j is 1. We compared the calculated amplitudes R_j^{calc} of the signal with the observed values R_j defining a root-mean-square deviation σ by:

$$\sigma(p_1, p_2, \ldots, p_n) = [\sum_j (R_j^{calc}(p_1, p_2, \ldots, p_n) - R_j^{exp})^2/N]^{\frac{1}{2}} \qquad (2)$$

where the sums are over the N values of j, and p's are the fitting parameters that produced the calculated spectrum. For our simulations, N was set equal to 1024.

The EPR spectra were simulated using EasySpin (v 4.5.0), a computational package developed by Stoll and Schweiger[34d] and based on Matlab (The MathWorks, Natick, MA, USA). EasySpin calculates EPR resonance fields using the energies of the states of the spin system obtained by direct diagonalization of the spin Hamiltonian (see Eq. 1). The EPR fitting procedure used a Monte Carlo type iteration to minimize the root-mean-square deviation, σ (see Eq. 2) between measured and simulated spectra. We searched for the optimum values of the following parameters: the principal components of g_A and g_B (i.e. g_{xA}, g_{yA}, g_{zA} and g_{xB}, g_{yB}, g_{zB}), the isotropic exchange J_o, the principal components of the dipole-dipole interaction tensor J (i.e. $J_{x'}$, $J_{y'}$, $J_{z'}$) and the peak-to-peak line-widths (ΔB_x, ΔB_y, and ΔB_z).

203

Mössbauer Studies: The presence of Fe in these materials strongly suggests using the Mössbauer Effect (ME) of ^{57}Fe to ascertain detailed properties of the Fe constituents. A ME spectrometer operated in the constant acceleration mode was combined with a liquid helium cryostat, and conventional data analysis programs for ^{57}Fe ME spectra were used. A ^{57}Co in Rh source provided the 14.4 KeV recoil-free ME γ-rays. The samples were contained in an O-ring sealed Lucite holder under an Ar atmosphere. The source and absorber were held at the same temperature for data taken over the range 1.5 to 300 K. Only data and results at 76 K are reported here showing one or two Fe sites and their isomer shifts (IS) and quadrupole splittings (ΔE_Q). The IS is related to the electronic state of the Fe, and the ΔE_Q to its environment. Of particular interest in these studies is the magnetic state of the Fe. No spontaneous ordering was observed at any temperature down to 1.5 K. Furthermore, no sample showed any hyperfine relaxation response; the Fe in the reported samples is non-magnetic. The isomer shift data exclude most usual Fe valences and spin values but do not provide an unambiguous assignment of the Fe state from ME data alone.

Electronic Structure Calculations: Density functional theory (DFT) calculations were carried out with the Gaussian 09 software (revision B.01)[35] and the ORCA software.[36] Geometry optimization calculations were carried out for the complexes using the crystal structures as starting points with the phenyl groups replaced by hydrogens to reduce the computational expense. The PBE exchange correlation functional (PBE exchange and PBE correlation)[37] was used for all calculations using a LANL2DZ basis set (5s5p3d+f) for Fe[38] with a 6-31G* basis set for all other elements using the spin-unrestricted molecular orbital approach. The LANL2DZ effective core potential was used for Fe.

Wavefunction stability tests were employed to ensure that the calculated wavefunction corresponds to the true electronic ground state. Time-dependent density functional theory calculations were also calculated with the Gaussian 09 software to search for low energy singlet excited states. Atomic spin densities and charges were evaluated using a Mulliken population analysis. Several calculations were repeated using the B3LYP functional[39] to ensure that the same general trends in the results were not dependent on the functional used. The ORCA software[36] was used to determine Mayer bond orders and to calculate the Moessbauer parameters for the complexes.[27]

Preparation of [(Ph₂PCH₂CH₂)₂PPh]FeBr₂ (12-Br₂): In the glove box, a 250 mL round-bottomed flask was charged with 0.250 g Triphos (0.468 mmol), 0.101 g (0.468 mmol) of FeBr₂, and approximately 75 mL of tetrahydrofuran. The resulting yellow solution was set to stir at an ambient temperature. After 17 hours, the reaction mixture was filtered through Celite and the filtrate was concentrated to yield a dark orange film. This material was scraped from the sides of the filter flask in the presence of approximately 5 mL of pentane and dried *in vacuo*. After repeating this process 2 additional times (to ensure removal of residual tetrahydrofuran), 0.327 g of a dark orange microcrystalline solid identified as **[κ^3-(Ph₂PCH₂CH₂)₂PPh]FeBr₂** was collected (93% yield). Analysis for $C_{34}H_{33}Br_2FeP_3$: Calcd. C, 54.41%; H, 4.40%. Found: C, 54.19%; H, 4.33%. Magnetic Susceptibility (Guoy Balance): μ_{eff}= 4.8 μ_B. ^{1}H NMR (tetrahydrofuran-d_8): δ (ppm) = 98.38 (2959.1 Hz, 2H, C*H₂*), 43.10 (1511.7 Hz, 2H, C*H₂*), 34.24 (1527.8 Hz, 2H, C*H₂*), 26.2 (855.48 Hz, 2H, C*H₂*), 16.3 (105.95 Hz, 4H, Ar-*H*), 11.74-11.20 (m, 16H, Ar-*H*), 9.94 (46.41 Hz, 1H, Ar-*H*), 3.07 (71.64 Hz, 2H, Ar-*H*), 2.44 (55.28 Hz, 2H, Ar-*H*).

Preparation of [(Ph₂PCH₂CH₂)₂PPh]FeCl₃ (12-Cl₃): In the glove box, a 250 mL round-bottomed flask was charged with 0.141 g (0.869 mmol) of $FeCl_3$ and approximately 50 mL of tetrahydrofuran resulting in the formation of yellow solution. A second solution containing 0.465 g Triphos (0.870 mmol) in approximately 15 mL of tetrahydrofuran was prepared and added drop-wise to the iron trichloride solution while stirring. The reaction mixture darkened from yellow to reddish-orange in color until the halfway point of addition, at which point it began to turn green in color. Upon stirring at ambient temperature for 90 min, the resulting emerald green solution was filtered through Celite and the solvent was evacuated. The resulting solid was washed twice with about 10 mL of diethylether and then twice with 10 mL of pentane to remove any residual Triphos or tetrahydrofuran. After drying under vacuum, 0.586 g (0.843 mmol, 97% yield) of a dark green solid identified as **[(Ph₂PCH₂CH₂)₂PPh]FeCl₃** was collected. Analysis for $C_{34}H_{33}Cl_3FeP_3$: Calcd. C, 58.59%; H, 4.74%. Found: C, 58.38%; H, 4.88%. Magnetic Susceptibility (Guoy Balance): μ_{eff} = 4.3 μ_B. ^{1}H NMR (tetrahydrofuran-d_8): δ (ppm) = 13.22 − 4.65 (m, Ar-H), -19.34 (615.72 Hz, 2H, CH_2), -24.32 (725.55 Hz, 2H, CH_2), -46.02 (1918.85 Hz, 2H, CH_2), -49.62 (2529.81 Hz, 2H, CH_2).

Preparation of [(Ph₂PCH₂CH₂)₂PPh]FeBr₃ (12-Br₃): In the glove box, a 250 mL round-bottomed flask was charged with 0.425 g of Triphos (0.796 mmol), 0.235 g (0.795 mmol) of $FeBr_3$ and approximately 100 mL of tetrahydrofuran. The resulting yellow solution was set to stir at ambient temperature. After 1 h, the reaction had turned dark red-orange in color. After 20 hours, the resulting bright orange solution was filtered through Celite and the solvent was evacuated to yield a yellow film. The material was scraped from the sides of the filter flask in the presence of approximately 5 mL of

pentane and then dried *in vacuo* to yield 0.571 g (0.688 mmol, 86% yield) of an olive green microcrystalline solid identified as **[(Ph₂PCH₂CH₂)₂PPh]FeBr₃**. Magnetic Susceptibility (Guoy Balance): μ_{eff} = 5.6 μ_B. ¹H NMR (tetrahydrofuran-d_8): δ (ppm) = 27.51 ppm (772.8 Hz), 9.84 (m), 6.55 (m), several resonances not located. ³¹P NMR (tetrahydrofuran-d_8): δ (ppm) = -22.10 (449.9 Hz).

Preparation of [κ³-(Ph₂PCH₂CH₂)₂PPh]Fe[κ²-(Ph₂PCH₂CH₂)₂PPh] [12-(κ²-Triphos)]: In the glove box, a 20 mL vial was charged with 0.159 g (0.213 mmol) of **12-Br₂** and approximately 15 mL of tetrahydrofuran. To this resulting yellow solution, 0.025 g (1.065 mmol, 5 equivalents) of sodium metal was added and the vial was set to stir. After 2 hours it had turned reddish-yellow in color. After 16 hours the resulting dark red solution was filtered through Celite and the solvent was evacuated to obtain a dark red film. It was washed with approximately 10 mL of pentane and then dried under vacuum to yield 0.076 g (0.068 mmol, 32% recrystallized yield) of a dark red microcrystalline solid identified as **[κ³-(Ph₂PCH₂CH₂)₂PPh]Fe[κ²-Ph₂PCH₂CH₂P(Ph)CH₂CH₂PPh₂].** Elemental Analysis for C₆₈H₆₆FeP₆: Calcd. C, 72.64% ; H, 5.87%. Found: C, 71.90%, H 5.71%. ¹H NMR (benzene-d_6) δ(ppm): 7.48-7.30 (m, 12H, *Phenyl*), 7.12-6.99 (m, 20H, *Phenyl*), 6.93 (t, *J =7.6 Hz,* 3H, *Phenyl*), 6.86 (m, 2H, *Phenyl*), 6.81 (m, 4H, *Phenyl*), 6.73 (m, 4H, *Phenyl*), 6.58 (t, *J = 8.0 Hz,* 2H, *Phenyl*), 2.72 (broad m, 1H, *CH₂P*), 2.42 (broad m, 1H, *CH₂P*), 2.18 (broad m, 2H, *CH₂P*), 2.04 (broad m, 3H, *CH₂P*), 1.75 (broad m, 4H, *CH₂P*), 1.31 (broad m, 4H, *CH₂P*), 0.82 (broad m, 1H, *CH₂P*).

¹³C NMR (benzene-d_6), δ (ppm): 146.2 (m, *i-aryl*), 145.9 (m, *i-aryl*), 145.4 (m, *i-aryl*), 144.5 (m, *i-aryl*), 143.5 (m, *i-aryl*), 141.2 (m, *i-aryl*), 140.4 (d, J_{CP} = 16.6 Hz, *i-aryl*), 140.0 (d, J_{CP} = 16.5 Hz, *i-aryl*), 135.1 (d, J_{CP} = 10.5 Hz, *aryl*), 134.7 (d, J_{CP} = 11.9 Hz,

aryl), 134.5 (d, J_{CP} = 8.5 Hz, *aryl*), 134.4 (s, *aryl*), 133.7 (d, J_{CP} = 8.4 Hz, *aryl*), 133.6 (s,

aryl), 133.4 (s, *aryl*), 133.3 (d, J_{CP} = 8.9 Hz, *aryl*), 132.4 (d, J_{CP} = 6.8 Hz, *aryl*), 131.4 (d,

J_{CP} = 7.0 Hz, *aryl*), 129.2 (d, J_{CP} = 6.0 Hz, *aryl*), 129.1 (s, *aryl*), 129.0 (d, J_{CP} = 5.7 Hz,

aryl), 128.9 (s, *aryl*), 128.5 (s, *aryl*), 128.3 (s, *aryl*), 128.0 (s, *aryl*), 127.9 (d, J_{CP} = 6.3

Hz, *aryl*), 127.7 (d, J_{CP} = 7.1 Hz, *aryl*), 127.6 (s, *aryl*), 127.4 (d, J_{CP} = 8.3 Hz, *aryl*),

127.1 (d, J_{CP} = 8.3 Hz, *aryl*), 126.8 (d, J_{CP} = 8.3 Hz, *aryl*), 126.4 (s, *aryl*), (Several aryl

resonances not located), 37.3 (m, *CH$_2$P*), 36.1 (m, *CH$_2$P*), 35.3 (m, *CH$_2$P*), 31.9 (m,

CH$_2$P), 30.0 (m, *CH$_2$P*), 27.8 (m, *CH$_2$P*), 25.2 (m, *CH$_2$P*), 23.6 (m, *CH$_2$P*). ^{31}P NMR

(benzene-d_6): δ (ppm) = 119.23 (m, Fe-*P*), 99.11 (m, Fe-*P*), 82.74 (m, Fe-*P*), 76.95 (m,

Fe-*P*), 68.24 (m, Fe-*P*), -12.08 (d, J_{PP} = 19.65 Hz, CH$_2$CH$_2$*P*Ph$_2$).

Preparation of [κ^3-(Ph$_2$PCH$_2$CH$_2$)$_2$PPh]Fe(Bpy) (12-Bpy). In glove box, a 250 mL

round-bottomed flask was charged with 0.208 g (0.278 mmol) of **12-Br$_2$**, 0.217 g (1.390

mmol, 5 equivalents) of bipyridine and approximately 100 mL of diethylether. The

mixture was allowed to cool at -35 ^{o}C for 30 min when a dark red color was observed.

Then to the mixture, 0.032 g (1.390 mmol, 5 equivalents) of sodium metal was added and

set to stir at ambient temperature. After 1 hour everything was dissolved and the resulting

solution had turned deep purple. It was stirred overnight. After 18 hours the solution was

filtered through Celite and the solvent was evacuated to obtain 0.202 g of a dark purple

microcrystalline solid. This was dissolved in approximately 10 mL of toluene and filtered

through Celite (to remove any residual salt resulted from the reaction). The filtrate was

again passed through another Celite column. The toluene was removed *in vacuo* to get a

dark solid (0.165g, 76%). The dark purple solid was dissolved in minimum amount of

diethyl ether (approximately 10 mL) and filtered through Celite again. The filtrate was

kept in freezer (-35 $^{\circ}$C) when dark purple color crystals were deposited at the bottom of the vial. After decanting the residual solvent the crystals were dried under vacuum to obtain purple microcrystalline solid (0.093 g, 45% recrystallized yield). ^{1}H NMR (benzene-d_6) δ(ppm): 8.23 (d, J =6.8 Hz, 1H, bpy), 7.96 (d, J =6.4 Hz, 1H, bpy), 7.61 (d, J = 8.4 Hz, 1H, bpy), 7.51 (m, 2H, aryl), 7.47 (d, J = 8.0 Hz, 1H, bpy), 7.05 (m, 4H, aryl), 7.01 (m, 9H, aryl), 6.83 (m, 6H, aryl), 6.76 (m, 5H, bpy & aryl), 6.66 (t, J =7.2 Hz, 1H, bpy), 6.14 (t, J = 6.4 Hz, 1H, bpy), 5.97 (t, J = 6.4 Hz, 1H, bpy), 2.40 (m, 2H, CH$_2$P), 1.82 (m, 6H, CH$_2$P); ^{13}C NMR (benzene-d_6) δ(ppm): 156.8 (s, bpy), 155.1 (d, J_{CP} = 11.7 Hz, bpy), 146.5 (s, aryl), 145.7 (s, aryl), 141.6 (m, aryl), 141.4 (m, aryl), 139.8 (m, aryl), 132.7 (m, aryl), 132.5 (m, aryl), 132.4 (s, aryl) 129.2 (s, aryl), 129.1 (s, aryl), 129.0 (m, aryl), 127.7 (s, aryl), 123.9 (s, bpy), 122.7 (s, bpy), 120.1(s, bpy), 116.5 (s, bpy), 115.4 (s, bpy), 112.2 (s, bpy). Two resonances not located. ^{31}P NMR (benzene-d_6): δ (ppm) = 112.93 (t, J_{PP} = 8.1 Hz, Fe-PPh), 91.59 (d, J_{PP} = 9.5 Hz, Fe-PPh$_2$).

Preparation of [κ^3-PhP(CH$_2$CH$_2$PPh$_2$)$_2$]Fe(η^4-C$_8$H$_8$) (12-COT). Method A: In the glovebox, a 20 mL scintillation vial was charged with 0.020 g (0.076 mmol) of Fe(COT)$_2$ and approximately 1 mL of benzene-d_6. While stirring, a solution of 0.040 g (0.075 mmol) Triphos in approximately 1 mL of benzene-d_6 was added dropwise. After approximately 1 min, an aliquot of the solution was taken and filtered through Celite into a J. Young tube. After 10 min, analysis of this aliquot by ^{1}H and ^{31}P NMR spectroscopy revealed that the reaction was near completion. Upon confirming spectroscopically that the reaction was complete after 1 hour, the fractions were recombined, filtered through Celite, and the solvent was evacuated to yield a red solid. After washing with 1 mL of pentane and 1 mL of Et$_2$O to remove a small amount of residual Triphos, 0.021 g (0.030

mmol, 40% yield) of **12-COT** was collected. **Method B:** A 100 mL round-bottomed flask was charged with 0.213 g of **12-Br$_2$** (0.284 mmol), 0.592 g (5.690 mmol) of 1,3,5,7-cyclooctatetraene (COT), and approximately 80 mL of diethyl ether. This slurry was placed in a -35 °C freezer for 20 minutes. After this time, freshly cut sodium metal (0.033 g, 1.422 mmol) was added to the slurry while cold. The reaction was set to stir while warming to room temperature. After 15 h, the resulting deep red solution was filtered through Celite and the Celite pad was washed with 15 mL of toluene to fully dissolve the product. The solvent was evacuated to yield a red solid. This material was washed 5 times with pentane (5 x 10 mL) to get rid of excess COT. Then it was washed five times with diethyl ether (5 x 5 mL) to remove any remaining free ligand. Drying *in vacuo* yielded 0.098 g (0.141 mmol, 49%) of a red solid identified as **12-COT**. Conducting this reaction with 10 eq. rather than 20 eq. of 1,3,5,7-cyclooctatetraene in tetrahydrofuran afforded a 1:1 ratio of **12-COT** to **12-κ^2-Triphos**. Analysis for C$_{42}$H$_{41}$FeP$_3$: Calcd. C, 72.63%; H, 5.95%; Found: C, 72.31% H, 5.66%. ^{1}H{^{31}P} NMR (benzene-*d$_6$*): δ (ppm) = 7.79 (t, *J* = 7.6 Hz, 2H, *phenyl*), 7.31 (t, *J* = 7.4 Hz, 2H, *phenyl*), 7.23 (t, *J* = 7.4 Hz, 1H, *phenyl*), 7.09 (t, *J* = 7.4 Hz, 4H, *phenyl*), 7.03 (m, 6H, *phenyl*), 6.88 (d, *J* = 7.0 Hz, 10H, *phenyl*), 4.93 (s, 8H, *COT*), 2.16 (m, 2H, *-CH$_2$*), 1.91 (m, 4H, *-CH$_2$*), 1.01 (m, 2H, *-CH$_2$*). ^{13}C NMR (benzene-*d$_6$*): δ (ppm) = 132.9 (m, *phenyl*), 132.5 (m, *phenyl*), 131.4 (m, *phenyl*), 129.7 (s, *phenyl*), 129.4 (s, *phenyl*), 129.1 (s, *phenyl*), 129.0 (s, *phenyl*), 128.9 (s, *phenyl*), 128.7 (s, *phenyl*), 128.4 (m, *phenyl*), 128.2 (m, *phenyl*), 127.2 (m, *phenyl*), 95.8 (s, *COT*), 32.22 (m, P*CH$_2$CH$_2$*P). ^{31}P{^{1}H} NMR (benzene-*d$_6$*): δ (ppm) = 116.33 (t, *J* = 7.8 Hz, Fe-*P*Ph), 95.71 (d, *J* = 7.8 Hz, Fe-*P*Ph$_2$).

Preparation of [H₃CC(CH₂PPh₂)₃]FeBr₂ (13-Br₂): In the glove box a 20 mL scintillation vial was charged with $FeBr_2$ (0.094 g, 0.435 mmol), Triphos* (0.271 g, 0.435 mmol) and approximately 15 mL of tetrahydrofuran. The resulting solution was set to stir at room temperature for six hours while it turned faint yellow in color. It was filtered through Celite and the solvent was evacuated to obtain a glassy film at the bottom of the filter flask, which was scraped with pentane, which was then decanted, twice (2 x 5 mL). Drying *in vacuo* yielded 0.310 g of a glassy solid (85%), identified as **13-Br₂**. Analysis for $C_{41}H_{39}FeBr_2P_3$: Calcd. C, 58.60%; H, 4.68%; Found: C, 58.57% H, 4.64%. Magnetic Susceptibility (Gouy Balance, 26 °C): μ_{eff} = 4.4 μ_B. ¹H NMR (tetrahydrofuran-d_8): δ (ppm) = 139.89 (peak width at ½ height = 5660 Hz), 57.61 (4590 Hz), 13.02 (735 Hz), 5.63 (321 Hz). ³¹P NMR (tetrahydrofuran-d_8): δ (ppm) = 21.91 (2651 Hz).

Preparation of [κ³-(Ph₂PCH₂)₃C(CH₃)]Fe[COT] (13-COT): A 100 mL round-bottomed flask was charged with 0.198 g of **13-Br₂** (0.236 mmol), 0.086 g (0.828 mmol) of 1,3,5,7-cyclooctatetraene (COT), and approximately 50 mL of diethyl ether. This slurry was placed in a -35 °C freezer for 25 minutes. After this time, freshly cut sodium metal (0.027 g, 1.182 mmol) was added to the slurry while cold. The reaction was set to stir while warming to room temperature. After 15 h, the resulting deep reddish-brown solution was filtered through Celite and the Celite pad was washed with 15 mL of toluene. The solvent was evacuated to yield a reddish-brown solid. This material was washed 5 times with pentane (5 x 10 mL) to get rid of excess COT and dried. The red solid was then dissolved in approximately 15 mL toluene and filtered through a Celite column. After evaporating the toluene, the red solid was washed five times with diethyl ether (5 x 4 mL) and it was dried completely to obtain 0.080 g (0.102 mmol, 43%) of red

crystals identified as **13-COT**. This complex was also prepared following the straightforward addition of Triphos* to Fe(COT)$_2$. Analysis for C$_{49}$H$_{47}$FeP$_3$: Calcd. C, 75.00%; H, 6.04%. Found: C, 74.64%; H, 6.28%. ^{1}H NMR (benzene-d_6): δ (ppm) = 6.93 (m, 18 H, *phenyl*), 6.82 (m, 12H, *phenyl*), 5.53 (s, 8H, *COT*), 2.00 (broad m, 6H, -*CH$_2$*), 0.993 (broad s, 3H, -*CH$_3$*). ^{13}C NMR (benzene-d_6): δ (ppm) = 143.5 (m, *phenyl*), 133.1 (m, *phenyl*), 128.0 (m, *phenyl*), 128.3 (m, *phenyl*), 95.7 (s, COT), 39.9 (m, *CH$_2$P*), 37.9 (m, *C*CH$_3$), 35.9 (m, *CH$_3$*). ^{31}P{^{1}H} NMR (benzene-d_6): δ (ppm) = 53.92 (s, *Fe-P*Ph$_2$).

Preparation of (Triphos)FeBr$_2$(CO) (12-Br$_2$(CO)): Under an inert atmosphere, a Schlenk tube was charged with 0.197 g (0.263 mmol) of **12-Br$_2$** in approximately 20 mL dry acetone. The tube was sealed and one atmosphere of CO was added to the frozen solution on a Schlenk line during a freeze-pump-thaw cycle. The solution was warmed to room temperature. The brown suspension turned deep green, which was stirred for 30 h at 23 °C. After 30 h the excess CO was evacuated on a Schlenk line and the resulting green suspension was heated for 1 h at 50 °C, while it turned into an orange suspension (this color change has alternatively been observed over the course of days at ambient temperature). Then the headspace of the tube was evacuated to remove any excess CO. Finally, the orange suspension was concentrated *in vacuo* and placed into a -35 °C freezer for 12 h. Filtration and drying yielded 0.125 g (0.161 mmnol, 61%) of an orange solid identified as **12-Br$_2$(CO)**. Analysis for C$_{35}$H$_{33}$P$_3$FeBr$_2$O: Calcd. C, 54.02%; H, 4.27%. Found: C, 53.16 %; H, 4.15 %. ^{1}H NMR (chloroform-d): 7.94 (m, 4H, *Ph*), 7.85 (m, 4H, *Ph*), 7.36-7.29 (m, 13H, *Ph*), 7.24-7.17 (m, 4H, *Ph*), 3.42 (m, 2H, C*H$_2$*), 3.28 (m, 2H, C*H$_2$*), 2.76 (m, 2H, C*H$_2$*), 2.66 (m, 2H, C*H$_2$*). ^{13}C NMR (chloroform-d): 219.76 (m, *CO*), 137.35 (*Ph*), 134.36 (*Ph*), 132.11 (*Ph*), 130.95 (*Ph*), 137.35 (*Ph*), 130.88 (*Ph*), 130.02

(*Ph*), 129.66 (*Ph*), 129.07 (*Ph*), 129.00 (*Ph*), 128.48 (*Ph*), 127.51 (*Ph*), 30.31 (*CH$_2$*), 27.15 (*CH$_2$*). ^{31}P NMR (chloroform-*d*): 134.62 (t, J_{P-P} = 22.38 Hz, *P*Ph), 56.73 (d, J_{P-P} = 21.54 Hz, *P*Ph$_2$). IR (KBr): ν_{CO} = 1957 cm^{-1}.

Observation of (Triphos)Fe(CO)$_2$ (12-(CO)$_2$) from 12-Br$_2$(CO): Under an inert atmosphere, a 20 mL vial was charged with 0.101 g (0.129 mmol) of **12-Br$_2$(CO)** in approximately 15 mL of toluene and cooled. Another vial containing a 3 mL toluene solution of NaEt$_3$BH (0.324 mL, 0.324 mmol) was also cooled. After 30 min, the NaEt$_3$BH solution was added slowly to the orange **12-Br$_2$(CO)** slurry. The vial was warmed to room temperature and stirred for 24 h. The resulting yellow solution was filtered through Celite and toluene was evacuated to obtain a yellow film. The film was scraped with pentane (5 x 4 mL) and dried to isolate 0.038 g (0.0588 mmol, 45%) of a bright yellow solid identified as **12-(CO)$_2$**.[16] This complex was also observed following Na/Hg reduction of **12-Br$_2$(CO).** ^{1}H NMR (benzene-*d$_6$*): 8.01 (m, 4H, *Ph*), 7.52 (m, 2H, *Ph*), 7.13-7.03 (m, 13H, *Ph*), 6.96-6.87 (m, 6H, *Ph*), 2.16 (m, 2H, C*H$_2$*), 1.95 (m, 2H, C*H$_2$*), 1.76 (m, 2H, C*H$_2$*), 1.57 (m, 2H, C*H$_2$*). ^{13}C NMR (benzene-*d$_6$*): 230.91 (m, *CO*), 223.70 (m, *CO*), 141.84 (m, *Ph*), 139.22 (s, *Ph*), 138.93 (s, *Ph*), 133.49 (m, *Ph*), 131.23 (m, *Ph*), 130.87 (s, *Ph*), 129.93 (s, *Ph*), 129.69 (s, *Ph*), 128.93 (m, *Ph*), 128.64 (m, *Ph*), 32.34 (m, *CH$_2$*), 30.23 (m, *CH$_2$*). ^{31}P NMR (benzene-*d$_6$*): 134.11 (t, J_{P-P} = 54.0 Hz, Ph*P*), 96.43 (d, J_{P-P} = 54.0 Hz, Ph$_2$*P*). IR (benzene-*d$_6$*): ν_{CO} = 1929, 1873 cm^{-1}.

Preparation of (Triphos)FeH(Br)(CO) (12-H(Br)(CO)): Under an inert atmosphere, a 100 mL round bottom flask was charged with 0.116 g (0.149 mmol) of **12-Br$_2$(CO)** in approximately 25 mL toluene and placed in a liquid N$_2$ cooled cold well. A 20 mL scintillation vial containing 0.149 mL (0.149 mmol) of NaEt$_3$BH (1 M solution in

toluene) in approximately 2 mL toluene was also cooled. After 30 min, the NaEt$_3$BH solution was slowly added to the toluene slurry of **12-Br$_2$(CO)** while stirring. The flask was warmed to room temperature and stirred for 2.5 h at what time the mixture had turned into an orange solution. It was filtered through Celite and the toluene was removed *in vacuo*. The orange-yellow film was dissolved in 5 mL toluene and filtered through a Celite column. The filtrate was layered with 1 mL diethylether and stored at -35 °C. Brown crystals were isolated (0.035 g, 0.0486 mmol, 32 %) and identified as **12-H(Br)(CO)**. Analysis for C$_{35}$H$_{34}$P$_3$FeBrO: Calcd. C, 60.11%; H, 4.90%. Found: C, 59.89%; H, 4.83%. ^{1}H NMR (chloroform-*d*): 8.01 (broad m, 4H, *Ph*), 7.87 (broad m, 4H, *Ph*), 7.42 (broad m, 8H, *Ph*), 7.35 (m, 7H, *Ph*), 7.30 (m, 2H, *Ph*), 2.78 (broad m, 2H, *CH$_2$*), 2.43 (broad m, 2H, *CH$_2$*), 2.25 (broad m, 2H, *CH$_2$*), 1.90 (broad m, 2H, *CH$_2$*), -7.06 (dt, *J* = 52.45 Hz, 63.06 Hz, 1H, *Fe-H*). {^{31}P}^{1}H NMR (chloroform-*d*): 8.00 (m, 4H, *Ph*), 7.87 (m, 4H, *Ph*), 7.44-7.40 (m, 8H, *Ph*), 7.35 (m, 7H, *Ph*), 7.29 (m, 2H, *Ph*), 2.81 (m, 2H, *CH$_2$*), 2.44 (m, 2H, *CH$_2$*), 2.25 (m, 2H, *CH$_2$*), 1.89 (m, 2H, *CH$_2$*), -7.06 (s 1H, *Fe-H*). ^{13}C NMR (chloroform-*d*): 215.84 (CO), 138.58 (m, *Ph*), 137.37 (m, *Ph*), 134.37 (m, *Ph*), 133.74 (m, *Ph*), 133.46 (m, *Ph*), 130.81 (m, *Ph*), 130.38 (m, *Ph*), 129.83 (m, *Ph*), 129.44 (m, *Ph*), 128.77 (m, *Ph*), 128.45 (m, *Ph*), 127.89 (m, *Ph*), 32.38 (m, *CH$_2$*), 30.87 (m, *CH$_2$*). ^{31}P NMR (chloroform-*d*): 138.55 (Ph*P*), 82.31 (Ph$_2$*P*). IR (benzene-*d$_6$*): ν_{CO} = 1950 cm^{-1}.

Preparation of (Triphos)FeH(η^2-BH$_4$) (12-H(BH$_4$)): Under an inert atmosphere, a 20 mL scintillation vial was charged with 0.144 g (0.186 mmol) of **12-Br$_2$(CO)** in approximately 15 mL dry THF. To the orange suspension, 2.2 eq. of NaBH$_4$ (0.0163 g, 0.431 mmol) was added and stirred at 23 °C for 4 d, after which time the orange

suspension had turned bright orange. This solution was then filtered through Celite and the tetrahydrofuran was evacuated. The resulting bright orange film was scraped from the vial twice with 5 mL of diethylether and dried. The resulting solid was then dissolved in a minimum amount of toluene and layered with diethyl ether and placed in a -35 °C freezer. Recrystallization yielded 0.078 g (0.1287 mmol, 69%) of bright orange crystals upon drying, which were identified as **12-H(BH$_4$)**. Analysis for C$_{34}$H$_{38}$P$_3$FeB: calcd. C, 67.37%; H, 6.32%. Found: C, 67.66%; H, 6.06%. ^{1}H NMR (benzene-d_6): 7.92 (m, 4H, *Ph*), 7.65 (m, 4H, *Ph*), 7.57 (m, 2H, *Ph*), 7.12 – 6.95 (m, 14H, *Ph*), 5.83 (bs, 2H, B*H$_2$*), 2.39 (m, 2H, C*H$_2$*), 2.18 (m, 2H, C*H$_2$*), 1.93 (m, 2H, C*H$_2$*), 1.42 (m, 2H, C*H$_2$*), -12.77 (bs, 1H, B*H*), -14.04 (bs, 1H, B*H*), -23.95 (pseudo q, 1H, Fe*H*). $\{^{31}$P$\}^1$H (benzene-d_6): 7.94 (broad m, 4H, *Ph*), 7.66 (broad m, 4H, *Ph*), 7.59 (m, 2H), 7.18 (s, 3H), 7.12 – 6.95 (m, 13H), 5.84 (s, 2H), 2.38 (s, 2H), 2.20 (s, 2H), 1.94 (s, 2H), 1.42 (s, 2H), -12.74 (s, 1H), -14.05 (s, 1H), -23.95 (s, 1H). ^{13}C NMR (benzene-d_6): 141.5, 139.7, 133.7, 132.5, 130.2, 129.4, 129.1, 128.7, 128.6, 128.3, 118.2, 33.8, 30.5. ^{31}P NMR (benzene-d_6): 145.3 (t, J_{P-P} = 32.4 Hz, Ph*P*), 89.6 (d, J_{P-P} = 32.4 Hz, Ph$_2$*P*).

Preparation of (Triphos)FeD(η^2-BD$_4$) (1-D(BD$_4$)): Under an inert atmosphere, a 20 mL scintillation vial was charged with 0.030 g (0.039 mmol) of **12-Br(CO)** in approximately 15 mL dry THF. To the suspension, 0.024 g (0.578 mmol) of NaBD$_4$ was added and stirred at room temperature for 4 d. The solution was filtered through Celite and the THF was removed. The resulting orange film was scraped with diethyl ether (2 x 5 mL) and dried to yield 0.018 g (0.030 mmol, yield = 80%) of an orange solid identified as **12-D(BD$_4$)**. ^{2}H NMR (benzene): 5.76 (broad s, B*D$_2$*), -12.99 (broad s, B-*D*-Fe), -14.13

(broad s, B-*D*-Fe), -24.27 (broad m, Fe-*D*). ^{31}P NMR (benzene): -145.54 (Ph*P*), -90.02

(Ph$_2$*P*).

5.10. References:

1. Iron dinitrogen complexes: (a) Crossland, J. L.; Tyer, D. R. *Coord. Chem. Rev.* **2010**, *254*, 1883-1894. (b) Rodriguez, M. M., Bill, E., Brennessel, W. W. & Holland, P. L. *Science* **2011**, *334*, 780-783. (c) Hazari, N. *Chem. Soc. Rev.* **2010**, *39*, 4044-4056. (d) Anderson, J. S.; Rittle, J.; Peters, J. C. *Nature* **2013**, *501*, 84-87. (e) Moret, M.-E.; Peters, J. C. *Angew. Chem. Int. Ed.* **2011**, *50*, 2063-2067. (f) Bart, S. C.; Lobkovsky, E.; Chirik, P. J. *J. Am. Chem. Soc.* **2004**, *126*, 13794. (g) Hendrich, M. P.; Gunderson, W.; Behan, R. K.; Green, M. T.; Mehn, M. P.; Betley, T. A.; Lu, C. C.; Peters, J. C. *Proc. Natl. Acad. Sci. U.S.A* **2006**, *103*, 17107-17112. (h) Field, L. D.; Guest, R. W.; Turner, P. *Inorg. Chem.* **2010**, *49*, 9086-9093. (i) Gilbertson, J. D.; Szymczak, N. K.; Tyler, D. R. *J. Am. Chem. Soc.* **2005**, *127*, 10184-10185.

2. Iron catalysis: (a) Plietker, B. *Iron Catalysis in Organic chemistry: Reactions and Applications.* Wiley-VCH, Weinhem, **2008**. (b) Bauer, E. *Iron Catalysis II*. Springer, Swizerland, **2015**. (c) Bauer, I.; Knölker, H.-J.; *Chem. Rev.*, **2015**, *115*, 3170–3387. (d) Bolm, C.; Legros, J.; Le Paih, J.; Zani, L. *Chem. Rev.*, **2015**, *104*, 6217-6254.

3. (a) Blanchard, S.; Derat, E.; Murr, M. D-E.; Fensterbank, L.; Malacria, M.; Mouries-Mansuy, V. *Eur. J. Inorg. Chem.* **2012**, 376-389. (b) Bart, S. C. Lobkovsky, E.; Chirik, P. J. *J. Am. Chem. Soc.* **2004**, *126*, 13794-13807. (c) Trovitch, R. J.; Lobkovsky, E.; Chirik, P. J. *J. Am. Chem. Soc.* **2008**, *130,* 11631-11640. (d) Chirik, P. J.; Wieghardt, K. *Science* **2010**, *327*, 794-795.

4. (a) Akhtar, M.; Ellis, P. D.; MacDiarmid, A. G.; Odom, J. D. *Inorg. Chem.* **1972**, *11*, 2917-2921. (b) Whitlesey, M. K.; Mawby, R. J.; Osman, R.; Perutz, R. N.; Field, L. D.; Wilkinson, M. P.; George, M. W. *J. Am. Chem. Soc.* **1993**, *115*, 8627-8637. (c) Tolman, C. A.; Ittel, S. D.; English, A. D.; Jesson, J. P. *J. Am. Chem. Soc.* **1979**, *101*, 1742-1751. (d) Luo, L.; Nolan, S. P.; *Inorg. Chem.* **1993**, *32*, 2410-2415. (e) Hughes, D. L.; Leigh, G. J.; Jimenez-Tenorio, M.; Rowley, A. T.; *J. Chem. Soc. Dalton Trans.* **1993**, 75-82. (f) Hills, A.; Hughes, D. L.; Jimenez-Tenorio, M.; Leigh, G. J.; Rowley, A. T.; *J. Chem. Soc. Dalton Trans.* **1993**, 3041-3049. (g) de los Ríos, Jiménez-Tenorio, M.; Jiménez-Tenorio, M. A; Puerta, M. C.; Valerga, P. *J. Organomet. Chem.* **1996**, *525*, 57-64. (h) Hall, D. A.; Leigh, G. J. *J. Chem. Soc. Dalton Trans.* **1996**, 3539-3541. (i) Field, L. D.; Messerle, B. A.; Smernik, R. J.; Hambley, T. W.; Turner, P. *Inorg. Chem.* **1997**, *36*, 2884-2892. (j) Field, L. D.; Thomas, I. P.; Hambley, T. W.; Turner, P. *Inorg. Chem.* **1998**, *37*, 612-618. (k) Louie, J.; Grubbs, R. H.; *Organometallics* **2001**, *20*, 481-484. (l) Gilbertson, J. D.; Szymczak, N. K.; Tyler, D. R. *Inorg. Chem.* **2004**, *43*, 3341-3343. (m) van Rijn, J. A.; Gouré, E.; Siegler, M. A.; Spek, A. L.; Drent, E.; Bouwman, E. *J. Organomet. Chem.*

2011, *696*, 1899-1903. (n) Nicolas, F.; Katharina, H.; Kimon, F.; Robert, L. *Dalton Trans.* **2013**, *42*, 11252-11261. (o) Bedford, R. B.; Brenner, P. B.; Carter, E.; Gallagher, T.; Murphy, D. M.; Pye, D. R. *Organometallics* **2014**, *33*, 5940-5943. (p) Yelle, R. B.; Crossland, J. L.; Szymczak, N. K.; Tyler, D. R. *Inorg. Chem.* **2009**, *48*, 861-871. (q) Casitas, A.; Krause, H.; Goddard, R.; Fürstner A. *Angew. Chem. Int. Ed.* **2015**, *54*, 1521-1526.

5. PNPFe: (a) Langer, R.; Leitus, G.; Ben-David, Y.; Milstein, D. *Angew. Chem.* **2011**, *123*, 2168-2172. (b) Langer, R.; Iron, M. A.; Konstantinovski, L.; Diskin-Posner, Y.; Leitus, G.; Ben-David, Y.; Milstein, D. *Chem. Eur. J.* **2012**, *18*, 7196-7209. (c) Srimani, D.; Diskin-Posner, Y.; Ben-David, Y.; Milstein, D. *Angew. Chem. Int. Ed.* **2013**, *52*, 14131-14134. (d) Alberico, E.; Sponholz, P.; Cordes, C.; Nielsen, M.; Drexler, H-J.; Baumann, W.; Junge, H.; Beller, M. *Angew. Chem. Int. Ed.* **2013**, *52*, 14162-14166. (e) Chakraborty, S.; Brennessel, W. W.; Jones, W. D. *J. Am. Chem. Soc.* **2014**, *136*, 8564-8567. (f) Qu, S.; Dai, H.; Dang, Y.; Song, C.; Wang, Z-X.; Guan, H. *ACS Catal.* **2014**, *4*, 4377-4388. (g) Koehne, I.; Schmeier, T. J.; Bielinski, E. A.; Pan, C. J.; Lagaditis, P. O.; Bernskoetter, W. H.; Takase, M. K.; Würtele, C.; Hazari, N.; Schneider, S. *Inorg. Chem.* **2014**, *53*, 2133-2143. (h) Fillman, K. L.; Bielinski, E. A.; Schmeier, T. J.; Nesvet, J. C.; Woodruff, T. M.; Pan, C. J.; Takase, M. K.; Hazari, N.; Neidig, M. L. *Inorg. Chem.* **2014**, *53*, 6066-6072. (i) Rivada-Wheelaghan, O.; Dauth, A.; Leitus, G.; Diskin-Posner, Y. *Inorg. Chem.* **2015**, *54*, 4526-4538. (j) Bonitatibus Jr., P. J.; Chakraborty, S.; Doherty, M. D.; Siclovan, O.; Jones, W. D.; Soloveichik, G. L. *Proc. Natl. Acad. Sci. U. S. A.* **2015**, *112*, 1687-1692. (k) Sharninghausen, L. S.; Mercado, B. Q.; Crabtree, R. H.; Hazari, N. *Chem. Commun.* **2015**, *51*, 16201-16204. (l) Zell, T.; Ben-David, Y.; Milstein, D. *Catal. Sci. Technol.* **2015**, *5*, 822-826. (m) Zell, T.; Milstein, D. *Acc. Chem. Res.* **2015**, *48*, 1979-1994. (n) Chakraborty, S.; Bhattacharya, P.; Dai, H.; Guan, H. *Acc. Chem. Res.* **2015**, *48*, 1995-2003. (o) Zhang, Y.; MacIntosh, A. D.; Wong, J. L.; Bielinski, E. A.; Williard, P. G.; Mercado, B. Q.; Hazari, N.; Bernskoetter, W. H. *Chem. Sci.* **2015**, *6*, 4291. (p) Chakraborty, S.; Lagaditis, P. O.; Förster, M.; Bielinski, E. A.; Hazari, N.; Holthausen, M. C.; Jones, W. D.; Schneider, S. *ACS Catal.* **2014**, *4*, 3994-4003.

6. PCPFe: (a) Xu, G.; Sun, H.; Li, X. *Organometallics* **2009**, *28*, 6090. (b) Bhattacharya, P.; Krause, J. A.; Guan, H. *Organometallics* **2011**, *30*, 4720-4729. (c) Zhao, H.; Sun, H.; Li, X. *Organometallics* **2014**, *33*, 3535. (d) Bhattacharya, P.; Krause, J. A.; Guan, H. *Organometallics* **2014**, *33*, 6113-6121. (e) Bhattacharya, P.; Krause, J. A.; Guan, H. *J. Am. Chem. Soc.* **2014**, *136*, 11153-11161. (f) Huang, S.; Zhao, H.; Li, X.; Wang, L.; Sun, H. *RSC Adv.* **2015**, *5*, 15660. (g) Murugesan, S.; Kirchner, K.; *Dalton Trans.* **2016**, *45*, 416-439.

7. Triphos iron complexes: (a) Davies, S. G.; Felkin, H.; Watts, O. *J. Chem. Soc. Chem Commun.* **1980**, *4*, 159-160. (b) Di Vaira, M.; Midollini, S.; Sacconi, L. *Inorg. Chem.* **1981**, *20*, 3430-3435. (c) Ghilardi, C. A.; Innocenti, P.; Midollini, S.; Orlandini, A. *J. Organomet. Chem.* **1982**, *231*, C78-C80. (d) Asam, A.; Janssen, B.; Huttner, G.; Zsolnai, L.; Walter, O. *Z. Naturforsch* **1993**, *48b*, 1707-1714. (e) Ghilardi, C. A.; Laschi, F.; Midollini, S.; Orlandini, A.; Scapacci, G.; Zanello, P. *J. Chem. Soc. Dalton Trans.* **1995**, 531-540. (f) Baker, P. K.; Meehan, M. M. *Inorg. Chim. Acta* **2000**, *303*, 17-23. (g)

O'Connor, J. M.; Hiibner, K.; Closson, A.; Gantzel, P. *Organometallics* **2001**, *20*, 1482-1485. (h) Guilera, G.; McGrady, G. S.; Steed, J. W.; Kaltsoyannis, N. *New J. Chem.* **2004**, *28*, 444-446. (i) Jaunky, P.; Schmalle, H. W.; Blacque, O.; Fox, T.; Berke, H. *J. Organomet. Chem.* **2005**, *690*, 1429-1455. (j) Guilera, G.; McGrady, G. S.; Steed, J. W.; Burchell, R. P. L.; Sirsch, P.; Deeming, A. J. *New J. Chem.* **2008**, *32*, 1573-1581. (k) Thoreson, K. A.; Follett, A. D.; McNeill, K. *Inorg. Chem.* **2010**, *49*, 3942-3949. (l) Dimmer, J.-A.; Wesemann, L. *Eur. J. Inorg. Chem.* **2011**, 235-240. (m) Li, P.; de Bruin, B.; Reek, J. N. H.; Dzik, W. I. *Organometallics* **2015**, *34*, 5009-5014. (n) Nishibayashi, Y.; Iwai, S.; Hidai, M. *J. Am. Chem. Soc.* **1998**, *120*, 10559-10560. (o) Hogarth, G.; Richards, I. *Inorg. Chem. Commun.* **2007**, *10*, 66-70. (p) Adam, F. I.; Hogarth, G.; Richards, I.; Sanchez, B. E. *Dalton Trans.* **2007**, *24*, 2495-2498.

8. Bpy : (a) Constable, E. C. *Adv. Inorg. Chem.* **1989**, *34*, 1-37. (b) Tom Dieck, H.; Franz, K.-D.; Hohmann, F. *Chem. Ber.* **1975**, *108*, 163-173. (c) Irwin, M.; Jenkins, R. K.; Denning, M. S.; Krämer, T.; Grandjean, F.; Long, G. J.; Herchel, R.; McGrady, J. E.; Goicoechea, J. M. *Inorg. Chem.* **2010**, *49*, 6160–6171. (d) Roitershtein, D.; Domingos, ~A.; Pereira, L. C. J.; Ascenso, J. R.; Marques, N. *Inorg. Chem.* **2003**, *42*, 7666–7673. (e) Scarborough, C. C.; Wieghardt, K. *Inorg. Chem.* **2011**, *50*, 9773-9793. (f) Chisholm, M. H.; Huffman, J. C.; Rothwell, I. P.; Bradley, P. G.; Kress, N.; Woodruff, W. H. *J. Am. Chem. Soc.* **1981**, *103*, 4945-4947. (g) Gore-Randall, E.; Irwin, M.; Denning, M. S.; Goicoechea, J. M. *Inorg. Chem.* **2009**, *48*, 8304–8316. (h) Echegoyen, L.; DeCian, A.; Fischer, J.; Lehn, J.-M. *Angew. Chem., Int. Ed. Engl.* **1991**, *30*, 838–840. (i) Bock, H.; Lehn, J.-M.; Pauls, J.; Holl, S.; Krenzel, V. *Angew. Chem., Int. Ed.* **1999**, *38*, 952–955. (j) Mukhopadhyay, T. K.; Feller, R. K.; Rein, F. N.; Henson, N. J.; Smythe, N. C.; Trovitch, R. J.; Gordon, J. C. *Chem. Commun.* **2012**, *48*, 8670-8672.

9. (a) Crabtree, R. H. *The Organometallic Chemistry of the Transition Metals*; John Wiley & Sons: Hoboken, NJ, 2009.

10. (a) Poremba, P.; Schmidt, H-G.; Noltemeyer, M.; Edelmann, F. T. *Organometallics* **1998**, *17*, 986-988. (b) Sygula, A.; Fronczek, F. R.; Rabideau, P. W. *J. Organomet. Chem.* **1996**, *526*, 389-391. (c) Hu, N.; Gong, L.; Jin, Z.; Chen, W. *J. Organomet. Chem.* **1988**, *352*, 61-66. (d) Jones, M. T.; de Boer, E. *Mol. Phys.* **1982**, *47*, 487-499. (e) Noordik, J. H.; van den Hark, T. E. M.; Mooij, J. J.; Klassen, A. A. K. *Acta Cryst.* **1974**, *B30*, 833-835.

11. Relevant COT complexes of iron for bond length survey: (a) Dickens, B.; Lipscomb, W. N. *J. Chem. Phys.* **1962**, *37*, 2084-2093. (b) Tsupreva, V. N.; Titov, A. A.; Filippov, O. A.; Bilyachenko, A. N.; Smol'yakov, A. F.; Dolgushin, F. M.; Agapkin, D. V.; Godovikov, I. A.; Epstein, L. M.; Shubina, E. S. *Inorg. Chem.* **2011**, *50*, 3325-3331. (c) Karlin, K. D.; Moisan, M. P.; Kustyn, M.; Dahlstrom, P. L.; Zubieta, J.; Raithby, P. R. *Cryst. Struct. Commun.* **1982**, *11*, 1945-1949. (d) Bassi, I. W.; Scordamaglia, R. *J. Organomet. Chem.* **1972**, *37*, 353-359. (e) Yu, Y.; Sun, J.; Chen, J. *J. Organomet. Chem.* **1997**, *533*, 13-23. (f) Lavallo, V.; El-Batta, A.; Bertrand, G.; Grubbs, R. H. *Angew. Chem. Int. Ed.* **2011**, *50*, 268-271. (g) Mukhopadhyay, T. K.; Flores, M.; Feller, R. K.;

Scott, B. L.; Taylor, R. D.; Paz-Pasternak, M.; Henson, N. J.; Rein, F. N.; Smythe, N. C.; Trovitch, R. J.; Gordon, J. C. *Organometallics* **2014**, *33*, 7101-7112.

12. For a discussion on the electrochemical reduction of CpCo(COT) see: (a) Moraczewski, J.; Geiger, Jr.; W. E. *J. Am. Chem. Soc.* **1981**, *103*, 4779-4787. (b) Baik, M.-H.; Schauer, C. K.; Ziegler, T. *J. Am. Chem. Soc.* **2002**, *124*, 11167-11181 and references therein.

13. Torrent, M.; Sola, M.; Frenking, G. *Chem. Rev.* **2000**, *100*, 439-493 and references therein.

14. Liu, T.; Li, B.; Popescu, C. V.; Bilko, A.; Pérez, L. M.; Hall, M. B.; Darensbourg, M. Y. *Chem. Eur. J.* **2010**, *16*, 3083-3089.

15. (a) Creutz, C. *Comments Inorg. Chem.* **1982**, *1*, 293. (b) Vlcek, A. A. *Coord. Chem. Rev.* **1982**, *43*, 39-62.

16. Felkin, H.; Lednor, P. W.; Normant, J.-M.; Smith, R. A. J. *J. Organomet. Chem.* **1978**, *157*, C64-C66.

17. Other relevant COT complexes for bond length survey: (a) Cr-COT complex: Brauer, D. J.; Krüger, C. *Inorg. Chem.* **1976**, *15*, 2511-2514. (b) CoCOT: Brennessel, W. W.; Young, Jr.; V. G.; Ellis, J. E. *Angew. Chem. Int. Ed.* **2002**, *41*, 1211-1215. (c) (η^4-COT)Zr(η^8-COT): Rogers, D. M.; Wilson, S. R.; Girolami, G. S. *Organometallics* **1991**, *10*, 2419-2424. (d) (η^4-COT)Zr(η^8-COT)(THF): Brauer, D. J.; Krüger, C. *J. Organomet. Chem.* **1972**, *42*, 129-137. (e) (η^5-Cp*)Zr(μ-η^8,η^2-COT)(η^4-COT)Zr(η^5-Cp*): Sinnema, P. J.; Meetsma, A.; Teuben, J. H. *Organometallics* **1993**, *12*, 184-189. (f) Mo-COT: Cotton, F. A.; Koch, S. A.; Schultz, A. J.; Williams, J. M. *Inorg. Chem.* **1978**, *17*, 2093-2098. (g) (η^4-COT)Ru(CO)$_3$: Cotton, F. A.; Eiss, R. *J. Am. Chem. Soc.* **1969**, *91*, 6593-6597. (h) Heck, J.; Lange, G.; Malessa, M.; Boese, R.; Bläser, D. *Chem. Eur. J.* **1999**, *5*, 659-668. (i) Brown, D. B.; Johnson, B. F. G.; Martin, C. M.; Parsons, S. *J. Organomet. Chem.* **1997**, *536-537*, 285-291. (j) Bieri, J. H.; Egolf, T.; van Philipsborn, W.; Piantini, U.; Prewo, R.; Ruppli, U.; Salzer, A. *Organometallics* **1986**, *5*, 2413-2425. (k) Cotton, F. A.; Koch, S. A.; Schultz, A. J.; Williams, J. M. *Inorg. Chem.* **1978**, *17*, 2093-2098.

18. For the purposes of this contribution, a C-C bond metrical parameter error limit of ±0.01 Å has been set for inclusion of a data set in electronic structure discussion.

19. . [(η^8-COT)Ti]$_2$(μ-η^4,η^4-COT): (a) Dierks, V. H.; Dietrich, H. *Acta Cryst.*, *Sect. B.* **1968**, *24*, 58-62. (b) Dietrich, H.; Dierks, H. *Angew. Chem. Int. Ed.* **1966**, *5*, 899.

20. [(2,6-(2,6-^{i}Pr$_2$-C$_6$H$_3$)C$_6$H$_3$)Cr]$_2$(μ-η^3,η^4-COT): Boynton, J. N.; Summerscales, O. T.; Grandjean, F.; Long, G. J.; Fettinger, J. C.; Power, P. P. *Organometallics* **2012**, *31*, 8559-8560.

21. Farmery, K.; Kilner, M.; Greatrex, R.; Greenwood, N. N. *J. Chem. Soc. A* **1969**, 2339-2345.

22. Dickson, D. P. E.; Berry, F. J. Mössbauer Spectroscopy; Cambridge University Press: Trowbridge, Great Britain, **1986**.

23. Hanson, A. W. *Acta Cryst.* **1962**, *15*, 930-933.

24. Calvo, R.; Isaacson, R. A.; Paddock, M. L.; Abresch,E. C.; Okamura,M. Y.; Maniero, A. L.; Brunel, L. C.; Feher G. *J. Phys. Chem. B.* **2001**, *105*, 4053-4057.

25. Klärner, F.-G. *Angew. Chem. Int. Ed.* **2001**, *40*, 3977-3981, and references therein.

26. Stratman, R. E.; Scuseria, G. E.; Frisch, M. J. *J. Chem. Phys.* **1998**, *109*, 8218-8224.

27. Römelt, M.; Ye, S.; Neese, F. *Inorg. Chem.* **2009**, *48*, 784-785.

28. Lavallo, V.; Grubbs, R. H. *Science* **2009**, *326*, 559-562.

29. Ben-Daat, H.; Hall, G. B.; Groy, T. L.; Trovitch, R. J. *Eur. J. Inorg. Chem.* **2013**, 4430-4442.

30. Pal, R.; Groy, T. L.; Bowman, A. C.; Trovitch, R. J. *Inorg. Chem.* **2014**, *53*, 9357-9365.

31. (a) Albright, T. A.; Burdett, J. K.; Whangbo, M.-H. *Orbital Interaction in Chemistry*; John Wiley & Sons: New York, **1985**, pp. 343-347. (b) Albright, T. A.; Burdett, J. K. *Problems in Molecular Orbital Theory*; Oxford University Press, New York, **1992**, pp. 205-206.

32. (a) King, R. B.; Kapoor, P. N.; Kapoor, R. N. *Inorg. Chem.* **1971**, *10*, 1841-1850. (b) Schaefer, B. A.; Margulieux, G.; Small, B. L.; Chirik, P. J. *Organometallics* **2015**, *34*, 1307-1320.

33. Mukhopadhyay, T. K.; Groy, T. L.; Smythe, N. C.; Gordon, J. C.; Trovitch, R. J. *J. Coord. Chem.* DOI: 10.1080/00958972.2016.1191631.

34. (a) Abragam, A.; Bleaney, B. *Electron Paramagnetic Resonance of Transition Ions.* Clarendon Press: Oxford, Great Britain, 1970; Chapter 9. (b) Bencini, A.; Gatteschi, D. *Electron Paramagnetic Resonance of Exchange Coupled Systems;* Springer: Berlin, 1990; Chapter 3. (c) Eaton, G. R.; Eaton, S. S. *In Biological Magnetic Resonance*; Berliner, L. J., Reuben, J., Eds.; Plenum: New York, 1989; Vol. 8, pp 339−396. (d) Stoll, S.; Schweiger, A. *J. Magn. Reson.* **2006**, *178*, 42−55.

35. Frisch, M. J.; Trucks, G. W.; Schlegel, H. B.; Scuseria, G. E.; Robb, M. A.; Cheeseman, J. R.; Scalmani, G.; Barone, V.; Mennucci, B.; Petersson, G. A.; Nakatsuji, H.; Caricato, M.; Li, X.; Hratchian, H. P.; Izmaylov, A. F.; Bloino, J.; Zheng, G.; Sonnenberg, J. L.; Hada, M.; Ehara, M.; Toyota, K.; Fukuda, R.; Hasegawa, J.; Ishida, M.; Nakajima, T.; Honda, Y.; Kitao, O.; Nakai, H.; Vreven, T.; Montgomery, Jr., J. A.; Peralta, J. E.; Ogliaro, F.; Bearpark, M.; Heyd, J. J.; Brothers, E.; Kudin, K. N.; Staroverov, V. N.; Kobayashi, R.; Normand, J.; Raghavachari, K.; Rendell, A.; Burant, J. C.; Iyengar, S. S.; Tomasi, J.; Cossi, M.; Rega, N.; Millam, J. M.; Klene, M.; Knox, J. E.; Cross, J. B.; Bakken, V.; Adamo, C.; Jaramillo, J.; Gomperts, R.; Stratmann, R. E.; Yazyev, O.; Austin, A. J.; Cammi, R., Pomelli, C.; Ochterski; J. W.; Martin, R. L.; Morokuma, K.; Zakrzewski, V. G.; Voth, G. A.; Salvador, P.; Dannenberg, J. J.; Dapprich, S.; Daniels, A. D.; Farkas, O.; Foresman, J. B., Ortiz, J. V.; Cioslowski, J.; Fox, D. J. Gas *Gaussian 09 Revision B.01*, Wallingford, CT, Gaussian Inc., 2009.

36. Neese, F. *WIREs Comput. Mol. Sci.* **2012**, *2*, 73-78.

37. Perdew, J. P.; Burke, K.; Ernzerhof, M. *Phys. Rev. Lett.* **1996**, *77*, 3865-3868.

38. Roy, L. E.; Hay, J.; Martin, R. L. *J. Chem. Theory Comput.* **2008**, *4*, 1029-1031.

39. Becke, A. D. *J. Chem. Phys.* **1993**, *98*, 5648-5652.

BIBILIOGRAPHY

Chapter 1

1. Role of homogeneous precious metal catalysts: (a) Chirik, P. J.; Wieghardt, K. *Science.* **2010**, *327*, 794-795. (b) Osborn, J. A.; Jardine, F. H.; Young, J. F.; Wilkinson, G. *J. Chem. Soc. A* **1966**, 1711-1732. (c) Yi, C. S.; Lee, D. W. *Organometallics* **1999**, *18*, 5152-5156. (d) Speier, J. L.; Webster, J. A.; Barnes, G. H. *J. Am. Chem. Soc.* **1957**, *79*, 974−979. (e) Troegel, D.; Stohrer, J. *Coord. Chem. Rev.* **2011**, *255*, 1440–1459. (f) Vougioukalakis, G. C.; Grubbs, R. H. *Chem. Rev.* **2010**, *110*, 1746-1787. (g) Nicolaou, K. C.; Bulger, P. G.; Sarlah, D. *Angew. Chem. Int. Ed.* **2005**, *44*, 4442-4489. (h) Beletskaya, I. P.; Cheprakov, A. V.; *Chem. Rev.* **2000**, *100*, 3009-3066.

2. (a) Junge, K.; Schröder, K.; Beller, M. *Chem. Commun.* **2011**, *47*, 4849−4859. (b) Le Bailly, B. A. F.; Thomas, S. P. *RSC Adv.* **2011**, *1*, 1435. (c) Bullock, R. M. *Catalysis without Precious Metals*; Wiley-VCH: Weinheim, Germany, **2010**. (d) Gosmini, C.; Beǵouin, J.-M.; Moncomble, A. *Chem. Commun.* **2008**, 3221−3233. (e) Gaillard, S.; Renaud, J.-L. *ChemSusChem* **2008**, *1*, 505−509. (f) Enthaler, S.; Junge, K.; Beller, M. *Angew. Chem. Int. Ed.* **2008**, *47*, 3317.

3. (a) Luca O. R.; Crabtree, R. H. *Chem. Soc. Rev.* **2013**, *42*, 1440-1459. (b) Chirik P. J.; Wieghardt, K. *Science* **2010**, *327*, 794-795.

4. (a) Stubbert, B. D.; Peters, J. C.; Gray, H. B. *J. Am. Chem. Soc.*, **2011**, *133*, 18070. (b) Luca, O. R.; Konezny, S. J.; Blakemore, J. D.; Saha, S.; Colosi, D. M.; Brudvig, G. W.; Batista, V. S.; Crabtree, R. H. *New J. Chem.*, **2012**, *36*, 1149. (c) Chaudhuri, P.; Hess, M.; Mu˙ller, J.; Hildenbrand, K.; Bill, E.; Weyhermüller, T.; Wieghardt, K. *J. Am. Chem. Soc.* **1999**, *121*, 9599.

5. Gibson, V. C.; Redshaw, C.; Solan, G. A. *Chem. Rev.* **2007**, *107*, 1745-1776.

6. (a) Small, B. L.; Brookhart, M.; Bennett, A. M. A. *J. Am. Chem. Soc.* **1998**, *120*, 4049-4050. (b) Britovsek, G. J. P.; Gibson, V. C.; Kimberley, B. S.; Maddox, P. J.; McTavish, S. J.; Solan, G. A.; White, A. J. P.; Williams, D. J. *Chem. Commun.* **1998**, 849-850.

7. (a) Bart, S. C.; Lobkovsky, E.; Bill, E.; Chirik, P. J. *J. Am. Chem. Soc.* **2004**, *126*, 13794-13807. (b) Trovitch, R. J.; Lobkovsky, E.; Bill, E.; Chirik, P. J. *Organometallics* **2008**, *27*, 1470. (c) Sylvester, K. T.; Chirik, P. J. *J. Am. Chem. Soc.* **2009**, *131*, 8772-8774. (d) Hoyt, J. M.; Schmidt, V. A.; Tondreau, A. M.; Chirik, P. J. *Science,* **2015**, *349*, 960-963.

8. (a) de Bruin, B.; Bill, E.; Bothe, E.; Weyhermüller, T.; Wieghardt, K. *Inorg. Chem.* **2000**, *39*, 2936-2947. (b) Knijnenburg, Q.; Gambarotta, S.; Budzelaar, P. H. M. *Dalton Trans.* **2006**, 5442-5448.

9. (a) Jørgensen, C. K. *Coord. Chem. Rev.*, **1966**, *1*, 164.   (b) Baker-Hawkes, M. J.; Billig, E.; Gray, H. B. *J. Am. Chem.   Soc*., **1966**, *88*, 4870-4875.

10. (a) Ben-Daat, H.; Hall, G. B.; Groy, T. L.; Trovitch, R. J. *Eur. J. Inorg. Chem.* **2013**, 4430−4442. (b) Pal, R.; Groy, T. L.; Bowman, A. C.; Trovitch, R. J. *Inorg. Chem.* **2014**, *53*, 9357-9365.

11. (a) Knijnenburg, Q.; Gambarotta, S.; Budzelaar, P. H. M. *Dalton Trans.* **2006**, 5442-5448. (b) Chirik, P. J.; Wieghardt, K. *Science* **2010**, *327*, 794-795.

12. (a) Valyaev, D. A.; Lavigne, G.; Lugan, N. *Coord. Chem. Rev.* **2016**, *308*, 191-235. (b) Trovitch, R. J. *Synlett* **2014**, *25*, 1638−1642.

13. (a) Zhang, W.; Loebach, J. L.; Wilson, S. R.; Jacobsen, E. N. *J. Am. Chem. Soc.* **1990**, *112*, 2801-2803. (b) Cavanaugh, M. D.; Gregg, B. T.; Cutler, A. R. *Organometallics* **1996**, *15*, 2764-2769. (c) Sampson, M. D.; Nguyen, A. D.; Grice, K. A.; Moore, C. E.; Rheingold, A. L.; Kubiak, C. P. *J. Am. Chem. Soc.* **2014**, *136*, 5460-5471.

14. Reardon, D.; Aharonian, G.; Gambarotta, S.; Yap, G. P. A. *Organometallics* **2002**, *21*, 786-788.

15. B. Cordero, V. Gómez, A. E. Platero-Prats, M. Revés, J. Echeverría, E. Cremades, F. Barragán, S. Alvarez, *Dalton Trans.* **2008**, 2832-2838.

16. Russell, S. K.; Bowman, A. C.; Lobkovsky, E.; Wieghardt, K.; Chirik, P. J. Eur. J. *Inorg. Chem.* **2012**, *2012*, 535−545.

17. (a) (37) Weil, J. A.; Bolton, J. R. Electron paramagnetic resonance: Elementary theory and practical applications; Wiley: Hoboken, NJ, **2007**. (b) Rieger, P. H. *Coord. Chem. Rev.* **1994**, *135/136*, 203−286.

Chapter 2

1. (a) Marciniec, B. *Hydrosilylation: A Comprehensive review on recent advances*. Springer, Berlin, Germany, **2010**. (b) Marciniec, B.; Guliñski, J. *J. Orgmet. Chem.* **1993**, *446*, 15-23. (c) Shaikh, N. S.; Junge, K.; Beller, M. *Org. Lett.* **2007**, *9*, 5429-5432.

2. (a) Enthaler, S.; Junge, K.; Beller, M. *Angew. Chem. Int. Ed.* **2008**, *47*, 3317-3321. (b) Troegel, D.; Stohrer, J. *Coord. Chem. Rev.* **2011**, *255*, 1440-1450. (c) Díez-González, S.; Nolan, S. P. *Org. Prep. Proc. Int.* **2007**, *39*, 523-529. (d) Shaikh, N. S.; Enthaler, S.; Junge, K.; Beller, M. *Angew. Chem. Int. Ed.* **2008**, *47*, 2497-2501.

3. (a) Speier, J. L. *Adv. Orgmet. Chem.* **1979**, *17*, 407-447. (b) Chatterjee, B.; Gunanathan, C. *Chem. Commun.* **2014**, *50*, 888-890. (c) Lewis, L. N.; Stein, J.; Gao, Y. Colborn, R. E.; Hutchins, G. *Platinum Metals Rev.* **1997**, *41*, 66-75. (d) Karstedt, B. D.

Platinum Complexes of Unsaturated Siloxanes and Platinum Containing Organopolysiloxanes. **1973**.

4. For leading Fe catalysts see: (a) Ruddy, A. J.; Kelly, C. M.; Crawford, S. M.; Wheaton, C. A.; Sydora, O. L.; Small, B. L.; Stradiotto, M.; Turculet, L. *Organometallics* **2013**, *32*, 5581−5588. (b) Yang, J.; Tilley, T. D. *Angew. Chem., Int. Ed*. **2010**, *49*, 10186−10188. (c) Blom, B.; Enthaler, S.; Inoue, S.; Irran, E.; Driess, M. *J. Am. Chem. Soc*. **2013**, *135*, 6703−6713. (c) Bhattacharya, P.; Krause, J. A.; Guan, H. *Organometallics* **2011**, *30*, 4720−4729. (e) Kandepi, V. V. K. M.; Cardoso, J. M. S.; Peris, E.; Royo, B. *Organometallics* **2010**, *29*, 2777−2782. (f) Tondreau, A. M.; Darmon, J. M.; Wile, B. M.; Floyd, S. K.; Lobkovsky, E.; Chirik, P. J. *Organometallics* **2009**, *28*, 3928− 3940. (g) Tondreau, A. M.; Lobkovsky, E.; Chirik, P. J. *Org. Lett*. **2008**, *10*, 2789−2792.

5. For leading Co examples, see: (a) Zhou, H.; Sun, H.; Zhang, S.; Li, X. *Organometallics* **2015**, *34*, 1479−1486. (b) Niu, Q.; Sun, H.; Li, X.; Klein, H.-F.; Flörke, U. *Organometallics* **2013**, *32*, 5235−5238. (c) Sauer, D. C.; Wadepohl, H.; Gade, L. H. *Inorg. Chem*. **2012**, *51*, 12948−12958. (d) Yu, F.; Zhang, X.-C.; Wu, F.-F.; Zhou, J.-N.; Fang, W.; Wu, J.; Chan, A. S. C. *Org. Biomol. Chem*. **2011**, *9*, 5652. (e) Brunner, H.; Amberger, K. J. *Organomet. Chem*. **1991**, *417*, C63− C65. (f) Nesbit, M. A.; Suess, D. L. M.; Peters, J. C. *Organometallics* **2015**, *34*, 4741.

6. For leading Ni examples, see: (a) Porter, T. M.; Hall, G. B.; Groy, T. L.; Trovitch, R. J. *Dalton Trans*. **2013**, *42*, 14689−14692. (b) Bheeter, L. P.; Henrion, M.; Brelot, L.; Darcel, C.; Chetcuti, M. J.; Sortais, J.-B.; Ritleng, V. *Adv. Synth. Catal*. **2012**, *354*, 2619−2624. (c) Postigo, L.; Royo, B. *Adv. Synth. Catal*. **2012**, *354*, 2613−2618. (d) Tran, B. L.; Pink, M.; Mindiola, D. J. *Organometallics* **2009**, *28*, 2234−2243. (e) Chakraborty, S.; Krause, J. A.; Guan, H. *Organo- metallics* **2009**, *28*, 582−586 and references cited therein. (f) MacMil- lan, S. N.; Hill Harman, W.; Peters, J. C. *Chem. Sci*. **2014**, *5*, 590−597. (g) Steiman, T. J.; Uyeda, C. *J. Am. Chem. Soc*. **2015**, *137*, 6104−6110.

7. For leading Cu examples, see: (a) Roy, S. R.; Sau, S. C.; Mandal, S. K. *J. Org. Chem*. **2014**, *79*, 9150−9160. (b) Albright, A.; Gawley, R. E. *J. Am. Chem. Soc*. **2011**, *133*, 19680−19683. (c) Yu, F.; Zhou, J.-N.; Zhang, X.-C.; Sui, Y.-Z.; Wu, F.-F.; Xie, L.-J.; Chan, A. S. C.; Wu, J. *Chem. - Eur. J*. **2011**, *17*, 14234−14240. (d) Zhang, X.-C.; Wu, F.-F.; Li, S.; Zhou, J.-N.; Wu, J.; Li, N.; Fang, W.; Lam, K. H.; Chan, A. S. C. *Adv. Synth. Catal*. **2011**, *353*, 1457−1462. (e) Díez-Gonza ́lez, S.; Escudero-Adań,E.;Benet-Buchholz,J.;Stevens,E.D.;Slawin,A.M. Z.; Nolan, S. P. *Dalton Trans*. **2010**, *39*, 7595−7606. (f) Fujihara, T.; Semba, K.; Terao, J.; Tsuji, Y. *Angew. Chem., Int. Ed*. **2010**, *49*, 1472− 1476. (g) Mostefaï, N.; Sirol, S.; Courmarcel, J.; Riant, O. *Synthesis* **2007**, 1265−1271.(h) Díez-Gonza ́lez, S.;Scott, N.M.;Nolan, S. P. Organometallics **2006**, 25, 2355−2358. (i) Lipshutz, B. H.; Lower, A.; Kucejko, R. J.; Noson, K. *Org. Lett*. **2006**, *8*, 2969−2972. (j) Díez- Gonza ́lez, S.; Kaur, H.; Zinn, F. K.; Stevens, E. D.; Nolan, S. P. *J. Org. Chem*. **2005**, *70*, 4784−4796. (k) Wu, J.; Ji, J.-X.; Chan, A. S. C. *Proc. Natl. Acad. Sci. U. S. A*. **2005**, *102*, 3570−3575. (l) Lee, D.; Yun, J. *Tetrahedron Lett*. **2004**, *45*, 5415−5417. (m) Kaur, H.; Zinn, F. K.; Stevens, E. D.; Nolan, S. P. *Organometallics*

2004, *23*, 1157−1160. (n) Lipshutz, B. H.; Noson, K.; Chrisman, W.; Lower, A. *J. Am. Chem. Soc.* **2003**, *125*, 8779−8789. (o) Lipshutz, B. H.; Noson, K.; Chrisman, W. *J. Am. Chem. Soc.* **2001**, *123*, 12917−12918. (p) Sirol, S.; Courmarcel, J.; Mostefai, N.; Riant, O. *Org. Lett.* **2001**, *3*, 4111−4113. (q) Brunner, H.; Miehling, W. *J. Organomet. Chem.* **1984**, *275*, C17− C21.

8. For leading Zn catalysts, see: (a) Rit, A.; Zanardi, A.; Spaniol, T. P.; Maron, L.; Okuda, J. *Angew. Chem., Int. Ed.* **2014**, *53*, 13273− 13277. (b) Lummis, P. A.; Momemi, M. R.; Lui, M. W.; McDonald, R.; Ferguson, M. J.; Miskolzie, M.; Brown, A.; Rivard, E. *Angew. Chem., Int. Ed.* **2014**, *53*, 9347−9351. (c) Łowicki, D.; Bezłada, A.; Mlynarski, J. *Adv. Synth. Catal.* **2014**, *356*, 591−595. (d) Boone, C.; Korobkov, I.; Nikonov, G. I. *ACS Catal.* **2013**, *3*, 2336−2340. (e) Pang, S.; Peng, J.; Li, J.; Bai, Y.; Xiao, W.; Lai, G. *Chirality* **2013**, *25*, 275−280. (f) Enthaler, S.; Schröder, K.; Inoue, S.; Eckhardt, B.; Junge, K.; Beller, M.; Drieβ, M. *Eur. J. Org. Chem.* **2010**, *2010*, 4893−4901. (g) Gajewy, J.; Kwit, M.; Gawroński, J. *Adv. Synth. Catal.* **2009**, *351*, 1055−1063. (h)Geŕard, S.; Pressel, Y.; Riant, O. *Tetrahedron: Asymmetry* **2005**, *16*, 1889−1891. (i) Bette, V.; Mortreux, A.; Savoia, D.; Carpentier, J.-F. *Adv. Synth. Catal.* **2005**, *347*, 289−302. (j) Bette, V.; Mortreux, A.; Savoia, D.; Carpentier, J.-F. *Tetrahedron* **2004**, *60*, 2837−2842. (k) Mastranzo, V. M.; Quintero, L.; Anaya de Parrodi, C. A.; Juaristi, E.; Walsh, P. J. *Tetrahedron* **2004**, *60*, 1781−1789. (l) Mimoun, H. *J. Org. Chem.* **1999**, *64*, 2582−2589. (m) Sattler, W.; Ruccolo, S.; Rostami Chaijan, M.; Nasr Allah, T.; Parkin, G. *Organometallics* **2015**, *34*, 4717.

9. (a) R. I. Khusnutdinov, A. R. Bayguzina, U. M. Dzhemilev, *Russ. J. Org. Chem.* **2012**, *48*, 309-348. (b) R. J. Trovitch, *Synlett* **2014**, *25*, 1638-1642. (c) Valyaev, D. A.; Lavigne, G.; Lugan, N. *Coord. Chem. Rev.* **2016**, *308*, 191-235.

10. B. T. Gregg, P. K. Hanna, E. J. Crawford, A. R. Cutler, *J. Am. Chem. Soc.* **1991**, *113*, 384-385.

11. (a) M. B. Cavanaugh, B. T. Gregg, A. R. Cutler, *Organometallics* **1996**, *15*, 2764-2769. (b) Z. Mao, B. T. Gregg, A. R. Cutler, *J. Am. Chem. Soc.* **1995**, *117*, 10139-10140.

12. S. U. Son, S-J. Paik, I. S. Lee, Y-A. Lee, Y. K. Chung, *Organometallics* **1999**, *18*, 4114-4118.

13. S. U. Son, S-J. Paik, Y. K. Chung, *J. Molecular Cat. A: Chem.* **2007**, *151*, 87-90.

14. V. K. Chidara, G. Du, *Organometallics* **2013**, *32*, 5034-5037.

15. Mukhopadhyay, T. K.; Flores, M.; Groy, T. L.; Trovitch, R. J. *J. Am. Chem. Soc.* **2014**, *136*, 882-885.

16. Ghosh, C; Mukhopadhyay, T. K.; Flores, M.; Groy, T. L.; Trovitch, R. J. *Inorg. Chem.* **2015**, *54*, 10398-10406.

17. Mukhopadhyay, T. K.; Groy, T. L.; Trovitch, R. J. *J. Am. Chem. Soc. (manuscript in preparation).*

18. LeBlanc, F. A.; Piers, W.; Parvez, M. *Angew. Chem., Int. Ed.* **2014**, *53*, 789−792.

19. Berk, S. C.; Kreutzer, K. A.; Buchwald, S. L. *J. Am. Chem. Soc.* **1991**, *113*, 5093−5095.

20. Le Bideau, F.; Henique, J.; Samuel, E.; Elschenbroich, C. *Chem. Commun.* **1999**, 1397−1398.

Chapter 3

1. For early hydrosilylation reviews see (a) Speier, J. L. *Adv. Organomet. Chem.* **1979**, *17*, 407-447. (b) Ojima, I. *Chem. Org. Silicon Compd.* **1989**, *2*, 1479-1526.

2. Speier, J. L.; Webster, J. A.; Barnes, G. H. *J. Am. Chem. Soc.* **1957**, *79*, 974-979.

3. Troegel, D.; Stohrer, J. *Coord. Chem. Rev.* **2011**, *255*, 1440-1459.

4. Chalk, A. J.; Harrod, J. F. *J. Am. Chem. Soc.* **1965**, *87*, 16-21.

5. Maruyama, Y.; Yamamura, K.; Nakayama, I.; Yoshiuchi, K.; Ozawa, F. *J. Am. Chem. Soc.* **1998**, *120*, 1421-1429, and references therein.

6. For leading examples see: (a) Deutsch, C.; Krause, N.; Lipshutz, B. H. *Chem. Rev.* **2008**, *108*, 2916-2927. (b) Morris, R. H. *Chem. Soc. Rev.* **2009**, *38*, 2282-2291. (c) Riener, K.; Högerl, M. P.; Gigler, P.; Kühn, F. E. *ACS Catal.* **2012**, *2*, 613-621. (d) Bleith, T.; Wadepohl, H.; Gade, L. H. *J. Am. Chem. Soc.* **2015**, *137*, 2456-2459.

7. Osborn, J. A.; Jardine, F. H.; Young, J. F.; Wilkinson, G. *J. Chem. Soc. A* **1966**, 1711-1732.

8. (a) Ojima, I.; Nihonyanagi, M.; Kogure, T.; Kumagai, M.; Horiuchi, S.; Nakatsugawa, K. *J. Organomet. Chem.* **1975**, *94*, 449-461. (b) Reyes, C.; Prock, A.; Giering, W. P. *Organometallics* **2002**, *21*, 546-554.

9. (a) Schneider, N.; Finger, M.; Haferkemper, C.; Bellemin-Laponnaz, S.; Hofmann, P.; Gade, L. H. *Angew. Chem. Int. Ed.* **2009**, *48*, 1609-1613. (b) Schneider, N.; Finger, M.; Haferkemper, C.; Bellemin-Laponnaz, S.; Hofmann, P.; Gade, L. H. *Chem.-Eur. J.* **2009**, *15*, 11515-11529.

10. (a) Gutsulyak, D. M.; Vyboishchikov, S. F.; Nikonov, G. I. *J. Am. Chem. Soc.* **2010**, *132*, 5950-5951. (b) Park, S.; Brookhart, M. *Organometallics* **2010**, *29*, 6057-6064. (c) Lipke, M. C.; Tilley, T. D. *J. Am. Chem. Soc.* **2014**, *136*, 16387-16398.

226

11. For first-row metal alkene hydrosilylation catalysts see: (a) Tondreau, A. M.; Atienza, C. C. H.; Weller, K. J.; Nye, S. A.; Lewis, K. M.; Delis, J. G. P.; Chirik, P. J. *Science* **2012**, *335*, 567-570. (b) Atienza, C. C. H.; Tondreau, A. M.; Weller, K. J.; Lewis, K. M.; Cruse, R. W.; Nye, S. A.; Boyer, J. L.; Delis, J. G. P.; Chirik, P. J. *ACS Catal*. **2012**, *2*, 2169-2172. (c) Tondreau, A. M.; Atienza, C. C. H.; Darmon, J. M.; Milsmann, C.; Hoyt, H. M.; Weller, K. J.; Nye, S. A.; Lewis, K. M.; Boyer, J.; Delis, J. G. P.; Lobkovsky, E.; Chirik, P. J. *Organometallics* **2012**, *31*, 4886-4893. (d) Peng, D.; Zhang, Y.; Du, X.; Zhang, L.; Leng, X.; Walter, M. D.; Huang, Z. *J. Am. Chem. Soc.* **2013**, *135*, 19154-19166. (e) Srinivas, V.; Nakajima, Y.; Ando, W.; Sato, K.; Shimada, S. *Catal. Sci. Tech.* **2015**, *5*, 2081-2084. (f) Chen, J.; Cheng, B.; Cao, M.; Lu, Z. *Angew. Chem. Int. Ed.* **2015**, *54*, 4661-4664. (g) Steinman, T. J.; Uyeda, C. *J. Am. Chem. Soc.* **2015**, *137*, 6104-6110. (h) Sunada, Y.; Noda, D.; Soejima, H.; Tsutsumi, H.; Nagashima, H. *Organometallics* **2015**, *34*, 2896-2906. (i) Buslov, I.; Becouse, J.; Mazza, S.; Montandon-Clerc, M.; Hu, X. *Angew. Chem. Int. Ed.* **2015**, *54*, 14523-14526. (j) Chen, C.; Hect, M. B.; Kavara, A.; Brennessel, W. W.; Mercado, B. Q.; Weix, D. J.; Holland, P. L. *J. Am. Chem. Soc.* **2015**, *137*, 13244-13247. (k) Noda, D.; Tahara, A.; Sunada, Y.; Nagashima, H. *J. Am. Chem. Soc.* **2016**, *138*, 2480-2483.

12. For leading Fe carbonyl hydrosilylation catalysts see: (a) Tondreau, A. M.; Lobkovsky, E.; Chirik, P. J. *Org. Lett.* **2008**, *10*, 2789-2792. (b) Tondreau, A. M.; Darmon, J. M.; Wile, B. M.; Floyd, S. K.; Lobkovsky, E.; Chirik, P. J. *Organometallics* **2009**, *28*, 3928-3940. (c) Kandepi, V. V. K. M.; Cardoso, J. M. S.; Peris, E.; Royo, B. *Organometallics* **2010**, *29*, 2777-2782. (d) Yang, J.; Tilley, T. D. *Angew. Chem. Int. Ed.* **2010**, *49*, 10186-10188. (e) Bhattacharya, P.; Krause, J. A.; Guan, H. *Organometallics* **2011**, *30*, 4720-4729. (f) Ruddy, A. J.; Kelly, C. M.; Crawford, S. M.; Wheaton, C. A.; Sydora, O. L.; Small, B. L.; Stradiotto, M.; Turculet, L. *Organometallics* **2013**, *32*, 5581-5588. (g) Blom, B.; Enthaler, S.; Inoue, S.; Irran, E.; Driess, M. *J. Am. Chem. Soc.* **2013**, *135*, 6703-6713. (h) Bleith, T.; Gade, L. H. *J. Am. Chem. Soc.* **2016**, *ASAP*.

13. For leading Co carbonyl hydrosilylation catalysts see: (a) Brunner, H.; Amberger, K. *J. Organomet. Chem.* **1991**, *417*, C63-C65. (b) Yu, F.; Zhang, X.-C.; Wu. F.-F.; Zhou, J.-N.; Fang, W.; Wu, J.; Chan, A. S. C. *Org. Biomol. Chem.* **2011**, *9*, 5652. (c) Sauer, D. C.; Wadepohl, H.; Gade, L. H. *Inorg. Chem.* **2012**, *51*, 12948-12958. (d) Niu, Q.; Sun, H.; Li, X.; Klein, H.-F.; Flörke, U. *Organometallics* **2013**, *32*, 5235-5238. (e) Zhou, H.; Sun, H.; Zhang, S.; Li, X. *Organometallics* **2015**, *34*, 1479-1486. (f) Nesbit, M. A.; Suess, D. L. M.; Peters, J. C. *Organometallics* **2015**, *34*, 4741-4752.

14. For leading Ni carbonyl hydrosilylation catalysts see: (a) Chakraborty, S.; Krause, J. A.; Guan, H. *Organometallics* **2009**, *28*, 582-586, and references therein. (b) Tran, B. L.; Pink, M.; Mindiola, D. J. *Organometallics* **2009**, *28*, 2234-2243. (c) Postigo, L.; Royo, B. *Adv. Synth. Catal.* **2012**, *354*, 2613-2618. (d) Bheeter, L. P.; Henrion, M.; Brelot, L.; Darcel, C.; Chetcuti, M. J.; Sortais, J.-B.; Ritling, V. *Adv. Synth. Catal.* **2012**, *354*, 2619-2624. (e) Porter, T. M.; Hall, G. B.; Groy, T. L.; Trovitch, R. J. *Dalton Trans*. **2013**, *42*, 14689-14692. (f) MacMillan, S. N.; Harman, W. H.; Peters, J. C. *Chem. Sci.* **2014**, *5*, 590-597.

15. For leading Cu carbonyl hydrosilylation catalysts see: (a) Brunner, H.; Miehling, W. *J. Organomet. Chem.* **1984**, *275*, C17-C21. (b) Sirol, S.; Courmarcel, J.; Mostefai, N.; Riant, O. *Org. Lett.* **2001**, *3*, 4111-4113. (c) Lipshutz, B. H.; Noson, K.; Chrisman, W. *J. Am. Chem. Soc.* **2001**, *123*, 12917-12918. (d) Lipshutz, B. H.; Noson, K.; Chrisman, W.; Lower, A. *J. Am. Chem. Soc.* **2003**, *125*, 8779-8789. (e) Kaur, H.; Zinn, F. K.; Stevens, E. D.; Nolan, S. P. *Organometallics* **2004**, *23*, 1157-1160. (f) Lee, D.; Yun, J. *Tetrahedron Lett.* **2004**, 5415-5417. (g) Wu, J.; Ji, J.-X.; Chan, A. S. C. *Proc. Natl. Acad. Sci., U.S.A.* **2005**, *102*, 3570-3575. (h) Díez-González, S.; Kaur, H.; Zinn, F. K.; Stevens, E. D.; Nolan, S. P. *J. Org. Chem.* **2005**, *70*, 4784-4796. (i) Díez-González, S.; Scott, N. M.; Nolan, S. P. *Organometallics* **2006**, *25*, 2355-2358. (j) Lipshutz, B. H.; Lower, A.; Kucejko, R. J.; Noson, K. *Org. Lett.* **2006**, *8*, 2969-2972. (k) Mostefaï, N.; Sirol, S.; Courmarcel, J.; Riant, O. *Synthesis* **2007**, *8*, 1265-1271. (l) Fujihara, T.; Semba, K.; Terao, J.; Tsuji, Y. *Angew. Chem. Int. Ed.* **2010**, *49*, 1472-1476. (m) Díez-González, S.; Escudero-Adán, E.; Benet-Buchholtz, J.; Stevens, E. D.; Slawin, A. M. Z.; Nolan, S. P. *Dalton Trans.* **2010**, *39*, 7595-7606. (n) Zhang, X.-C.; Wu, F.-F.; Li, S.; Zhou, J.-N.; Wu, J.; Li, N.; Fang, W.; Lam, K. H.; Chan, A. S. C. *Adv. Synth. Catal.* **2011**, *353*, 1457-1462. (o) Yu, F.; Zhou, J.-N.; Zhang, X.-C.; Sui, Y.-Z.; Wu, F.-F.; Xie, L.-J.; Chan, A. S. C.; Wu, J. *Chem. Eur. J.* **2011**, *17*, 14234-14240. (p) Albright, A.; Gawley, R. E. *J. Am. Chem. Soc.* **2011**, *133*, 19680-19683. (q) Roy, S. R.; Sau, S. C.; Mandal, S. K. *J. Org. Chem.* **2014**, *79*, 9150-9160.

16. For leading Zn carbonyl hydrosilylation catalysts see: (a) Mimoun, H. *J. Org. Chem.* **1999**, *64*, 2582-2589. (b) Mastranzo, V. M.; Quintero, L.; de Parrodi, C. A.; Juaristi, E.; Walsh, P. J. *Tetrahedron* **2004**, *60*, 1781-1789. (c) Bette, V.; Mortreux, A.; Savoia, D.; Carpentier, J.-F. *Tetrahedron* **2004**, *60*, 2837-2842. (d) Bette, V.; Mortreux, A.; Savoia, D.; Carpentier, J.-F. *Adv. Synth. Catal.* **2005**, *347*, 289-302. (e) Gérard, S.; Pressel, Y.; Riant, O. *Tetrahedron: Asym.* **2005**, *16*, 1889-1891. (f) Gajewy, J.; Kwit, M.; Gawroński, J. *Adv. Synth. Catal.* **2009**, *351*, 1055-1063. (g) Enthaler, S.; Schröder, K.; Inoue, S.; Eckhardt, B.; Junge, K.; Beller, M.; Drieβ, M. *Eur. J. Org. Chem.* **2010**, 4893-4901. (h) Pang, S.; Peng, J.; Li, J.; Bai, Y.; Xiao, W.; Lai, G. *Chirality* **2013**, *25*, 275-280. (i) Boone, C.; Korobkov, I.; Nikonov, G. I. *ACS Catal.* **2013**, *3*, 2336-2340. (j) Łowicki, D.; Bezłada, A.; Mlynarski, J. *Adv. Synth. Catal.* **2014**, *356*, 591-595. (k) Lummis, P. A.; Momemi, M. R.; Lui, M. W.; McDonald, R.; Ferguson, M. J.; Miskolzie, M.; Brown, A.; Rivard, E. *Angew. Chem. Int. Ed.* **2014**, *53*, 9347-9351. (l) Rit, A.; Zanardi, A.; Spaniol, T. P.; Maron, L.; Okuda, J. *Angew. Chem. Int. Ed.* **2014**, *53*, 13273-13277. (m) Sattler, W.; Ruccolo, S.; Chaijan, M. R.; Allah, T. N.; Parkin, G. *Organometallics* **2015**, 34, 4717-4731.

17. (a) Enthaler, S.; Junge, K; Beller, M. *Angew. Chem. Int. Ed.* **2008**, *47*, 3317-3321. (b) Plietker, B. *Iron Catalysis in Organic Chemistry*; Wiley-VCH: Weinheim, Germany, **2008**.

18. Collman, J. P.; Hegedus, L. S.; Norton, J. R.; Finke, R. G. In *Principles and Applications of Organotransition Metal Chemistry*. University Science Books, Sausalito, CA, 1987, pp. 306-333.

19. In Metsänen, T. T.; Gallego, D.; Szilvási, T.; Driess, M.; Oestreich, M. *Chem Sci.* **2015**, *6*, 7143-7149, a peripheral mechanism which does not involve iron mediated organometallic pathways has been proposed. While the Ni and Zn catalysts described in refs 14a and 16m are believed to catalyze carbonyl hydrosilylation via insertion into M-H followed by Si-H σ-bond metathesis, the leading Co catalyst for this transformation (ref 13f) relies on borane-assisted Si-H activation and carbonyl insertion into the resulting Co-Si bond.

20. (a) Valyaev, D. A.; Lavigne, G.; Lugan, N. *Coord. Chem. Rev.* **2016**, 308, 191-235. (b) Trovitch, R. J. *Synlett* **2014**, *25*, 1638-1642.

21. (a) Igarashi, M.; Fuchikami, T. *Tetrahedron Lett.* **2001**, *42*, 1945-1947. (b) Zheng, J.; Chevance, S.; Darcel, C.; Sortais, J.-B. *Chem. Commun.* **2013**, *49*, 10010-10012.

22. (a) Mao, Z.; Gregg, B. T.; Cutler, A. R. *J. Am. Chem. Soc.* **1995**, *117*, 10139-10140. (b) Cavanaugh; M. D.; Gregg, B. T.; Cutler, A. R. *Organometallics* **1996**, *15*, 2764-2769. (c) Son, S. U.; Paik, S.-J.; Lee, I. S.; Lee, Y.-A.; Chung, Y. K.; Seok, W. K.; Lee, H. N. *Organometallics* **1999**, *18*, 4114-4118. (d) Son, S. U.; Paik, S.-J.; Chung, Y. K. *J. Mol. Catal. A: Chem.* **2000**, *151*, 87-90.

23. Ghosh, C.; Mukhopadhyay, T. K.; Flores, M.; Groy, T. L.; Trovitch, R. J. *Inorg. Chem.* **2015**, *54*, 10398-10406.

24. Chidara, V. K.; Du, G. *Organometallics* **2013**, *32*, 5034-5037.

25. Mukhopadhyay, T. K.; Flores, M.; Groy, T. L.; Trovitch, R. J. *J. Am. Chem. Soc.* **2014**, *136*, 882-885.

26. Zhou, W.; Marquard, S. L.; Bezpalko, M. W.; Foxman, B. M.; Thomas, C. M. *Organometallics* **2013,** *32*, 1766-1772.

27. Wang, Y.; Gu, P; Wang, W. Wei, H. *Catal. Sci. Technol.* **2014**, *4*, 43-46.

28. (a) Du, G.; Fanwick, P. E.; Abu-Omar, M. M. **2007**, *129*, 5180-5187. (b) Ison, E. A.; Trivedi, E. R.; Corbin, R. A.; Abu-Omar, M. M. **2005**, *127*, 15374-15375.

29. Pal, R.; Groy, T. L.; Bowman, A. C.; Trovitch, R. J. *Inorg. Chem.* 2014, *53*, 9357-9365.

30. Benkeser, R. A.; Landesman, H.; Foster, D. J. *J. Am. Chem. Soc.* **1952**, *74*, 648-650.

31. Ben-Daat, H.; Hall, G. B.; Groy, T. L.; Trovitch, R. J. *Eur. J. Inorg. Chem.* **2013**, 4430-4442.

Chapter 4

1. Walter, M. G.; Warren, E. L.; McKone, J. R.; Boettcher, S. W.; Mi, Q.; Santori, E. A.; Lewis, N. S. *Chem. Rev.* **2010**, *110*, 6446-6473.

2. (a) Gust, D.; Moore, T. A.; Moore, A. L. *Acc. Chem. Res.* **2009**, *42*, 1890-1898. (b) Gust, D.; Moore, T. A.; Moore, A. L. *Acc. Chem. Res.* **2001**, *34*, 40-48. (c) Gust, D.; Moore, T. A.; Moore, A. L. *Acc. Chem. Res.* **1993**, *26*, 198-205.

3. Nocera, D. G. *Acc. Chem. Res.* **2012**, *45*, 767-776.

4. For representative Fe catalysts see: (a) Roy S.; Mazinani, S. K. S.; Groy, T. L.; Gan, L.; Tarakeshwar, P.; Mujica, V.; Jones, A. K. *Inorg. Chem.* **2014**, *53*, 8919-8929. (b) Darmon, J. M.; Raugei, S.; Liu, T.; Hulley, E. B.; Weiss, C. J.; Bullock, R. M.; Helm, M. L. *ACS Catal.* **2014**, *4*, 1246-1260. (c) Gloaguen, F.; Rauchfuss, T. B. *Chem. Soc. Rev.* **2009**, *38*, 100-108.

5. For representative Co catalysts see: (a) McCrory, C. C. L.; Uyeda, C.; Peters, J. C. *J. Am. Chem. Soc.* **2012**, *134*, 3164-3170. (b) Dempsey, J. L.; Brunschwig, B. S.; Winkler, J. R.; Gray, H. B. *Acc. Chem. Res.* **2009**, *42*, 1995-2004. (c) Jacques, P.-A.; Artero, V.; Pécaut, J.; Fontecave, M. *Proc. Natl. Acad. Sci. U.S.A.* **2009**, *106*, 20627-20632. (d) Hu, X.; Brunschwig, B. S.; Peters, J. C. *J. Am. Chem. Soc.* **2007**, *129*, 8988-8998. (e) Artero, V.; Fontecave, M. *Coord. Chem. Rev.* **2005**, *249*, 1518-1535.

6. For representative Ni catalysts see: (a) Gan, L.; Groy, T. L.; Tarakeshwar, P.; Mazinani, S. K. S.; Shearer, J.; Mujica, V.; Jones, A. K. *J. Am. Chem. Soc.* **2015**, 137, 1109-1115. (b) Helm, M. L.; Stewart, M. P.; Bullock, R. M.; DuBois, M. R.; DuBois, D. L. *Science* **2011**, *333*, 863-866. (c) Kilgore, U. J.; Roberts, J. A. S.; Pool, D. H.; Appel, A. M.; Stewart, M. P.; DuBois, M. R.; Dougherty, W. G.; Kassel, W. S.; Bullock, R. M.; DuBois, D. L. *J. Am. Chem. Soc.* **2011**, *133*, 5861-5872. (d) Wilson, A. D.; Shoemaker, R. K.; Miedaner, A.; Muckerman, J. T.; DuBois, D. L.; DuBois, M. R. *Proc. Natl. Acad. Sci. U.S.A.* **2007**, *104*, 6951-6956. (e) Wilson, A. D.; Newell, R. H.; McNevin, M. J.; Muckerman, J. T.; DuBois, M. R.; DuBois, D. L. *J. Am. Chem. Soc.* **2006**, *128*, 358-366.

7. Lewis, N. S.; Nocera, D. G. *Proc. Natl. Acad. Sci. U.S.A.* **2006**, *103*, 15729-15735.

8. Crabtree, G. W.; Dresselhaus, M. S; Buchanan, M. V. *Phys. Today* **2004**, *57*, 39-44.

9. (a) Benson, E. E.; Kubiak, C. P.; Sathrum, A. J.; Smieja, J. M. *Chem. Soc. Rev.* **2009**, *38*, 89-99. (b) Kumar, B.; Llorente, M.; Froehlich, J.; Dang, T.; Sathrum, A.; Kubiak, C. P. *Annu. Rev. Phys. Chem.* **2012**, *63*, 541-69.

10. (a) Schneider, J.; Jia, H.; Muckerman, J. T.; Fujita, E. *Chem. Soc. Rev.* **2012**, *41*, 2036-2051. (b) Doherty, M. D.; Grills, D. C.; Muckerman, J. T.; Polyansky, D. E.; Fujita, E. *Coord. Chem. Rev.* **2010**, *254*, 2472-2482. (c) Fujita, E. *Coord. Chem. Rev.* **1999**, *185-186*, 373-384.

11. For Fe catalysts see: (a) Costentin, C.; Passard, G.; Robert, M.; Savéant, J.-M. *Proc. Natl. Acad. Sci. U.S.A.* **2014**, *111*, 14990-14994. (b) Costentin, C.; Passard, G.; Robert, M.; Savéant, J.-M. *J. Am. Chem. Soc.* **2014**, *136*, 11821-11829. (c) Costentin, C.; Drouet, S.; Robert, M.; Savéant, J.-M. *Science* **2012**, *338*, 90-94. (d) Thammavongsy, Z.; Seda, T.; Zakharov, L. N.; Kaminsky, W.; Gilbertson, J. D. *Inorg. Chem.* **2012**, *51*, 9168-9170. (e) Chen, J.; Szalda, D. J.; Fujita, E.; Creutz, C. *Inorg. Chem.* **2010**, *49*, 9380-9391. (f) Grodkowski, J.; Neta, P. *J. Phys. Chem. A* **2000**, *104*, 4475-4479. (g) Dhanasekaran, T.; Grodkowski, J.; Neta, P.; Hambright, P.; Fujita, E. *J. Phys. Chem. A* **1999**, *103*, 7742-7748. (h) Grodkowski, J.; Behar, D.; Neta, P. Hambright, P. *J. Phys. Chem. A* **1997**, *101*, 248-254. (i) Bhugun, I.; Lexa, D.; Savéant, J.-M. *J. Am. Chem. Soc.* **1996**, *118*, 1769-1776. (j) Bhugun, I.; Lexa, D.; Savéant J.-M. *J. Am. Chem. Soc.* **1994**, *116*, 5015-5016. (k) Hammouche, M.; Lexa, D.; Momenteau, M.; Savéant J.-M. *J. Am. Chem. Soc.* **1991**, *113*, 8455-8466. (l) Hammouche, M.; Lexa, D.; Savéant J.-M. *J. Electroanal. Chem.* **1988**, *249*, 347-351.

12. For Co catalysts see: (a) Ogata, T.; Yamamoto, Y.; Wada, Y.; Murakoshi, K.; Kusaba, M.; Nakashima, N.; Ishida, A.; Takamuku, S.; Yanagida, S. *J. Phys. Chem.* **1995**, *99*, 11916-11922. (b) Ogata, T.; Yanagida, S.; Brunschwig, B. S.; Fujita, E. *Energy Convers. Manage.* **1995**, *36*, 669-672. (c) Matsuoka, S.; Yamamoto, K.; Ogata, T.; Kusaba, M.; Nakashima, N.; Fujita, E.; Yanagida, S. *J. Am. Chem. Soc.* **1993**, *115*, 601-609. (d) Fujita, E.; Szalda, D. J.; Creutz, C.; Sutin, N. *J. Am. Chem. Soc.* **1988**, *110*, 4870-4871. (e) Fisher, B.; Eisenberg, R. *J. Am. Chem. Soc.* **1980**, *102*, 7363-7365.

13. For Ni catalysts see: (a) Thoi, V. S.; Chang, C. J. *Chem. Commun.* **2011**, *47*, 6578-6580. (b) Simón-Manso, E.; Kubiak, C. P. *Organometallics* **2005**, *24*, 96-102. (c) Fujita, E.; Brunschwig, B. S.; Ogata, T.; Yanagida, S. *Coord. Chem. Rev.* **1994**, *132*, 195-200. (d) Craig, C. A.; Spreer, L. O.; Otvos, J. W.; Calvin, M. *J. Phys. Chem.* **1990**, *94*, 7957-7960. (e) Daniele, S.; Ugo, P.; Bontempelli, G.; Fiorani, M. *J. Electroanal. Chem.* **1987**, *219*, 259-271. (f) Beley, M.; Collin, J.-P.; Ruppert, R.; Sauvage, J.-P. *J. Am. Chem. Soc.* **1986**, *108*, 7461-7467. (g) Meshitsuka, S.; Ichikawa, M.; Tamaru, K. *J. Chem. Soc., Chem. Commun.* **1974**, 158-159.

14. Bourrez, M.; Molton, F.; Chardon-Noblat, S.; Deronzier, A. *Angew. Chem. Int. Ed.* **2011**, *50*, 9903-9906.

15. (a) Smieja, J. M.; Benson, E. E.; Kumar, B.; Grice, K. A.; Seu, C. S.; Miller, A. J. M.; Mayer, J. M.; Kubiak, C. P. *Proc. Natl. Acad. Sci. U.S.A.* **2012**, *109*, 15646-15650. (b) Smieja, J. M.; Kubiak, C. P. *Inorg. Chem.* **2010**, *49*, 9283-9289. (c) Kumar, B.; Smieja, J. M.; Kubiak, C. P. *J. Phys. Chem. C* **2010**, *114*, 14220-14223. (d) Johnson, F. P. A.; George, M. W.; Hartl, F.; Turner, J. J. *Organometallics* **1996**, *15*, 3374-3387. (e) Sullivan, B. P.; Bolinger, C. M; Conrad, D.; Vining, W. J.; Meyer, T. J. *J. Chem. Soc.,*

Chem. Commun. **1985**, 1414-1416. (f) Hawecker, J.; Lehn, J.-M.; Ziessel, R. *J. Chem. Soc., Chem. Commun.* **1984**, 328-330.

16. Smieja, J. M.; Sampson, M. D.; Grice, K. A.; Benson, E. E.; Froehlich, J. D.; Kubiak, C. P. *Inorg. Chem.* **2013**, *52*, 2484-2491.
17. Sampson, M. D.; Nguyen, A. D.; Grice, K. A.; Moore, C. E.; Rheingold, A. L.; Kubiak, C. P. *J. Am. Chem. Soc.* **2014**, *136*, 5460-5471.

18. Takeda, H.; Koizumi, H.; Okamoto, K.; Ishitani, O. *Chem. Commun.* **2014**, *50*, 1491-1493.

19. Walsh, J. J.; Neri, G.; Smith, C. L.; Cowan, A. J. *Chem. Commun.* **2014**, *50*, 12698-12701.

20. For an example of Mn-catalyzed proton reduction see: (a) Valyaev, D. A.; Peterleitner, M. G.; Semeikin, O. V.; Utegenov, K. I.; Ustynyuk, N. A.; Sournia-Saquet, A.; Lugan, N.; Lavigne, G. J. Organomet. Chem. 2007, 692, 3207–3211. (b) Hou, K.; Poh, T.; Fan, W. Y. *Chem. Commun.* **2014**, *50*, 6630

21. For recent contributions see: (a) Riplinger, C.; Sampson, M. D.; Ritzmann, A. M.; Kubiak, C. P. *J. Am. Chem. Soc.* **2014**, *136*, 16285-16298. (b) Bourrez, M.; Orio, M.; Molton, F.; Vezin, H.; Duboc, C.; Deronzier, A.; Chardon-Noblat, S. *Angew. Chem. Int. Ed.* **2014**, *53*, 240-243. (c) Grills, D. C.; Farrington, J. A.; Layne, B. H.; Lymar, S. V.; Mello, B. A.; Preses, J. M.; Wishart, J. F. *J. Am. Chem. Soc.* **2014**, *136*, 5563-5566.

22. (a) Zeng, Q.; Tory, J. Hartl, F. *Organometallics* **2014**, *33*, 5002-5008. (b) Vollmer, M. V.; Machan, C. W.; Clark, M. L.; Antholine, W. E.; Agarwal, J.; Schaefer III, H. F.; Kubiak, C. P.; Walensky, J. R. *Organometallics* **2015**, *34*, 3-12.

23. (a) Agarwal, J.; Stanton III, C. J.; Shaw, T. W.; Vandezande, J. E.; Majetich, G. F.; Bocarsly, A. B.; Schaefer III, H. F. *Dalton Trans.* **2015**, 44, 2122-2131. (b) Agarwal, J.; Shaw, T. W; Stanton III, C. J.; Majetich, G. F.; Bocarsly, A. B.; Schaefer III, H. F. *Angew. Chem. Int. Ed.* **2014**, *53*, 5152-5155.

24. (a) Mukhopadhyay, T. K.; Feller, R. K.; Rein, F. N.; Henson, N. J.; Smythe, N. C.; Trovitch, R. J.; Gordon, J. C. *Chem. Commun.* **2012**, *48*, 8670-8672. (b) Scarborough, C. C.; Wieghardt, K. *Inorg. Chem.* **2011**, *50*, 9773-9793, and references therein. (c) Irwin, M.; Jenkins, R. K.; Denning, M. S.; Krämer, T.; Grandjean, F.; Long, G. J.; Herchel, R.; McGrady, J. E.; Goicoechea, J. M. *Inorg. Chem.* **2010**, *49*, 6160-6171. (d) Kraft, S. J.; Fanwick, P. E.; Bart, S. C. *Inorg. Chem.* **2010**, *49*, 1103-1110. (e) Roitershtein, D.; Domingos, Ã.; Pereira, L. C.; J.; Ascenso, J. R.; Marques, N. *Inorg. Chem.* **2003**, *42*, 7666-7673. (f) Schultz, M.; Boncella, J. M.; Berg, D. J.; Tilley, T. D.; Anderson, R. A.; *Organometallics* **2001**, *21*, 460-472. (g) Evans, W. J.; Drummond, D. K. *J. Am. Chem. Soc.* **1989**, *111*, 3329-3335.

25. (a) Porter, T. M.; Hall, G. B.; Groy, T. L.; Trovitch, R. J. *Dalton Trans.* **2013**, *42*, 14689-14692. (b) Khusniyarov, M. M.; Weyhermüller, T. Bill, E.; Wieghardt, K. *J. Am. Chem. Soc.* **2009**, *131*, 1208-1221, and references therein. (c) Muresan, N.; Lu, C. C.; Ghosh, M.; Peters, J. C.; Abe, M.; Henling, L. M.; Weyhermöller, Bill, E.; Wieghardt, K. *Inorg. Chem.* **2008**, *47*, 4579-4590. (d) Muresan, N.; Chlopek, K.; Weyhermüller, T.; Neese, F.; Wieghardt, K. *Inorg. Chem.* **2007**, *46*, 5327-5337. (e) Khusniyarov, M. M.; Harms, K.; Burghaus, O.; Sundermeyer, J. *Eur. J. Inorg. Chem.* **2006**, 2985-2996.

26. (a) Bart, S. C.; Chlopek, K.; Bill, E.; Bouwkamp, M. W.; Lobkovsky, E.; Neese, F.; Wieghardt, K.; Chirik, P. J. *J. Am. Chem. Soc.* **2006**, *128*, 13901-13912. (b) Knijnenburg, Q.; Gambarotta, S.; Budzelaar, P. H. M. *Dalton Trans.* **2006**, 5442-5448. (c) de Bruin, B.; Bill, E.; Bothe, E.; Weyhermüller, T.; Wieghardt, K. *Inorg. Chem.* **2000**, *39*, 2936-2947.

27. Mukhopadhyay, T. K.; Flores, M.; Groy, T. L.; Trovitch, R. J. *J. Am. Chem. Soc.* **2014**, *136*, 882-885.

28. Cavanaugh, M. D.; Gregg, B. T.; Cutler, A. R. *Organometallics* **1996**, *15*, 2764-2769.

29. Trovitch, R. J. *Synlett* **2014**, 25, 1638-1642.

30. Ben-Daat, H.; Hall, G. B.; Groy, T. L.; Trovitch, R. J. *Eur. J. Inorg. Chem.* **2013**, 4430-4442.

31. Russell, S. K.; Bowman, A. C.; Lobkovsky, E.; Wieghardt, K.; Chirik, P. J. *Eur. J. Inorg. Chem.* **2012**, 535-545.

32. Gennaro, A.; Isse, A. A.; Vianello, E. *J. Electroanal. Chem.* **1990**, *289*, 203-215.

33. Hydrosilylation reactions using (^{Ph2PPr}PDI)Mo(CO) have recently been found to proceed following phosphine donor dissociation. Please see: Pal, R.; Groy, T. L.; Bowman, A. C.; Trovitch, R. J. *Inorg. Chem.* **2014**, *53*, 9357-9365.

34. Jaguar, version 8.1, Schrodinger, LLC, New York, NY, 2013.

35. (a) Perdew, J. P.; Burke, K.; Ernzerhof, M. *Phys. Rev. Lett.* **1996**, *77*, 3865-3868. (b) Perdew, J. P.; Burke, K.; Ernzerhof, M. *Phys. Rev. Lett.* **1997**, *78*, 1396.

36. Rassolov, V.; Pople, J. A.; Ratner, M.; Windus, T. L. *J. Chem. Phys.* **1998**, *109*, 1223-1229.

37. Mukhopadhyay, T. K.; MacLean, N. L.; Gan, L.; Ashley, D. C.; Groy, T. L.; Baik, M.-H.; Jones, A. K.; Trovitch, R. J. *Inorg. Chem.* **2015**, *54*, 4475.

Chapter 5

1. Iron dinitrogen complexes: (a) Crossland, J. L.; Tyer, D. R. *Coord. Chem. Rev.* **2010**, *254*, 1883-1894. (b) Rodriguez, M. M., Bill, E., Brennessel, W. W. & Holland, P. L. *Science* **2011**, *334*, 780-783. (c) Hazari, N. *Chem. Soc. Rev.* **2010**, *39*, 4044-4056. (d) Anderson, J. S.; Rittle, J.; Peters, J. C. *Nature* **2013**, *501*, 84-87. (e) Moret, M.-E.; Peters, J. C. *Angew. Chem. Int. Ed.* **2011**, *50*, 2063-2067. (f) Bart, S. C.; Lobkovsky, E.; Chirik, P. J. *J. Am. Chem. Soc.* **2004**, *126*, 13794. (g) Hendrich, M. P.; Gunderson, W.; Behan, R. K.; Green, M. T.; Mehn, M. P.; Betley, T. A.; Lu, C. C.; Peters, J. C. *Proc. Natl. Acad. Sci. U.S.A* **2006**, *103*, 17107-17112. (h) Field, L. D.; Guest, R. W.; Turner, P. *Inorg. Chem.* **2010**, *49*, 9086-9093. (i) Gilbertson, J. D.; Szymczak, N. K.; Tyler, D. R. *J. Am. Chem. Soc.* **2005**, *127*, 10184-10185.

2. Iron catalysis: (a) Plietker, B. *Iron Catalysis in Organic chemistry: Reactions and Applications*. Wiley-VCH, Weinhem, **2008**. (b) Bauer, E. *Iron Catalysis II*. Springer, Swizerland, **2015**. (c) Bauer, I.; Knölker, H.-J.; *Chem. Rev.*, **2015**, *115*, 3170–3387. (d) Bolm, C.; Legros, J.; Le Paih, J.; Zani, L. *Chem. Rev.*, **2015**, *104*, 6217-6254.

3. (a) Blanchard, S.; Derat, E.; Murr, M. D-E.; Fensterbank, L.; Malacria, M.; Mouries-Mansuy, V. *Eur. J. Inorg. Chem.* **2012**, 376-389. (b) Bart, S. C. Lobkovsky, E.; Chirik, P. J. *J. Am. Chem. Soc.* **2004**, *126*, 13794-13807. (c) Trovitch, R. J.; Lobkovsky, E.; Chirik, P. J. *J. Am. Chem. Soc.* **2008**, *130*, 11631-11640. (d) Chirik, P. J.; Wieghardt, K. *Science* **2010**, *327*, 794-795.

4. (a) Akhtar, M.; Ellis, P. D.; MacDiarmid, A. G.; Odom, J. D. *Inorg. Chem.* **1972**, *11*, 2917-2921. (b) Whitlesey, M. K.; Mawby, R. J.; Osman, R.; Perutz, R. N.; Field, L. D.; Wilkinson, M. P.; George, M. W. *J. Am. Chem. Soc.* **1993**, *115*, 8627-8637. (c) Tolman, C. A.; Ittel, S. D.; English, A. D.; Jesson, J. P. *J. Am. Chem. Soc.* **1979**, *101*, 1742-1751. (d) Luo, L.; Nolan, S. P.; *Inorg. Chem.* **1993**, *32*, 2410-2415. (e) Hughes, D. L.; Leigh, G. J.; Jimenez-Tenorio, M.; Rowley, A. T.; *J. Chem. Soc. Dalton Trans.* **1993**, 75-82. (f) Hills, A.; Hughes, D. L.; Jimenez-Tenorio, M.; Leigh, G. J.; Rowley, A. T.; *J. Chem. Soc. Dalton Trans.* **1993**, 3041-3049. (g) de los Ríos, Jiménez-Tenorio, M.; Jiménez-Tenorio, M. A; Puerta, M. C.; Valerga, P. *J. Organomet. Chem.* **1996**, *525*, 57-64. (h) Hall, D. A.; Leigh, G. J. *J. Chem. Soc. Dalton Trans.* **1996**, 3539-3541. (i) Field, L. D.; Messerle, B. A.; Smernik, R. J.; Hambley, T. W.; Turner, P. *Inorg. Chem.* **1997**, *36*, 2884-2892. (j) Field, L. D.; Thomas, I. P.; Hambley, T. W.; Turner, P. *Inorg. Chem.* **1998**, *37*, 612-618. (k) Louie, J.; Grubbs, R. H.; *Organometallics* **2001**, *20*, 481-484. (l) Gilbertson, J. D.; Szymczak, N. K.; Tyler, D. R. *Inorg. Chem.* **2004**, *43*, 3341-3343. (m) van Rijn, J. A.; Gouré, E.; Siegler, M. A.; Spek, A. L.; Drent, E.; Bouwman, E. *J. Organomet. Chem.* **2011**, *696*, 1899-1903. (n) Nicolas, F.; Katharina, H.; Kimon, F.; Robert, L. *Dalton Trans.* **2013**, *42*, 11252-11261. (o) Bedford, R. B.; Brenner, P. B.; Carter, E.; Gallagher, T.; Murphy, D. M.; Pye, D. R. *Organometallics* **2014**, *33*, 5940-5943. (p) Yelle, R. B.; Crossland, J. L.; Szymczak, N. K.; Tyler, D. R. *Inorg. Chem.* **2009**, *48*, 861-871. (q) Casitas, A.; Krause, H.; Goddard, R.; Fürstner A. *Angew. Chem. Int. Ed.* **2015**, *54*, 1521-1526.

5. PNPFe: (a) Langer, R.; Leitus, G.; Ben-David, Y.; Milstein, D. *Angew. Chem.* **2011**, *123*, 2168-2172. (b) Langer, R.; Iron, M. A.; Konstantinovski, L.; Diskin-Posner, Y.; Leitus, G.; Ben-David, Y.; Milstein, D. *Chem. Eur. J.* **2012**, *18*, 7196-7209. (c) Srimani, D.; Diskin-Posner, Y.; Ben-David, Y.; Milstein, D. *Angew. Chem. Int. Ed.* **2013**, *52*, 14131-14134. (d) Alberico, E.; Sponholz, P.; Cordes, C.; Nielsen, M.; Drexler, H-J.; Baumann, W.; Junge, H.; Beller, M. *Angew. Chem. Int. Ed.* **2013**, *52*, 14162-14166. (e) Chakraborty, S.; Brennessel, W. W.; Jones, W. D. *J. Am. Chem. Soc.* **2014**, *136*, 8564-8567. (f) Qu, S.; Dai, H.; Dang, Y.; Song, C.; Wang, Z-X.; Guan, H. *ACS Catal.* **2014**, *4*, 4377-4388. (g) Koehne, I.; Schmeier, T. J.; Bielinski, E. A.; Pan, C. J.; Lagaditis, P. O.; Bernskoetter, W. H.; Takase, M. K.; Würtele, C.; Hazari, N.; Schneider, S. *Inorg. Chem.* **2014**, *53*, 2133-2143. (h) Fillman, K. L.; Bielinski, E. A.; Schmeier, T. J.; Nesvet, J. C.; Woodruff, T. M.; Pan, C. J.; Takase, M. K.; Hazari, N.; Neidig, M. L. *Inorg. Chem.* **2014**, *53*, 6066-6072. (i) Rivada-Wheelaghan, O.; Dauth, A.; Leitus, G.; Diskin-Posner, Y. *Inorg. Chem.* **2015**, *54*, 4526-4538. (j) Bonitatibus Jr., P. J.; Chakraborty, S.; Doherty, M. D.; Siclovan, O.; Jones, W. D.; Soloveichik, G. L. *Proc. Natl. Acad. Sci. U. S. A.* **2015**, *112*, 1687-1692. (k) Sharninghausen, L. S.; Mercado, B. Q.; Crabtree, R. H.; Hazari, N. *Chem. Commun.* **2015**, *51*, 16201-16204. (l) Zell, T.; Ben-David, Y.; Milstein, D. *Catal. Sci. Technol.* **2015**, *5*, 822-826. (m) Zell, T.; Milstein, D. *Acc. Chem. Res.* **2015**, *48*, 1979-1994. (n) Chakraborty, S.; Bhattacharya, P.; Dai, H.; Guan, H. *Acc. Chem. Res.* **2015**, *48*, 1995-2003. (o) Zhang, Y.; MacIntosh, A. D.; Wong, J. L.; Bielinski, E. A.; Williard, P. G.; Mercado, B. Q.; Hazari, N.; Bernskoetter, W. H. *Chem. Sci.* **2015**, *6*, 4291. (p) Chakraborty, S.; Lagaditis, P. O.; Förster, M.; Bielinski, E. A.; Hazari, N.; Holthausen, M. C.; Jones, W. D.; Schneider, S. *ACS Catal.* **2014**, *4*, 3994-4003.

6. PCPFe: (a) Xu, G.; Sun, H.; Li, X. *Organometallics* **2009**, *28*, 6090. (b) Bhattacharya, P.; Krause, J. A.; Guan, H. *Organometallics* **2011**, *30*, 4720-4729. (c) Zhao, H.; Sun, H.; Li, X. *Organometallics* **2014**, *33*, 3535. (d) Bhattacharya, P.; Krause, J. A.; Guan, H. *Organometallics* **2014**, *33*, 6113-6121. (e) Bhattacharya, P.; Krause, J. A.; Guan, H. *J. Am. Chem. Soc.* **2014**, *136*, 11153-11161. (f) Huang, S.; Zhao, H.; Li, X.; Wang, L.; Sun, H. *RSC Adv.* **2015**, *5*, 15660. (g) Murugesan, S.; Kirchner, K.; *Dalton Trans.* **2016**, *45*, 416-439.

7. Triphos iron complexes: (a) Davies, S. G.; Felkin, H.; Watts, O. *J. Chem. Soc. Chem Commun.* **1980**, *4*, 159-160. (b) Di Vaira, M.; Midollini, S.; Sacconi, L. *Inorg. Chem.* **1981**, *20*, 3430-3435. (c) Ghilardi, C. A.; Innocenti, P.; Midollini, S.; Orlandini, A. *J. Organomet. Chem.* **1982**, *231*, C78-C80. (d) Asam, A.; Janssen, B.; Huttner, G.; Zsolnai, L.; Walter, O. *Z. Naturforsch* **1993**, *48b*, 1707-1714. (e) Ghilardi, C. A.; Laschi, F.; Midollini, S.; Orlandini, A.; Scapacci, G.; Zanello, P. *J. Chem. Soc. Dalton Trans.* **1995**, 531-540. (f) Baker, P. K.; Meehan, M. M. *Inorg. Chim. Acta* **2000**, *303*, 17-23. (g) O'Connor, J. M.; Hiibner, K.; Closson, A.; Gantzel, P. *Organometallics* **2001**, *20*, 1482-1485. (h) Guilera, G.; McGrady, G. S.; Steed, J. W.; Kaltsoyannis, N. *New J. Chem.* **2004**, *28*, 444-446. (i) Jaunky, P.; Schmalle, H. W.; Blacque, O.; Fox, T.; Berke, H. *J. Organomet. Chem.* **2005**, *690*, 1429-1455. (j) Guilera, G.; McGrady, G. S.; Steed, J. W.; Burchell, R. P. L.; Sirsch, P.; Deeming, A. J. *New J. Chem.* **2008**, *32*, 1573-1581. (k) Thoreson, K. A.; Follett, A. D.; McNeill, K. *Inorg. Chem.* **2010**, *49*, 3942-3949. (l)

Dimmer, J.-A.; Wesemann, L. *Eur. J. Inorg. Chem.* **2011**, 235-240. (m) Li, P.; de Bruin, B.; Reek, J. N. H.; Dzik, W. I. *Organometallics* **2015**, *34*, 5009-5014. (n) Nishibayashi, Y.; Iwai, S.; Hidai, M. *J. Am. Chem. Soc.* **1998**, *120*, 10559-10560. (o) Hogarth, G.; Richards, I. *Inorg. Chem. Commun.* **2007**, *10*, 66-70. (p) Adam, F. I.; Hogarth, G.; Richards, I.; Sanchez, B. E. *Dalton Trans.* **2007**, *24*, 2495-2498.

8. Bpy : (a) Constable, E. C. *Adv. Inorg. Chem.* **1989**, *34*, 1-37. (b) Tom Dieck, H.; Franz, K.-D.; Hohmann, F. *Chem. Ber.* **1975**, *108*, 163-173. (c) Irwin, M.; Jenkins, R. K.; Denning, M. S.; Kr€amer, T.; Grandjean, F.; Long, G. J.; Herchel, R.; McGrady, J. E.; Goicoechea, J. M. *Inorg. Chem.* **2010**, *49*, 6160–6171. (d) Roitershtein, D.; Domingos, ~A.; Pereira, L. C. J.; Ascenso, J. R.; Marques, N. *Inorg. Chem.* **2003**, *42*, 7666–7673. (e) Scarborough, C. C.; Wieghardt, K. *Inorg. Chem.* **2011**, *50*, 9773-9793. (f) Chisholm, M. H.; Huffman, J. C.; Rothwell, I. P.; Bradley, P. G.; Kress, N.; Woodruff, W. H. *J. Am. Chem. Soc.* **1981**, *103*, 4945-4947. (g) Gore-Randall, E.; Irwin, M.; Denning, M. S.; Goicoechea, J. M. *Inorg. Chem.* **2009**, *48*, 8304–8316. (h) Echegoyen, L.; DeCian, A.; Fischer, J.; Lehn, J.-M. *Angew. Chem., Int. Ed. Engl.* **1991**, *30*, 838–840. (i) Bock, H.; Lehn, J.-M.; Pauls, J.; Holl, S.; Krenzel, V. *Angew. Chem., Int. Ed.* **1999**, *38*, 952–955. (j) Mukhopadhyay, T. K.; Feller, R. K.; Rein, F. N.; Henson, N. J.; Smythe, N. C.; Trovitch, R. J.; Gordon, J. C. *Chem. Commun.* **2012**, *48*, 8670-8672.

9. (a) Crabtree, R. H. *The Organometallic Chemistry of the Transition Metals*; John Wiley & Sons: Hoboken, NJ, 2009.

10. (a) Poremba, P.; Schmidt, H-G.; Noltemeyer, M.; Edelmann, F. T. *Organometallics* **1998**, *17*, 986-988. (b) Sygula, A.; Fronczek, F. R.; Rabideau, P. W. *J. Organomet. Chem.* **1996**, *526*, 389-391. (c) Hu, N.; Gong, L.; Jin, Z.; Chen, W. *J. Organomet. Chem.* **1988**, *352*, 61-66. (d) Jones, M. T.; de Boer, E. *Mol. Phys.* **1982**, *47*, 487-499. (e) Noordik, J. H.; van den Hark, T. E. M.; Mooij, J. J.; Klassen, A. A. K. *Acta Cryst.* **1974**, *B30*, 833-835.

11. Relevant COT complexes of iron for bond length survey: (a) Dickens, B.; Lipscomb, W. N. *J. Chem. Phys.* **1962**, *37*, 2084-2093. (b) Tsupreva, V. N.; Titov, A. A.; Filippov, O. A.; Bilyachenko, A. N.; Smol'yakov, A. F.; Dolgushin, F. M.; Agapkin, D. V.; Godovikov, I. A.; Epstein, L. M.; Shubina, E. S. *Inorg. Chem.* **2011**, *50*, 3325-3331. (c) Karlin, K. D.; Moisan, M. P.; Kustyn, M.; Dahlstrom, P. L.; Zubieta, J.; Raithby, P. R. *Cryst. Struct. Commun.* **1982**, *11*, 1945-1949. (d) Bassi, I. W.; Scordamaglia, R. *J. Organomet. Chem.* **1972**, *37*, 353-359. (e) Yu, Y.; Sun, J.; Chen, J. *J. Organomet. Chem.* **1997**, *533*, 13-23. (f) Lavallo, V.; El-Batta, A.; Bertrand, G.; Grubbs, R. H. *Angew. Chem. Int. Ed.* **2011**, *50*, 268-271. (g) Mukhopadhyay, T. K.; Flores, M.; Feller, R. K.; Scott, B. L.; Taylor, R. D.; Paz-Pasternak, M.; Henson, N. J.; Rein, F. N.; Smythe, N. C.; Trovitch, R. J.; Gordon, J. C. *Organometallics* **2014**, *33*, 7101-7112.

12. For a discussion on the electrochemical reduction of CpCo(COT) see: (a) Moraczewski, J.; Geiger, Jr.; W. E. *J. Am. Chem. Soc.* **1981**, *103*, 4779-4787. (b) Baik, M.-H.; Schauer, C. K.; Ziegler, T. *J. Am. Chem. Soc.* **2002**, *124*, 11167-11181 and

references therein.

13. Torrent, M.; Sola, M.; Frenking, G. *Chem. Rev.* **2000**, *100*, 439-493 and references therein.

14. Liu, T.; Li, B.; Popescu, C. V.; Bilko, A.; Pérez, L. M.; Hall, M. B.; Darensbourg, M. Y. *Chem. Eur. J.* **2010**, *16*, 3083-3089.

15. (a) Creutz, C. *Comments Inorg. Chem.* **1982**, *1*, 293. (b) Vlcek, A. A. *Coord. Chem. Rev.* **1982**, *43*, 39-62.

16. Felkin, H.; Lednor, P. W.; Normant, J.-M.; Smith, R. A. J. *J. Organomet. Chem.* **1978**, *157*, C64-C66.

17. Other relevant COT complexes for bond length survey: (a) Cr-COT complex: Brauer, D. J.; Krüger, C. *Inorg. Chem.* **1976**, *15*, 2511-2514. (b) CoCOT: Brennessel, W. W.; Young, Jr.; V. G.; Ellis, J. E. *Angew. Chem. Int. Ed.* **2002**, *41*, 1211-1215. (c) (η^4-COT)Zr(η^8-COT): Rogers, D. M.; Wilson, S. R.; Girolami, G. S. *Organometallics* **1991**, *10*, 2419-2424. (d) (η^4-COT)Zr(η^8-COT)(THF): Brauer, D. J.; Krüger, C. *J. Organomet. Chem.* **1972**, *42*, 129-137. (e) (η^5-Cp*)Zr(μ-η^8,η^2-COT)(η^4-COT)Zr(η^5-Cp*): Sinnema, P. J.; Meetsma, A.; Teuben, J. H. *Organometallics* **1993**, *12*, 184-189. (f) Mo-COT: Cotton, F. A.; Koch, S. A.; Schultz, A. J.; Williams, J. M. *Inorg. Chem.* **1978**, *17*, 2093-2098. (g) (η^4-COT)Ru(CO)$_3$: Cotton, F. A.; Eiss, R. *J. Am. Chem. Soc.* **1969**, *91*, 6593-6597. (h) Heck, J.; Lange, G.; Malessa, M.; Boese, R.; Bläser, D. *Chem. Eur. J.* **1999**, *5*, 659-668. (i) Brown, D. B.; Johnson, B. F. G.; Martin, C. M.; Parsons, S. *J. Organomet. Chem.* **1997**, *536-537*, 285-291. (j) Bieri, J. H.; Egolf, T.; van Philipsborn, W.; Piantini, U.; Prewo, R.; Ruppli, U.; Salzer, A. *Organometallics* **1986**, *5*, 2413-2425. (k) Cotton, F. A.; Koch, S. A.; Schultz, A. J.; Williams, J. M. *Inorg. Chem.* **1978**, *17*, 2093-2098.

18. For the purposes of this contribution, a C-C bond metrical parameter error limit of ±0.01 Å has been set for inclusion of a data set in electronic structure discussion.

19. . [(η^8-COT)Ti]$_2$(μ-η^4,η^4-COT): (a) Dierks, V. H.; Dietrich, H. *Acta Cryst.*, *Sect. B.* **1968**, *24*, 58-62. (b) Dietrich, H.; Dierks, H. *Angew. Chem. Int. Ed.* **1966**, *5*, 899.

20. [(2,6-(2,6-^{i}Pr$_2$-C$_6$H$_3$)C$_6$H$_3$)Cr]$_2$(μ-η^3,η^4-COT): Boynton, J. N.; Summerscales, O. T.; Grandjean, F.; Long, G. J.; Fettinger, J. C.; Power, P. P. *Organometallics* **2012**, *31*, 8559-8560.

21. Farmery, K.; Kilner, M.; Greatrex, R.; Greenwood, N. N. *J. Chem. Soc. A* **1969**, 2339-2345.

22. Dickson, D. P. E.; Berry, F. J. Mössbauer Spectroscopy; Cambridge University Press: Trowbridge, Great Britain, **1986**.

23. Hanson, A. W. *Acta Cryst.* **1962**, *15*, 930-933.

24. Calvo, R.; Isaacson, R. A.; Paddock, M. L.; Abresch,E. C.; Okamura,M. Y.; Maniero, A. L.; Brunel, L. C.; Feher G. *J. Phys. Chem. B.* **2001**, *105*, 4053-4057.

25. Klärner, F.-G. *Angew. Chem. Int. Ed.* **2001**, *40*, 3977-3981, and references therein.

26. Stratman, R. E.; Scuseria, G. E.; Frisch, M. J. *J. Chem. Phys.* **1998**, *109*, 8218-8224.

27. Römelt, M.; Ye, S.; Neese, F. *Inorg. Chem.* **2009**, *48*, 784-785.

28. Lavallo, V.; Grubbs, R. H. *Science* **2009**, *326*, 559-562.

29. Ben-Daat, H.; Hall, G. B.; Groy, T. L.; Trovitch, R. J. *Eur. J. Inorg. Chem.* **2013**, 4430-4442.

30. Pal, R.; Groy, T. L.; Bowman, A. C.; Trovitch, R. J. *Inorg. Chem.* **2014**, *53*, 9357-9365.

31. (a) Albright, T. A.; Burdett, J. K.; Whangbo, M.-H. *Orbital Interaction in Chemistry*; John Wiley & Sons: New York, **1985**, pp. 343-347. (b) Albright, T. A.; Burdett, J. K. *Problems in Molecular Orbital Theory*; Oxford University Press, New York, **1992**, pp. 205-206.

32. (a) King, R. B.; Kapoor, P. N.; Kapoor, R. N. *Inorg. Chem.* **1971**, *10*, 1841-1850. (b) Schaefer, B. A.; Margulieux, G.; Small, B. L.; Chirik, P. J. *Organometallics* **2015**, *34*, 1307-1320.

33. Mukhopadhyay, T. K.; Groy, T. L.; Smythe, N. C.; Gordon, J. C.; Trovitch, R. J. *J. Coord. Chem. (just accepted)*.

34. (a) Abragam, A.; Bleaney, B. *Electron Paramagnetic Resonance of Transition Ions.* Clarendon Press: Oxford, Great Britain, 1970; Chapter 9. (b) Bencini, A.; Gatteschi, D. *Electron Paramagnetic Resonance of Exchange Coupled Systems;* Springer: Berlin, 1990; Chapter 3. (c) Eaton, G. R.; Eaton, S. S. *In Biological Magnetic Resonance*; Berliner, L. J., Reuben, J., Eds.; Plenum: New York, 1989; Vol. 8, pp 339−396. (d) Stoll, S.; Schweiger, A. *J. Magn. Reson.* **2006**, *178*, 42−55.

35. Frisch, M. J.; Trucks, G. W.; Schlegel, H. B.; Scuseria, G. E.; Robb, M. A.; Cheeseman, J. R.; Scalmani, G.; Barone, V.; Mennucci, B.; Petersson, G. A.; Nakatsuji, H.; Caricato, M.; Li, X.; Hratchian, H. P.; Izmaylov, A. F.; Bloino, J.; Zheng, G.; Sonnenberg, J. L.; Hada, M.; Ehara, M.; Toyota, K.; Fukuda, R.; Hasegawa, J.; Ishida, M.; Nakajima, T.; Honda, Y.; Kitao, O.; Nakai, H.; Vreven, T.; Montgomery, Jr., J. A.; Peralta, J. E.; Ogliaro, F.; Bearpark, M.; Heyd, J. J.; Brothers, E.; Kudin, K. N.; Staroverov, V. N.; Kobayashi, R.; Normand, J.; Raghavachari, K.; Rendell, A.; Burant, J.

C.; Iyengar, S. S.; Tomasi, J.; Cossi, M.; Rega, N.; Millam, J. M.; Klene, M.; Knox, J. E.; Cross, J. B.; Bakken, V.; Adamo, C.; Jaramillo, J.; Gomperts, R.; Stratmann, R. E.; Yazyev, O.; Austin, A. J.; Cammi, R., Pomelli, C.; Ochterski; J. W.; Martin, R. L.; Morokuma, K.; Zakrzewski, V. G.; Voth, G. A.; Salvador, P.; Dannenberg, J. J.; Dapprich, S.; Daniels, A. D.; Farkas, O.; Foresman, J. B., Ortiz, J. V.; Cioslowski, J.; Fox, D. J. Gas *Gaussian 09 Revision B.01*, Wallingford, CT, Gaussian Inc., 2009.

36. Neese, F. *WIREs Comput. Mol. Sci.* **2012**, *2*, 73-78.

37. Perdew, J. P.; Burke, K.; Ernzerhof, M. *Phys. Rev. Lett.* **1996**, *77*, 3865-3868.

38. Roy, L. E.; Hay, J.; Martin, R. L. *J. Chem. Theory Comput.* **2008**, *4*, 1029-1031.

39. Becke, A. D. *J. Chem. Phys.* **1993**, *98*, 5648-5652.

APPENDIX A

Copyright and Permissions

Part of Chapter 1 have been taken from (a) Ghosh, C.; Mukhopadhyay, T. K.; Flores, M.; Groy, T. L.; Trovitch, R. J. *Inorg. Chem.* **2015**, *54*, 10398-10406. (b) Mukhopadhyay, T. K.; Flores, M.; Groy, T. L.; Trovitch, R. J. *J. Am. Chem. Soc.* **2014**, *136*, 882-885.

ACS Publications
Most Trusted. Most Cited. Most Read.

Title: A Highly Active Manganese Precatalyst for the Hydrosilylation of Ketones and Esters

Author: Tufan K. Mukhopadhyay, Marco Flores, Thomas L. Groy, et al

Publication: Journal of the American Chemical Society

Publisher: American Chemical Society

Date: Jan 1, 2014

Copyright © 2014, American Chemical Society

PERMISSION/LICENSE IS GRANTED FOR YOUR ORDER AT NO CHARGE

BACK | CLOSE WINDOW

241

Part of Chapter 4 have been taken from Mukhopadhyay, T. K.; MacLean, N. L.; Gan, L.; Ashley, D. C.; Groy, T. L.; Baik, M. -H.; Jones, A. K.; Trovitch, R. J. *Inorg. Chem.* **2015**, *54*, 4475-4482.

Part of Chapter 5 have been taken from (a) Mukhopadhyay, T. K.; Feller, R. K.; Rein, F. N.; Henson, N. J.; Smythe, N. C.; Trovitch, R. J.; Gordon, J. C. *Chem. Commun.* **2012**, *48*, 8670-8672. (b) Mukhopadhyay, T. K.; Flores, M.; Feller, R. K.; Scott, B. L.; Taylor, R. D.; Paz-Pasternak, M.; Henson, N. J.; Rein, F. N.; Smythe, N. C.; Trovitch, R. J.; Gordon, J. C. *Organometallics* **2014**, *33*, 7101-7112.

BIOGRAPHICAL SKETCH

Tufan K. Mukhopadhyay was born and raised at Panduka, which is a small village at in West Bengal, India. He started his educational career at Nadiha High School and after finishing matriculation, he went to Manbhum Victoria Institution at Purulia for higher secondary degree. He completed his Batchelor in Science (B. Sc.) with a first class in Chemistry Honors from Ramananda Centenary College, Laulara, Purulia., where he acquired the interest for research in chemistry. After B. Sc., Tufan joined Indian Institute of Technology, Madras (IITM) as a Master of Science (M. Sc.) student, where he spent two years. He worked with Prof. Santosh J. Gharpure to fulfill M. Sc. dissertation, where he studied the synthesis of N-fused indoles from the cyclization of vinylogous carbamates. Completing M. Sc. in 2010, Tufan spent one more year at IITM working with Prof. Indrapal Singh Aidhen on carbohydrate chemistry, where he published a second author paper in *Eur. J. Org. Chem*. After that he came to Arizona State University in 2011 as a graduate student and joined the first research group of Prof. Ryan J. Trovitch. In Prof. Trovitch's lab, Tufan worked on the development of homogeneous manganese and iron catalysts, where he characterized a series of low valent manganese complexes that are remarkably efficient for carbonyl hydrosilylation. He was also selected for the Outstanding Graduate Research Assistant award by the School of Molecular Sciences in 2016. During the doctoral research, he has acquired various skills and immense knowledge in the field of inorganic and organometallic chemistry. He hopes to work on small molecule activation using metal ligand cooperativity with Prof. Nathaniel Szymczak at University of Michigan, Ann Arbor, starting at June 2016. Tufan is interested to pursue his scientific quest further by conducting independent research in the field of renewable energy development.